DEVELOPMENT OF A PREDICTIVE MODEL FOR THE WEATHERING OF OIL IN THE PRESENCE OF SEA ICE

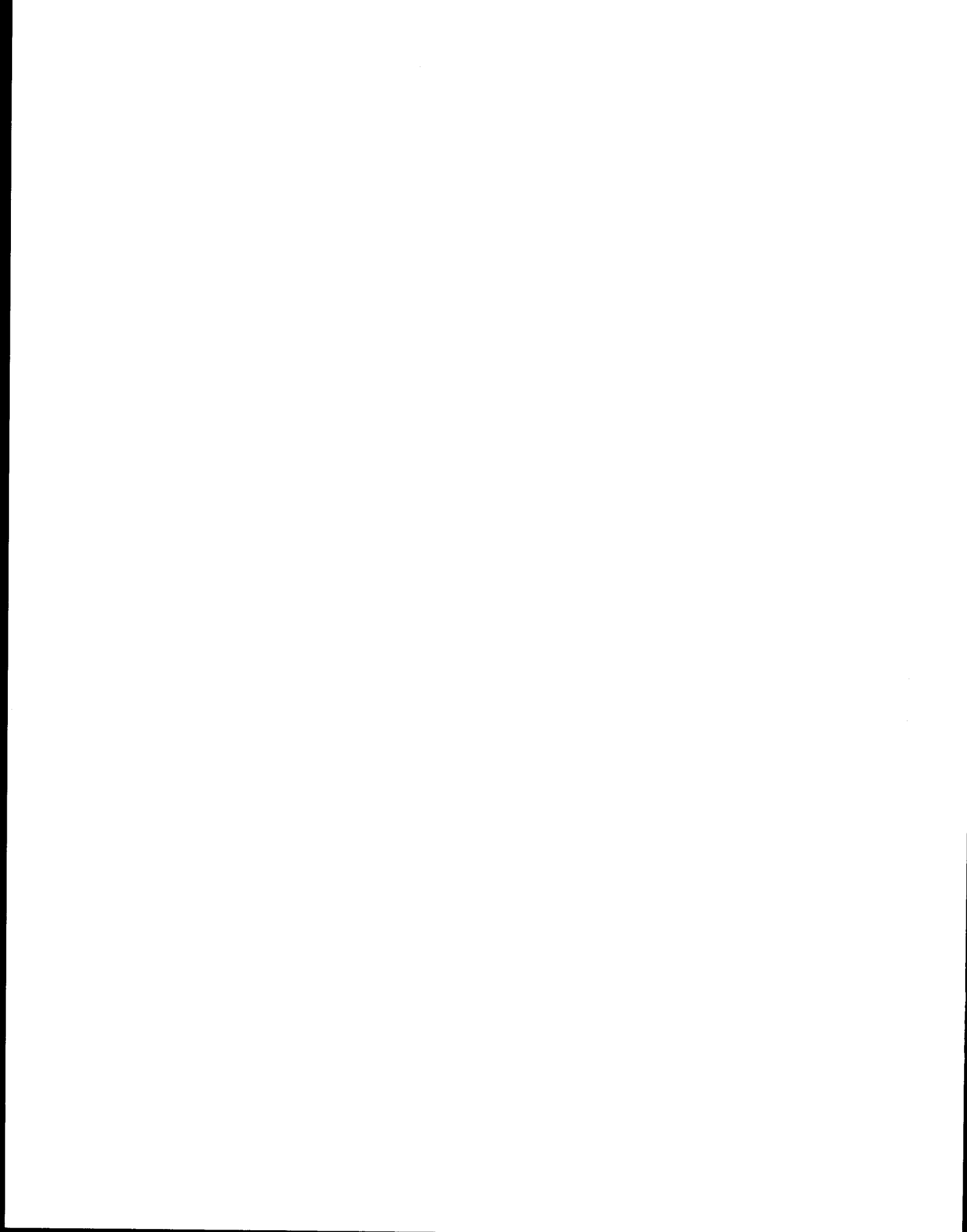by

James R. Payne, G. Daniel McNabb, Jr., Lon E. Hachmeister,
Bruce E. Kirstein, John R. Clayton, Jr., Charles R. Phillips,
Robert T. Redding, Cheryl L. Clary, Gary S. Smith, and Garry H. Farmer

Applied Environmental Sciences Department
Science Applications International Corporation
10260 Campus Point Drive
San Diego, California 92121

Final Report
Outer Continental Shelf Environmental Assessment Program
Research Unit 664

October 1987

ACKNOWLEDGMENTS

ABSTRACT

The objective of this program has been to develop a predictive model that describes the qualitative and quantitative weathering of spilled oil and refined petroleum products in the presence of first-year and multi-year ice. To achieve this objective and verify model predictions, cold-room and field experiments were performed to provide suitable data for describing time-series changes in the physical and chemical properties of oil spilled in the presence of first-year and multi-year ice in various configurations. For modeling purposes, fresh and weathered crude oil were characterized as distillable cut fractions (i.e., pseudocomponents). In addition, specific mechanisms for enhancing the transport of spilled oil components to the benthic environment were recognized during this program, and additional studies were completed to investigate these potentially significant dispersion/dissolution processes. Results from these studies and the development of the computer model provide a significant contribution toward OCSEAP's goal of developing predictive capabilities for defining the magnitude of the impacts from OCS oil and gas activities to exposed Arctic and sub-Arctic biota.

TABLE OF CONTENTS

153

TABLE OF CONTENTS (Continued)

154

TABLE OF CONTENTS (Continued)

155

TABLE OF CONTENTS (Continued)

LIST OF FIGURES

159

160

LIST OF FIGURES (Continued)

161

LIST OF TABLES

165

LIST OF TABLES (Continued)

166

167

1.
INTRODUCTION

Beginning in 1979, Science Applications Inc., now Science Applications International Corporation (SAIC), undertook the development of a computer-driven model for simulating the weathering behavior of crude oil and refined petroleum products released in open ocean environments (Payne et al., 1984a). The weathering model included algorithms describing evaporation, dissolution, water-in-oil emulsification, spreading of oil on the sea surface, and predicted percent oil remaining in a slick as a function of open ocean weathering conditions. The model algorithms are based on physical properties data and the physical/chemical partitioning behavior of oil driven by dynamic equilibria and mass transfer coefficients. Model verification was completed by outdoor sub-arctic wave tank studies in which quantitative data on evaporation, dissolution, water-in-oil emulsification, microbial degradation, and adsorption onto suspended particulate material were obtained and compared with the model-predicted values for the first three processes. As a logical extension of that program, SAIC undertook a modeling and experimental program to evaluate specific changes in the physical and chemical properties of oil due to weathering in arctic environments in the presence of first-year and multi-year sea ice.

This report contains the results of the oil-in-ice studies and describes the model development or modifications to the existing Open Ocean Oil-Weathering Model Code that enable predictions to be made for oil weathering behavior in the presence of first-year and multi-year ice. The following section (2) is an Executive Summary which includes conclusions and implications from these studies that are relevant for OCSEAP's purpose of analyzing OCS oil and gas development in the Arctic.

Background information is presented in Section 3 describing the structure and characteristics of first-year and multi-year ice and their interactions with oil. Much of this existing information on the behavior of oil in ice is based on observations from spills under simulated blowout conditions (e.g., DOME, 1981; Nelson and Allen, 1981). Although results from such cited studies are relevant to discussions of oil-in-ice behavior (and possible spill

cleanup methods), no previous attempts have been made to measure specific mass transfer rates and the changes in physical and chemical properties of oil due to weathering processes as are required for predictive modeling.

Section 4 contains information on controlled coldroom wavetank experiments that were undertaken to quantify changes in the physical and chemical properties of oil spilled in the presence of simulated first-year and multi year ice. The experiments were designed to generate data necessary for predicting rates of oil dispersion, dissolution, evaporation, and water-in-oil emulsification in arctic environments where sea ice is an important, if not controlling, factor in oil weathering. Descriptions are presented of not only frazil and slush ice formation under turbulent conditions, but also how columnar ice growth in less turbulent regimes will ultimately affect the qualitative and quantitative behavior of whole crude oil released into "first-year" and "multi-year" ice systems. The construction and utilization of the experimental flow-through wave tank and the cold room at the NOAA Kasitsna Bay laboratory are also discussed. Specifically, the ability to simulate not only the structure and behavior of first-year and multi-year ice, but also the interactions of spilled oil with sea ice in the scaled-down wave tank (i.e., relative to natural spill conditions) was a major concern for the wave tank studies. Consequently, a limited field data collection and observation program was undertaken in the Chukchi Sea in February/March 1984 to provide additional information on real and simulated "first-year" ice properties and also on possible scaling problems. In this effort, first-year ice samples were collected in the Chukchi Sea to compare crystal structure and salinity characteristics of the field ice with those of simulated "first-year" wave tank ice. Conductivity (salinity) and temperature measurements were obtained for the first-year ice and subsurface water in the field and compared with equivalent values from the wave tank studies. The results of these and other "scaling" field studies are presented in Section 4.

Section 5 contains information on a more extensive field effort that was undertaken in the Chukchi Sea in February/March 1985. Based on information in the open literature as well as the results of the wave tank studies in Section 4, this field effort was designed to investigate the possible transport

of dissolved hydrocarbon compounds from an oil spill in open, re- freezing lead systems to benthic environments beneath surface ice fields. Descriptions of the laboratory and field efforts as well as the experimental results and their possible environmental relevance are presented in this section.

Section 6 presents a discussion of the endproduct numerical model that has been generated to predict additional weathering behavior of oil in the presence of first-year and multi-year sea ice. Analytical data and qualitative (descriptive) information derived from both the Kasitsna Bay wave tank experiments and the Chukchi Sea field programs were taken into account and incorporated into the on-going development of NOAA's Oil Weathering Model. In addition to the wave tank and field efforts, controlled diffusion experiments were performed in the laboratory to measure component-specific dissolution rates from an oil slick into a well-stirred water column at ambient (cold water) conditions. The results were used to generate partition coefficients for individual true boiling point distillate oil cuts. These results are also presented in Section 6, and they were taken into account for the oil-in-ice model.

By virtue of this building process, the oil-in-ice model is similar to, and compatible with, the previously developed open-ocean oil-weathering model (CUTVP2). Both models are based on a pseudo-component characterization of the parent crude oil or refined product, and they calculate a material balance after specified periods of exposure. Additional modifications to the oil weathering code were made during the execution of this program to allow predictions regarding changes in physical properties (e.g., rheological) of the oil using a "fractioned weathered" parameter (as defined by Dr. Donald Mackay of the University of Toronto). The algorithms required for developing the new oil-in-first-year and oil-in-multi-year ice model code are described in this section.

In addition to the discussion of the model, Section 6 also includes a brief description of an application of the model to a real-world spill-of-opportunity. On 21 January 1984 the M/V Cepheus went aground on the west side of Knik Arm almost due west of Carin Point near Anchorage, AK. Approximately 200,000 gallons of JP-5 fuel were released into the water. SAIC collected and

171

performed appropriate analyses of oil samples from the <u>Cepheus</u>. These analytical results were then introduced into the code for the model, and the output was provided to NOAA HAZMAT in support of their spill response effort.

Section 7 describes the relevant Quality Assurance/Quality Control (QA/QC) procedures employed and the results obtained during the completion of this program. It includes a description of instrument calibration frequency, the levels of precision and accuracy obtained as reflected in replicate analyses, spike and recovery determinations, method and system blanks, and results from analyses of interim reference materials supplied by the NOAA/NMF QA lab in Seattle. Limits of detection and methods used to define them are also presented.

Section 8 contains the Bibliography for all cited references, and Appendices A & B present FORTRAN code descriptions for component specific dissolution from oil slicks and dispersed oil droplets, respectively.

A User's Guide for the oil-in-ice model is provided as a separate document. This guide includes information on topics such as model access, model prompts and model output, and contains a complete listing of the NOAA/ SAIC Oil Ice-Weathering Code.

EXECUTIVE SUMMARY--CONCLUSIONS AND IMPLICATIONS RELEVANT TO OCSEAP'S ANALYSIS OF OUTER CONTINENTAL SHELF OIL AND GAS DEVELOPMENT IN THE ARCTIC

The ultimate objective of this research effort was the development of a computer model that predicts the chemical and physical weathering behavior of oil released in the presence of first-year and multi-year sea ice. Several different oil-ice configurations have been incorporated into the model, including: 1) oil released on top of or under first-year or multi-year ice; 2) oil released in melting first-year or multi-year ice; and 3) oil weathering in the absence of ice. The third option represents the code from the previous NOAA sponsored open-ocean oil weathering model. In addition, bounding calculations have been performed to estimate dissolved component-specific concentrations resulting from oil released in first-year or multi-year ice lead systems that are subject to refreezing and thawing events. Additional model development completed during this program included the encoding of algorithms to use data from the NOAA oil weathering model for generating bulk physical properties of oil based on the Mackay "fraction weathered" formulation. The model uses a pseudo-component approach based on distillate cut fractions to characterize and generate physical properties for the spilled product under environmental conditions specified by the model user. Therefore, the model can consider any specified whole crude oil or refined petroleum product (e.g., fuel oil, gasoline, aircraft fuel, Bunker C, etc.).

Data were collected during both wave tank experiments and field sampling programs in the Chukchi Sea to assist in the development and verification of the oil-in-ice weathering model. Data obtained from both wave tank experiments and field observations yielded comparable results when the inherent scaling differences between these two regimes are considered. For example, the similarities in sea ice behavior and properties between wave tank and field studies included the mechanisms for ice growth and decay sequences of ice types (i.e., frazil, grease, and columnar ice), ice crystal structures, general ice morphology (e.g., smooth first-year ice versus ridge and keel systems in pack and/or multi-year ice), and vertical salinity profiles in the ice and water column layers. These similarities between the wave tank and field observations suggest that data derived from the wave tank studies for oil-ice interactions

are relevant to anticipated oil-ice interactions in field situations. Output from the model was used in support of a spill response effort by NOAA HAZMAT for a spill-of-opportunity when the M/V Cepheus went aground near Anchorage, AK and released approximately 200,000 gallons of JP-5 fuel oil into ice-covered waters. Results from the model output helped to predict rates of oil loss in the ice covered waters. However, time series samples of the spilled product could not be obtained because of the extremely dynamic nature of the ice and the transient behavior of the easily dispersed and volatile fuel oil. Thus, field verification of model predictions from an oil spill in ice-covered waters still awaits a future opportunity.

The oil-in-ice wave tank studies provided several findings that are important for predicting the weathering behavior of oil in the presence of first-year and/or multi-year sea ice. The significant findings are summarized in the following paragraphs.

One of the most important aspects of the oil-in-ice experiments was the role of ice morphology in controlling the rate and extent of stable water-in-oil emulsion formation. Melting first-year ice produced substantial amounts of slush ice and a water-in-oil emulsion of Prudhoe Bay crude oil containing up to 60% water was formed within four hours of the onset of wave agitation in this slush ice field. In contrast, rotting multi-year ice appeared to have a much lower tendency to produce a slush ice matrix during melting, and formation of the stable water-in-oil emulsions occurred over a relatively longer period of time. Therefore, data from the wave tank experiments suggest that the presence of a slush ice matrix and wave-generated turbulence promote the formation of stable water-in-oil emulsions. Emulsification presumably is the result of subjecting oil to microscale turbulence from the wave-induced grinding between slush ice crystals. Rapid formation of stable water-in-oil emulsions is important to potential spill cleanup and containment approaches, and for in situ burning from considerations of the lowered combustability of water-in-oil emulsions. Furthermore, it was observed that these water-in-oil emulsions had a density (specific gravity) which was intermediate between slush ice and seawater, and that they tended to reside just below the surface of the slush ice

174

fields. Therefore, under actual spill conditions, emulsified oil in the presence of relatively thick slush ice (e.g., 10 cm) may be extremely difficult to locate or observe from helicopters or fixed-wind aircraft.

Wave-turbulence induced compression and pumping of oil onto the surface of pancake ice was also observed in the wave tank experiments. This surfaced oil can become trapped by ridges of frozen slush ice that form around the edges of the pancake ice surfaces. At the same time, wave turbulence in the broken ice fields simulated in the cold-room wave tanks was responsible for rapid and appreciable increases in concentrations of dispersed oil droplets in the water column due to enhanced dispersion. This resulted in significant increases of dissolved-component concentrations; however, in the presence of slush ice, this dispersion (and concomitant dissolution) quickly became self-limiting with the rapid onset of stable water-in-oil emulsions that were characterized by high in situ oil viscosities.

It is expected that the long-term dispersion behavior of oil under similar sea ice conditions in the field would be dependent on the nature and composition of the oil. For example, if a refined oil product was released into seawater in the presence of slush ice and minor levels of turbulence, then dispersion of the refined product might continue for longer periods of time than would be expected for a crude oil. Refined products (as opposed to crude oils) generally do not contain surface active compounds that are important for stabilizing water-in-oil emulsions. Thus, small scale turbulence generated by the grinding of ice crystals could actually enhance the dispersion of refined oil products. In turn, this could lead to elevated water column levels of dispersed oil droplets and also dissolved compounds (e.g., more water-soluble aromatic compounds) due to high surface to volume ratios inherent to small oil droplets.

The importance of modeling a well-stirred versus a diffusion controlled oil slab (pool) has been considered from a theoretical standpoint throughout the development of the existing NOAA oil weathering models. Wave tank experiments completed during this program have now demonstrated that the diffusion controlled mechanism must be incorporated into future predictions of

rates of evaporation from emulsified slicks and from thicker pools of oil stranded on floating ice surfaces. Diffusion controlled evaporation of lower molecular weight components from oil pools was verified for the first time during the oil on ice weathering experiments. Significant differences in the retention of lower molecular weight components occured as a function of depth in the oil pool. In wave tank experiments involving interactions between oil and slush ice, water-in-oil emulsification occurred before significant evaporative losses of lower molecular weight components could occur. This situation is different from that encountered during open ocean oil weathering scenarios where evaporative losses of lower molecular weight components from surface oil are not only relatively rapid but also important to the subsequent behavior of the oil. Thus, once a stable emulsion has formed in the presence of first-year ice and agitation, delayed evaporative losses of lower molecular weight components would be expected because evaporation from these emulsions is a diffusion controlled process. Under such conditions, modeling the evaporation and dissolution behavior of components from the water-in-oil emulsion would require a combination of well-stirred and diffusion controlled algorithms.

Evaporation of lower molecular components from oil confined within brine channels in sea ice was also observed during wave tank experiments. Migration of oil in brine channels is severely retarded due to high viscosities of oils that are maintained at low (<0°C) temperatures. Furthermore, temperature gradients can exist within thick ice systems between the upper ice surface that is at or near the ambient temperature of the overlying air and the lower ice surface that is usually at thermal equilibrium with the underlying seawater. Therefore, migration rates for oil in brine channels may also vary as a function of depth in the ice field. Nevertheless, dissolved gases can still be released from the oil, which results in a selective partitioning of lower molecular weight components while the oil is still trapped in the brine channels. However, this phenomenon is probably not important for modeling oil weathering in the presence of sea ice because selective component evaporation would only affect the upper-most portions of oil in the brine channels. The actual release of the majority of the volatile gases from the trapped oil would be retarded until the bulk oil reached the surface of the ice or water.

In addition to these studies of direct interactions between oil and sea ice, a mechanism for transporting dissolved hydrocarbons to bottom waters in the presence of sea ice was investigated in this program. During the initial stages of sea ice formation (i.e., frazil, grease and/or columnar ice growth), brine is extruded from the ice to the adjacent seawater, which results in a localized increase in the salinity (and, thus, density) of this water. In the absence of turbulent mixing and dilution, the higher density water can sink as a relatively discrete mass in a process known as brine cabling. Hydrocarbons from a surface oil spill that dissolve in the water mass (e.g., water-soluble, lower molecular weight aromatic compounds) can be transported along with the salt toward the bottom by such processes with minimal dilution. Preliminary field studies performed during February/March 1984 in the Chukchi Sea, and experimental wave tank studies, suggested a transport mechanism for dissolved oil compounds. An experimental spill with a combined aromatic compound cocktail was performed in an open but refreezing lead system near Pt. Franklin in the Chukchi Sea in February/March 1985. Subsequent analyses of water samples collected from beneath the surface ice yielded measurable concentrations of both benzene and toluene at selected sampling sites and depths. Furthermore, the actual distributions of these concentrations could be explained by a brine cabling scenario that was compatible with accompanying near bottom current and hydrographic measurements (i.e., salinity, temperature and density). Therefore, results of this field effort demonstrated the transport of dissolved hydrocarbon compounds to bottom waters by brine cabling. This process has important implications for potential spills from drilling activities during periods of ice-growth or from accidental oil or refined product releases from tankers or barges in open lead systems.

3.1   FORMATION CHARACTERISTICS OF ICE IN SEAWATER

Formation of ice in seawater requires in situ temperatures below the freezing point of the water. However, the physical conditions of the water at the time of the freezing will determine the nature of the ice formed. Depending on these conditions, one or more of the following initial ice types can result: 1) frazil ice, 2) slush ice and 3) columnar ice (Martin, 1979). Although each type of ice has unique characteristics, all three are characterized by having high surface salinities due to the exclusion of sea salts during the freezing process.

In general, the first type of sea ice formed is frazil ice. It is generated directly from supercooled seawater that is subjected to turbulence (e.g., from wind and/or wave action) at a sufficient level that direct, smooth surface ice freezing at the air-sea interface does not occur. Studies of the morphology of frazil crystals formed in saline solutions indicate that their shapes can include either two-dimensional circular discs (Martin, 1981a) or three-dimensional configurations with thin fingers and plates protruding in directions other than the main crystal axis (Hanley and Tsang, 1984). Individual saline frazil crystals are approximately 1×10^{-3} meters in diameter and $1\text{-}10 \times 10^{-6}$ meters in thickness (Martin and Kauffman, 1981). They are also surrounded by brine films that are generated in the freezing process. Due to this salt rejection, the brine immediately surrounding the crystal has a higher salinity than that of the surrounding water. This results in a lower freezing point for the water around the crystal, and imparts an inherent resistance to continued growth of the crystal (Hanley and Tsang, 1984). Under appropriate conditions, frazil crystals may be generated throughout a water column. Once formed, they will rise to the surface since their densities are less than that of the ambient seawater.

Martin (1981a) summarizes four situations that can produce the formation of frazil ice crystals in seawater. First, cold winds blowing across regions of open water (e.g., polynyas adjacent to shorelines or leads further

178

out to sea) can result in frazil formation. If the open water has sufficient fetch, Langmuir circulation patterns can "herd" frazil ice into streaks parallel to the direction of the wind and/or cause the frazil to accumulate against some downwind, solid object (e.g., the edge of a lead or a shoreline). Second, seawater adjacent to the face of an ice shelf or iceberg can generate frazil crystals by either direct cooling of the water or upward movement of a cold, deep seawater mass (parcel) to a depth where pressure effects (i.e., freezing point depression) result in the water being cooled below its freezing point. Third, frazil crystals may form between water masses of different salinities (e.g., when a layer of fresh melt water at its freezing point lies over a layer of seawater at its freezing point). And, fourth, slow drainage of cold dense brine from sea ice can lead to the formation of frazil ice layers beneath the ice.

Regardless of the mechanism responsible for the initiation of frazil formation, frazil crystals frequently accumulate in masses at the air-water interface or under-ice surface. This can be due to either the inherent buoyancy of the crystals themselves (i.e., they rise to surfaces) or wind and current advection phenomena. Such accumulations of frazil crystals are known as grease (or slush) ice. Armstrong et al. (1966) define grease ice as "a later stage of freezing than frazil ice, where the spicules and plates of ice have coagulated to form a thick soupy layer on the surface of the water". Under the influence of wave or wind agitation, the original structure of the source frazil crystals may be degraded in a grease ice field by turbulent grinding action. Martin (1981b) notes that grease ice consists of approximately 3 parts ice to 7 parts seawater (by mass). In particular, grease ice accumulations are known to occur against the downwind edges of leads that are perpendicular to the direction of the wind (see Figure 3-1; Bauer and Martin, 1983) and in convergence zones of Langmuir circulation patterns that are parallel to the direction of the wind (Pollard, 1977). Areas of frazil and grease ice formation as described in the preceding several paragraphs are common in marginal seas such as the Bering and Chukchi Seas (Martin and Kauffman, 1981) and the Weddell Sea (Gill, 1973). Grease ice formation was observed in open leads off Point Barrow, Alaska during the field efforts in this NOAA program.
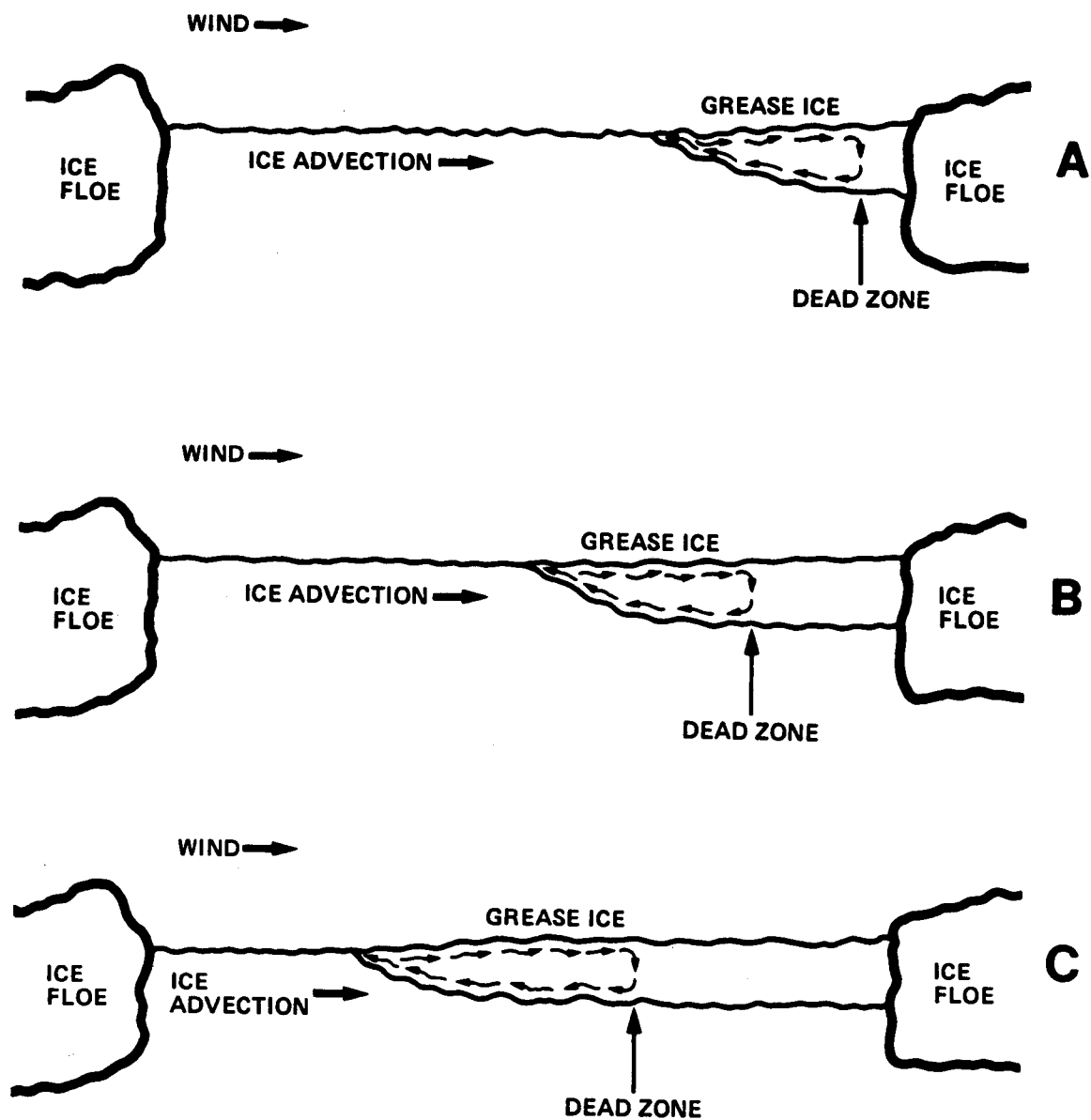
Figure 3-1.—Schematic Overview Depicting the Growth and Downwind Accumulation of Grease Ice in an Open Lead. The dead zone denotes area where ice thickness dampens wave turbulence and internal circulation within ice. (Adapted from Bauer and Martin, 1983.)

The second type of ice that can be formed in seawater is slush ice. Martin (1979) states that it is generated in surface waters when blowing snow accompanies wind. If the ambient air and water temperatures are sufficiently low, the snow will persist in the water to form a mixture of snow crystals and seawater. From a practical standpoint, however, it is difficult to distinguish snow/seawater slush from accumulations of frazil crystals (i.e., grease ice) in surface waters. Therefore, for the purposes of this report the terms slush ice and grease ice will be used interchangeably for a common ice type.

Columnar ice consists of long, individual crystals or platelets that have a vertical orientation. Figure 3-2 shows a portion of an ice fragment containing columnar ice that was collected from ice fields in the Chukchi Sea during this program. The common vertical planar orientation of the ice crystals is illustrated in the figure. Columnar ice growth may continue up to depths of approximately 1-2 meters during the ice growing season (Martin, 1979; Martin, 1984, personal communication). In typical ice cores the lower 10-40 mm of columnar ice is called the skeletal layer. This layer charactristically is highly porous and fragile, which will facilitate the adsorption or incorporation of any oil that might be released or driven beneath the ice layer (Martin, 1979).

A physical requirement for the formation of columnar ice is the existence of calm or quiescent conditions in the water column. Thus, agitation of the water due to wave or wind action must be sufficiently small to allow for the orderly, non-random vertical growth of columnar ice crystals. Such conditions may result from either an absence of both wave and wind action or an induced "damping" of these turbulent forces by an overlying layer of a more viscous material such as grease or slush ice (or oil as described later in this study).

3.2   CHARACTERISTICS OF FIRST-YEAR ICE

By definition, first-year ice has existed only for the current growth season. It may comprise any or all of the ice types described in Section 3.1 (i.e., congealed frazil ice and/or grease ice, slush ice, or columnar ice).

Figure 3-2.--Columnar Ice in the Chukchi Sea.

First-year ice usually grows to a thickness of approximately 1-2 meters, with a predominantly columnar ice crystal structure beneath a near-surface layer of congealed frazil or grease ice (Martin, 1979).

The salinity of sea ice varies with the age and degree of exposure to changing thermal regimes (Weeks and Weller, 1984). As mentioned previously, one feature common to the formation of all first-year ice forms is the occurrence of high salt concentrations on the surface due to rejection of sea salts during the freezing process. The resulting frozen surface brine can crystallize into small (20-50 mm) salt "flowers" with salinities ranging from 45-95 ppt (Martin, 1979). Salt "flowers" have been observed in field samples of ice from the Beaufort Sea (Martin, 1979) and the Chukchi Sea (this study, see Section 4.3), and they were also generated in the artificial "first-year" ice growth wave tank experiments summarized in this report (Sections 4.2.1 and 4.4.1). The high surface ice salinities due to brine rejection determine not only subsequent surface properties of the ice but also contribute to the formation and propagation of brine channels through the ice. As noted in Martin (1979), brine channels form between crystal facies of the ice with channel diameters up to 10 mm. Smaller feeder channels run diagonally between platelet boundaries. Development of brine channels in first-year ice can occur throughout the growth season, although the size and spatial frequency of the channels increases as the ice warms. The most extensive development of brine channels occurs in the spring when air and ice temperatures increase toward the freezing point. The presence of brine channels represents an important mechanism for the vertical migration of oil spilled underneath first-year ice, and was investigated during the wave tank studies described in Section 4.2.2.

Melting of first-year ice may occur in the following sequence: 1) ice warm-up and brine drainage; 2) formation of surface melt ponds with increasing levels of solar radiation; and 3) decomposition into slush and broken ice (Martin, 1979). As the surface layers of the ice are heated, the highly saline surface ice melts and forms liquid brine pools. Brine drainage channels are then formed in the surface ice layers with interior temperatures greater than

-4°C.   These brine channels eventually extend throughout the depth of the ice floe, and represent a major mechanism for the vertical (downward) flux of salt and the upward flux of entrapped oil if present (see Section 4.2.2).

In the months of June and July in the Arctic, sufficient solar radiation is available to melt the surface saline layer of first-year ice. As the pond water absorbs more heat, this ice melt tends to form large ponds that gradually expand both horizontally and vertically in the ice. This tendency toward radial expansion may also be enhanced if oil lenses are present in the ice.   Once an oil lens is liberated from the ice, the oil floats to the surface of the melt pond. Thermal convection from the heating of this dark surface oil promotes even more rapid melting of the surrounding ice, with an accompanying expansion of the original pond size (Martin, 1979; NORCOR, 1975). Melting of ice that has been advected to the marginal ice zone is also promoted by interaction with warmer water, and melting of ice along the northern coastal zone in the Beaufort Sea can be promoted by river overflow in the late spring and early summer.

3.3   CHARACTERISTICS OF MULTI-YEAR ICE

Multi-year ice describes ice that has survived for more than one growth season.   Since this ice may have been subjected to several partial thaw and refreeze cycles, the brine rejection process will have had multiple opportunities to be expressed (Weeks and Weller, 1984). Therefore, multi-year ice may be characterized by lower salinities, as well as lower abundances of internal brine channels than in first-year ice.

Multi-year ice occurs primarily in offshore regions that are not stabilized by attachment to shorelines (see Section 3.4). Ice in offshore regions normally is in constant motion, resulting in repeated breaking and reworking of the ice and the formation of surface and bottom ridge systems and rubble fields surrounded by refrozen first-year ice leads.   Therefore, multi-year ice is usually characterized by much greater bottom relief than first-year ice (Kovacs, 1977; Ackley et al., 1974). Due to this greater bottom relief, multi-year ice is more likely than first-year ice to "feel" water

184

currents moving beneath the ice. This will lead to a greater tendency for multi-year ice to be set in motion by currents, with an accompanying increased tendency for fracturing and breakup resulting in the formation of offshore open leads. First-year ice then forms when newly opened water leads in the multi-year ice field refreeze. Therefore, multi-year ice fields normally consist of a combination of multi-year and first-year ice. Since offshore open water leads can occur in multi-year ice fields (as described here), the phenomenon of brine cabling (see Section 3.5.2) is relevant to multi-year ice fields as well as first-year ice fields. The higher bottom relief of multi-year ice can also influence the character of the water currents beneath the ice by causing increased eddy turbulence due to bottom ice roughness. This can enhance the general mixing properties of the water, which will become important in explaining hydrocarbon distributions observed in the field brine cabling study in Section 5.3. Independent of the brine cabling phenomenon, the higher relief on the underside of multi-year ice can also be important for direct entrapment of oil released or driven beneath ice surfaces (see Section 3.5.1.3).

3.4   NATURAL ICE FORMATIONS IN ALASKAN ARCTIC MARINE REGIONS AND THEIR RELATION TO BOTTOM MORPHOLOGY

Relative to the shoreline on the northern coast of Alaska, three zones of ice cover occur: (1) the fast ice zone; (2) the pack ice zone; and (3) the area of intersection between the two zones (Reimnitz et al., 1978). A schematic representation of these zones is presented in Figure 3-3. Figure 3-4 illustrates the formation sequence for ice types that can occur in these different zones.

For the most part, the fast ice zone includes floating and bottom-fast ice that has formed near the shore each year, although it may also include occasional multi-year ice floes and/or remnants of grounded ridges. Fast ice is subject to movement and deformation by winds during the first few months of its formation. Eventually, however, it becomes immobilized and is usually protected by the shore on one side and grounded fast ice ridges on the other. The fast ice zone normally tends to be relatively flat and undeformed since the initial movement and deformation phases occur for only a relatively short time during its formation.

185
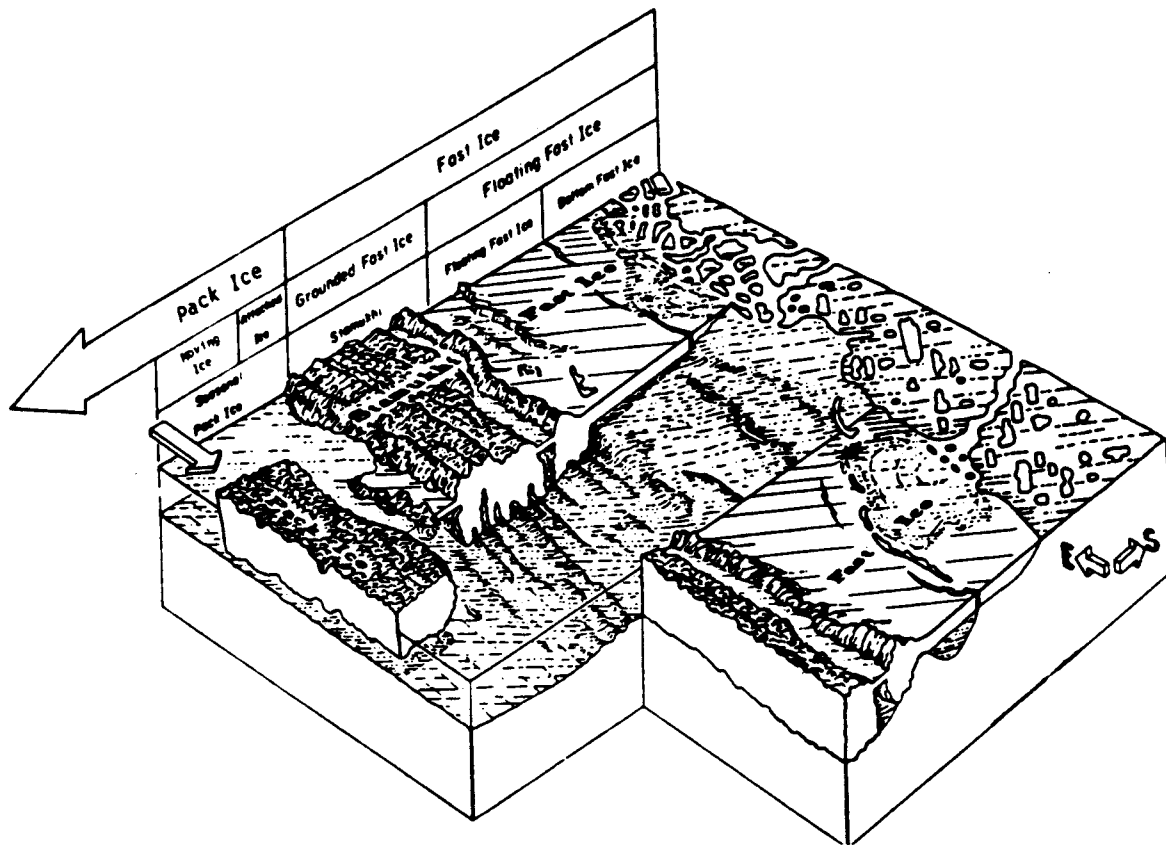
Figure 3-3.--Seasonal Development of Ice Zonation in Relation to Bottom Morphology. (Adapted by Tau Rho Alpha, from Reimnitz et al., 1977.)
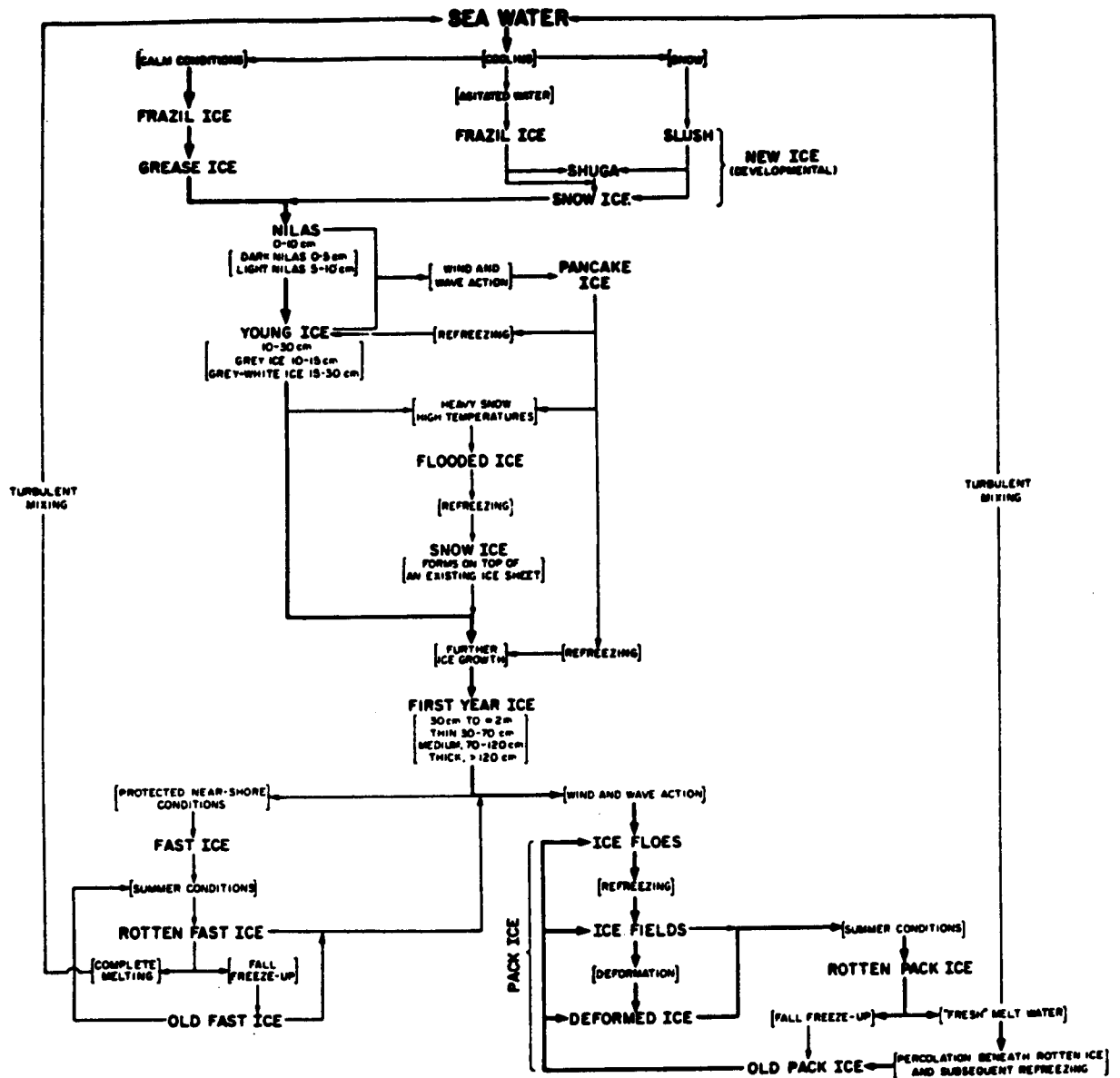
Figure 3-4.--Sea-ice Terminology in Genetic Sequence (Weeks, 1978).

The zone of seasonal pack ice is further offshore from the fast ice, and can contain a substantial portion of multi-year ice. Since the seasonal pack ice is not directly attached to the shore, winds and water currents tend to keep it in almost constant motion. Cracks frequently open in pack ice to form leads that quickly freeze over with thin layers of first-year ice. The latter phenomenon is one reason that pack ice normally comprises some mixture of first-year and multi-year ice (see Section 3.3). It is also possible to have additional growth of columnar ice (i.e., first-year ice) below multi-year ice structures (depending on their thickness). In any event, some of the leads that open in pack ice will be closed by movements of the ice, which breaks and piles up both old and new ice to form ridges and rubble fields. The result is an ice field characterized by a relatively high degree of structural relief.

The area where the moving pack ice meets the stationary shore-fast ice is a highly active shear zone. A great amount of ice deformation takes place in this area, which is characterized by heavy ice ridging and highly irregular ice features. Water depths are often in the range of 10-30 meters. Since many of the ice ridge keels can be deeper than this, this active shear zone is often characterized by bands of grounded ice ridges. These grounded sea-ice formations formed as a result of "ice heaping" are known as "stamukhi" (Zubov, 1945). Reimnitz et al., (1978) refer to this area of ice ridges and hummocks seaward of the fast-ice zone as the "stamukhi zone" (see Figure 3-3).

A fourth zone of very dynamic ice activity that also has great importance for considerations of oil-ice interactions is the marginal ice zone (MIZ). The MIZ includes the boundary region between ice and open water, and the affected regions on each side of the boundary. The location of the MIZ can vary seasonally and spatially relative to shorelines. However, a common characteristic of all MIZ areas is the complex and rapidly changing interplay between the atmosphere, the ice and the ocean on a variety of temporal and spatial scales. Processes that affect conditions in the MIZ include ocean fronts and eddies, changes in the roughness of both the ice and associated open water surfaces, and wind and atmospheric circulation patterns driven by local surface temperature gradients. Further, ocean convection or circulation

patterns are influenced by sea ice formation (brine generation) and ice break-up and melting (fresh-water generation at the surface) as controlled by varying temperature conditions and the effects of waves and ocean swells.

3.5   INTERACTIONS OF OIL AND ICE

The behavior and fate of oil spilled in regions of ice covered sea-water will depend upon factors including not only the type of oil or distillate product released but also where it is released (i.e., under the ice or in open leads) and the state of the ice growth at the time of the spill. In general, interactions between oil and sea ice can be divided into two types of processes: 1) those that "capture" oil and 2) those that "transport" oil. "Capture" processes will include 1) entrainment of oil by grease or slush ice and by rafted or ridged first-year and multi-year ice, 2) interactions of oil with smooth, unbroken first-year ice and 3) interactions between ocean waves, oil and ice floes at the edge of the ice. "Transport" processes will include 1) interactions of oil with Langmuir circulation patterns in near-shore polynyas (consistent open water regions along the lee-sides of shorelines such as the area south of St. Lawrence Island and parts of the Chukchi Sea) or more transient offshore leads where grease ice occurs, 2) general advection of oil by large-scale ice movements and 3) specific advection of oil associated with ice bands that form at the ice edge. More detailed background information regarding these "capture" and "transport" processes will be presented in Sections 3.5.1 and 3.5.2, respectively.

3.5.1   "Capture" or Incorporation Processes Contributing to Oil-Sea Ice Interactions

Mechanisms for the incorporation of oil into a sea ice cover will vary with both the morphology of the ice and the season. Oil may be incorporated into new ice forming in leads, it may seep upwards to the ice surface through cracks or unconsolidated ridges in the ice cover, or it may be frozen into existing ice by new ice growth.

3.5.1.1 Oil Release in a Grease Ice Field

Martin and Kauffman (1981) described the general movement patterns of ice in the initial formation stages of grease or slush ice fields under the influence of waves that propagate into an ice slurry (see Figure 3-1). Surface waves can "herd" the grease ice against a solid object (e.g., the edge of a lead) where the radiation stress from the wave action will create a thickness increase in the ice wedge with distance into the ice layer. Grease ice is an excellent wave absorber because it has a nonlinear viscosity that increases as the ice concentration increases and the shear rate decreases. As a result, the wedge of grease ice will divide into separate regions approximating liquid and solid behavior, and these regions will be separated by an abrupt transition zone termed the "dead zone". Ahead of the dead zone, the waves propagate as heavily damped water waves; behind the dead zone, they propagate as elastic waves. If oil is spilled in the wave field just in front of a grease ice wedge, most of the oil will end up on the surface of the ice beyond the dead zone, with some oil droplets circulating in the grease ice field ahead of the dead zone. The exact distribution of oil intrapped in the grease ice and on the ice surface will be largely controlled by the oil's inhearent density (and degree of weathering or water-in-oil emulsification). Oils with densities higher than the grease ice (0.917 g/ml) may be subject to greater encapsulation (Payne et al., 1984b and Wilson and Mackay 1986). Similar oil distributions would be expected in grease ice accumulations that arise due to Langmuir circulation patterns. Therefore, if oil were spilled in a polynya or open lead where grease ice was forming, then some of the oil would be expected to accumulate in local dead zones and/or Langmuir convergence zones, and a smaller fraction would be dispersed into oil droplets by breaking waves and would circulate around both grease ice and Langmuir rotors.

Once grease ice begins to solidify, ice "pancakes" are observed to form in the grease ice field. Martin (1981b) demonstrated that crude oil released beneath grease ice pancakes in a wave field appeared in cracks around the pancakes. The oscillating motion of the pancakes then drove the oil laterally through the cracks and pumped some of it onto the ice floes. However, the grease ice did retard the rise of the oil to the ice surface and its lateral

spreading within the cracks. Therefore, in the case of oil spilled beneath a wind-agitated field of pancake ice, one would expect that a certain fraction of the oil would be "pumped" onto the surface of the ice, while the remainder would be bound up in or below the grease ice/pancake ice system.

3.5.1.2 Oil Released on Top of a Solid Ice Field

If oil were released onto the surface of solidified ice (first-year or multi-year) by either direct spills or working its way up through forming ice, the spreading properties of the oil would become important to its eventual fate and composition. Snow cover or ice ridges would confine the oil and thus limit the extent of its spreading. In contrast, strong winds and/or horizontal seepage would tend to increase areal spreading (NORCOR, 1975). The weathering of oil on the ice surface during winter would be relatively slow due to cold temperatures, reduced solar radiation, and diffusion-controlled restriction of component evaporation resulting from limited surface area, greater oil layer thickness and the lack of turbulent mixing. However, during the spring thaw, melt pools would form rapidly on oil-covered ice surfaces due to increased absorption of solar radiation (Martin, 1979). The subsequent thinning of the oil slick would accelerate weathering processes. Martin (1979) concluded that oil spread on the surface of ice would eventually be released into surface waters after the oil either melted through the ice or flowed off its edges.

3.5.1.3 Oil Released Underneath a Solid Ice Field

Consideration of the spreading properties of oil will also be important for estimating the fate and composition of oil released under a solid ice field. Factors affecting this spreading will include the density and viscosity of the oil, the degree of under-ice roughness, the in situ water current velocities and the "porosity" of the ice (e.g., brine channels and skeletal layers of columnar ice). All effect the capacity of the ice to contain subsurface releases of oil.

Bottom Ice Roughness and Oil Containment Potential

If new ice forms in calm conditions, the underside of the ice is usually relatively flat and smooth. Depending on a balance between surface tension, viscosity and density, oil can then spread beneath this ice to some equilibrium thickness. Values for equilibrium slick thicknesses have been reported to range from approximately 5-12 mm for refined oils with densities in the range of crude oils (Cox et al., 1980). Minimum stable drop thicknesses for crude oil under ice have been reported to be approximately 5-10 mm (Lewis, 1976). Using these values for slick thicknesses and assuming a completely smooth surface, Thomas (1984) has estimated that approximately 8000 m^3 of oil can spread beneath each km^2 of ice in the absence of currents or ice motion.

However, the underside of sea ice is generally not perfectly smooth. Therefore, each km^2 of sea ice will actually be able to contain more oil than the above estimate. Furthermore, under-ice roughness will vary between fast ice, pack ice and ice in the stamukhi zone.

The nearshore areas of fast ice normally tend to be relatively flat and undeformed. The under-ice roughness in these areas is determined primarily by spatial variations in snow cover that cause differences in sub-surface ice growth rates. Barnes et al. (1979) reported that snow cover on surface ice accumulates in drifts parallel to the prevailing wind direction, and that these drifts are fairly stable throughout the ice season. The drifts in turn insulate the ice from the much colder overlying ambient air, causing reduced ice growth beneath the drifts. Therefore, the underside of the surface ice takes on an undulating appearance. As the ice continues to grow through the winter, these subsurface undulations become more pronounced.

An impulse radar system has been used to map the under-ice relief of fast ice zones at various places in Prudhoe Bay in the early spring (Kovacs, 1977, 1979; Kovacs et al., 1981). From the resulting contour maps, these

192

authors estimated that the volume of under-ice voids lying above the mean ice draft (i.e., the oil containment potential) was 10,000-35,000 m^3km^{-2} for areas of undeformed fast ice. For areas of slightly deformed ice, the void volume estimate was as high as 60,000 m^3km^{-2}.

In the pack ice zone, the degree of under-ice roughness increases since the ice is in constant motion and subject to repeated breaking and reworking processes. This region contains not only first-year ice floes and pressure ridges but also variable amounts of multi-year ice and refrozen leads. Under multi-year ice, there is a very substantial increase in void volume that could contain oil. Kovacs (1977) profiled the underside of a multi-year ice floe and estimated that 293,000 m^3km^{-2} of void space existed above the mean draft of approximately 4.3 meters. Other investigators (Ackley et al., 1974) have also reported greater relief under multi-year ice than under first-year ice.

Under-ice Currents and Oil Spreading

Under-ice currents can contribute to the spread of oil beneath sea ice. Until it is completely encapsulated by new ice growth, oil can be moved beneath ice by differential currents of sufficient magnitude until either solid objects are encountered or the currents cease.

Relationships between differential current speed, bottom roughness, and the movement of oil under ice have been evaluated in Cox et al. (1980). These investigators concluded that the threshold differential current velocity required for moving oil beneath an absolutely smooth ice surface was approximately 3-7 cm/sec. For an ice roughnesses of 1 and 10 mm, the threshold velocities were 12-16 cm/sec and 22-25 cm/sec, respectively. For current speeds above these threshold velocities, oil would be moved at some fraction of the current speed. Oil trapped upstream of large obstructions could also be "flushed out" at current velocities in the range of 15-25 cm/sec. In general terms, Cox et al. (1980) concluded that oil spilled beneath an ice cover would not be transported by currents until the relative current velocities were in the range of 15-25 cm/sec. At velocities less than this critical value, a

193

typical ice field would have substantial oil spill containment capacity. Under-ice currents can range from 2 to 5 cm/sec in parts of the multi-year Beaufort ice pack (Kawalik and Untersteiner, 1978), and Aagaard (1981) reported similar current speeds 10 m below the ice on the Beaufort inner-shelf in 30 to 40 meter depths north of Prudhoe Bay. It should be noted that these measurements were not in the region of the Beaufort Sea extension of the Alaskan Coastal current where Aagaard (1981) has reported average under-ice currents ranging from 25-30 cm/sec. Matthews (1981) used sub-surface and bottom drifters to estimate currents in a wide variety of areas in the central Beaufort shelf. He reported under-ice currents in the range of 7 to 10 cm/sec and near-bottom currents of 0.5 to 2 cm/sec. Near bottom currents (1 meter above the sediment) were measured at 1 to 4 cm/sec under floating shore-fast ice at depths of 20 m in the Beaufort Sea northeast of Pt. Barrow and at 20 to 30 m in the Chukchi Sea near Pt. Franklin as part of this program (see Table 5-7, Section 5.3).

It should be emphasized that the preceeding velocity estimates must be considered as current speeds <u>relative</u> to an under-ice surface. If the ice field is also in motion, then the critical values for current speeds would have to be adjusted to arrive at velocities <u>relative</u> to the under-ice surface.

Effects of Ice Growth, Structural Characteristics and Brine Channels on Oil Retention Under Sea Ice

Oil released into water beneath sea ice will rise through the water column and be trapped on the underside of the ice. If this oil becomes associated with the porous skeletal layer of columnar ice during periods of active ice growth, it will remain essentially static until the ice begins to warm (Martin, 1979). During periods of ice growth, an ice lip will also form as horizontal platelets around subsurface pools of trapped oil (Martin, 1979). Depending on the seasonal conditions, an ice sheet could then continue to grow under the oil and eventually completely trap the oil.

As noted in Section 3.2, first-year ice in particular is characterized by the presence of brine channels that have their origin in the initial

194

freezing process. The importance of these brine channels to the migration of subsurface or encapsulated oil becomes especially important during warming periods. As the ice begins to warm, brine pools maintained as "salt flowers" on the ice surface over winter as well as brine trapped between the columnar ice crystals begins to drain down through the ice. By the time the air and ice temperature approach freezing point values, the brine channels normally extend throughout the ice. Once the channels connect the surface and bottom of the ice, dense brines drain through the ice and escape from the under ice surface. Oil that was initially trapped under or in the ice may then begin to appear on the upper ice surface due to density-mediated migration of the oil up through the open brine channel pathways. Oil that surfaces through these channels will float in surface melt ponds. If such ponds do not exist, they soon form as the oil darkens the surface of the ice and further enhances absorption of solar radiation.

3.5.2   "Transport" Processes Contributing to Oil-Sea Ice Interactions

Once oil becomes associated with ice by any of the processes discussed in Section 3.5.1, it has the potential to be physically transported to areas substantially removed from the initial point of release. Some of these transport processes can be of substantial magnitude, as evidenced by rates of movement for ice of up to 130 km/day along the Chukchi Sea coast following an ice breakout through the Bering Strait (Lewbel, 1984). More detailed information on potential spatial transport of oil by ice can be found in numerous publications such as Martin and Bauer (1981), Martin (1981b), Pease (1981), and Lewbel and Gallaway (1984).

Other less direct mechanisms may also contribute to the spatial transport of dissolved oil components. For example, the previously mentioned expulsion of sea salts from ice during the initial freezing process may play a role in hydrocarbon transport. In addition to the expulsion of brine to ice surfaces, the freezing process also rejects salts to the water below the ice. As discussed in Kozo (1983) and Schumacher et al. (1983), this can produce water parcels that have higher salinities (and thus densities) than the surrounding water. These water masses can sink in the surrounding water column

195

by a process known as brine cabling. If dissolved oil compounds or neutral density oil droplets become incorporated into these denser saline water parcels (i.e., in conjunction with the salts, that are excluded from the ice crystal lattice during the freezing process), then this brine cabling mechanism provides a possible route for the transport of either dissolved or dispersed oil components to benthic environments. This concept of transport of oil compounds by brine cabling was evaluated in both wave tank and field studies for this program, and the results are presented in Sections 5.2 and 5.3, respectively.

3.6   COMPUTER MODELING OF OIL WEATHERING IN THE PRESENCE OF SEA ICE

Previous studies by Payne et al. (1984a) have measured and modeled the physical and chemical properties of oil during weathering in an open-ocean environment. However, oil weathering in the presence of sea ice will be highly dependent on the oil/ice configuration. Modeling oil weathering processes under sea ice will be different in virtually all respects from oil weathering on the open ocean, primarily because oil released under sea ice will not be subjected to a similar weathering environment. Nevertheless, any approach to modeling the oil/ice system must be compatible with existing open-ocean weathering models (i.e., Payne et al., 1984a) because the oil eventually is exposed to the same weathering processes when the oil migrates to the ice/air interface or the ice finally breaks up. In addition, if oil is released in broken ice, or if escaping gas from a subsurface blowout causes a bubble or crack in relatively thin ice (DOME, 1981), then this oil would also be subject to a combination of open-ocean and oil-in-ice weathering processes. In either case the ice can refreeze and prevent further short-term evaporative losses (depending on the season and weather conditions). Eventual break-up of the ice with the spring/summer thaw ultimately will release the oil, possibly at appreciable distances from the initial point of oil release. When this occurs, evaporation, dissolution, dispersion, spreading, water-in-oil emulsification, and other weathering processes considered in the open-ocean model will again become important. The currently used True Boiling Point (TBP) or pseudo-component oil-characterization for open-ocean weathering processes has been

196

incorporated into SAIC's model for oil-ice interactions, and this approach is, by design, entirely compatible with the open-ocean oil-weathering model (Section 6.4).

In modeling oil under ice with the oil still in contact with water, the mass transfer processes considered are dispersion and dissolution. Dispersion will not be an important weathering mechanism when under-ice turbulence levels are low and under-ice currents are sufficiently small such that the oil will remain stationary against the ice (DOME, 1981). Thus, in most oil releases below land-fast first-year ice, the only mass transfer process expected to be of importance is dissolution. Dispersion may become important, however, in the shear zone, in moving pack ice, or in areas with stronger tidal currents. Furthermore, dispersion will certainly become an important process when the ice breaks up and wave-induced turbulence in the broken ice field pumps oil onto the ice surface and into the water column.

4.
COLD ROOM/WAVE TANK STUDIES

Laboratory studies were completed during this program to measure rates of oil weathering in the presence of simulated first-year and multi-year sea ice. Experiments were conducted using natural seawater in a flow-through wave tank system constructed in a specially designed cold room at the NOAA-Kasitsna Bay Laboratory (Figures 4-1A and 4-1B). Artificially generated sea ice was produced to simulate actual arctic or sub-arctic ice conditions (as described in Martin, 1981).

During the first-year sea ice experiments, fresh Prudhoe Bay crude oil was added below the grease- and columnar-ice layer to simulate a subsurface release. Results from these studies are described in detail in the Final Report for RU640 (Payne et al., 1984b). The multi-year ice experiments involved repeated simulated freeze/thaw cycles, ridge construction and several oil/ice scenarios. The physical and chemical weathering behavior of the oil was evaluated through time series measurements of the oil during freezing and thawing conditions.

4.1   DESCRIPTION OF THE COLD ROOM AND WAVE TANK SYSTEM

A flow-through seawater wave tank constructed in the cold room of the Kasitsna bay Laboratory is illustrated schematically in Figures 4-2A and 4-2B. Seawater for the wave tank was pumped through PVC pipe from a depth of 3 meters below lower low tide in Kasitsna Bay. The PVC pipes were flushed for a minimum of two weeks prior to the initiation of the tank tests to reduce potentials for background (phthalate) contamination. Seawater blanks were also collected and analyzed prior to each of the tank experiments. Several under ice differential current regimes were generated by varying the seawater flow rate into and out of the tank. During the first-year ice experiments, seawater was introduced into the tank at a flow rate of 1 liter/minute (equivalent to a current speed of 0.003 cm/sec), while the flow rate was ~3 liters/minute (0.01 cm/sec) during the multi-year ice experiments. These seawater flow rates result in one tank volume turnover (~1870 1) every 1.25 days in the oil in fist-year ice and every
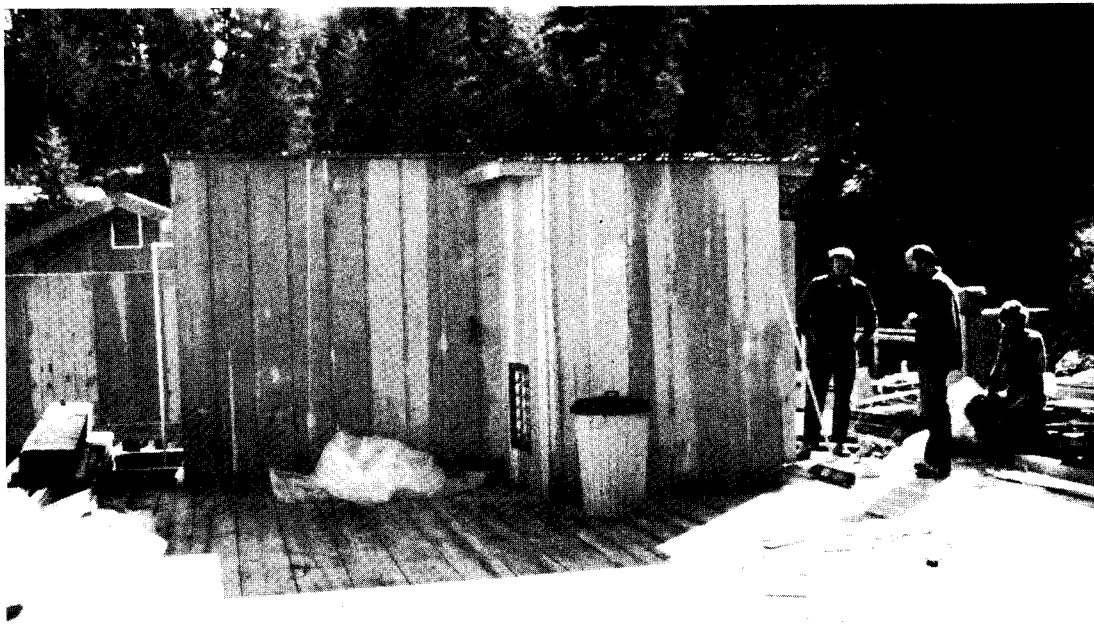
Figure 4-1A.--Outside View of the Compressor Room and Cold Room Used for Oil/Ice Studies at Kasitsna Bay.
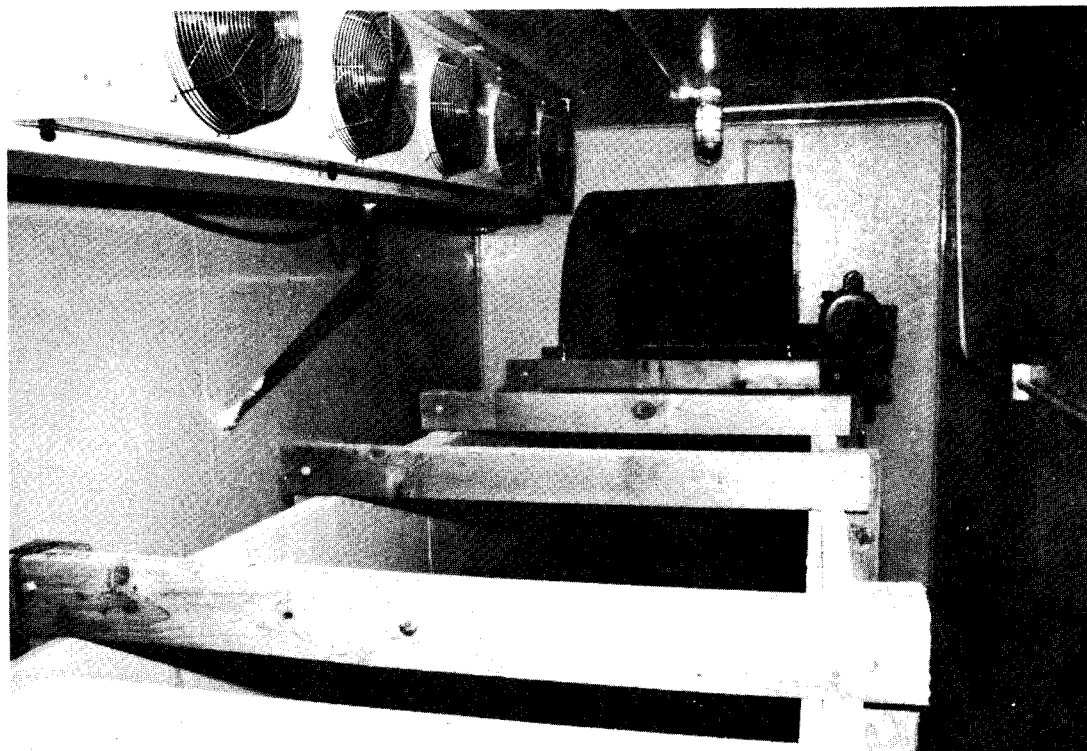
Figure 4-1B.--Wave Tank System and Five Blower Evaporator Unit Inside the Cold Room at Kasitsna Bay. The paddle wheel system at the far end of the tank was later replaced by the hinged system described in the text and shown schematically in Figure 4-2A.

Quartz Heaters (Height Adjustable)

1 HP Motor

Incoming Seawater

Paddle

Overflow

Sampling
Ports

Ice Surface

36"

25¼"

Side View
(Support braces
not shown)

6"

Thermister
Array

View Ports

11'6"

Adjustable
Pitch Cam

32½"

Top View

Thermister Array

Support
Braces

1 HP Motor
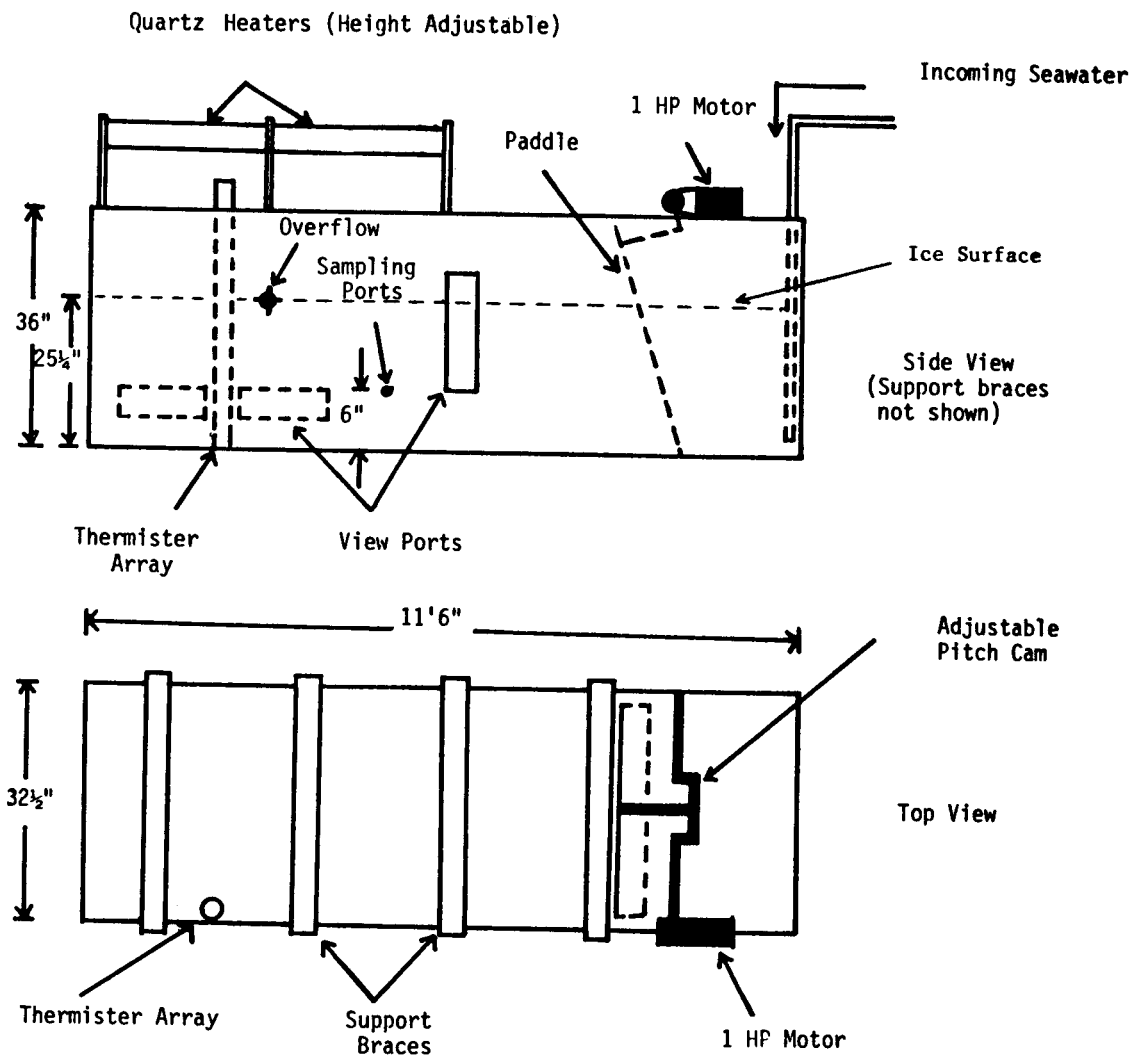
Figure 4-2A.--Ice/Wave Tank Dimensions (not to scale).
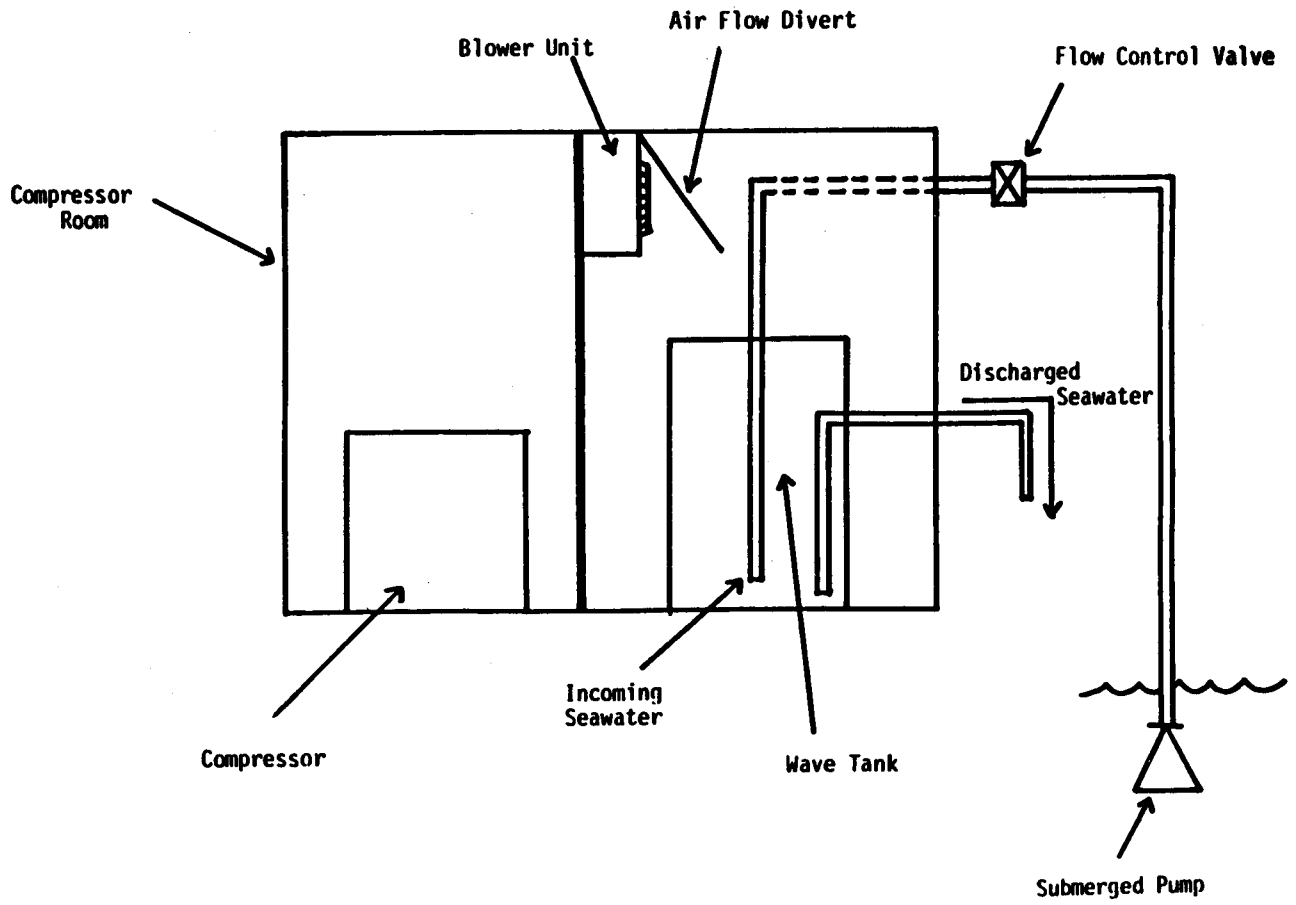
Figure 4-2B.—General Layout of the Flow-Through Cold Room System.

10 hours in the oil in multi-year ice experiments, respectively. In both instances, the differential under-ice currents were intended to simulate advective removal of dissolved components and dispersed oil droplets. Higher flow velocities would of course have been desirable to simulate a wider variety of differential currents as would be expected under landfast and pack ice. However, flow rates were restricted by the cooling capacity of the evaporator unit and 5 horse-power compressor used to refrigerate the cold room and lower the ambient water temperature from +4°C (as encountered outside at Kasitsna Bay during the winter months) to approximately -1.7°C for ice growth inside the wave tank. If higher water flow velocities had been used, then the desired ice regimes could not have been generated.

4.2   SIMULATED FIRST-YEAR ICE TANK STUDIES

4.2.1   Generation of First-Year Ice

A profile of the desired ice/oil configuration for a simulated sub-surface oil discharge under first year ice, shown schematically in Figure 4-3, consists of an upper 5 cm layer of frazil/frozen grease ice above a 4 cm layer of columnar ice. Oil would be added beneath the columnar ice, and then additional ice formation would be initiated to entrap the oil within the ice block.

The ice thicknesses were constrained both by the refrigeration capabilities and flow-through seawater systems. The maximum ice growth of the tank system can be calculated using the differential form of the equation of Anderson (1961):

$$(2D + 0.051) \, WD = 2.8 \times 10^{-5} \, (T_w - T_a)Wt \tag{1}$$

where   D is the initial ice thickness in meters,
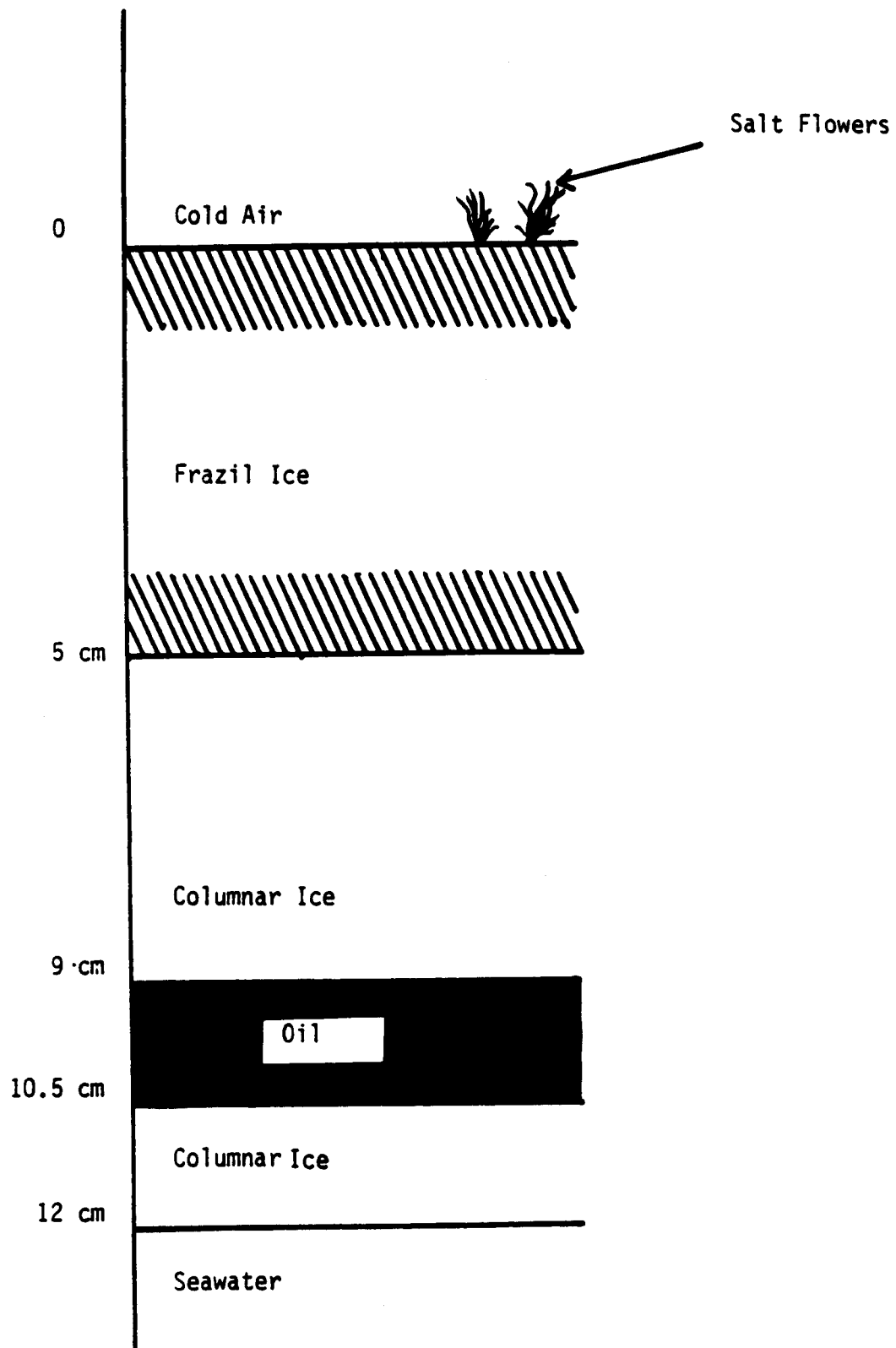
Figure 4-3.--Diagram of Desired Ice-Oil Configuration.

WD is the ice growth in time interval Wt,

T_w is the water temperature assumed at freezing point -1.7°C),

T_a is the air temperature (-30°C),

and Wt is the time interval in hours.

For an initial ice thickness of 10cm, ice growth over a one hour period is WD - 3.2 mm, which equals the growth of ice necessary to cool seawater at the flow rate of 2.4 liters/minutes. Minimum water flow rates in the tank are 1 liter/ minute, thus oil could only be spilled in depths less than 10 cm (Martin, 1984; personal communication during site visit at Kasitsna Bay).

During initial ice formation, the incoming seawater was supercooled to -1.8°C in the presence of wave turbulence. Wave turbulence then was reduced allowing the formation of frazil ice crystals on the water surface. Frazil ice growth occurred within 1 to 2 minutes after the wave generator was turned off, with a 3-5 knot wind and a room temperature of -30°C. Wave turbulence was re-initiated to drive the frazil ice crystals into the water column and encourage the formation of grease ice and slush ice. Frazil ice crystals were observed throughout the water column, and grease ice accumulated to a depth of approximately 4 cm before the paddle system was turned off three hours later. Vertical temperature profiles during all ice experiments were monitored with a thermister array. Figure 4-4 shows the time-series temperature profiles of air, ice, and seawater in the wave tank during growth of grease ice. A chronology of the ice formation and oil spill events is presented in Table 4-1.

Within three hours of the initial frazil ice formation, a 5 cm layer of grease ice covered 80% of the tank surface. A 4 cm layer of columnar ice was then grown over the next 20-21 hours below the grease ice layer prior to initiating the subsurface oil spill (see Table 4-1). Additional columnar ice growth was allowed to occur below the spilled oil to simulate oil-in-ice encapsulation as illustrated in Figure 4-3. Figures 4-5 and 4-6 show an ice core with the frozen grease ice on the surface and the columnar ice immediately beneath it. This core was obtained during initial ice growth stages and, as
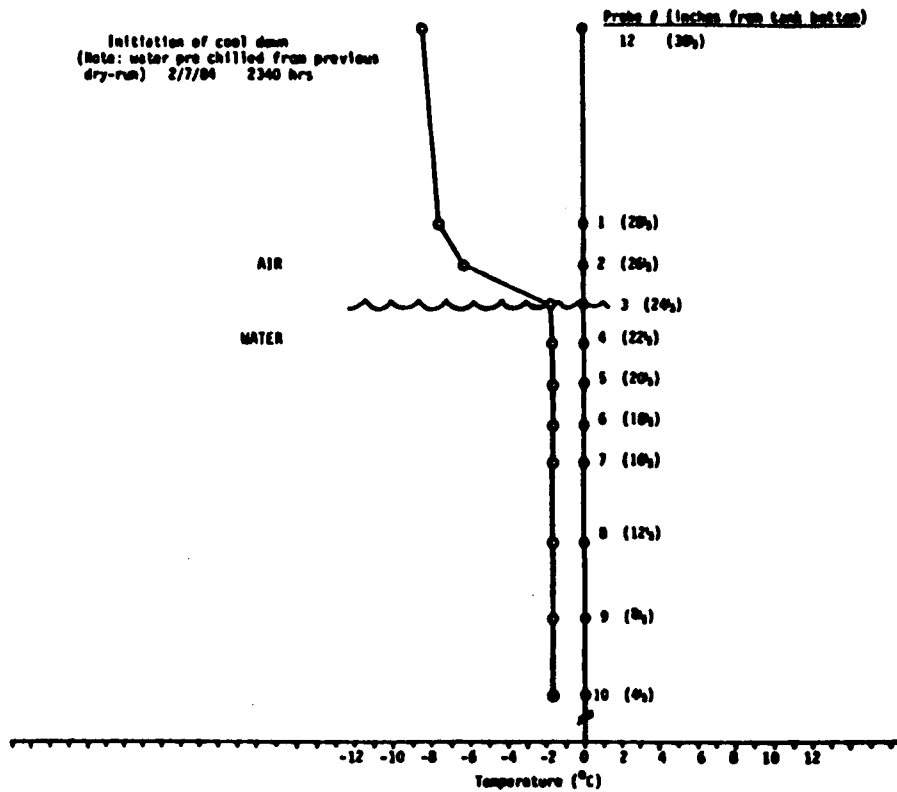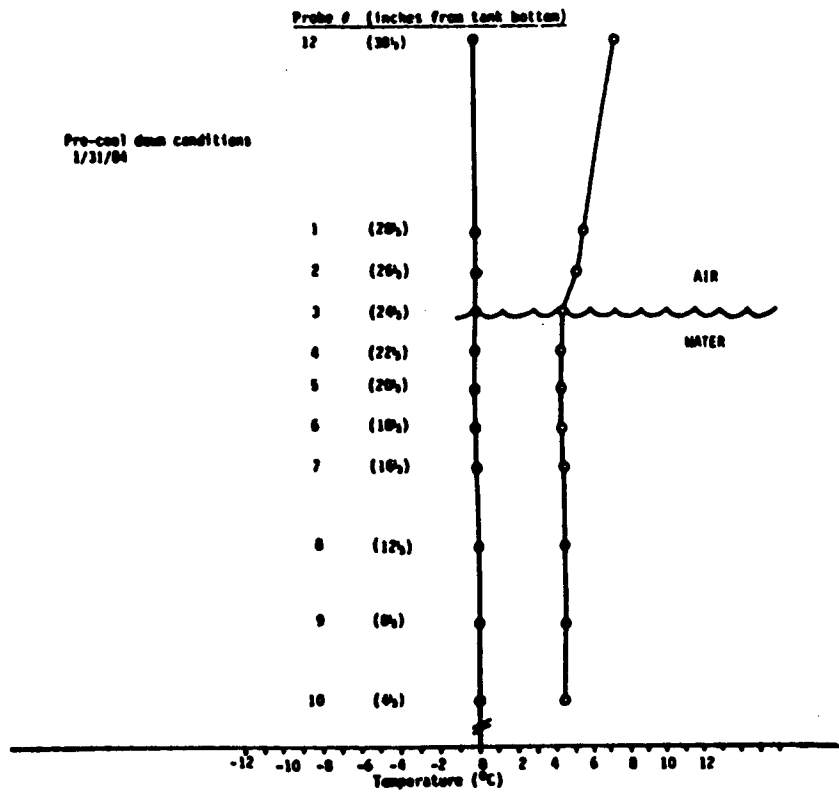
Figure 4-4.—Temperature/Depth Profiles Obtained During Oil/Ice Interaction
Experiment. (See also Table 4-1 for a time-series chronology of events in the
cold-room experiments.)

205

Figure 4-4.--(Continued)

Figure 4-4.--(Continued)

Figure 4-4.--(Continued)

208
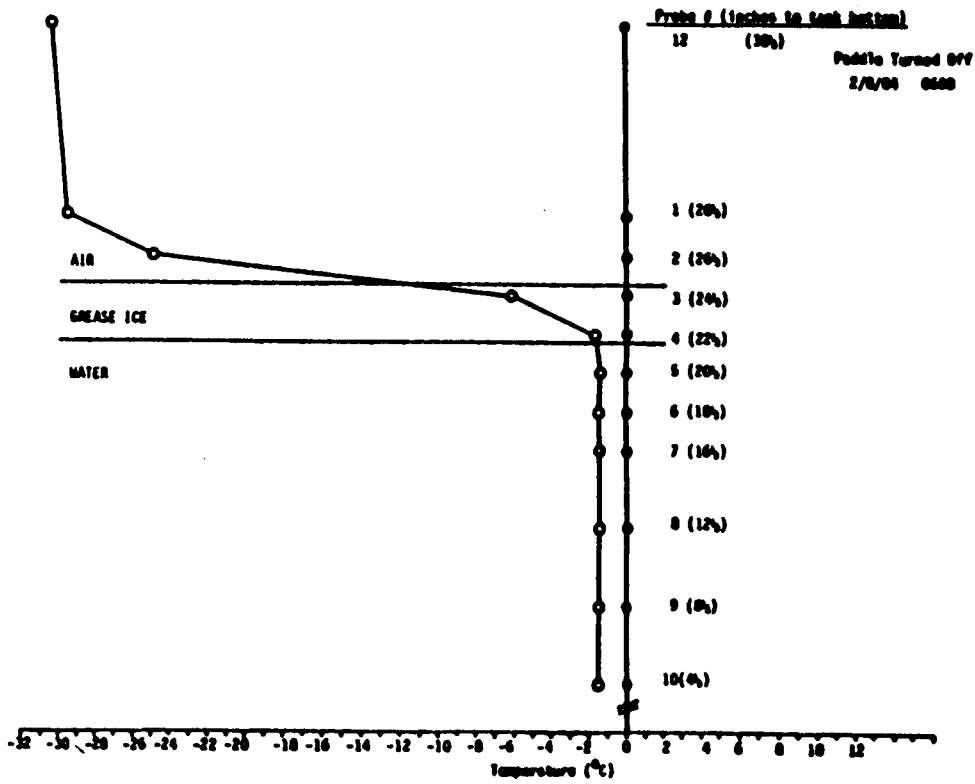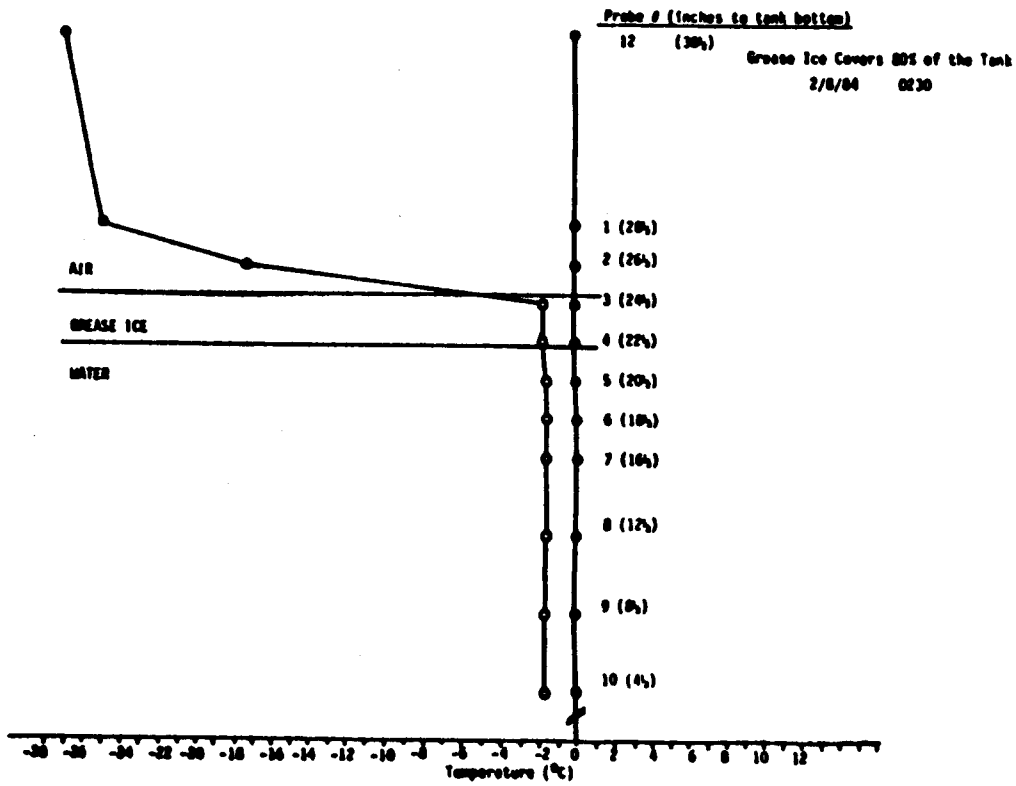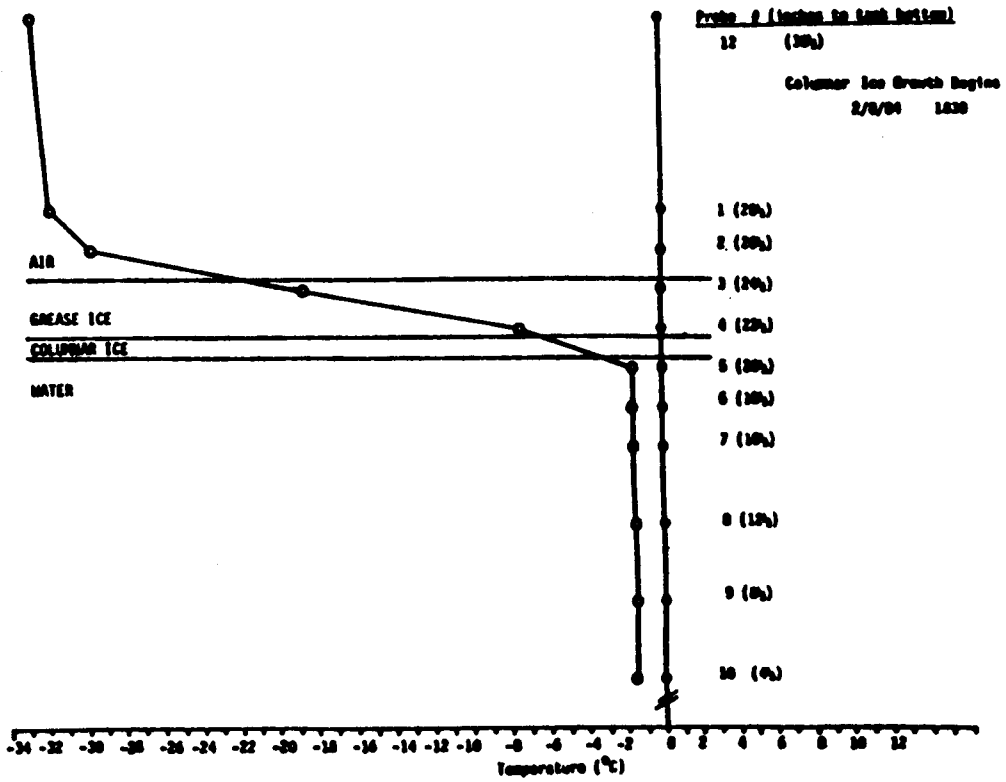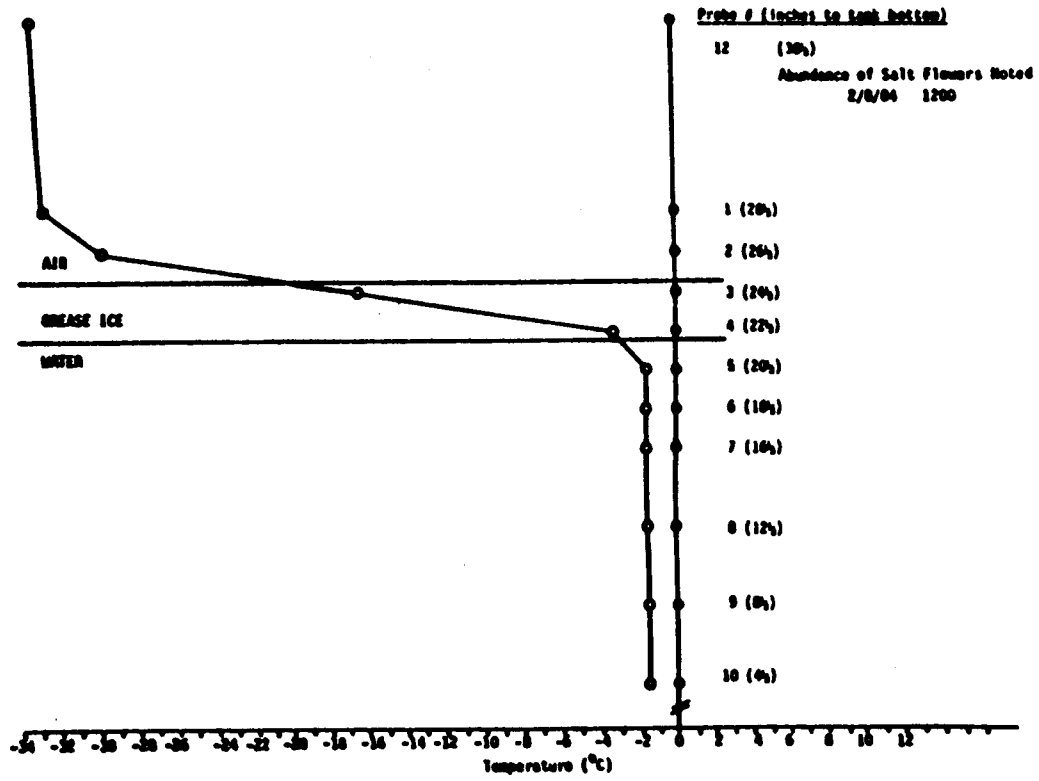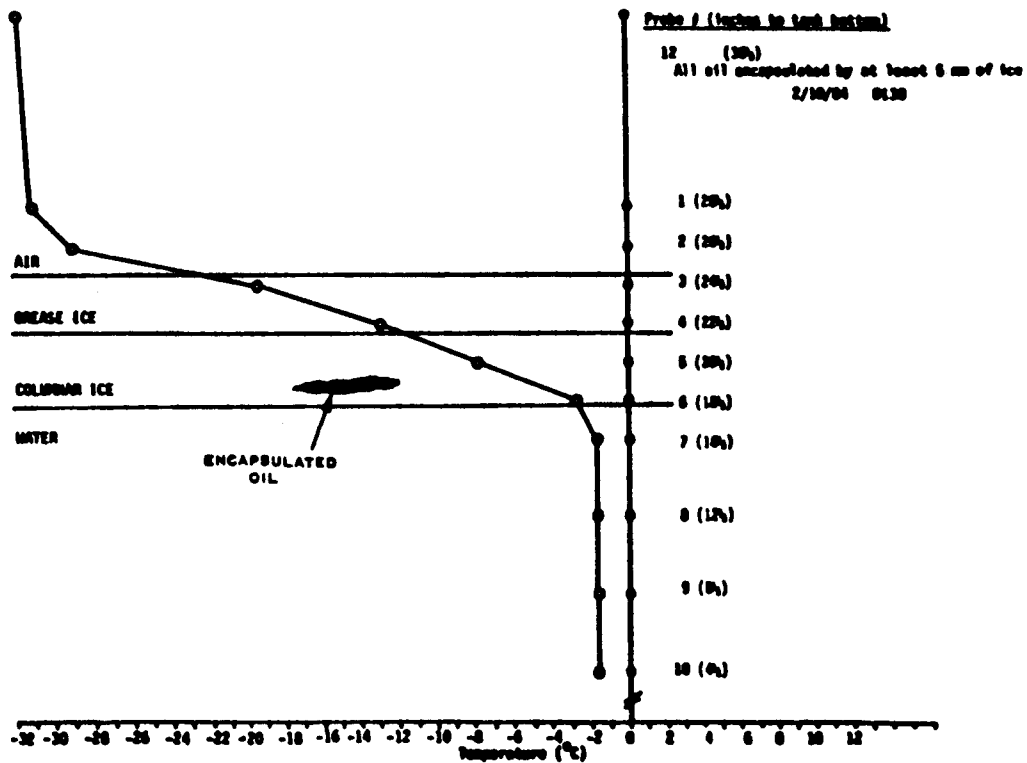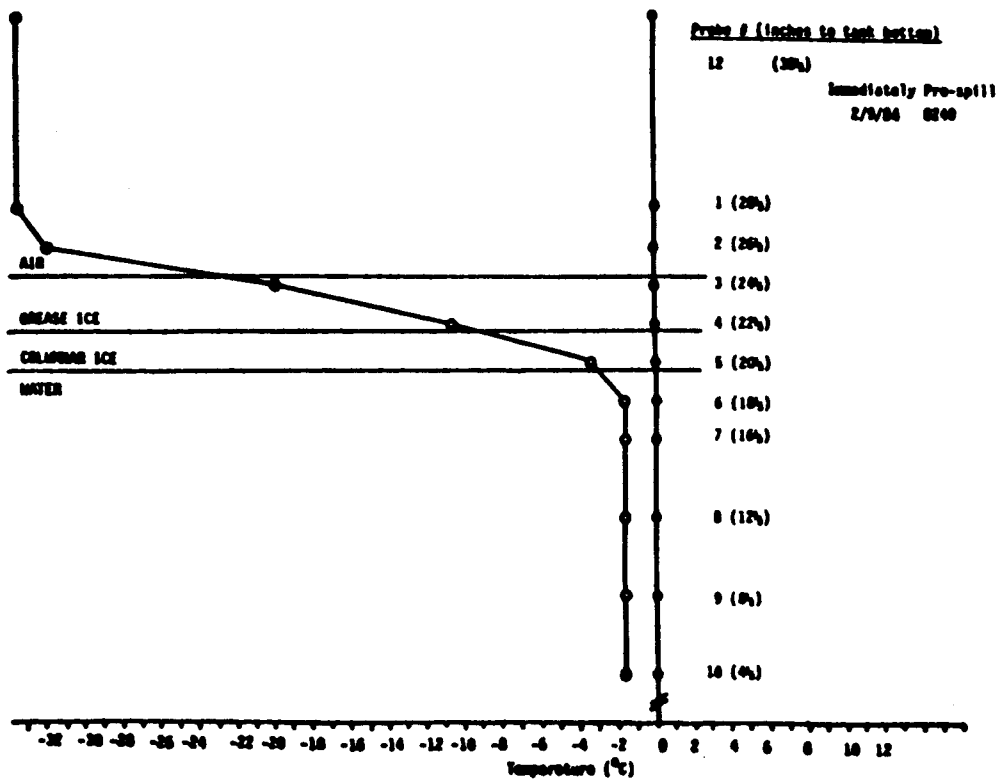
Table 4-1.--Chronology of Times and Dates of Significant Events Occurring
During the Oil/Ice Wave Tank Experiment.

Date/Time		Flow Rate (1/min)	Significant Event Description
2/7	2340	-	Initiation of cool down
2/8	0130	-	Grease ice over 2/3 of the tank
"	0220	-	" " 2" thick
"	0315	-	Wave generation terminated
"	0330	2.4	Grease ice 3" thick-surface skin formed
"	0600	1.1	Abundance of salt flowers
"	1300	-	First appearance of columnar ice
"	1500	1.1	3" grease ice + 1/2 " columnar ice
"	1830	.84	3" grease ice + 1" columnar ice
2/9	0100	.88	3" grease ice + 2" columnar ice
"	0500	-	5 liter spill of PB crude complete
"	1100	.80	3" grease ice + 2 1/2 " columnar ice-even with oil pools
"	1900	.94	3" grease ice + 3 1/2" columnar ice-oil encapsulation complete
2/10	0900	.88	3" grease ice + 4 1/2 " columnar ice
"	1630	-	3" grease ice + 5 1/4 " columnar ice-initial brine channeling
2/11	2100	.76	3" grease ice 5 3/4 " columnar ice
2/13	1200	-	Initiation of thaw
"	1800	.68	3" grease ice + 6 1/4 " columnar ice-pools of brine
2/14	0430	-	First oil surfacing
"	0630	.67	3" grease ice + 6 3/4 " columnar ice-maximum ice thickness
2/15	1930	.62	Open leads introduced
"	2315	.64	Ice 5 1/2 " thick-90% columnar
2/16	0130	.67	10% of the oil has surfaced
"	1000	-	Oil removed for distillation
2/18	1730	1.7	Break-up (wave action initiated)
2/20	1200	1.8	4" grease ice
2/22	1100	1.8	Ice free
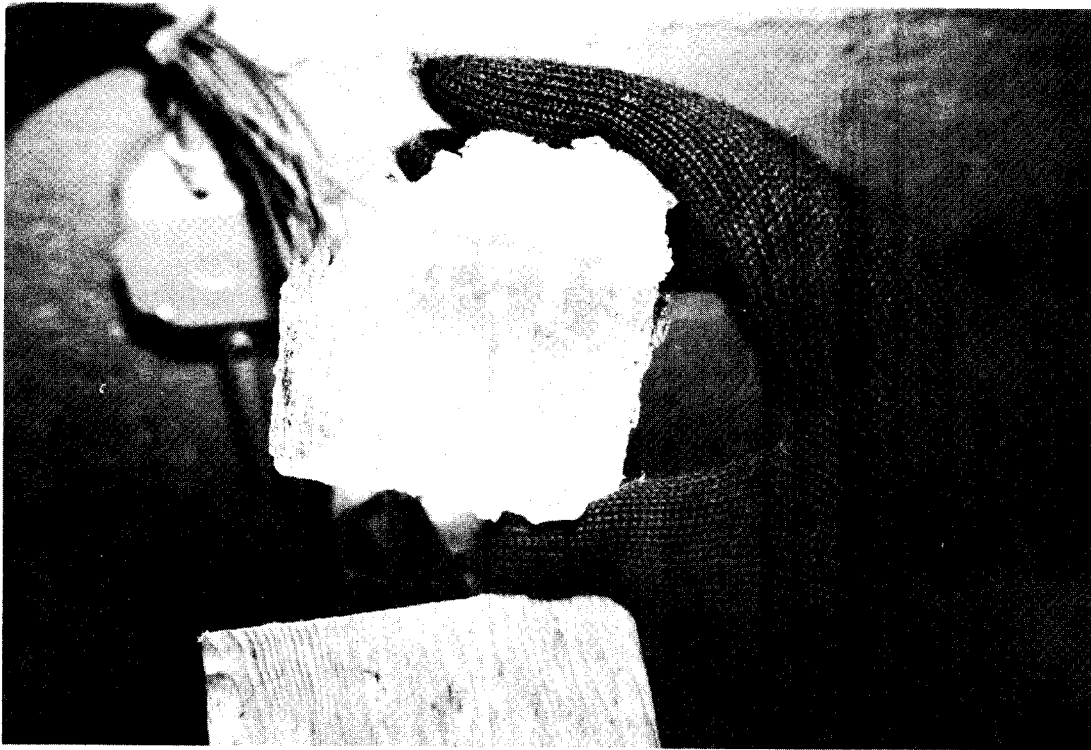
Figure 4-5.--Side view of Ice Core Obtained from Wave Tank System Illustrating the Discontinuity Between the Frozen Grease Ice (top) and the Columnar Ice (bottom). Most of the 3-5 inches of grease ice which was on top of the columnar ice was lost during sampling.
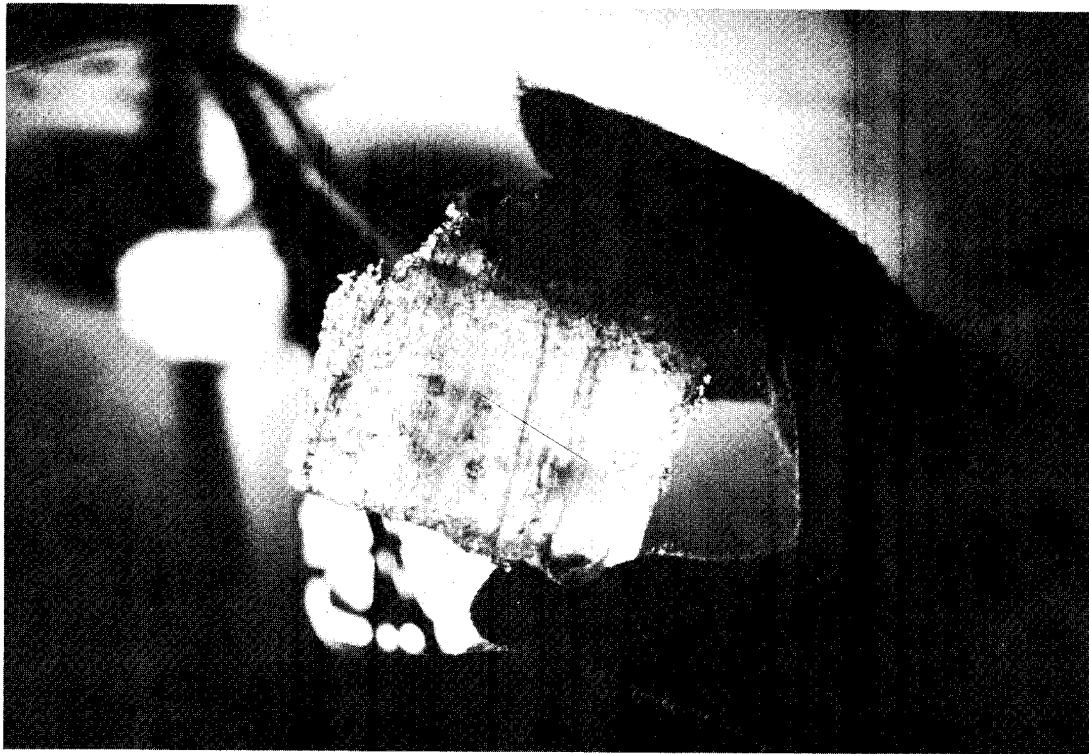
Figure 4-6.--Same Ice Sample as Described in Figure 4-5 with Backlighting to Better Illustrate the Crystal Structure of the Columnar Ice.

such, the columnar ice was only 10 cm thick at the time of sampling. Most of the 5 to 6 cm layer of grease ice originally present on the top of the core was lost during extrusion of the core. The abrupt transition apparent between the grease ice and columnar ice is also characteristic of cores from first-year ice collected in the field (Martin, 1979).

Salinity data collected during the ice formation experiments are summarized in Table 4-2.

Characteristics of the structural morphology (e.g., crystal orientation) and salinity measurements for ice formed in the wave tank were similar to those observed in actual field samples of ice in the Chukchi Sea (see Section 4.3.1 for comparisons).

4.2.2   Oil/Ice Interactions

When the ice layer in the tank consisted of 5-6 cm of surface grease ice and 4 to 6 cm of columnar ice, 5 liters of fresh Prudhoe Bay crude oil were introduced below the ice layer through a Teflon tube. Following addition of oil to the tank, oil droplets congealed immediately underneath the ice and some oil pooling was observed in under-ice depressions generated by placing styrofoam blocks on the upper ice surface to simulate snow drifts. Figure 4-7 shows one such pool of oil adjacent to the underwater thermister array, and also illustrates the formation of millimeter to 2 cm diameter oil droplets under the ice layer.

An under ice depression was intentionally formed near one of the vertical view ports to permit observations of the accumulation of the oil in this under-ice cavity. Within 23 hours the spilled oil was completely encapsulated by a 5 mm (minimum) layer of columnar ice. An additional 12 cm of columnar ice was then generated beneath the oil lens, and the spill remained entrapped within the columnar ice until a thaw cycle was initiated.

211

Table 4-2.—Salinities of Various Ice Types and Brines Obtained During the Oil/Sea Ice Interaction Experiment.

Sample type	Salinity ($^o/_{oo}$) of samples at—						
	Pre-freeze-up	Initial ice formation (1/30/84 2100)	Solid ice (1/31/84 1230)	Maximum ice thickness (2/2/84 2200)	Thaw initiation (2/3/84 1100)	8 hours into thaw (2/3/84 1900)	36 hours after breakup (2/6/84 2100)
Seawater	34.1	37.1	--	31.1	--	--	30.4
Grease ice	--	29.2	--	--	--	--	10.5
Surface brine	--	--	85.0	76.4	0.5	12.0	47.0 (residing inside pancake ice)
Ice at:							
surface	--	--	27.7	17.5	--	5.8	10.5 (rim of pancake ice)
2" depth	--	--	--	13.3	--	5.5	--
4" depth	--	--	--	12.5	--	9.5	--
6" depth	--	--	--	14.2	--	--	--
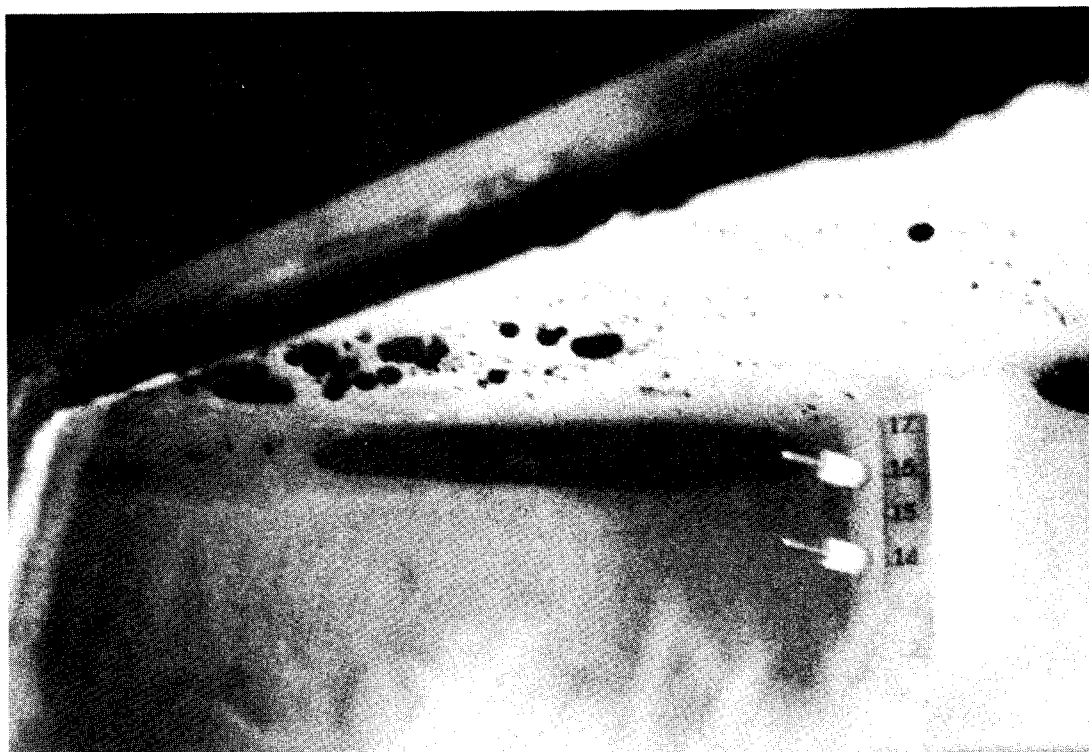
Figure 4-7.--Oil Pooling in Under-Ice Depressions Just After the Spill.

Approximately four days after the spilled oil was entrapped in the lower ice layer, a thaw cycle was initiated. Water column measurements of dissolved and dispersed hydrocarbons were completed over this period to insure that the system (which was constantly being exposed to fresh seawater flow) had returned to near "background" levels before initiation of the thaw. Just before initiation of the thaw cycle a significant temperature gradient was observed in the frozen grease ice and columnar ice (Figure 4-8), which at this point had reached a total thickness of 15-17 cm. Within 48 hours of initiation of the thaw cycle, the temperature gradient in the ice began to break down, which resulted in both melting of the surface grease ice and formation of standing pools of brine on top of the ice along with brine channel drainage.
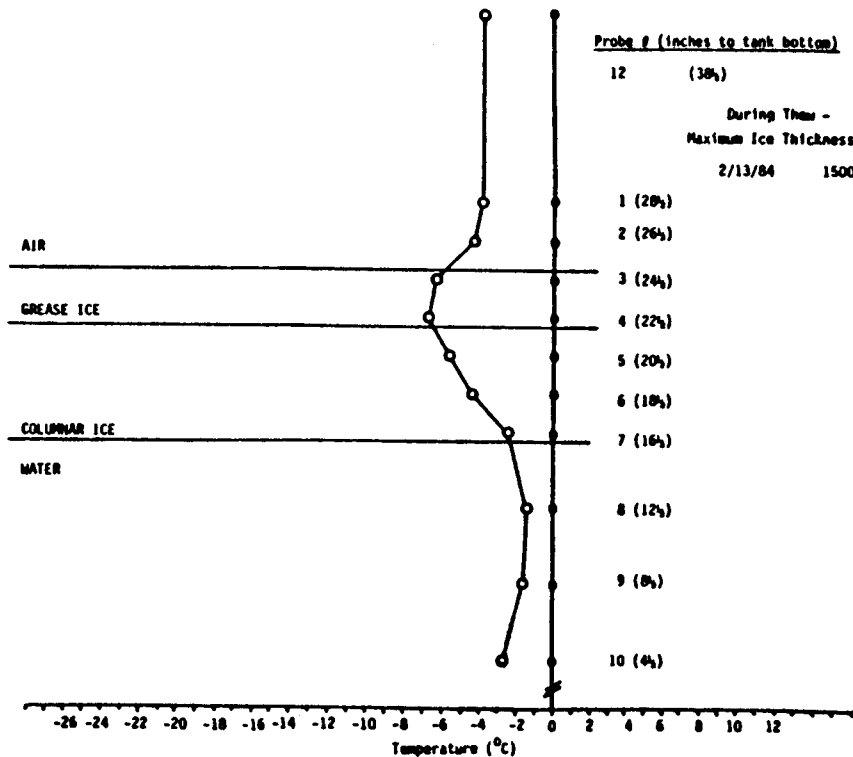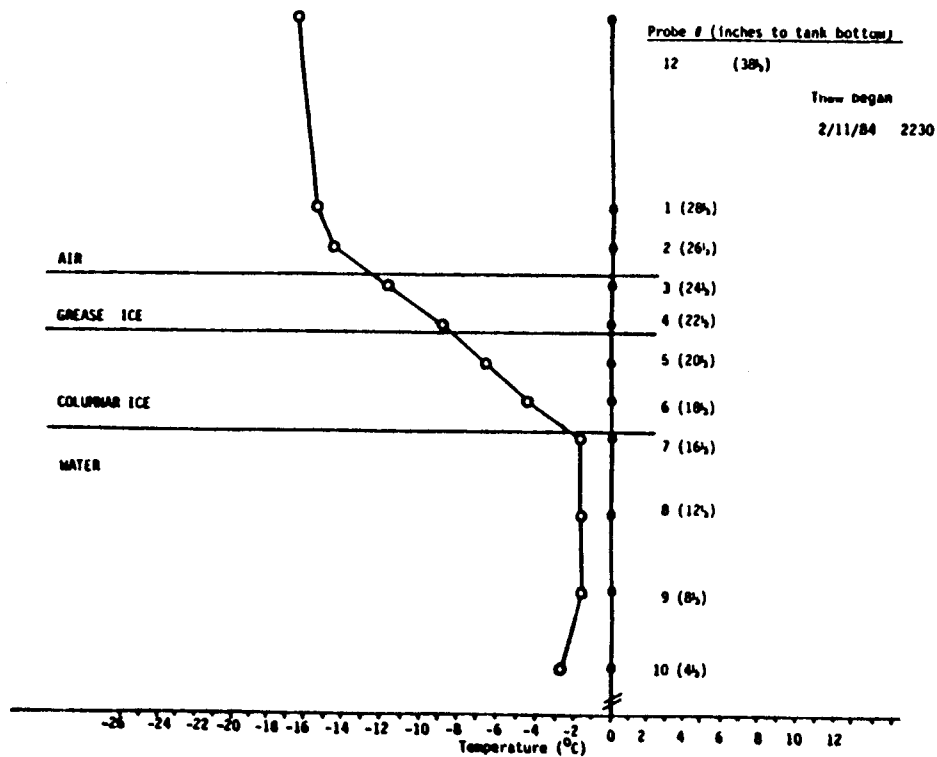
Figure 4-8.—Temperature/Depth Profiles Obtained During Oil/Ice Interaction
Experiment. (See also Table 4-1 for time-series chronology of events in the
cold-room experiments.)

214

First Appearance of Oil on Ice Surface

2/14/84   1030

Probe # (inches to tank bottom)

12   (30½)

1 (28½)

2 (26½)

AIR

3 (24½)

GREASE ICE

4 (22½)

5 (20½)

6 (18½)

COLUMNAR ICE

7 (16½)

WATER

8 (12½)

9 (8½)

10 (4½)

-28 -26 -24 -22 -20 -18 -16 -14 -12 -10 -8 -6 -4 -2 0 2 4 6 8 10 12

Temperature (°C)

Brine Channel Formation Complete

2/15/84   0600

Probe # (inches to tank bottom)

12   (30½)

Standing Pools of Brine

1 (28½)

2 (26½)

AIR

3 (24½)

GREASE ICE

4 (22½)

5 (20½)

COLUMNAR ICE

6 (18½)

7 (16½)

WATER

8 (12½)

9 (8½)

10 (4½)

-28 -26 -24 -22 -20 -18 -16 -14 -12 -10 -8 -6 -4 -2 0 2 4 6 8 10 12

Temperature (°C)

Figure 4.8.--(Continued)

A 71 cm diameter test floe was cut in the center of the ice to facilitate brine channel drainage and oil migration in a floating ice patch. This test floe was left in place, but its buoyancy was not restrained by the surrounding fast-ice layers which were held in place by the tank walls. With this circular test floe, time-series brine channel drainage and oil migration could be measured on ice behaving under natural buoyancy conditions. The remaining ice in the tank which was fast against the tank walls was also used for monitoring oil migration. However, slight changes in the water level due to partial blockage of the drainage pipe may have affected the migration rates in the fast ice, although this was not a factor in the central test floe.

A pool of oil trapped adjacent to the vertical viewport allowed observation of oil migration during initial formation of brine channels. Figure 4-9 shows the initiation of this brine channel migration, with a pocket of dissolved gases (methane, ethane, propane, and butane) leading the oil phase. Figure 4-10 shows the brine channels as outlined on the glass window and additional migration of the oil with time. While this migration was subject to "wall effects", the elapsed time for the oil to reach the surface was approximately the same as that observed for the floating ice floe. Chromatographic measurements of oil samples, obtained by penetrating the brine channel from above with a syringe, showed that some evaporation and loss of low molecular weight compounds occurred before the oil reached the ice surface.

Such losses would be diffusion controlled, however, and would not affect the bulk of the oil still residing in the trapped pool beneath the ice surface. Approximately four hours after the test floe had been cut out of the fast ice surface the first oil surfaced through the circular test floe.

Estimates of oil flow rates through the brine channels were derived from the amount of surface oil measured (area x thickness) on the test floe over time. In addition, time series photographs were used to document the changes and arrive at the volume and rate estimates listed in Table 4-3. The data in Table 4-3 were used to evaluate the brine channel migration predictions

216

Table 4-3.--Experimentally Determined Oil Migration Rates.

Elapsed Time(hrs)	Area (cm^2)	Thickness (cm)	Volume (mls)	Average Rate (mls/hr)
4.3	9.1	.05	.45	.11
10.2	1.4	.30	.87	.09
16.8	52.8	.22	11.9	.71
25.0	279	.46	129	5.2
35.8	269	.83	224	6.2
88.0	1260	.30	378	4.3

by Cox et al. (1980). The expression, given by Cox et al. (1980), for the minimum brine channel diameter that will allow oil migration (d_i) is:

$$d_i = \frac{4\sigma_{ow}}{\delta} \cdot \frac{\cos \alpha}{(L_w-L_o)g} \qquad (2)$$

where, for the experimental spill, σ_{ow} is the oil/water interfacial tension (24.2 g/sec^2), α is angle of contact (0), ω is the under ice oil lens thickness (2.5 cm), L_w is the water density (1.03 g/cm^3), L_o is the oil density (.92 g/cm^3), δ is the slick thickness and g is the gravitational constant (980 cm/sec^2). Using these values to solve for d_i indicates a minimum brine channel diameter of 3.6 mm, which seems reasonable in light of observations made in the wave tank and published brine channel diameters from oil spill studies completed in the field (Martin, 1979).

The rise rate velocity is given by:

$$\mu_z = \frac{(L_w-L_o)g\ \delta d^2}{32\ L\mu} \qquad (3)$$

217

Figure 4-9.--Initial Migration of Encapsulated Oil as Viewed Through Vertical Viewport. Note gas bubbles above migrating oil surface due to the slow release of volatile components during the brine channel migration. Photograph was taken at 1900 hours, 2/10/84.

Figure 4-10.--Continued Brine Channel Migration as Observed Through Vertical Viewport at 2245 Hours, 2/10/84. The location of brine channel drainage from the surface is illustrated by outlining the brine pools with Magic Marker.

where L_w, L_o, g, and δ are as before, d is the brine channel diameter (.36 cm), L is the ice thickness (5.7 cm), and μ is the oil viscosity (5.5 g cm^{-1} sec^{-1}). Solving for μ_z, a rise rate of .35 mm/sec was determined. This value is lower by a factor of two than the rise rate of 0.7 mm/sec determined experimentally by Martin (1979). However, slight changes in in situ oil viscosity (while still in the ice) or even a slight (1.4 fold) difference in brine channel diameter could result in a factor of two change in μ_z.

Finally, the volume flow rate to the surface can be expressed by:

$$V = \frac{\Pi d^2}{4} \mu_z N'A \qquad (4)$$

where d is as before, μ_z is the rise rate velocity (.035 cm/sec), N' is the number of brine channels per area (.01/cm^2) and A is the area of the spill (209 cm^2). Solving for V, with the experimentally determined data, indicates that the volume of oil deposited on the surface as a function of time should be approximately 27 mls/hr. This value is somewhat high when compared to the experimentally determined values presented in Table 4-3. However, other factors which may need to be taken into consideratin to explain the differences between calculated and observed flow rates include: 1) the depth of the oil pool in the ice, 2) the rate of temperature increase (totally controlled by laboratory conditions), 3) the fact that the laboratory ice was relatively thin ($\leq$ 10 cm), 4) the fact that the oil lens was initially trapped in columnar ice 4 cm below a 5 cm thick canopy of refrozen grease ice, 5) uncertainties in the number of brine channels/unit area in the laboratory and field studies and 6) the influence of the oil after it has surfaced with additional ice ablation and melting. Obviously, additional refinement of the modeling of oil migration in brine channels appears warranted; however, to our knowledge this is the first comparison of measured data with predictions based on Cox's approach.

Approximately 6 hours after the first brine channel oil migration was noted in the circular test floe, the oil had pooled in approximately five areas; the largest oil pool was approximately 1 cm in diameter. Approximately 24 hours later, several oil pools, the largest of which was estimated to be 5 cm long, were noted in the test floe. With increased absorption of infrared energy these pools then led to enhanced oil spreading and ice melting as reflected in the temperature profiles shown in Figure 4-11. Approximately 3 days later an estimated 90% of the oil was present on the ice/water surface. Gas chromatographic analysis of this surface oil pool illustrated that lower boiling distillate cuts up through TBP cut 7 (BP 282-304°F; Payne et al., 1984a) had been removed by evaporative weathering (see Figure 4-20; Section 4.2.4).

Three days after the thaw was initiated (Table 4-1), the ice was quite rotten and was manually broken up into 60-80 cm diameter floes. The paddle system was then later turned back on to generate 6-8 cm waves to examine the effects of light turbulence on oil weathering behavior in the presence of grease ice and test ice floes. The micro-scale turbulence introduced by the grinding of the ice floes against one another, and the grinding action of the frazil ice and grease ice crystals between the major floes, significantly enhanced the formation of a stable water-in-oil emulsion. The 4-6 cm wave oscilliations in the grease ice also led to a pumping action, as described by Lee et al. (1974), causing the oil to collect on the ice floes and around the rims. Subsurface observations and water sampling (see Section 4.2.3) illustrated that elevated levels of dispersed oil in the water column also resulted from this small scale turbulence which causes oil droplets to disperse. Dispersion quickly became self-limiting, however, due to the rapid (within 4 hours) formation of a water-in-oil emulsion (mousse) and drastic increases in oil viscosity.

A further observation was that the water-in-oil emulsion formed in the tank was not neutrally buoyant and, in fact, had a density (0.982 g/ml) such that most of the larger emulsified oil patches resided immediately below the grease ice on the water surface. The larger mousse balls were approximately 5 to 8 cm in diameter. With continued agitation and eventual melting of the

10% of the Oil Resides on Ice Surface

2/16/84   1115

Probe # (inches to tank bottom)

12   (30½)

1 (28½)
2 (26½)
3 (24½)
4 (22½)
5 (20½)
6 (18½)
7 (16½)
8 (12½)
9 (8½)
10 (4½)

AIR

COLUMNAR ICE

WATER

Temperature (°C)

Compressor & Paddle on -90% Oil (as Mousse) Resides Under Grease Ice.

2/20/84   1100

Probe # (inches to tank bottom)

12   (30½)

1 (28½)
2 (26½)
3 (24½)
4 (22½)
5 (20½)
6 (18½)
7 (16½)
8 (12½)
9 (8½)
10 (4½)

AIR

MIXTURE OF ICE FLOES AND GREASE ICE

WATER

Temperature (°C)

Figure 4-11.—Temperature/Depth Profiles Obtained During Oil/Ice Interaction Experiment. (See also Table 4-1 for a time-series chronology of events in the cold-room experiments.)

222

Some Mousse has surfaced

2/21/84   1200

Probe # (inches to tank bottom)

12   (38½)

1 (28½)

2 (26½)

3 (24½)

AIR

4 (22½)

GREASE ICE

5 (20½)

WATER

6 (18½)

7 (16½)

8 (12½)

9 (8½)

10 (4½)

-26 -24 -22 -20 -18 -16 -14 -12 -10 -8 -6 -4 -2 0 2 4 6 8 10 12

Temperature (°C)

Ice Free

2/22/84   1100

Probe # (inches to tank bottom)

12   (38½)

1 (28½)

2 (26½)

AIR

3 (24½)

WATER

4 (22½)

5 (20½)

6 (18½)

7 (16½)

8 (12½)

9 (8½)

10 (4½)

-24 -22 -20 -18 -16 -14 -12 -10 -8 -6 -4 -2 0 2 4 6 8 10 12

Temperature (°C)
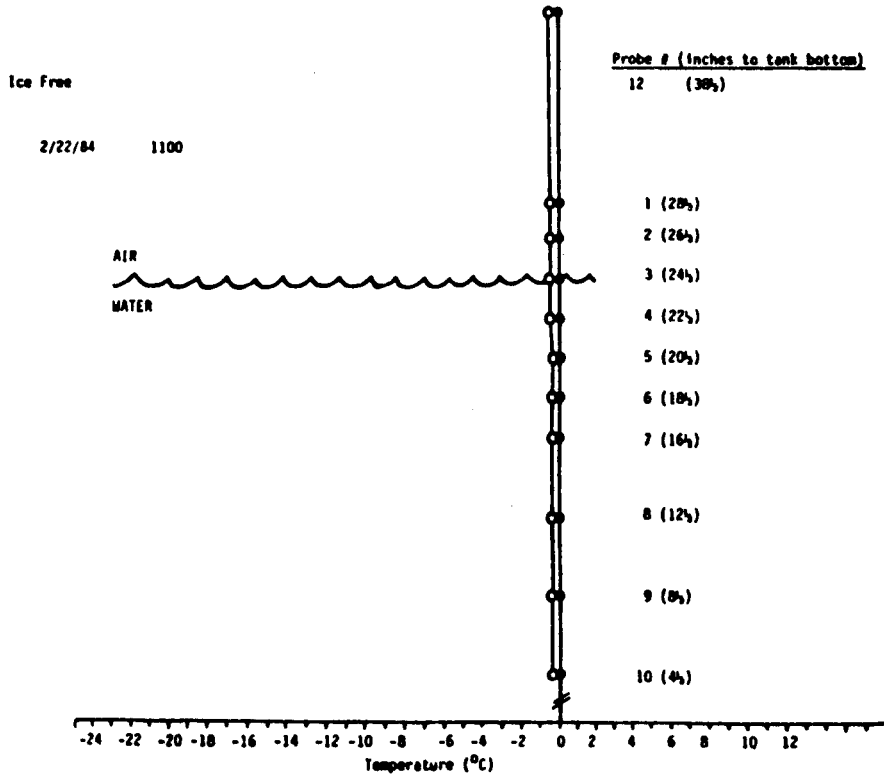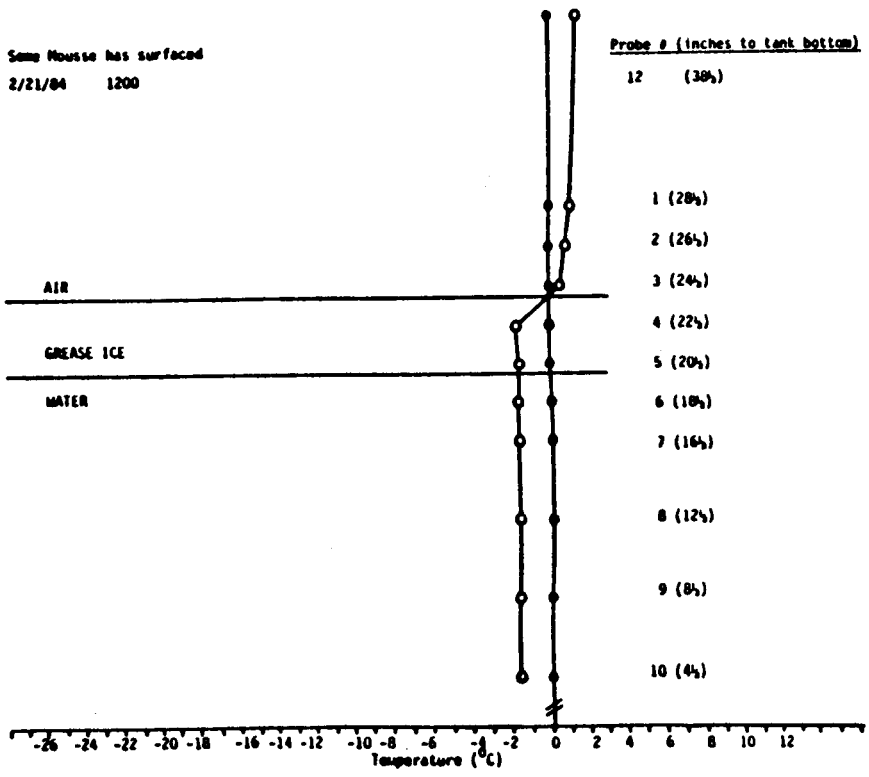
Figure 4-11.--(Continued)

223

grease ice (Table 4-1), the emulsified water-in-oil mixture eventually surfaced in the open water between the ice floes. Similar observations have been reported by Wilson and Mackay (1986). In their experiments rotating-shaker generated water-in-oil emulsions and Sudan Red dyed white oil (Bayol 35; SG 0.790) plus tetrachloroethylene (SG 1.615) mixtures were incorporated into agitated fresh-water grease ice contained in 3500 ml graduated beakers. These waterin-oil emulsions and the oil/chlorinated solvent mixtures had densities ranging from 0.92 to 0.98 g/ml). The reported density of the fresh water grease ice was 0.917 g/ml. Thus, when Wilson and Mackay poured an artificially generated water-in-oil emulsion (with a density of 0.946 g/ml) into the beaker with the grease ice and stirred it, an estimated 80 to 90% of the oil was incorporated. In the Kurdistan incident where No. 6 fuel oil was spilled in ice covered waters in Cabot Strait, the measured oil density was again qreater than the grease ice density and only slightly less dense than the water (C-Core, 1975). As a result, it was reported that the oil often resided beneath the grease ice, and as much as 50% of the oil was estimated to be entrained in the brash ice to a depth of 1 meter.

Tables 4-4 through 4-6 present rheological properties data for the emulsified oil generated in the cold room/wave tank experiments completed at Kasitsna Bay. The oil/water interfacial surface tension in the emulsified oil did not change throughout the duration of the experiment but remained at approximately 25-26 dynes per centimeter. Like-wise, the oil/air interfacial surface tension did not change during the emulsification process. Comparisons between changes in the rheological properties of mousse generated under open ocean/ice-free conditions (Payne, et al. 1984a) and those in mousse in the presence of artificial first-year ice can be made by examining the data in Tables 4-4 through 4-6 and Figure 4-12. A smooth decrease in oil/water interfacial surface tension from 27 to 13 dynes per centimeter was observed during open ocean oil weathering processes, with the oil/air interfacial surface tension showing values very similar to those observed in the ice tank system. Thus, in the presence of ice a stable water-in-oil emulsion was generated even without the change in oil/water interfacial surface tension noted under open-ocean weathering conditions.

Table 4-4.—Interfacial Tension (Oil/Water) and Surface Tension (Oil/Air) Obtained at Various Times During the Oil/Sea Ice Interaction Experiment.

Sample State[a]	Oil/Water Interfacial Tension (dynes/cm)	Oil/Air Surface Tension (dynes/cm)
Fresh crude (pre-spill)	26.2	33.4
Oil approaching the ice surface through brine channels (oil temp. @ 1.8°C – ambient measurement)	24.2	36.8
Pooled oil after surfacing	23.4	34.7
Mousse – 4 hrs after break-up	25.8	35.9
Mousse – 12 hrs after break-up	27.3	35.2
Mousse – 4 days after break-up	26.7	36.7

[a]Except where noted. all measurements were obtained after sample equilibration at room temperature.

Table 4-5.—Water Content (% by weight) in Oil Weathered in the Presence of Sea Ice.

Sample Description	Sampling Time and Date	Water Content[a](%)
Fresh Prudhoe Bay Crude	Pre-Spill	<.01
Oil Encapsulated by Ice	0600 2/16/84	4.3
Freshly Exposed Oil	1100 2/16/84	7.4
Mousse – 4 hrs after break-up	1600 2/18/84	64
Mousse – 11 hrs after break-up	2230 2/18/84	65
Mousse – 3 days after break-up	1330 2/21/84	64
Mousse – 4 days after break-up	2200 2/22/84	66

[a]Water content determined by Karl Fischer titration or ASTM 1796.

Table 4-6.--Oil Viscosities at Various Times and Temperatures Obtained During the Oil/Sea Ice Interaction Experiment.

Sample State	Oil Temperature (°C)[a]	Viscosity (centipoise)
Fresh Crude (pre-spill)	20.0	50
Oil approaching the ice surface through brine channels	1.0	550
Oil on ice surface (~10% remaining in the ice)	2.1	500
Weathering oil - 11 hrs after break-up	-2.0	25,000
Weathering oil - 11 hrs after break-up	38	1,100
Mousse - 36 hrs after break-up	-2.5	30,000
Mousse - 36 hrs after break-up	38	1,200
Mousse - 4 days after break-up	1.0	30,000
Mousse - 4 days after break-up	38	1,400

[a]Except for 38°C cases, viscosities were taken at experimental ambient temperatures.
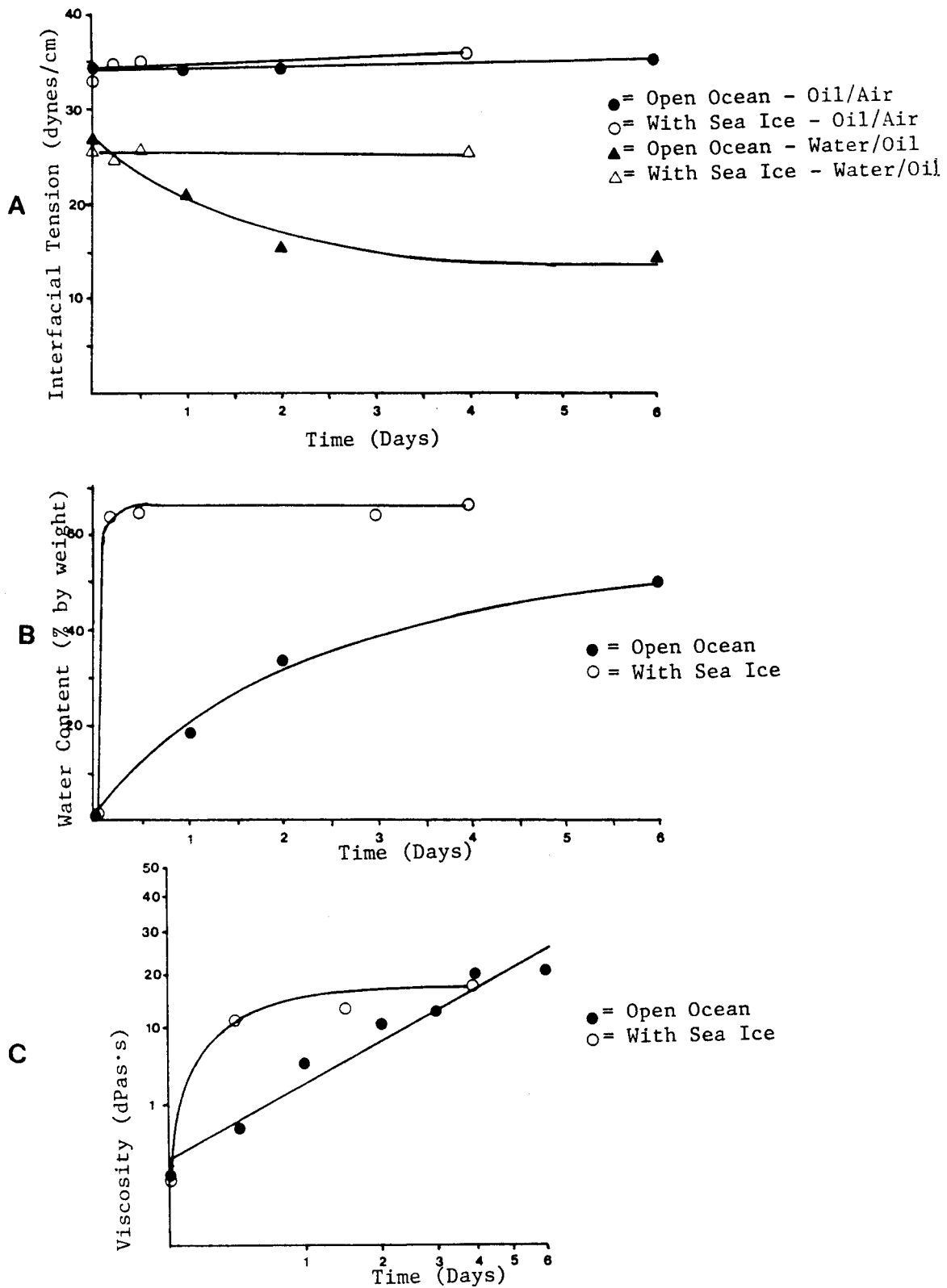
Figure 4-12.--Comparison of Oil Weathering Rheological Properties Between
Open Ocean and with Sea Ice Present.   (A) interfacial tension, (B) water
incorporation, and (C) viscosity.

227

For comparison, water content in the mousse reached 64% within 4 hours after ice break-up and initiation of wave turbulence (Table 4-5), whereas water build-up in a stable water-in-oil emulsion did not occur in open-ocean test tank studies for 12 days, and then only in a smooth increasing pattern (see Figure 4-12).

Large increases in viscosity were measured in the water-in-oil emulsion generated in the wave tank systems (Table 4-6). Fresh oil, as it surfaced through the brine channels had a viscosity of 550 centipoise at 1°C, whereas mousse formed four hours after the onset of turbulence exhibited a viscosity of 25,000 cp at -2°C. When this sample was warmed in the laboratory to 38°C for more standard (100°F) viscosity testing, a value of 1,100 centiporse was obtained. For comparison, the viscosities of mousse formed in open ocean oil weathering experiments approach 1,100 centipoise (at 38°C) only after 3-4 days of weathering under subarctic conditions (Payne et al., 1984a). Maximum oil viscosities approached 30,000 centipoise at ambient (-2.5°C) temperatures and 1,400 centipoise at 38°C after 4 days during the oil-in-ice experiments.

4.2.3   Compound Specific Partitioning and Whole Oil Droplet Dispersion

Aliquots of fresh Prudhoe Bay crude oil and samples of weathered oil and water from the wave tank were collected before spill initiation and at regular intervals during the experiment, respectively, for subsequent chemical analyses. The aliphatic and aromatic fractions of each of these samples as well as true boiling point (TBP) distillate cuts, were characterized for chemical and rheological properties by methods described in Payne et al. (1984a).

Concentrations of specific dissolved aromatic hydrocarbons in the water column are presented in Tables 4-7A and 4-7B for post-spill and post-ice break-up cycles, respectively. Time series profiles of dissolved aromatic hydrocarbon concentrations, shown in Figure 4-13 illustrate the slight increase in dissolved hydrocarbon concentrations in the water column immediately after subsurface oil release with a decrease in hydrocarbon concentrations after oil encapsulation in the ice during Day 3 to Day 4. With the initiation of wave

Table 4-7A.--Time Series Dissolved Hydrocarbon Concentrations (µg/liter) in the Presence of Sea Ice Before and During Encapsulization. Note: Open leads refers to the presence of several small open water leads resulting from cutting a 71-cm-diameter test floe in the center of the tank. Temperature regimes during the experiment can be seen in Figures 4-4, 4-8, and 4-11.

| Compound | KOVAT | Prespill | POST SPILL TIME | | | | | | | | | | | Open Leads | | |
			2 Hours	4 Hours	6 Hours	9 Hours	13 Hours	17 Hours	28 Hours	36 Hours	2 Days	3 Days	4 Days	5 Days	7 Days	9 Days
Ethylbenzene	854	ND[a]	.635	.690	.799	1.29	.455	.907	.482	.926	.126	.0583	.0308	.0890	.695	3.01
m,p-xylene	866	.460	2.53	2.79	3.40	4.41	2.00	3.32	2.83	3.45	.850	.453	.362	.751	2.76	10.9
o-xylene	891	.246	1.11	1.22	1.50	1.97	.868	1.46	1.07	1.54	.341	.185	.147	.291	1.22	5.12
Isopropylbenzene	921	ND	.0594	.0661	.0757	.112	.0504	.0874	.0694	.0941	.0253	ND	.0227	ND	.0784	.281
N-propylbenzene	950	ND	.0753	.0814	.0944	.145	.0618	.108	.0830	.127	.0284	ND	ND	ND	.106	.463
C_3-benzene	960	ND	.294	.321	.382	.524	.233	.393	.340	.446	.111	.0736	.0557	.119	.405	1.63
C_3-benzene	966	ND	.0985	.0978	.116	.163	.0706	.121	.102	.146	.0313	.0226	ND	.0346	.139	.553
1,3,5-trimethylbenzene	978	ND	.130	.154	.176	.226	.108	.179	.163	.205	.0497	.0270	.0258	.0511	.180	.847
C_3-benzene	992	ND	.358	.397	.502	.603	.291	.481	.436	.567	.131	.0891	.0685	.154	.519	2.02
C_4-benzene	1020	ND	.214	.238	.213	.365	.163	.266	.178	.240	.114	.0585	.0575	.144	.318	1.13
Tetramethylbenzene	1107	ND	.0972	.107	.146	.135	.101	.127	.0865	.150	ND	.0252	ND	ND	ND	.201
Naphthalene	1180	ND	.235	.289	.368	.502	.245	.360	.329	.520	.0868	.0578	.0376	.0832	.418	1.15
2-methylnaphthalene	1290	ND	.103	.129	.230	.281	.107	.214	.195	.348	.0611	.0405	.0285	.0702	.400	1.08
1-methylnaphthalene	1307	ND	.0952	.122	.158	.209	.104	.151	.148	.254	.0476	.0381	.0316	.0554	.296	.869
1,1'-biphenyl	1375	ND	ND	ND	ND	.0246	ND	.0204	ND	.0416	ND	.0263	ND	.0323	.0336	ND
2,6-dimethylnaphthalene	1399	ND	.0630	.0852	.11	ND	.0668	.0899	.0891	.103	.0358	.0384	.0218	.0468	.0278	.869
C_2-naphthalene	1414	ND	ND	ND	ND	.0313	ND	.0232	ND	.0464	ND	ND	ND	ND	.0561	.114
C_2-naphthalene	1433	ND	.0383	.0549	.0747	.0809	.0254	.0532	ND	.0690	ND	ND	ND	ND	.145	.257
C_2-naphthalene	1448	ND	ND	ND	ND	ND	ND	ND	ND	ND	ND	ND	ND	ND	ND	ND
2,3,5-trimethylnaphthalene	1558	ND	.0255	.0340	.0414	ND	.0274	.0326	ND	.0595	ND	ND	ND	ND	.0576	ND
Dibenzothiophene	1746	ND	ND	.0465	.0571	.0507	.0389	.0413	ND	.0475	ND	.0462	ND	ND	.0338	.142
Phenanthrene	1773	ND	ND	.0334	ND	.0532	.0249	ND	ND	.0686	ND	.0283	ND	ND	.150	ND
Total Resolved Compounds	—	2.77	8.60	9.42	26.8	34.0	6.25	15.7	13.6	18.5	4.92	4.71	3.69	3.99	12.6	66.0
Unresolved Compounds	—	0	8.27	7.92	19.8	14.0	6.89	6.83	4.50	14.0	0	0	0	0	12.5	20.7

[a] ND indicates "not detected".

Table 4-7B.--Time Series Dissolved Hydrocarbon Concentrations (µg/liter) in the Presence of Sea Ice After Ice Breakup and Initiation of Wave Turbulence. Wave action was initiated at 0 minutes on day 9 post spill (see also Figure 4-13).

Compound	KOVAT	POST BREAK-UP TIME											
		15 min	1 hr	2 hrs	4 hrs	8 hrs	12 hrs	24 hrs	48 hrs	3 days	4 days	5 days	6 days
Ethylbenzene	854	13.6	15.2	17.5	26.7	-	12.0	3.45	1.61	.476	.104	ND[a]	ND
m,p-xylene	866	47.4	54.4	62.9	98.3	58.6	47.2	15.8	9.80	4.27	1.36	.262	.108
o-xylene	891	22.9	27.8	32.5	52.0	34.3	27.9	10.1	5.87	2.54	.956	.209	ND
Isopropylbenzene	921	1.63	2.28	2.47	4.00	3.23	2.62	1.04	.745	.378	.104	ND	ND
N-propylbenzene	950	2.48	3.32	4.25	7.38	5.89	4.86	2.14	1.71	.907	.292	ND	ND
C$_3$-benzene	960	9.27	12.3	15.8	25.7	21.7	17.8	8.11	6.49	3.34	1.26	.385	.173
C$_3$-benzene	966	3.38	4.42	5.92	9.74	8.50	7.09	3.38	2.82	1.55	.601	.204	ND
1,3,5-trimethylbenzene	978	4.11	5.63	7.46	12.1	10.8	8.87	4.27	3.47	1.82	.819	.255	.124
C$_3$-benzene	992	11.9	16.4	21.6	34.5	32.4	27.1	13.8	11.8	6.46	2.67	.918	.475
C$_4$-benzene	1020	6.84	9.88	13.8	21.7	21.6	17.9	9.55	8.20	4.73	2.10	.749	.534
Tetramethylbenzene	1107	2.18	2.14	2.40	2.18	1.80	1.17	.340	.133	ND	ND	ND	ND
2-methylnaphthalene	1290	8.19	12.4	19.8	27.8	36.4	34.4	27.3	33.2	28.2	18.7	9.14	6.67
1-methylnaphthalene	1307	6.24	9.87	15.6	21.9	29.5	27.9	22.5	25.1	21.5	14.8	7.43	5.59
1,1-biphenyl	1375	.857	1.41	2.24	3.32	4.68	4.48	3.54	4.06	3.64	2.66	1.48	1.23
2,6-dimethylnaphthalene	1399	1.33	1.97	3.16	4.50	6.06	6.35	5.50	6.49	5.67	4.25	2.07	1.70
C$_2$-naphthalene	1414	1.34	1.89	2.92	4.00	5.35	5.00	4.83	5.66	4.98	3.38	1.50	1.39
C$_2$-naphthalene	1433	.391	.530	.807	1.17	1.69	1.48	1.25	1.60	1.43	.881	.363	.366
C$_2$-naphthalene	1448	.420	.513	1.11	1.50	2.12	2.14	1.57	1.96	1.77	1.42	.619	.591
2,3,5-trimethylnaphthalene	1558	.635	.706	.946	1.11	1.31	1.28	1.02	1.26	1.12	.851	.433	.431
Dibenzothiophene	1746	.228	.280	.350	.534	.679	.759	.595	.896	.870	.769	.296	.350
Phenanthrene	1773	.190	.232	.340	.508	.686	.650	.660	.951	.860	.744	.333	.404
Total Resolved Compounds	-	306.0	363.0	441.0	632.0	502.0	444.0	246.0	222.0	160.0	88.0	39.0	26.9
Unresolved Compounds	-	104.0	148.0	136.0	213.0	249.0	197.0	115.0	78.6	49.6	22.3	0	0

[a]ND indicates "not detected".

230
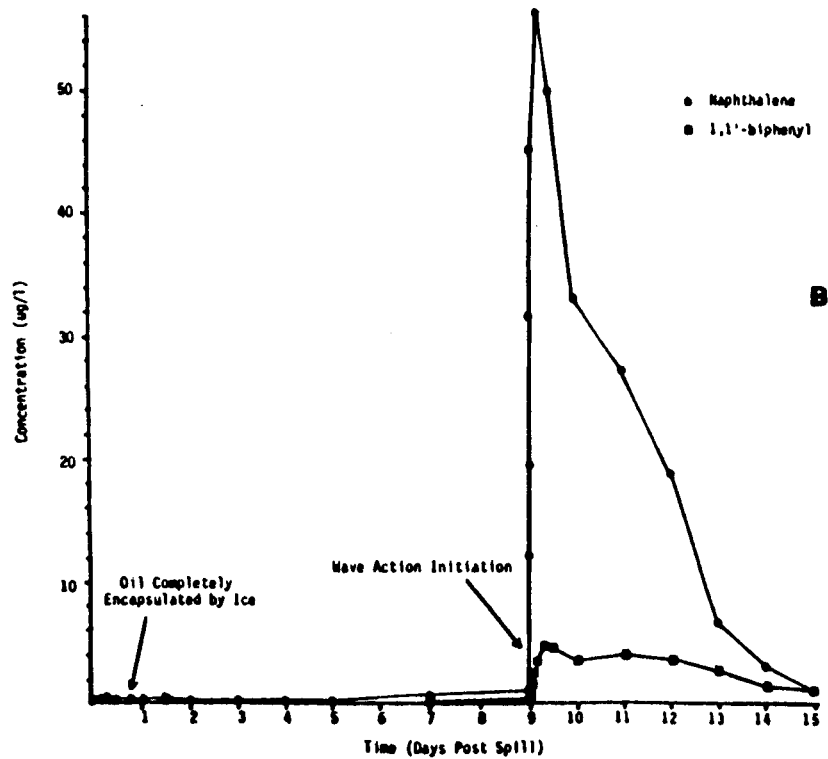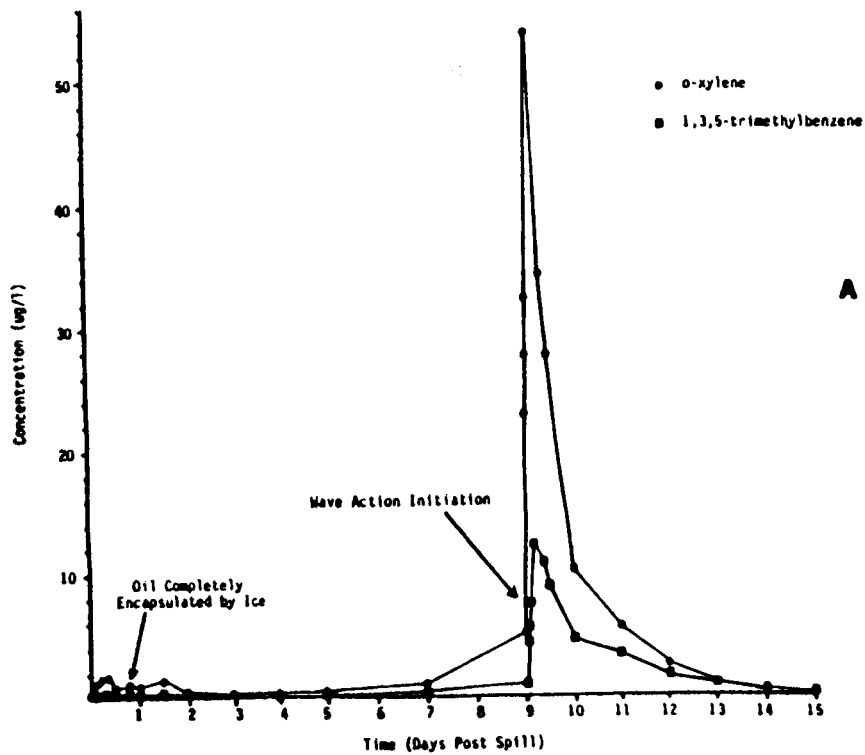
Figure 4-13.—Time Series Dissolved Hydrocarbon Concentrations with Sea Ice
Present. (A) o-xylene and 1,3,5-trimethylbenzene; (B) naphthalene and
1,1'-biphenyl; and (C) total resolved compounds and UCM.

231
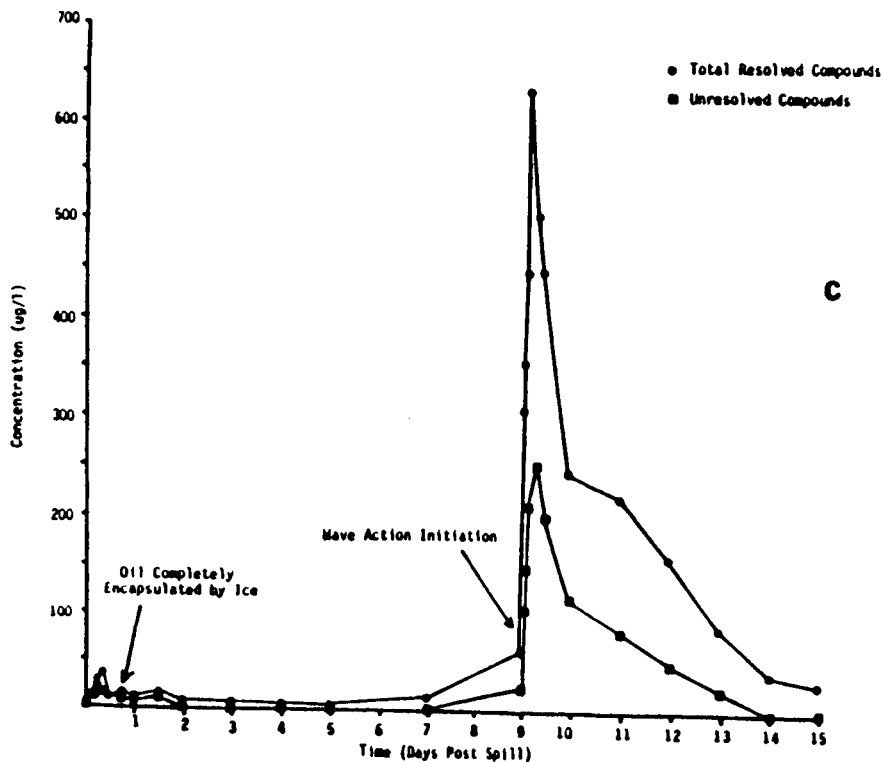
Note: the 71 cm circular test floe
for brine channel oil migration
studies was installed on day
five and additional leads were
cut in the ice canopy on day
7 (see Table 4-1). Some
dispersion of oil droplets
resulting in enhanced dis-
solution inadvertently
occurred during these
activities.

Figure 4-13.--(Continued)

232

turbulence after ice break-up on Day 9, however, an approximate 50-fold increase in dissolved hydrocarbon concentrations was observed for the compounds ortho-xylene, trimethylbenzene, naphthalene, and 1,1-biphenyl. The total resolved components and unresolved complex mixtures, as determined by FID-GC analyses, increased by factors of 700 and 300, respectively, after wave turbulence was introduced. The immediate spike in the total resolved component concentrations, due to the initiation of wave turbulence, was followed by a gradual decline (over 6 days) in water column concentrations due to the combined effects of subsurface advection and evaporative loss from the water surface.

Flame ionization detector gas chromatograms are presented in Figure 4-14 for methylene chloride extracts of: (a) a pre-spill seawater blank; (b) a water sample collected 9 hours after the subsurface release; and (c) a water sample collected five days after the initiation of the spill but before ice break-up. The chromatogram in Figure 4-14B for the 9 hour sample shows the presence of dissolved lower molecular weight aromatic hydrocarbons in the alkyl-substituted benzene through alkyl-substituted naphthalene range. After oil encapsulation and continued under-ice water column flushing of one tank-volume every 1.25 days (simulating 0.006 cm/sec subsurface currents), the water column was significantly cleaner after 5 days, as shown in the chromatogram in Figure 4-14C. AT higher under ice currents in the field, this process would obviously occur over a shorter time frame.

The thaw cycle in the tank system was initiated after the water column concentrations of dissolved aromatic hydrocarbons had returned to near pre-spill levels (see Figure 4-13). Immediately after ice break-up and initiation of wave turbulence, water column samples were again collected. Figure 4-15 presents the FID/GC profiles of the dissolved aromatic hydrocarbons in the water column with sea ice present: chromatogram A corresponds to a sample collected 8 hours after initial break-up, chromatogram B is from a water column sample collected 4 days after ice break-up, and chromatogram C shows the hydrocarbon components present in a sample collected after 6 days. Many of the lower molecular weight components were lost within six days due to evaporation and advective removal of the water from the wave tank system.
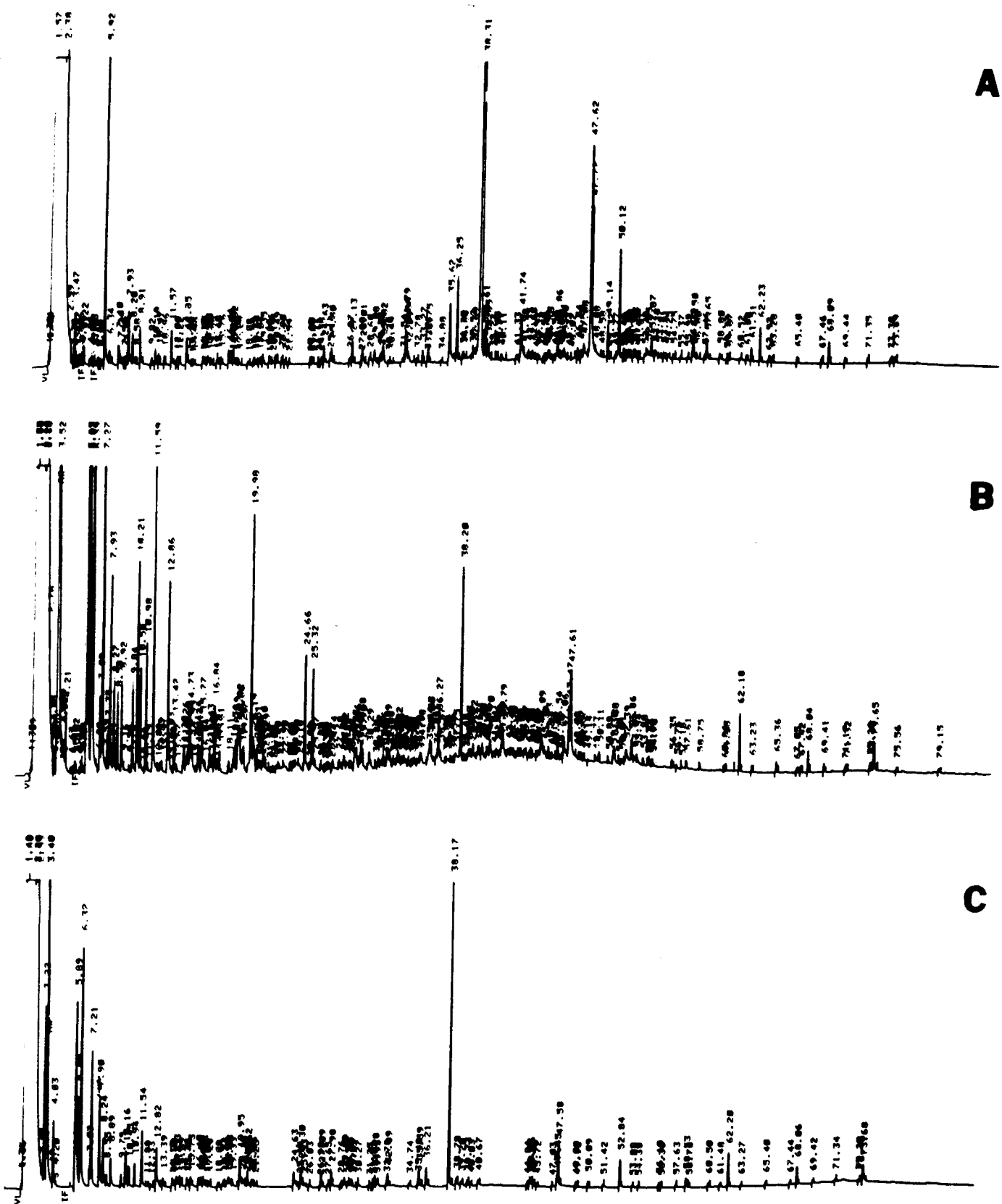
Figure 4-14.--FID-GC Chromatographic Profiles Depicting Hydrocarbons Dissolved in the Water Column with Sea Ice Present. (A) prespill; (B) 9 hours post spill; and (C) 5 days post spill (before ice breakup).

234
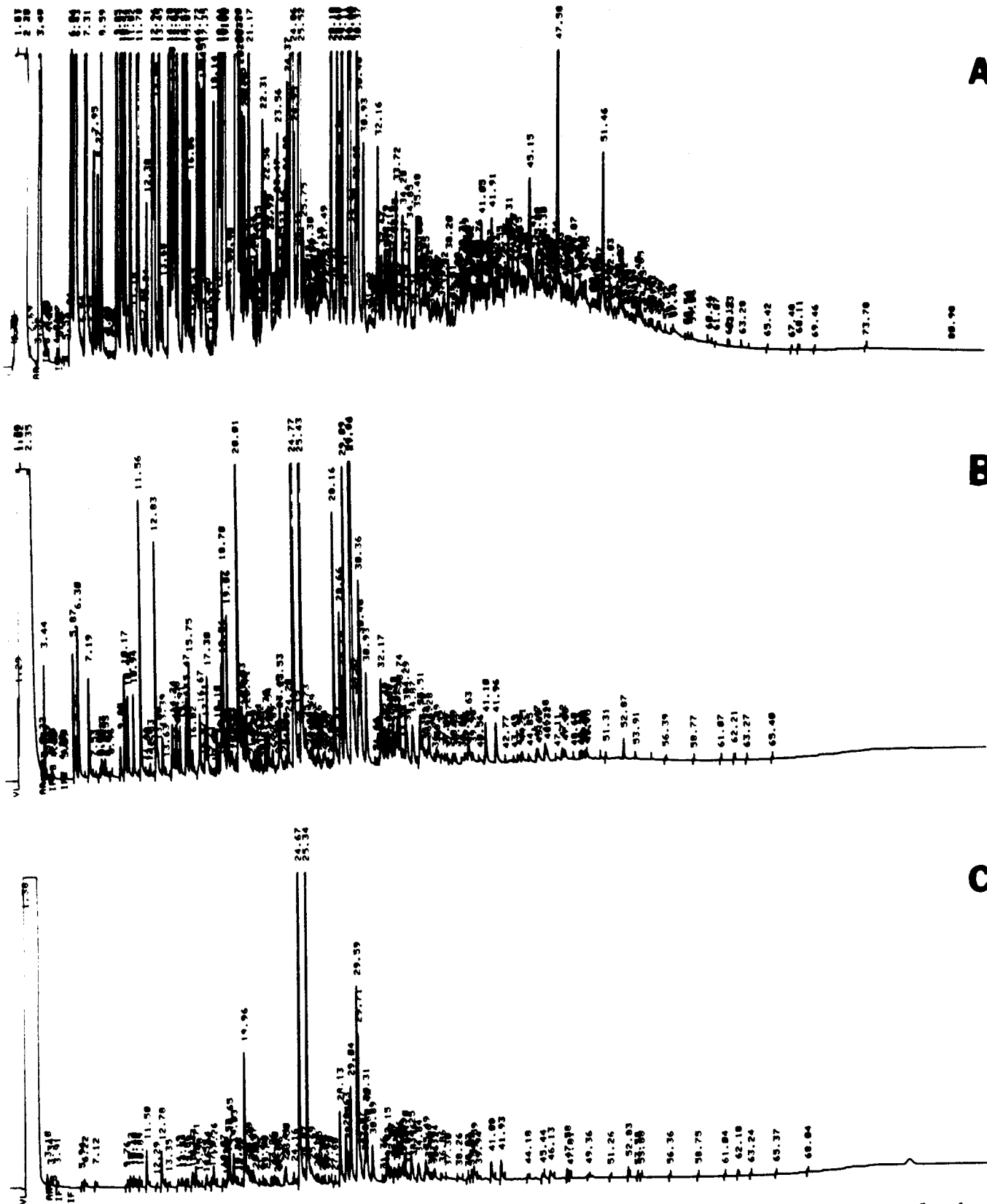
Figure 4-15.--FID-GC Chromatographic Profiles Depicting Hydrocarbons Dissolved in the Water Column with Sea Ice Present. (A) 8 hours; (B) 4 days; and (C) 6 days after ice breakup.

Water samples collected throughout the post spill and post break-up phases were also filtered for analyses of dispersed oil fractions, as described in Payne et. al. (1984a). Time series concentrations of dispersed oil concentrations in the tank are presented in Table 4-8. Concentrations of total resolved and unresolved complex mixture (UCM) aliphatic hydrocarbons (representing the dispersed oil phase) remained low (generally less than 10 μg/liter) throughout the post-spill period, with only relatively small changes from the pre-spill to the post-spill levels. In contrast, levels of dispersed total resolved and UCM hydrocarbons increased by two to three orders of magnitude following the break-up of the ice and onset of 4-6 cm wave turbulence. Maximum resolved and unresolved concentrations were measured 12 hours after ice break-up, although levels subsequently decreased to approximate pre-spill conditions at six days after break-up. Time series concentrations of total resolved and unresolved components in the dispersed oil phase are shown in Figures 4-16A and 4-16B, respectively. These data indicate that very little of the oil is dispersed into the water column during encapsulation by the ice, which occurred approximately 24 hours after the spill.

Detectable levels of some of the medium molecular weight alkanes (from nC_{12} to nC_{20}) were apparent 13 to 17 hours after the spill. This weak pulse of dispersed oil suggests a delayed mixing of oil micelles down to the depth of the sampling port, approximately 50 cm below the bottom of the ice layer. By 24 hours after the spill, all of the oil had been encapsulated by the ice; however, the concentration of the total resolved components continued to increase up to 36 hours post-spill. Beyond 36 hours, concentrations of individual alkanes and the UCM dropped to pre-spill levels. Chromatograms of the dispersed oil extracts are shown in Figure 4-17. The presence of some of the intermediate molecular weight alkanes, as well as a small UCM "hump", are apparent in the chromatogram of the 13 hour sample (Figure 4-17B) relative to the clean baseline and general absence of a series of n-alkane peaks for the chromatograms of pre-spill and 24 hour filter extract samples.

Table 4-8.—Time Series Dispersed Oil Concentrations (µg/liter) in the Presence of Sea Ice. Turbulence was initiated 9 days after the spill.

Compound	POST SPILL TIME								POST BREAK-UP TIME (9 DAYS +)							
	Prespill	4 hrs	6 hrs	13 hrs	17 hrs	36 hrs	2 days	9 days	1 hr	4 hrs	8 hrs	12 hrs	24 hrs	2 days	4 days	6 days
$N\text{-}C_9$	ND[a]	ND	ND	ND	ND	ND	ND	ND	.336	.427	.929	1.54	ND	ND	ND	ND
$N\text{-}C_{10}$	ND	ND	ND	ND	ND	ND	ND	ND	2.03	3.89	6.11	7.92	1.95	2.11	.226	ND
$N\text{-}C_{12}$	ND	ND	ND	.00686	.00875	ND	ND	ND	12.2	18.4	25.0	29.9	15.9	15.6	2.15	ND
$N\text{-}C_{14}$	ND	ND	ND	.0108	.0280	ND	ND	ND	17.2	22.1	30.0	36.7	23.5	23.1	3.83	ND
$N\text{-}C_{17}$	ND	ND	ND	.0580	.0233	ND	ND	ND	12.6	15.6	21.9	24.7	17.5	17.8	3.67	.265
Pristane	ND	ND	ND	.00971	.0122	ND	ND	ND	6.87	8.11	10.9	11.9	8.80	8.93	2.48	.451
$N\text{-}C_{18}$	ND	ND	ND	.0860	.0540	.0268	ND	ND	11.3	13.7	19.0	21.6	15.1	15.8	3.45	.232
Phytane	ND	ND	ND	.0197	.0293	ND	ND	ND	6.63	7.56	9.99	10.7	8.40	7.95	2.47	.0330
$N\text{-}C_{20}$	ND	ND	ND	.00935	.0131	ND	ND	ND	8.03	10.1	15.6	15.5	12.7	11.1	3.35	.0419
Total Resolved	1.23	1.14	2.25	4.75	4.21	6.76	2.09	2.84	310	402	507	592	403	387	93.0	3.21
UCM[b]	0	0	0	3.81	5.41	0	0	0	1050	1480	1990	2120	1860	1510	309	0

a - ND indicates "not detected'

b - 'Unresolved complex mixture'
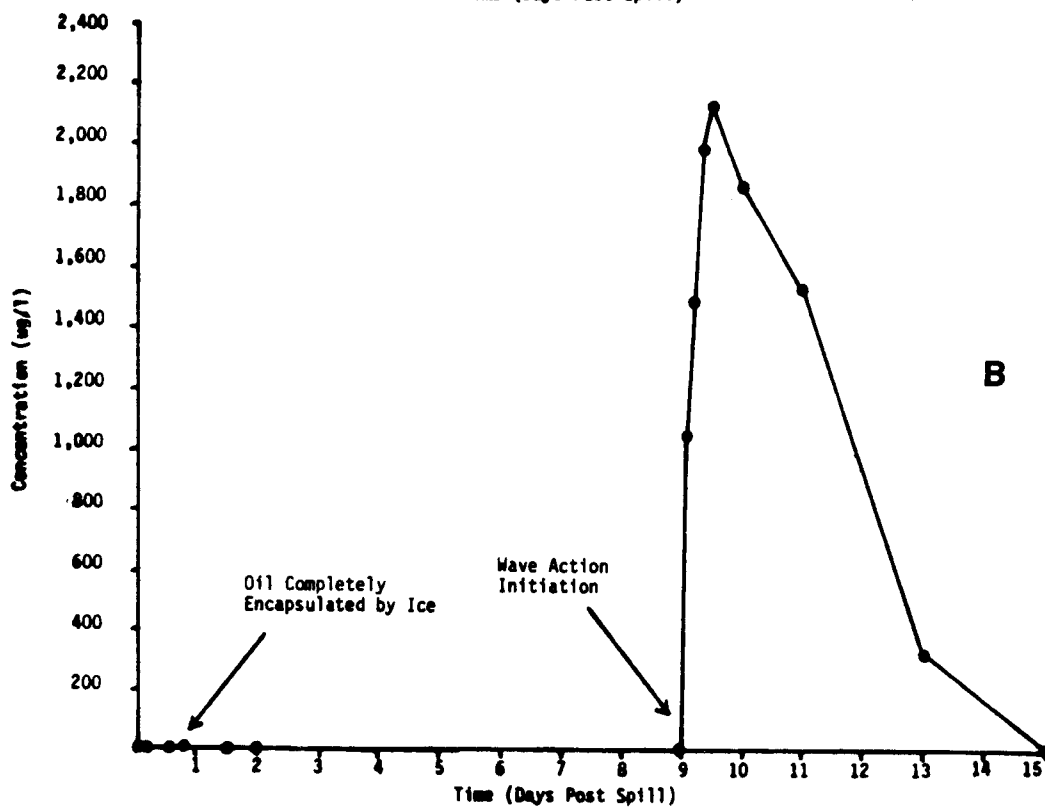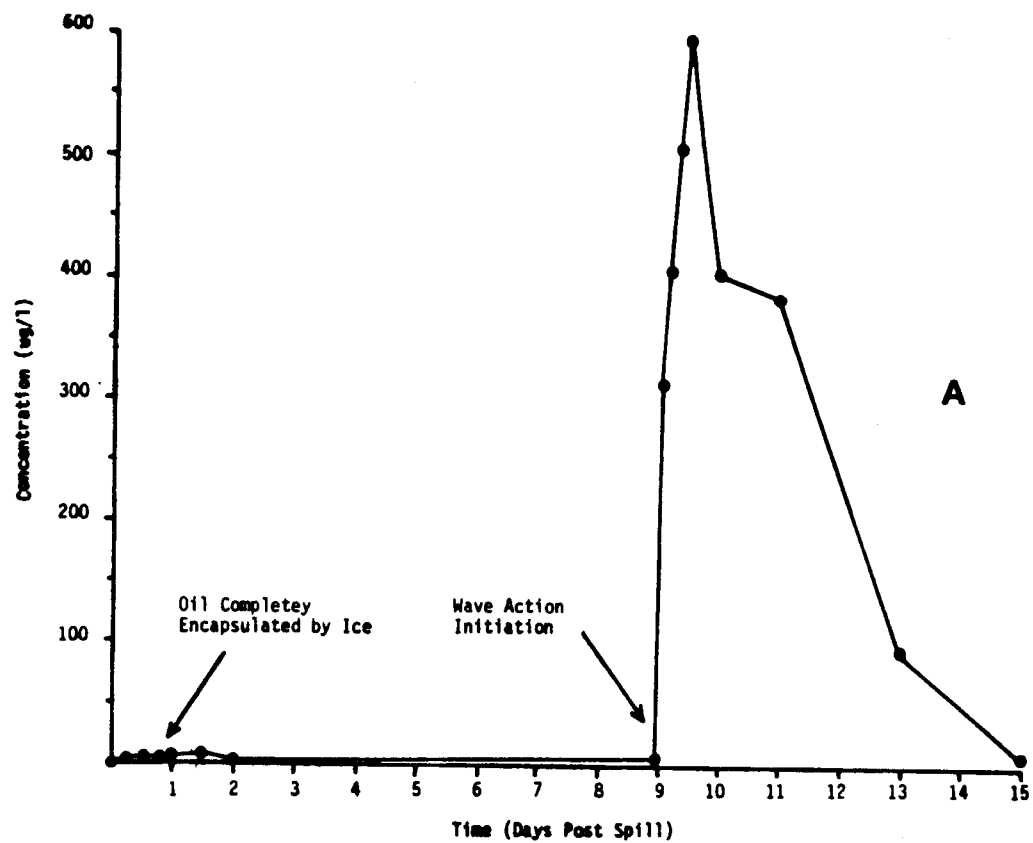
Figure 4-16.—Time Series Water Column Concentration of (A) Total Resolved Dispersed Oil Compounds, and (B) Unresolved Dispersed Oil Compounds.

238
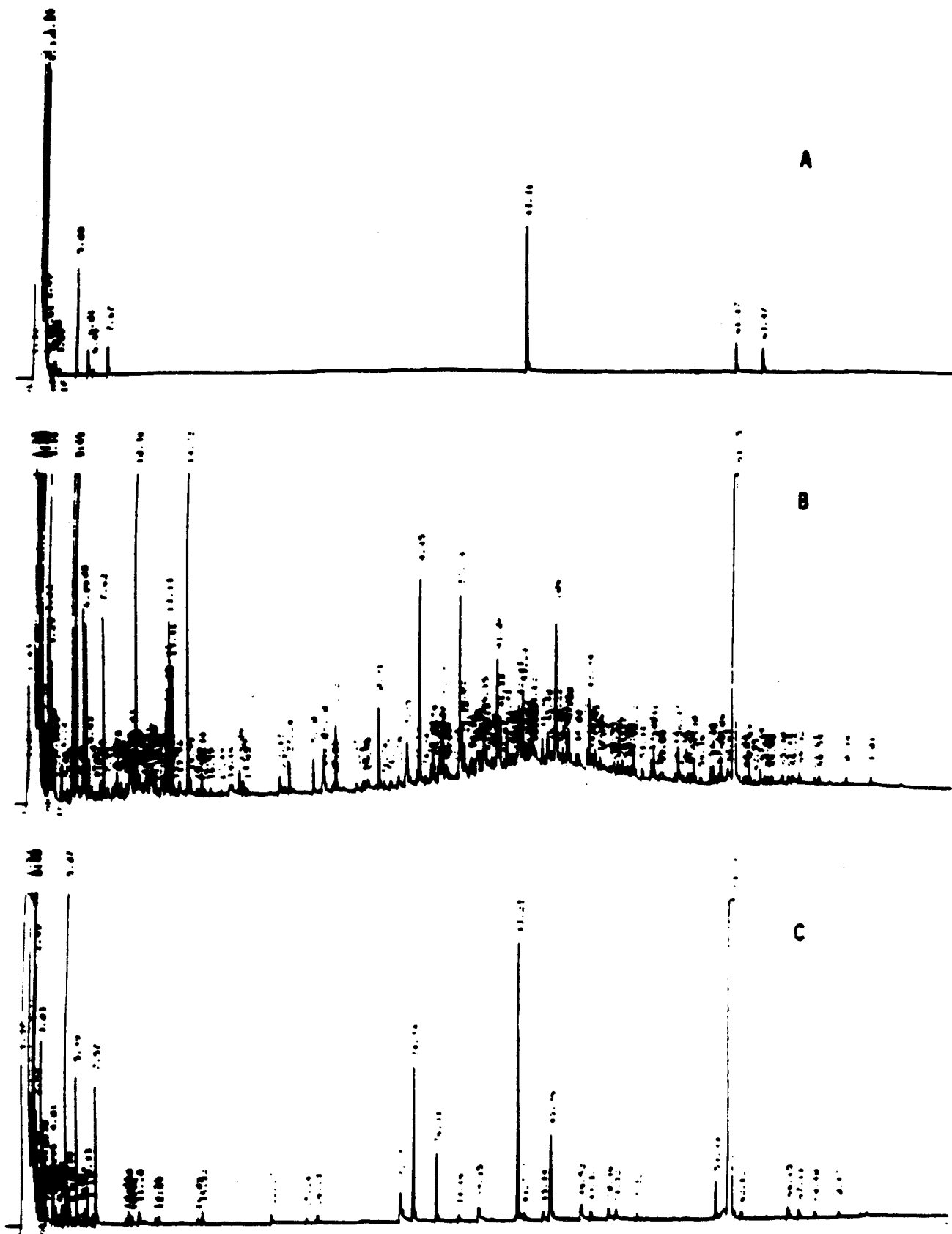
Figure 4-17.--FID-GC Chromatograms of 0.45-μm Glass Fiber Filter Extracts
Depicting Dispersed Oil in the Water Column During Ice Encapsulation:
(A) prespill, (B) 13 hours, and (C) 24 hours post spill.

239

Following the break-up of ice in the tank, concentrations of most of the individual n-alkanes increased with time up to 12 hours. Concentration subsequently decreased over the next six days to approximate pre-break-up levels with the formation of high viscosity water-in-oil emulsions which inhibited further dispersion. The presence of lower molecular weight n-alkanes (nC_9 through nC_{14}) was not detectable in the water column after six days. A series of peaks corresponding to the intermediate and higher molecular weight n-alkanes are apparent in the chromatogram of the filter extracts of the one hour and four day post-break-up samples (Figures 4-18A and B, respectively). Most, if not all of the lower molecular weight n-alkanes below nC_{10} (TBP Cut 7) are not as prominent in either the one hour or four day samples, suggesting a rapid loss due to evaporation and dissolution. The significantly reduced number of resolved intermediate and higher molecular weight compounds in the filter extract from the six day sample reflects the nearly complete inhibition of dispersed oil droplets in the water due to the formation of the high viscosity, water-in-oil emulsion (see Tables 4-5 and 4-6 and Figure 4-12).

4.2.4 Oil Phase Chemistry

Oil samples were also obtained from ice cores during the thawing cycle and analyzed by FID/GC. Chromatograms of the oil both immediately after it was released from ice encapsulation and after it had been exposed at the water surface for 3 hours are shown in Figure 4-19. Qualitatively, the chromatographic profiles appear identical, indicating little, if any, evaporative loss. However, other chromatograms obtained from oil in the brine channels showed some evaporative losses of lower molecular weight alkanes in the methane through heptane range. Due to the extremely high viscosity (550 centipoise) of oil at the ice temperatures during brine channel migration, the evaporative behavior is believed to be diffusion-controlled, producing a gradient of more highly evaporated oil nearer to the surface. Thus, in the bulk oil sample shown in Figure 4-19C, there appears to be little evaporative loss.

240
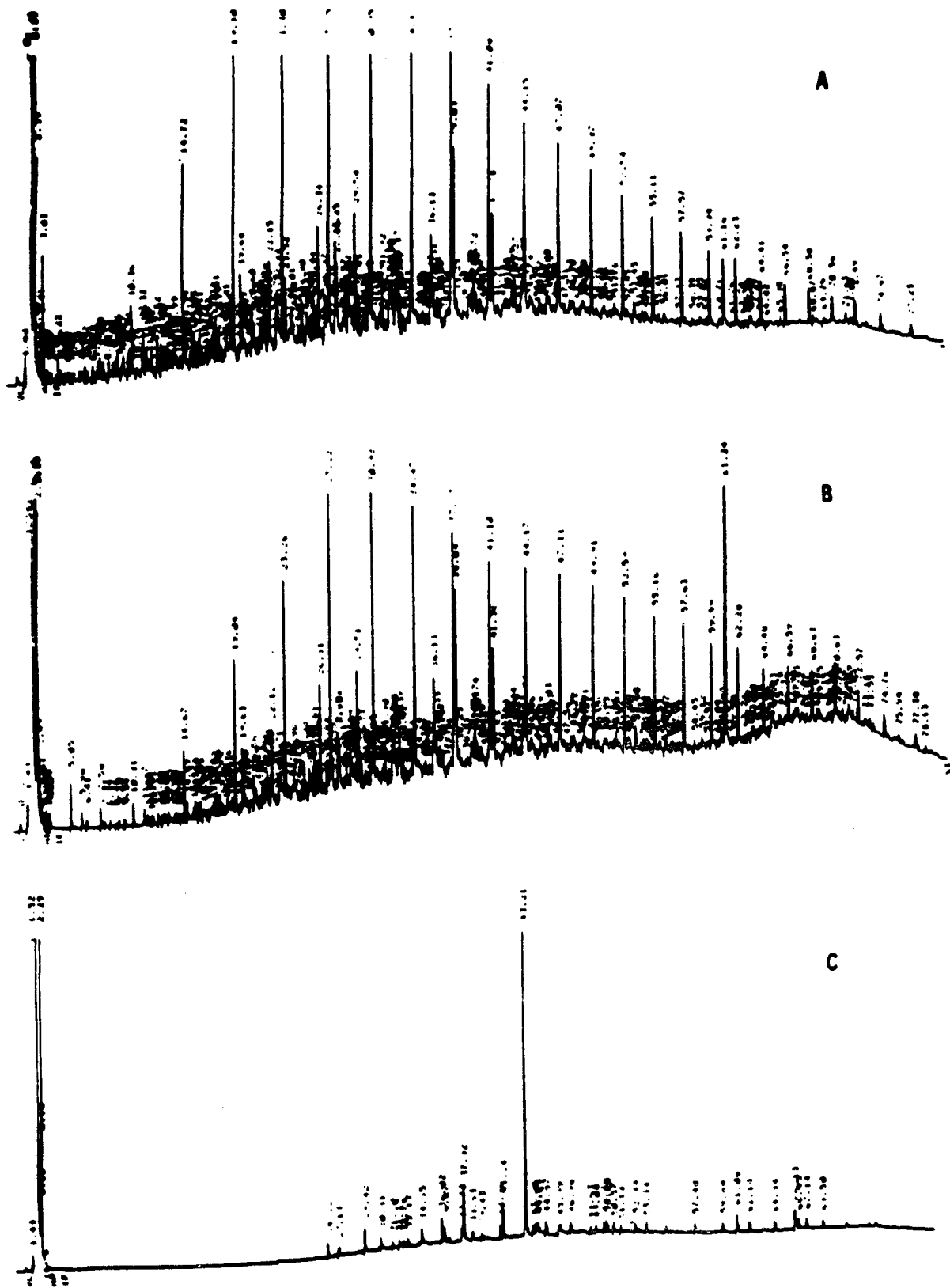
Figure 4-18.--FID-GC Chromatograms of 0.45-μm Glass Fiber Filter Extracts Depicting Dispersed Oil in the Water Column After Ice Breakup: (A) 1 hour, (B) 4 days, and (C) 6 days after breakup.
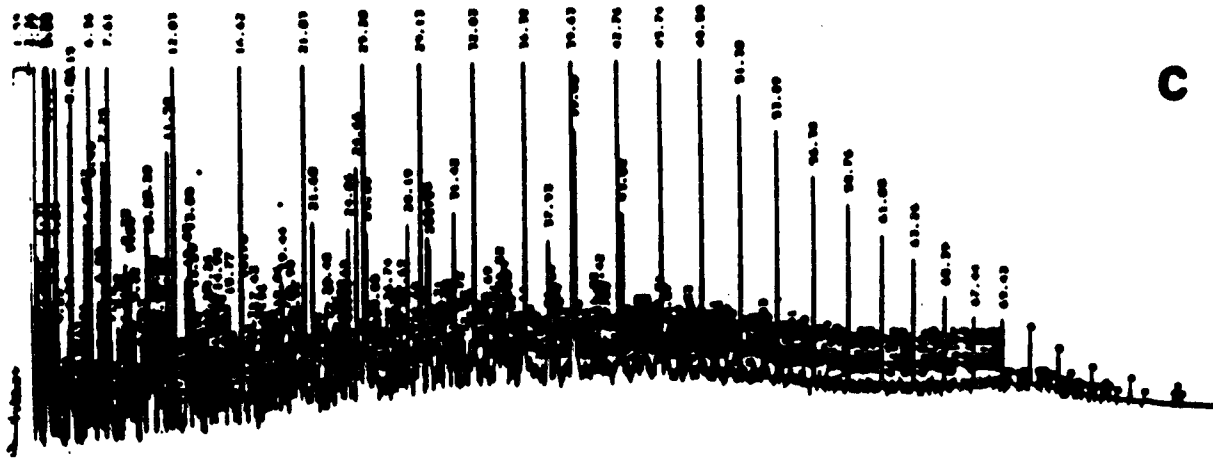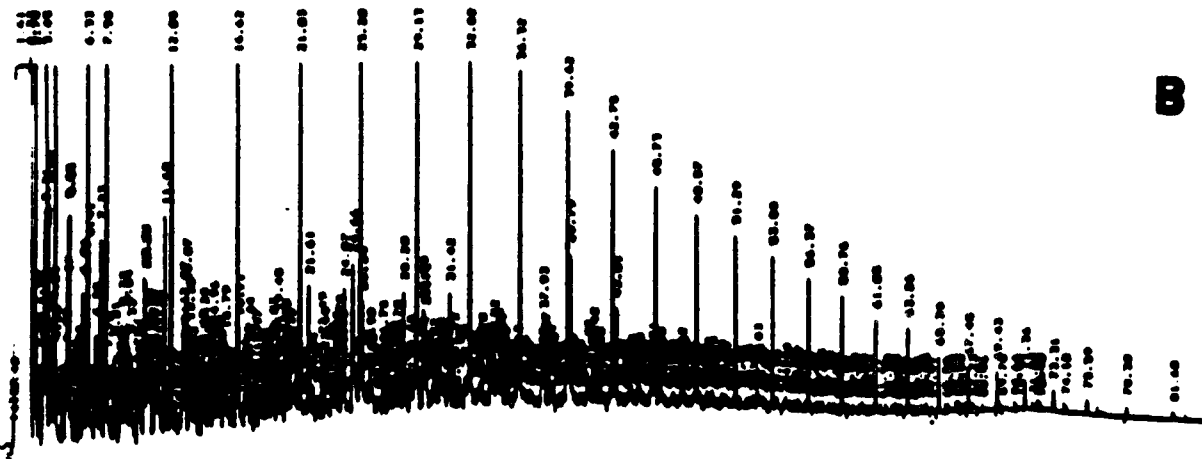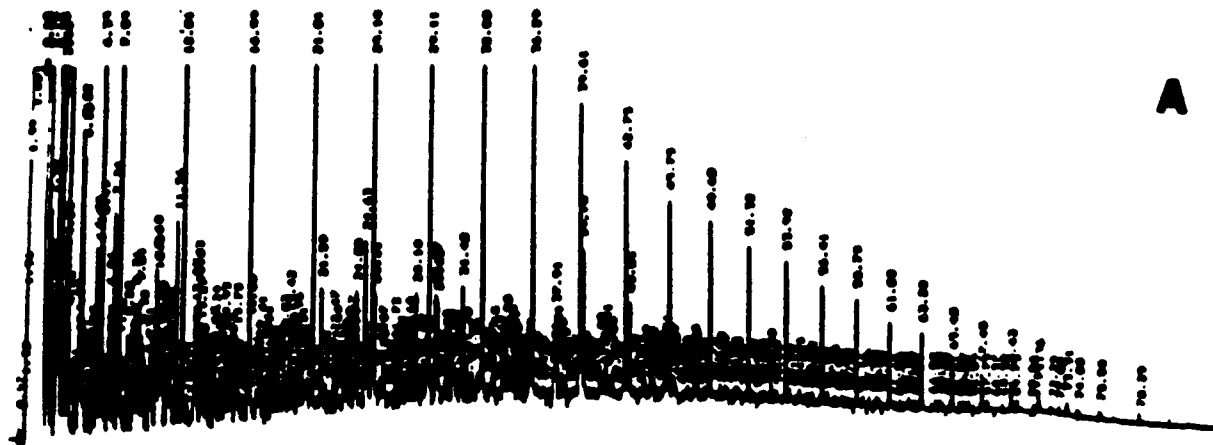
Figure 4-19.--FID-GC Chromatograms of Oil Weathering in the Presence of Sea Ice: (A) fresh Prudhoe bay crude oil; (B) encapsulated oil; and (C) bulk oil exposed for 3 hours.

242

In other cases, however, there was evidence of loss of lower molecular weight components from the oil even as it was migrating through the brine channels. Figure 4-9 (in Section 4.2.2) illustrated the presence of a gas pocket above the upwardly migrating oil. In several other ice floes, it was possible to sample the oil before it had migrated through the brine channel and reached the surface. Oil was removed with a syringe tip from a depth of approximately 5 cm below the ice/air interface through a brine channel having a diameter of approximately 3 millimeters. Figure 4-20 presents chromatograms obtained on: (A) encapsulated oil, (B) an oil sample obtained from the brine channel below the ice/air interface, and (C) a sample from a 5 mm deep oil pool which had migrated through a brine channel and flowed over the ice surface. Even at a depth of approximately 5 cm into the brine channel, some evaporative loss of lower molecular weight components below nC_9 had occurred. After this oil surfaced and had been exposed at the surface for 48 hours, the thicker whole oil mass showed loss of compounds below nC_{10} and nC_{11} (Figure 4-20C). This is equivalent to evaporative loss of most if not nearly all lower boiling components contained in TBP distillate cuts up through cut 7 (BP 282-304°F; Payne, et al. 1984a). With the oil in a thicker pool on the ice surface, diffusion-controlled evaporation is believed to predominate simulataneous weathering processes.

The possibility of diffusion-controlled evaporative weathering has been considered during earlier oil weathering investigations (Payne et al., 1981, 1984a). This process was investigated during these cold room wave tank experiments. An overflow of oil, which occurred during a temporary blockage of the seawater drain line, spread to varying thicknesses on the ice surface allowing the investigation of the diffusion controlled process. The oil spread out in a wedge from the point of origin to a final film thickness of less than 1 mm on the ice surface. This entire oil mass was then exposed to a 5 knot wind at an ambient average temperatue of -20°C. After 12 hours of exposure, samples of the less than 1 mm thick oil on the ice were obtained by carefully scraping the ice surface, melting the shavings, and then extracting the water for petroleum hydrocarbon measurements. Depth profiles in the thicker portion
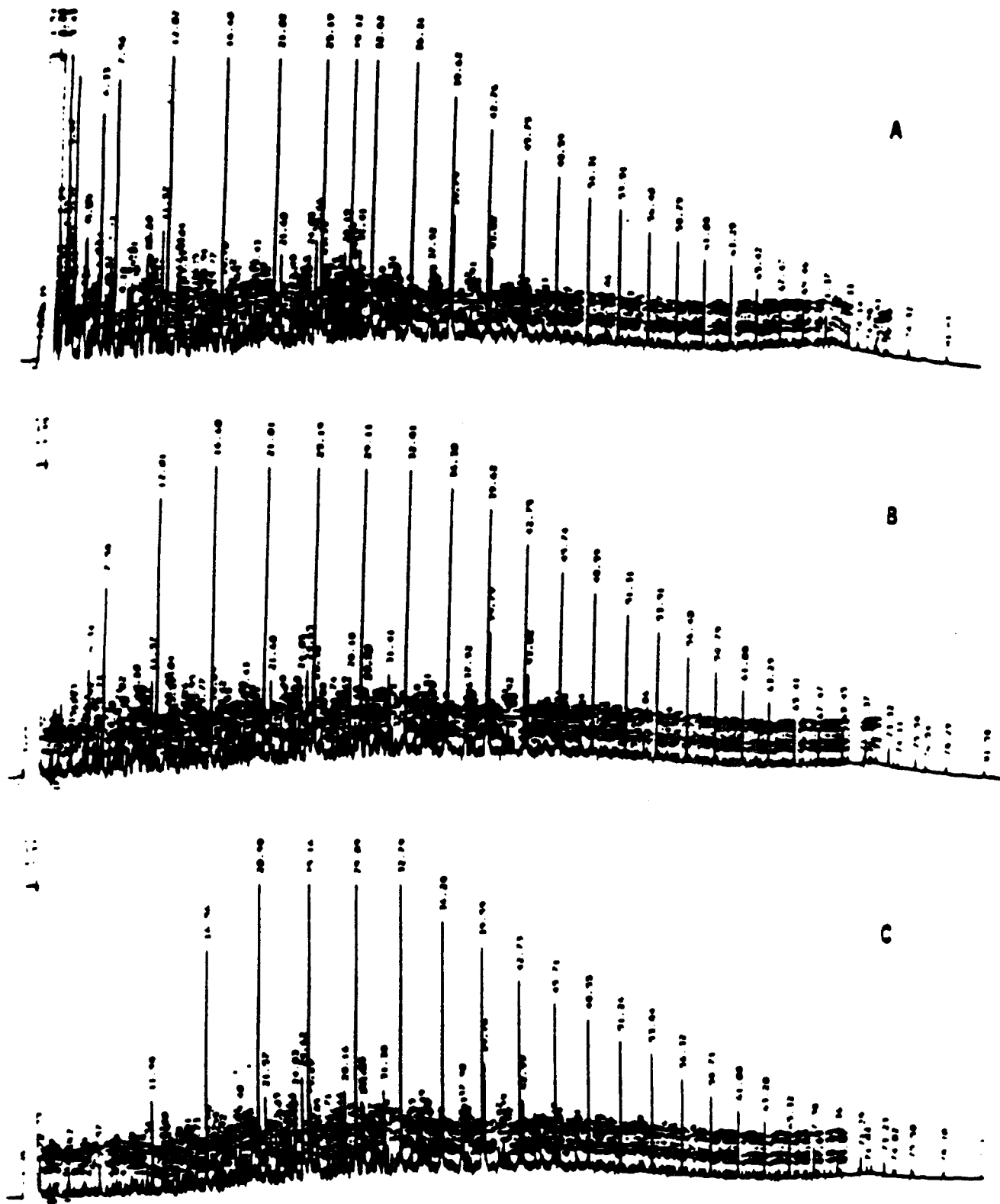
Figure 4-20.--FID-GC Chromatograms of Wave/Ice Tank Oil Samples: (A) fully encapsulated by ice, (B) during upward brine channel migration, and (C) exposed on the ice surface for 48 hours.

244

of the wedged shape oil were also obtained to investigate differential evaporation with depth into the sample. Figure 4-21 presents the gas chromatograms obtained on the samples. As the chromatogram in Figure 4-21A illustrates, compounds with molecular weights less than nC_{14} (B.P. ~480°F) were completely removed within the 12 hour period from the 1 mm thick film. An oil sample obtained with a 2 mm thick film showed loss of compounds only below nC_{12}; B.P. ~420°F (Figure 4-21B). The oil samples at deeper intervals of 4 and 5 mm yielded the chromatograms shown in Figure 4-21C and 4-21D, respectively. In these samples, only components with boiling points below 300-350°F are missing. Clearly, the differential residence time of the lower molecular weight components at depth in the film is established. Thus, in thicker oil pools stranded on ice surfaces, evaporation of the complete mass of oil will be diffusion controlled. The differences in evaporation rates due to different film thicknesses must be considered in the weathering model algorithms. The approach to modeling evaporation from a diffusion controlled slab was presented in the Open Ocean Oil Weathering Final Report (Payne et al., 1984a). A modeling approach of the analogous dissolution from a diffusion controlled slab is described in Section 6.0 of this report. To our knowledge, however, these are the first data that actually demonstrate the diffusion controlled process and verify its importance in accurately modeling oil weathering behavior.

There currently is only a mathematical model which describes the diffusive transport of _specific_ molecular species through a stagnant slab of oil with evaporation at the oil-air interface. This model is not useable for an entire (whole) crude because of two reasons: First the diffusivities of pseudocomponents (used to described whole oil) have never been measured, and second, the actual diffusion-evaporation process results in a moving boundary that has never been incorporated into a model that describes concentration as a function of position. The primary reason for concluding that a diffusion-controlled weathering phenomenon was observed in the experiments described here is that the oil was not uniform in concentration as a function of depth. Therefore, species were transporting due to diffusion to the oil-air interface (no complete mixing).
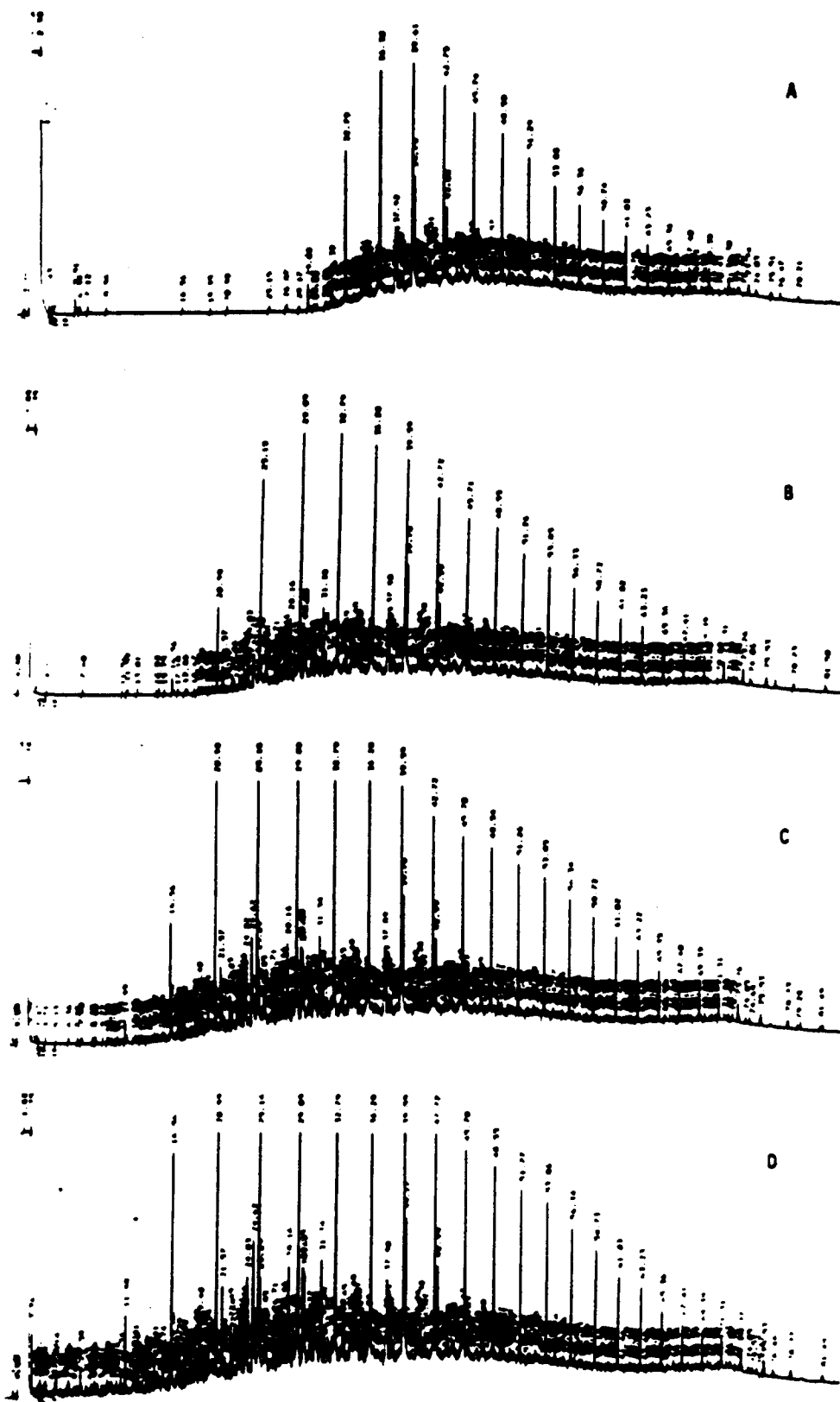
Figure 4-21.--FID-GC Chromatograms of Oil Stranded on the Ice Surface with Oil Thickness of (A) 1 mm, (B) 2 mm, (C) 4 mm, and (D) 5 mm. These samples had been exposed to evaporative weathering under a 5-knot wind at -20°C for approximately 12 hours.

The time-series changes in hydrocarbon composition with the formation of stable water-in-oil emulsions were monitored by collecting and analyzing (FID-GC) bulk oil samples from the oil/water emulsion. Some evaporative weathering of the emulsion had occurred, although most of the lower molecular components were still present in this mixture (Figure 4-22). Comparisons between the aliphatic concentrations in fresh oil, encapsulated oil, exposed oil, and mousse are shown in Table 4-9. Relative to concentrations in fresh oil, significant losses of n-alkanes below nC_{12} were observed in exposed and emulsified oil, and losses of nC_8 through nC_{10} were particularly apparent in the mousse samples. During open ocean oil weathering with Prudhoe Bay Crude oil, comparable stable water-in-oil emulsion formation was not observed until evaporative weathering resulted in much greater losses of the lower molecular weight components (Payne et al., 1984a).

Whole Prudhoe Bay crude oil contains 36% non-distilled residuum which partially comprises surfactants that are important for formation of stable water-in-oil emulsions. Surfactant materials such as asphaltenes, higher molecular weight waxes (n-alkanes), and metalloporphyrin compounds serve to stablize whole water-in-oil emulsions and coat water droplets (Payne and Phillips, 1985). This prevents water/water droplet coalescence and phase separation (for additional data on the chemical and physical properties of fresh and artificially weathered Prudhoe Bay crude please refer to Payne et al; 1984a).

With the rapid onset of mousse formation due to the micro-scale turbulence of grinding grease ice and the ice floes, experiments were undertaken to attempt to quantify the percent asphaltenes and waxes in this emulsified mass. As noted earlier, stable water-in-oil emulsion formation was not observed in the outdoor (ice free) wave tank experiments until significant evaporation and/or generation of surface active materials, by a combination of photochemical and microbial degradation processes, had occurred.
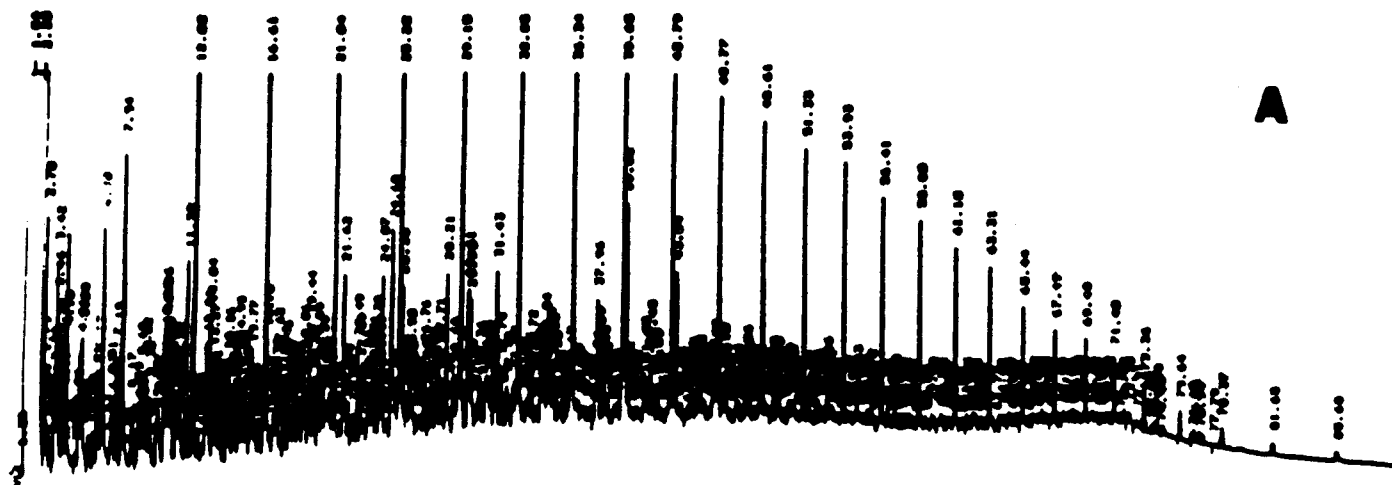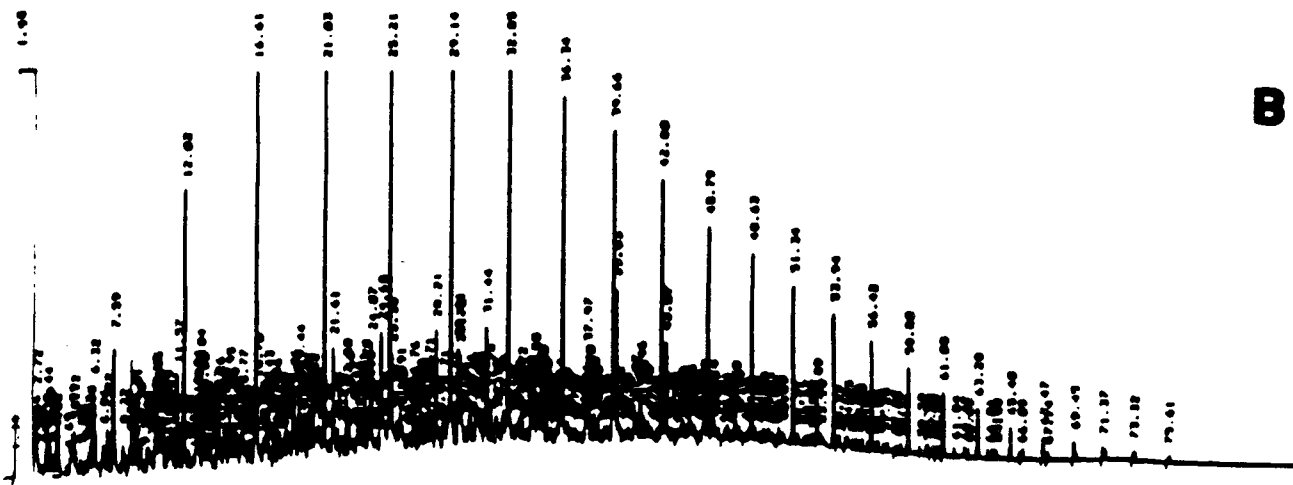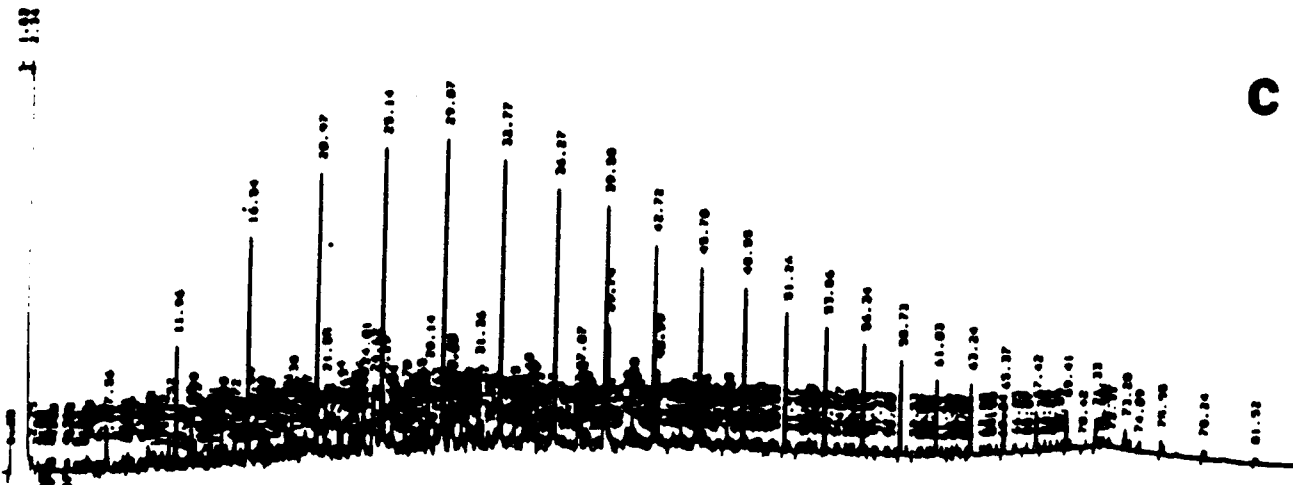
Figure 4-22.--FID-GC Chromatograms of Emulsified Oil Weathering in the Presence of Sea Ice: (A) oil exposed for 32 hours, (B) oil exposed for 57 hours, and (C) subsurface mousse obtained two days after ice breakup.

Table 4-9.--Aliphatic Hydrocarbon Concentrations (μg/g) in Crude Oil as it Weathers in the Presence of Sea ice.

Compound		Oil sample description			
	Fresh	Encapsulated	Exposed 32 hours	Exposed 57 hours[a]	Mousse--2 days after breakup[a]
N-C$_8$	3,670	2,590	432	228	ND[b]
N-C$_9$	5,160	4,520	3,570	2,520	426
N-C$_{10}$	5,680	5,500	3,760	3,640	1,540
N-C$_{11}$	4,520	4,520	3,550	3,840	2,270
N-C$_{12}$	4,960	4,950	4,140	4,760	3,280
N-C$_{15}$	4,490	3,820	3,670	4,460	3,350
N-C$_{17}$	3,630	3,210	3,210	3,820	3,060
Pristane	1,790	1,630	1,660	2,140	1,650
N-C$_{18}$	2,960	2,610	2,620	2,980	2,490
Phytane	1,540	1,490	1,470	1,530	1,410
N-C$_{20}$	2,240	2,130	2,160	2,220	1,950
N-C$_{25}$	1,800	1,420	1,690	1,140	1,400
Total resolved compounds	144,000	127,000	112,000	184,000	70,900
Unresolved compounds	412,000	297,000	309,000	240,000	309,000

[a] Concentrations corrected for water content.

[b] Not detected.

A sample of the stable mousse from the wave tank ice chamber was re-moved and subjected to deasphaltization and dewaxing using the procedures of Bridie et al. (1980). Essentially, dewaxing was completed by dissolving the mousse into a six-fold dilution of methylethylketone:dichloromethane (1:1) at a temperature of -10° to -20°C. On standing for approximately 3 hours the waxes precipitate and can be filtered from the whole crude oil. Asphalts are removed by taking the dewaxed oil and completing a 30-fold dilution in n-pentane at the -10° to -20°C temperature. With this procedure, the percent wax in the weathered mousse from the wave tank was determined to be 4.6% and the asphalts were 7.4% (by weight). In fresh Prudhoe Bay crude oil the wax and asphalt content were measured at 3.9 and 3.7%, respectively. Thus, with evaporative losses of the lower molecular weight components, the relative percent of wax and asphalt in the mousse (compared with the fresh oil) is observed to increase. However, this increase is not believed to be large enough to account for the observed mousse stability, and the rapid onset of a stable emulsion must instead be attributed to the water temperature (-1.7°C) and the micro-scale turbulence introduced by the grinding action of the grease ice crystals.

4.3   CHUKCHI SEA FIELD OBSERVATIONS AND COMPARISONS WITH FIRST-YEAR ICE DURING TANK EXPERIMENTS

During February and March, 1984, the Oil Weathering Program was expanded to include a limited survey of ice structure and behavior in the Chukchi Sea. Helicopter overflights and observations of ice floe behavior and ice growth in open cracks and leads, as well as ice coring for ice salinity determinations and conductivity, temperature, depth (CTD) casts in the Chukchi sea, were performed. The purpose of the field observations and measurements was to facilitate comparisons of ice structure and temperature/salinity profiles observed in the wave tank experiments with actual conditions in first year ice fields. Results from these activities are described in this section.

Three station transects (B, C and D) west of Point Barrow were occupied during this field program (Figure 4-23). The sea ice encountered in the Chukchi Sea was characterized as a mixture of first-year and multi-year ice with fractured ice blocks (rubble fields) and numerous ice ridges (Figures 4-24 and 4-25). In addition, salt flowers similar to those formed in the wave tank at Kasitsna Bay were observed on the ice surface in the Chukchi Sea, and these are also characteristic of the rejection/exudation of brine in newly formed ice (Martin, 1979). Extremely sporadic (intermittent) multi-year ice ridges were characterized (as best as possible) by smoothed surface relief of elevated ridges (>3 m), excessive snow accumulation compared to adjacent floes and pans, and extremely low salinities (~3-5 ppt) where ice samples could be collected. In general, it was not easy to differentiate between first and multi-year ice in the study area, and the characterization was qualitative at best.

During the field observations in March 1984, the ambient air temperature was -38°C. Under these conditions, grease ice and frazil ice formation was observed in numerous open lead systems, along with accumulations of grease ice in both the dead zone and against the ice floes. The presence of the grease ice attenuated the small wind-induced chop within the open leads, and the ice formation sequence was similar to that observed during the previous first-year ice wave tank experiments at Kasitsna Bay (Section 4.2). In addition to the grease ice, hundreds of ice chunks ranging from 15 to 20 cm in thickness were piled up along the leads. These ice chunks were believed to represent one to two days of ice growth, which occurred after the lead first opened. The chunks were then pushed onto the adjacent ice when the lead closed due to differential motion of adjacent pans.

Several ice cores were collected near the open lead system near Station D2 to compare the crystal structure with that of the ice formed in the Kasitsna Bay wave tank. A columnar ice fragment from first year ice growth is shown in Figure 3-2 (Section 3.1). The parallel alignment of the vertically oriented ice crystals is similar to the structure of the columnar ice grown in
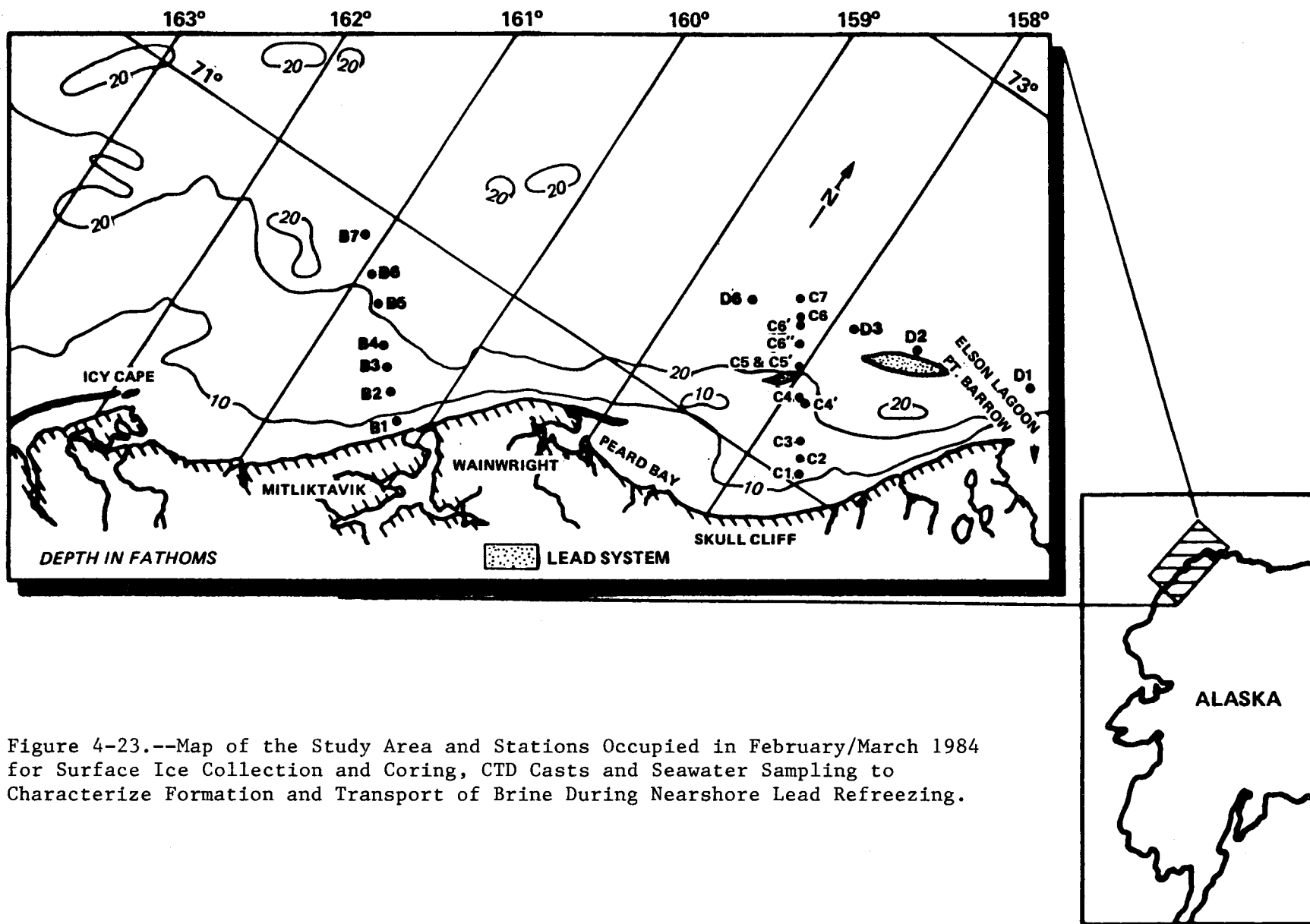
Figure 4-23.--Map of the Study Area and Stations Occupied in February/March 1984 for Surface Ice Collection and Coring, CTD Casts and Seawater Sampling to Characterize Formation and Transport of Brine During Nearshore Lead Refreezing.

Figure 4-24.--Rubble Field of Fractured Ice Observed in the Chukchi Sea During February 1984.

Figure 4-25.--Ice Ridge Adjacent to Large Smooth Pan Studied During Ice Measurements in the Chukchi Sea in February/March 1984.

the wave tank (Figures 4-5 and 4-6 in Section 4.2.1). In the field, however, columnar ice may form to depths from 1 to 2 meters during the growing season (Martin, personal communication).

At many of the station locations CTD casts were taken for tracing subsurface water masses. In addition, ice samples were collected for salinity determinations for comparison with ice surface salinity measurements during the wave tank experiments. Table 4-10 presents salinity data obtained from ice samples collected near Point Barrow in the Chukchi Sea. Ice salinities ranged from 3.5 ^{o}/oo in a columnar ice sample to 45 ^{o}/oo in a thin brine-coated surface ice sample from a new lead. Water samples associated with the ice cores had salinities of approximately 29 ^{o}/oo whereas a sample of surface brine had a salinity of 62°/oo. These salinities were similar to the corresponding measurements obtained from ice, seawater, and surface brine samples collected during wave tank experiments (see Table 4-2).

Sea water salinity and temperature measurements were made at a series of stations from approximately 5 km to 50 km offshore (see Figure 4-23 for Station locations). Salinity data from CTD casts along a transect off Wainwright are plotted in Figure 4-26. The profiles suggest that relatively high salinity waters (>33 ^{o}/oo) are generated from the brine produced during nearshore ice formation. During periods of ice growth in the Chukchi Sea, particularly in nearshore polynyas, salt extruded during frazil ice and grease ice formation may be responsible for localized increases in sea water salinities (Bauer and Martin, 1983; Kozo, 1983). The denser and more saline waters that accompany ice formation subsequently sink to the bottom and result in the near-bottom increases in sea water salinity shown in Figure 4-27. The denser bottom waters eventually may be transported by gravity flow in an offshore direction and accumulate in topographic basins or valleys. A similar brine transport mechanism has been suggested previously by McPhee (1980).

Table 4-10.--Salinities of Various Ice Types Obtained During Chukchi Sea
Ice Investigations.

Field Site #[a]	Depth or Description	Salinity (o/oo)
C-1	10"	11.5
"	12"	7.5
C-2	10"	16.1
"	18"	15.0
"	Water	28.7
C-3	Surface Brine	61.9
"	3"	14.3
"	12"	15.4
C-4	24"	12.5
C-5	Water	29.1
C-6	2"	21.5
"	24"	8.0
C-6*	12"	8.3
"	36"	12.5
C-7	6"	11.0
"	8"	8.3
"	12"	9.0
"	24"	10.2
D-2	Overflow 1[c]	18.0
"	Overflow 2	17.5
D-3	Columnar Ice - 10"	3.5
D-6	Surface Ice	21.0
New Lead[b]	Thin New Ice	45.3
" "	Thick New Ice	14.1
" "	Columnar Ice	4.7

[a]Site # designated by field study according to Lon Bachmeister
[b]Not an official field site
[c]Overflow ice samples obtained at two different locations at site D-2

255

CTD Station #
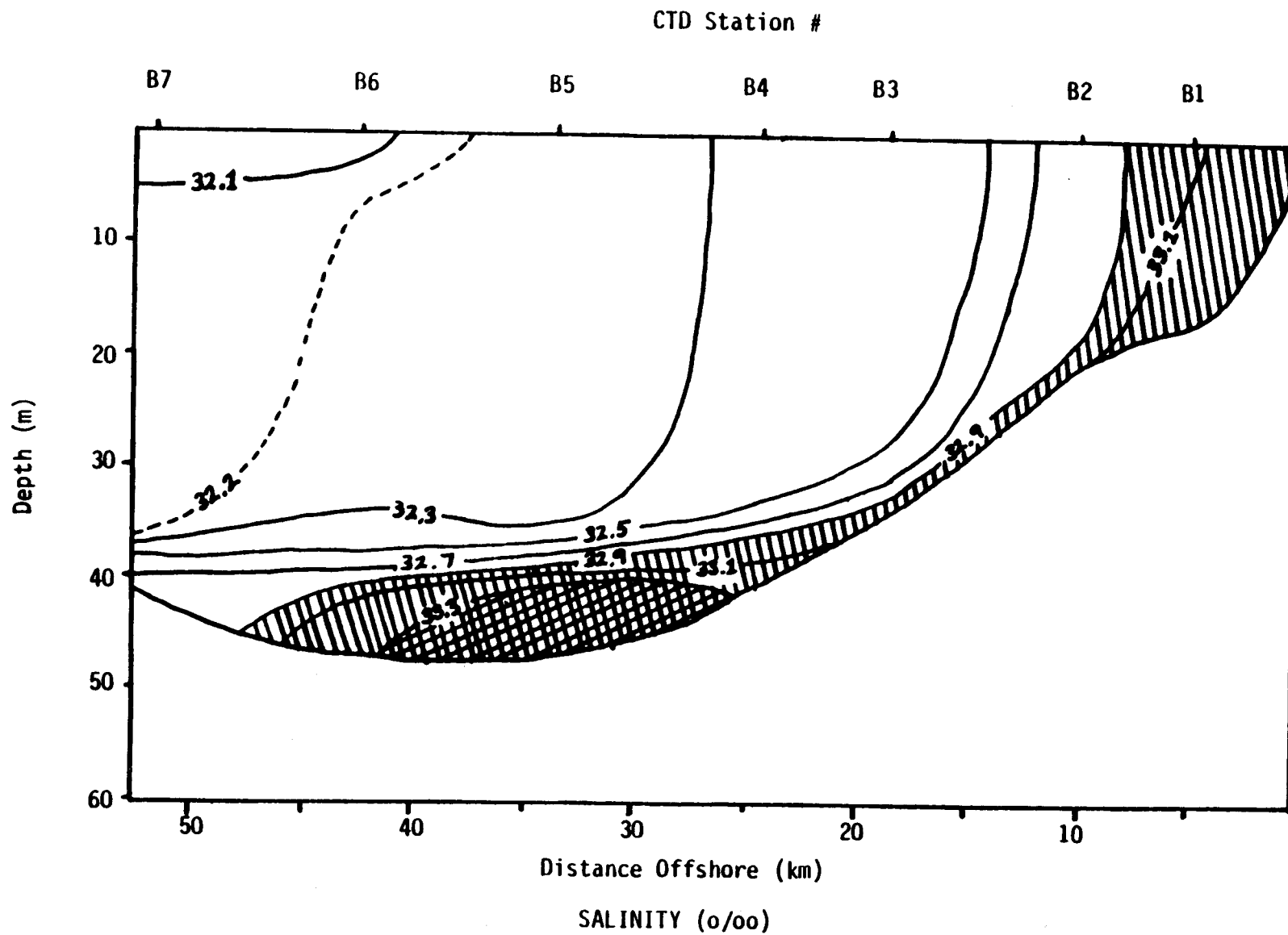
Figure 4-26.—Salinity Section off Wainwright, Alaska from March 1984.
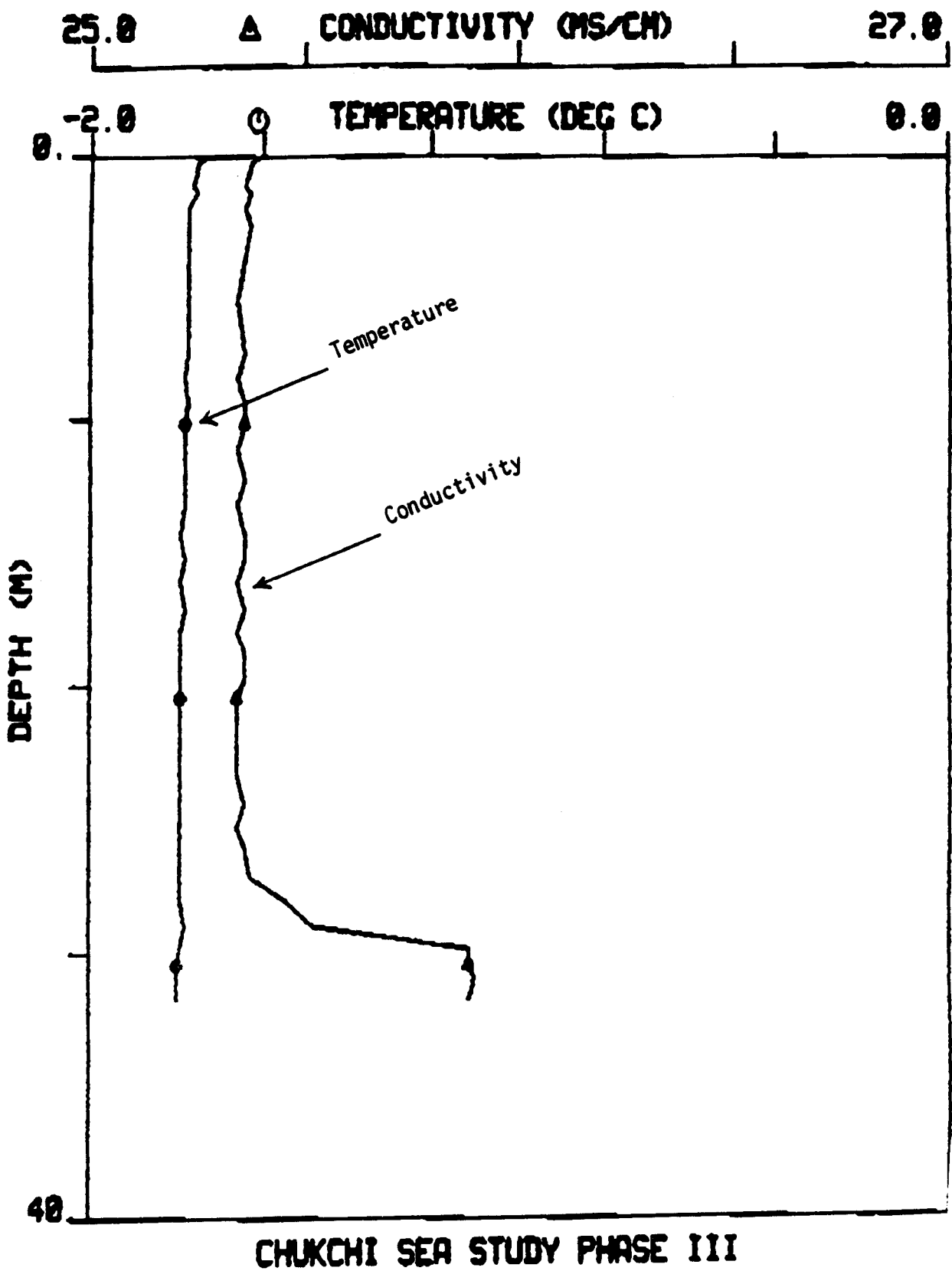
Figure 4-27.—Temperature and Conductivity Profile from Near Station B2, 15 km Offshore. (See Figure 4-23 for station locations.)

4.4   LABORATORY SIMULATED MULTI-YEAR ICE TANK STUDIES

4.4.1   Generation of Multi-Year Ice

The experimental studies designed to investigate and verify the modeled behavior of oil spilled in or under first-year and/or multi-year ice required careful control of a wide variety of environmental parameters. These include the following: cooling and heating temperature conditions (including infrared radiation) to control ice growth and decay; the structure (macro and micro) of the simulated first- and multi-year sea ice; the rates of under ice currents to remove extruded brine generated during ice growth and dispersed oil droplets and dissolved aromatic components resulting from a spill; and the energy regime necessary to generate wave turbulence, which is crucial to both realistic initial formation of frazil and grease ice crystals and the subsequent deterioration of first- and multi-year ice floes/pans during melting and break-up. In the following section, the results of wave tank studies with oil in "pseudo multi-year" ice are considered.

A slightly modified or "pseudo multi-year" ice growth approach was utilized to simulate multi-year ice that has undergone more extensive brine channel drainage. A methodology was designed wherein simulated first-year ice was grown to a depth of 10 to 18 cm (including columnar ice) and then subjected to a partial thaw to induce brine channel drainage. The solid ice sheet was then mechanically broken into 50 cm by 75 cm blocks and subjected to additional wave turbulence for periods of up to 2-4 hrs, which allowed for further removal of salt brine from ice surfaces. With continued wave turbulence, the air temperature was intentionally reduced to -30°C to allow refreezing, with ridging and rubble field formation occurring during ice growth in the new leads. This process was repeated several times, creating a small scale simulation of the broken rubble fields, ice ridges, and multi-year floes that were observed in the Chukchi Sea (Section 4.3). Ice and seawater samples were collected for salinity determinations and for comparisons with field observations. The following section describes the processes and events and the data collected during the pseudo multi-year ice experiment. Table 4-11

presents a chronology of the times and dates of significant events that occurred during this experiment. Table 4-12 presents values for salinities of simulated first-year and multi-year ice, brine and seawater measured during the experiment as described in the following sections and outlined in Table 4-11.

The cold room and wave tank were basically configured as described in Section 4.1 for oil/first-year ice experiments, with the exception that a heat exchanger was installed on the tank discharge and incoming seawater lines so that flow-through seawater conditions could be maintained at higher flow rates without excessive strain on the cooling system and/or undesirable heating of the seawater in the wave tank. A nominal flow of 2.5 to 3 liters/min of -0.5 to -0.8°C seawater was supplied to the tank to simulate desired under-ice currents of 0.01 cm/sec. This flow rate resulted in one tank volume turnover (1870 liters) approximately every ten hours.

Following an initial cooling of the seawater temperature to -1.8°C, frazil platelets ranging from 1 to 5 mm across and 0.1 mm thick formed uniformly throughout the tank to a depth of 1 m. After an additional 1.5 hrs, slush ice had accumulated over the entire tank surface. Three and one-half hours after the first frazil ice was noted, the slush ice was approximately 10 cm thick over most of the tank, and three 20 cm diameter pieces of pancake ice formed near the dead zone at the quiet end of the tank. Wave generation was terminated at that time, and the surface ice was allowed to congeal and freeze in place.

Later, the entire ice surface was completely frozen, with the exception of several brine pools (several mm deep) with salinities of 56 °/oo (Table 4-12). These pools eventually evaporated and were replaced by salt flowers there and elsewhere in the tank. Approximately 24 hours after the first appearance of frazil ice, the solid slush ice surface was 14 cm at the vertical viewing window, and the first growth of columnar ice was noted. The air, ice, and water temperature profile was similar to that shown in Figure 4-4 for first-year ice.

Table 4-11.--Chronology of Times and Dates of Significant Events Occurring During the Oil/Multi-Year Ice Wave Tank Experiments.

Date	Time	Flow Rate (l/min)	Significant Event Description
3/15	1720	-	Initiation of cool down
"	2250	3.2	Frazil ice throughout tank
3/16	0020	2.8	Grease ice 3" thick
"	0225	2.4	Wave generation terminated
"	1915	3.5	Appearance of salt flowers
"	2300	3.2	First appearance of columnar ice
3/17	1315	3.0	4" grease ice + 1 1/2" columnar ice
"	2230	2.8	Initiation of thaw
3/18	0930	-	4" grease ice + 2" columnar ice - brine pools
"	2000	-	Initial brine channel formation
3/19	1410	-	Wave turbulence initiated - ridge system established
"	1440	-	Turbulence terminated - cool down initiated
3/21	1100	2.5	Open leads and pressure ridge formed
"	1720	-	Open leads refrozen 1/4 to 1/2"
3/22	1440	2.4	700 ml PB Crude Oil Spill
3/23	0240	3.0	1/2" columnar ice under oil
"	1440	2.5	1 1/2 - 2" columnar ice under oil
3/24	0030	2.5	Initiation of thaw
3/25	1215	2.6	Initiation of turbulence
3/26	0210	-	Brine channel oil migration
"	1500	-	Emulsification of oil - degradation of multi-year ice

Table 4-12.—Salinities During an Oil Spill in Multi-Year Ice Chamber Experiment.

Sampling Time		Sampling Description	Salinity (%)
Date	Time		
3/15/85	2200	Tank Seawater	30.9
"	2250	Frazil Ice	21.9
3/16/85	0040	Grease Ice	17.7
"	1030	Top 1 cm Ice Surface	56.0
3/17/85	1600	Tank Seawater	30.5
"	"	Top 1 cm Ice Surface	59.3
"	2300	Salt Flowers	100.0
3/18/85	1045	Tank Seawater	30.2
"	"	Pooled Surface Brine	57.5
"	1930	Columnar Ice Under Ridge	10.1
3/19/85	2200	Tank Seawater	29.1
"	"	Grease Ice from Open Lead	24.4
3/20/85	1200	Surface of Refrozen Lead Ice	60.3
3/21/85	1300	Tank Seawater	30.4
"	"	Ridge Frozen into Lead	4.3
"	"	Columnar Ice from Ridge System	1.8
3/22/85	2030	Tank Seawater 6 hrs Post Spill	31.6
3/23/85	0240	Tank Seawater 12 hrs Post Spill	31.1
"	1440	Tank Seawater 24 hrs Post Spill	31.0
3/25/85	1100	Tank Seawater 3 days Post Spill	30.3
"	"	Columnar Ice from Ridge System	8.5
"	1630	Tank Seawater 4 hrs Post Break-up	31.0
3/26/85	0100	Tank Seawater 12 hrs Post Break-up	29.2
3/28/85	1200	Tank Seawater 3 days Post Break-up	29.7
"	"	Multi-Year Ice	8.9

Twenty-four hours of additional columnar ice growth was allowed until a 5 cm layer had accumulated beneath 10 cm of frozen slush ice at the vertical window. At that time, the cold room was allowed to stand open overnight at -5 to -2°C to initiate the first "Spring" thaw (Table 4-11). Later, a quartz infrared heater was installed 1 m above the tank and the ice was illuminated for several hours while the room temperature was maintained at -5 to -10°C to initiate brine channel formation and drainage.

A 15 cm by 45 cm chunk of ice was physically cut from the center of the tank and two similar sized pieces were pryed from the tank walls to create a 45 cm wide "lead" across the entire width of the tank. The remaining slush/columnar ice in front of the paddle was loosened. Two large blocks of ice, which had been removed from the surface, were forced by hand under the leading edge of the remaining fast ice in the tank to form a ridge system at that end of the tank.

A subsequent freeze and ice breakup cycle was performed to build up the simulated "multi-year" ice ridge keel system. In so doing, surface- and under-ice relief was generated with blocks of older ice which had now undergone two and one-half freeze/thaw cycles providing appropriate ice conditions for the oil release experiment. The surface ice relief exceeded 20 cm where ridging occurred, and the under-ice relief encompassed a range of 8-35 cm. The newly opened lead system was refrozen to a depth of 4-6 cm in preparation for the spill event. Most of the ridge surfaces and keels were fairly smoothed over due to the various freeze/thaw cycles. The new ice in the lead was 4 cm thick and no longer plastic. Salt flowers were abundant in the newly refrozen lead, but did not occur elsewhere because the remainder of the ice field had undergone numerous freeze/thaw cycles and surface rinses which lowered salinities considerably (Table 4-12). A 0.3 meter wide lead, approximately one meter long, was cut from side-to-side at the paddle end of the wave tank, and a large chunk of refrozen grease ice was left in the center of the intended experimental lead.

4.4.2   Oil/Multi-Year Ice Interactions

A measured volume of 750 mls of fresh Prudhoe Bay crude oil was added to the experimental lead using a funnel and Teflon tubing to prevent inadvertent spillage onto adjacent ice surfaces.   Oil was released at a depth of approximately 2.5 cm below the water surface in the open lead, and little of the oil was injected underneath the ice surface. The oil spread to form pools in small patches, approximately 4-5 cm in diameter on the quesant, open water in the lead system, and the total volume introduced was measured by difference. After the initial addition, no oil was visible on the under-ice surface and, likewise, no oil was observed on the under-ice ridges.   The seawater temperature was -1.7°C at the time of the spill, and the cold room temperature was maintained at -3 to -8°C.

Water samples were obtained by pumping 20 liter volumes through a small hole drilled in the ridge system between the nearshore rubble field and end of the tank ridge zone through a 293 mm diameter glass fiber filter in a Millipore stainless steel filter unit. This procedures allowed differentiation of dispersed and dissolved aromatic hydrocarbon components in the water column. Water samples were collected at 0, 1, 3, 6, 10, 12, 24, 48 and 72 hours following the initial spill event.   After three days a break-up event was initiated and additional water samples were collected at 1, 4, 8, 12, and 24 hours and then again at 3 days and 5 days post-break-up. As in the oil/first-year ice experiments, oil samples were collected at various intervals to measure rheological properties, including oil/air and oil/water interfacial surface tension, oil viscosity, and percent water uptake due to water-in-oil emulsification.

Approximately 50 minutes after the spill, the paddle was turned on in very short bursts to simulate the pumping action of a closing lead system. With the first 3-4 cm wave, the oil was observed to wash onto the ice surface adjacent to the lead where it was trapped in the 3-5 cm ice rubble, chips of columnar ice, and around the base of small (5-8 cm) ridges in the upper ice surface, such that an estimated 3-5% of the oil was prevented from returning to

the lead. As the paddle went through a complete revolution and seawater was also deposited on the upper ice surface, oil was observed to spread out in a colored sheen on top of the ice floe adjacent to the paddle. Where standing water was present, the oil flowed evenly over the ice. With a complete paddle revolution, oil was also observed to wash over the nearshore ice in the fast ice zone and pool in areas adjacent to the vertical window and in ridge and rubble ice structures approximately 50 cm from the open lead. At this time, additional oil droplets were noted impinging on the under-ice surface of the ridge systems adjacent to the vertical window. Oil that was not trapped in surface ice depressions flushed slowly backwards towards the open lead system. The horizontal extent of the oil flowing over the ice was limited to the 50 cm closest to the lead opening by the presence of a 5-10 cm ridge system of blocks which prevented further spreading. The ice edge adjacent to the paddle was then positioned to trap the oil in the lead system and prevent it from running back to the paddle area and behind it. As a result of the several "ice push" incidents, there was a considerable amount of oil forced up onto the near lead refrozen ice. Most of this pooled in areas up to approximately 3 mm thick.

On the underside of the smooth ice and ridge keels adjacent to the experimental lead, several very small oil drops could be observed on the ridge side closest to the paddle turbulence. These impinged as small droplets ranging in size from barely visible to up to 2 millimeters. The average size of most droplets was about 1 millimeter in diameter or slightly smaller. In an effort to drive a slightly larger quantity of oil under the ice ridge system the paddle turbulence was again initiated and pulses approaching 1/2 cycle were used. These pulses caused a considerable volume of oil to be washed over the ice surface, and a small volume of the oil (estimated 5-10%) was observed to disperse under the ice surface and impinge on the under-ice ridge system. Considerable amounts of the oil were washed on the upper ice surface nearly to the first ridge system 50 cm from the experimental lead. However, considerable amounts of oil still drained back into the open lead system.

Approximately 1-1/2 hours after the initiation of the spill, most of the oil, which had been in the swash zone on the fast ice immediately next to the lead had been washed off and returned to the oil pool in the open lead. There was still approximately 200 or 250 mls of oil stranded on the ice surface, which was not subject to drainage into the lead system, and these pools were allowed to remain to monitor evaporation weathering. Approximately 2 hours after the initiation of the spill, the compressor unit was turned back on to initiate a partial re-freeze. An estimated 90% of the open lead was covered by a thin film of oil.

During collection of the 3 hour water sample, the oil in the refrozen lead system was on a thin layer of freshly growing ice, estimated by penetration with a syringe to be about 1 or 2 millimeters thick. Under these conditions with limited direct water contact, the potential for addition dissolution of hydrocarbons was clearly minimized. Oil covered 80-90% of the experimental lead system, and in areas where oil did not coat the lead system, ice formed to a depth of approximately 1-3 millimeters. Freezing under the oil, was allowed to continue for at least another three hour period. At that time, ice thicknesses directly under the oil and in the open areas adjacent to the oil were examined to see if the oil imparted some differential rate of ice growth in this system. As suggested by Ross, et al. (1977), Walker (1975) and Wilson and Mackay (1986), any difference, if noted, was not significant under the calm test conditions examined in this experiment.

Six hours after initiation of the spill, most of the thicker oil in the lead system had been undergrown by 3-7 millimeters of columnar ice. The oil itself set up as a viscous film which pooled on the ice surface, and the oil thickness was measured to be 1 to 3 mm thick. Deeper pools of oil were observed on the stranded ice floe of grease and columnar ice intentionally frozen in the center of the lead. Elsewhere, oil which had been stranded in pools on the fast ice adjacent to the vertical window and ridge system appeared unchanged, although it had weathered by evaporation over the 6-hour period since all turbulence had been terminated.

In certain areas, stranded oil pooled to an estimated depth of 1 to 2 mm, and chips of broken ice, which had been generated during the breakout events and deposited in the "swash zone", had collected oil coatings over 90% of their surface. Larger 8 to 10 cm pieces of ice were unstained although they were coated with oil around the base. Several pools of oil formed higher on the fast-ice surface, on the lee side of several ridge systems. These pools which had been driven onto the ice surface during the wave turbulence approached 1 cm in thickness in several places. The washing effect of waves caused oil on the smoother areas to be removed almost completely with each wave pulse. During water flooding the oil tended to float off the ice into the open lead system and was only later caught by the capillary systems of the ice after water had drained through. Surprisingly, the stranded oil was very fluid to the touch despite the -23°C temperature conditions, and it did not exhibit a crust or more viscous surface layer.

Based on observations of oil behavior during the first 12 hours after the spill, it was noted that the oil floating on the water surface behaved very much like slush ice. It was herded by the wind from the refrigeration system into quiet zones against ice floes. Then under varying conditions of light wind, the oil spread out to some uniform thickness (1-5 mm) controlled by the volume spilled, the viscosity of the oil, and the area of the lead system available. Once this spreading occurred, the oil then cooled rapidly and with wave dampening due to the higher oil viscosities at ice formation temperatures, columnar ice growth then occurred beneath it. Modeling such conditions should be possible in that the oil could be considered as a diffusioncontrolled slab with no turbulence or diffusive mixing allowed. The only parameters required to model such a system would be the area of the lead and the volume of the oil spilled.

At this point in the experiment, it was apparent that three separate oil-weathering scenarios could be examined. The first was oil spilled into a refreezing lead system under calm conditions where grease and columnar ice soon formed beneath the oil surface. In this instance, the oil weathers by evapora- tion only as a diffusion controlled slab, as if it were spilled on top of solid

266

ice. The second case was oil spilled beneath the ice surface, where it was subject only to dissolution weathering before being encapsulated by additional ice growth (as considered during the oil in first-year ice spill scenarios in Section 4.2 of this report). Finally, although it was not occurring at the time, it was clear that the experiment could be modified by initiating a gradual thaw to evaluate conditions where oil was spilled into a decaying older pack-ice or multi-year ice field in which ice would break-up and decay due to wave turbulence and warming (air and water) conditions.

Very little additional change or activity was noted in the pooled oil after the lead froze over, so to investigate oil weathering behavior during the break up of older pack ice, a break-up event was initiated 3 days after the oil spill. The first paddle surge resulted in a water wash over the oil-covered refrozen lead system. Some of the oil on that lead system immediately started flowing from the edges of the refrozen lead. Oil then was washed from the refrozen lead system onto the swash zone of the fast ice where the thicker portions of oil remained fairly intact. The oil was still amazingly fluid and was observed to flow smoothly over the ice surface, spreading out in bands that were dark brown in color; no colored sheen was observed at the initiation of break-up. Greater than 98% of the oil which had been on the refrozen lead was eventually washed from its surface within five to seven minutes of the start of wave turbulence. All of this oil was observed to flow back and forth with each passing 3-5 cm wave onto the adjacent fast ice front. With continued paddle turbulence, oil droplets were forced beneath the fast ice surface where they impinged on the skeletal layer of the columnar ice under the ice surface. Much of the oil washed off the upper swash zone of the fast ice and into the backwater area immediately adjacent to the vertical windows. Oil floated on the stranded water surface as the seawater filled in and ran among the ridge systems frozen in the blocks of columnar ice associated with the simulated "multi-year" ridge buildup.

After the majority of oil was removed from the refrozen lead, where it was originally released, pockets of oil droplets (up to one cm in diameter) could be observed still frozen in the ice. Evidently these small volumes of

oil were trapped in columnar ice during the downward ice growth phase. The contribution of these trapped oil droplets was estimated to be much less than 1% of the total volume added to the tank.

Within 20 minutes of the onset of surface wave turbulence, the oil which had previously been stranded in the swash zone eventually was washed clear and onto the water surface. There was evidence of small pockets of oil that had frozen into deeper cracks in the swash zone, but these were not yet affected. The entire under-ice surface was coated with millimeter to 5.5 cm diameter oil droplets (Figure 4-28) within one hour of the onset of 4-6 cm wave turbulence. Oil which washed from the lead area accumulated in small pools in the ridge zone and on the under surface of the ice. Some oil migrated up through the columnar ice system. Also present under the ice were chips of grease and columnar ice blocks of 2-8 cm diameter, which broke away from the main stationary ice body and were forced under the fast ice by the action of the wave turbulence. With each passing wave, oil appeared to be forced into and through the under-ice capillary system to the point that it had penetrated the brine channels and the skeletal layer by as much as 3 or 4 millimeters.

Over 90% of the oil released in the tank eventually impinged on the bottom of the ice. It is possible that this behavior could also occur with waves breaking against larger pack- or multi-year ice pans, not just on shorefast ice. That is, larger pans with diameters greater than 10 meters would have sufficient size and momentum associated with them that wave and current turbulence could tend to wash slightly over and under their edges if surface and subsurface relief was not too extensive. Such wind and current induced under ice oiling was noted in the Bouchard #65 spill in Buzzards Bay (Arctec Inc., 1977, and Deslauriers et al., 1979) under pack ice during the Kurdistan spill in Cabot Straight (C-Core, 1975) and in a spill of No. 6 fuel oil in the Gulf of the St. Lawrence River, Canada near Matane, Quebec where the slick was driven by winds across open water only to become intrained within a shoreline field of grease and pancake ice (Wilson and Mackey 1986). Smaller floes on the other hand may tend to ride over waves or swells with less turbulent interaction such that less oil may be trapped beneath then. With

Figure 4-28.--Underwater Photograph of Dispersed Oil Droplets Entrained in the Under-Ice Ridge Keel System Nearest the Newly Opened Lead (Vertical Window) 5 Minutes after the Introduction of Quarter-cycle Paddle Pulsed Turbulence During the Breakup Event.

such turbulence under larger floes, any submerged oil (if present) could be subject to dissolution and not evaporation weathering.

Time-series measurements showed that oil deposited earlier beneath the ice (immediately after the spill) had migrated 3 or 4 millimeters into the columnar ice structure. Later arriving oil was deposited as emulsified droplets with higher viscosities.. With continued thawing these oil droplets then moved through the columnar ice until they reached the angular ridge systems imbedded in the ice earlier during the ridge formation and multiple re-freezing process. At this point, the oil was subject to differential entrapment and migration at different angles into the ridge system where columnar ice directions were no longer vertical. With continued thaw, this material would be released to the water column, although it would be delayed for some time when the migrating oil interacts with columnar ice with a different crystal structure orientation due to freezing of blocks and chunks of ice in a random orientation during multi- year ice ridge formation.

4.4.3 Compound-Specific Partitioning, Whole Oil Droplet Dispersion and Oil Phase Chemistry

Figure 4-29 presents flame ionization detector gas chromatograms obtained on representative oil samples from the surface of the refrozen lead and oil pooled on the multi-year ice floes as a function of time. Figure 4-29A is the time zero starting crude oil, which is characterized by even and odd n-alkanes from nC_7 through nC_{32} along with a wide variety of other resolved components in the KOVAT INDEX range of 700 to 3200. Evaporative losses of compounds below nC_{10} represented the major weathering process during the 48 hours following the spill (Figure 4-29B). Break-up of the refrozen lead containing most of the oil, then re-injected the partially weathered oil into the water column. It should be noted that although many of the lower molecular weight compounds appear to be lost by evaporation, there were still sufficient concentrations of many mono-cyclic aromatics such as toluene, o,m,p-xylene and ethyl-benzene that dissolved hydrocarbon levels in the water column were elevated one hour post-break-up (e.g. see Table 4-13). The final chromatogram shown in Figure 4-29C is of a surface oil sample obtained 4 days post-break-up. At this

270
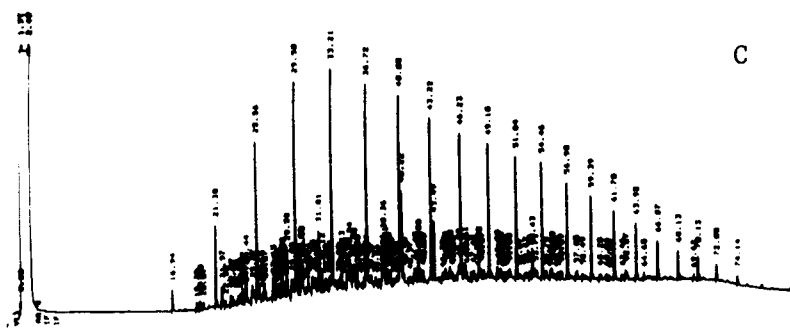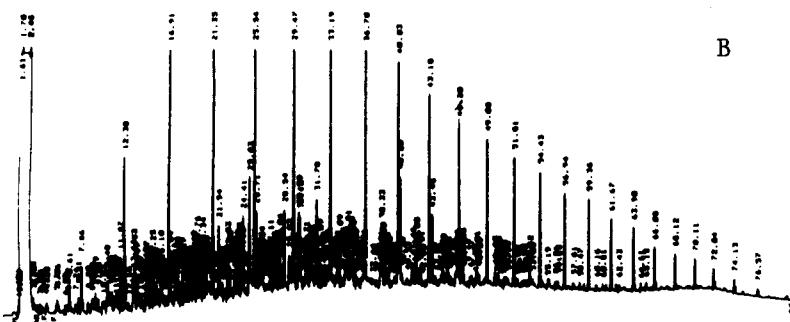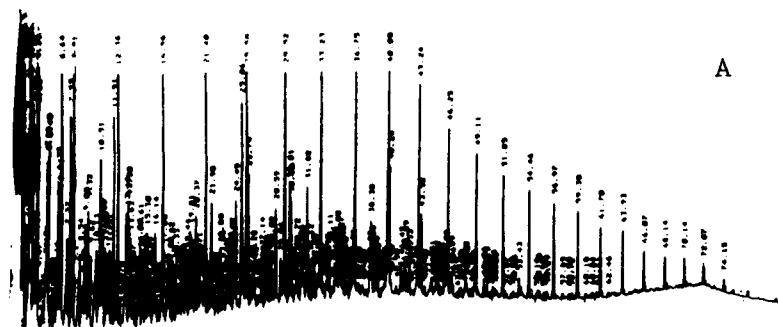
Figure 4-29.--GC-FID Chromatograms Depicting Prudhoe Bay Crude Oil Spilled in Multi-Year Ice: (A) time 0 (prespill), (B) 48 hours post spill (surface of refrozen lead), and (C) 4 days post breakup.

271

point the oil had weathered considerably; it had undergone moderate water-in-oil emulsification (to be discussed later) and a combination of evaporation and dissolution losses had removed all compounds below nC_{11}.

Figure 4-30 presents FID gas chromatograms for the filtered (dissolved) whole seawater extracts obtained at several time points throughout the experiment. Chromatogram 4-30A presents a time zero pre-spill blank, and is characterized by a few low level compounds intrinsic to the seawater system of Kasitsna Bay plus an internal standard. Chromatogram 4-30B shows those dissolved aromatic hydrocarbons present 3 hours after the spill. At this time, many lower and intermediate molecular weight compounds through the alkyl-substituted naphthalenes are present in the seawater, despite the fact columnar ice was already forming under the oil pooled in the refreezing lead. Several wave pulses immediately after the spill distributed dispersed hydrocarbons beneath the ridge system, but subsequent columnar ice formation effectively separated the surface oil from the water column. The continued tank volume turnover every 10 hours cleansed the water column of these lower molecular weight aromatics, such that concentrations of all contaminants had been reduced significantly 3 days post-spill (Figure 4-30C). Figure 4-30D shows the chromatographic profile of dissolved aromatics measured in the water column one hour post-break-up; at this point the oil had undergone significant diffusion-controlled evaporation weathering while stranded in above-ice pools in the lead system. Nevertheless, dissolved aromatics were released when oil droplets dispersed into the water column and impinged on the under-ice surface. This significant dissolved aromatic hydrocarbon pulse presumably reflects the increased surface area due to the 6-10 cm wave induced formation of less than 1 micron to 1 millimeter sized oil droplets which coated the entire under-ice surface. Thus, even though many lower molecular weight compounds had been removed by evaporation, significant concentrations remained to allow for an elevated concentration of these aromatics immediately after the break-up event. Finally, chromatogram 4-30E shows the residual higher molecular weight compounds still remaining in the water column five days after the break-up. Notably, the chromatogram is characterized by naphthalene, 1- and 2-methyl-naphthalene, and alkyl-substituted naphthalenes and phenanthrenes.
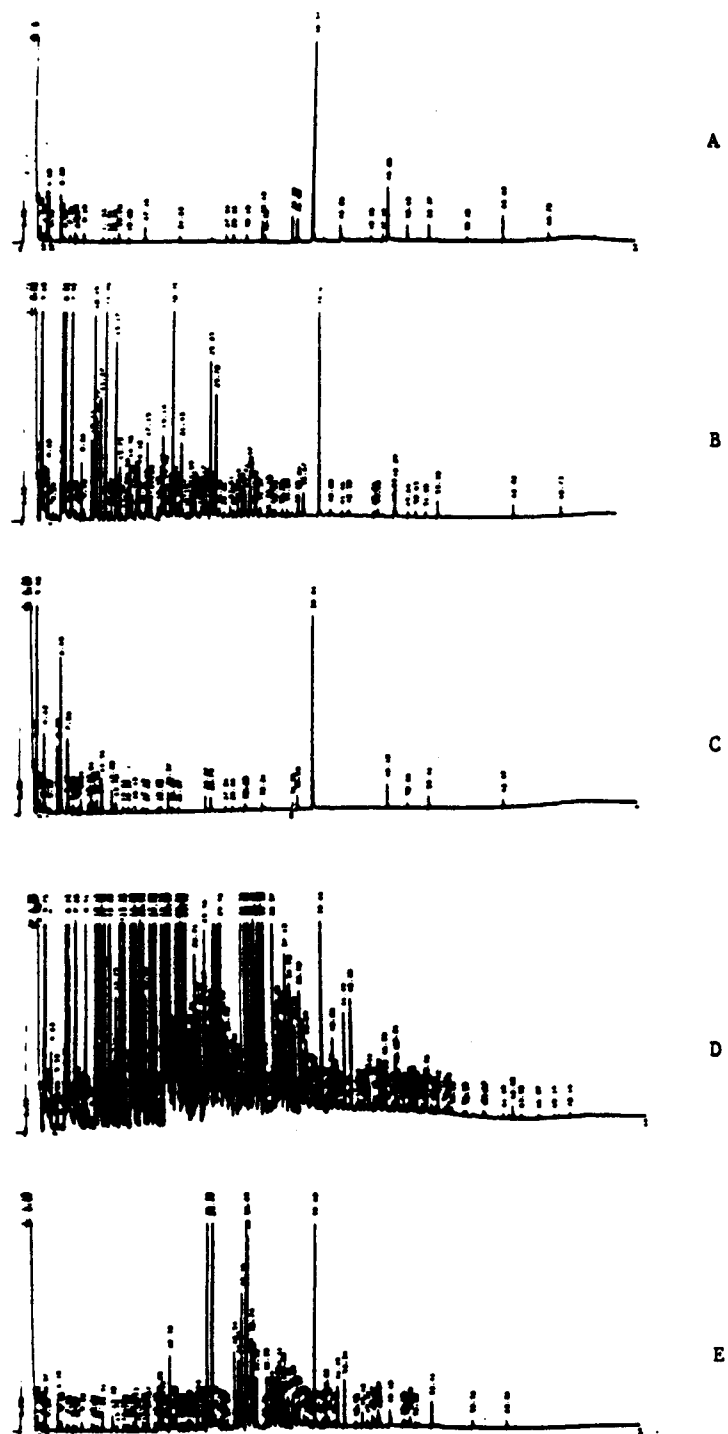
Figure 4-30.—GC-FID Chromatograms of Extracts of Seawater Obtained During the Oil/Multi-Year Ice Interaction Experiment: (A) time 0 (prespill), (B) 3 hours post spill, (C) 3 days post spill, (D) 1 hour post breakup, and (E) 5 days post breakup.

273

Summary concentration profiles of individual and total aromatic hydrocarbons in the water column are presented in Figure 4-31. Specifically, Figure 4-31A shows the sum of the total resolved and unresolved complex mixture (UCM) compounds in the dissolved fraction versus time during the spill event. The total resolved compounds, and several lower molecular weight aromatics including toluene, o,m,p-xylene, and ethylbenzene (i.e., Figure 4-31B and Figure 4-31D), displayed elevated concentrations in the water column immediately after the spill event. The total resolved plus unresolved complex mixture compounds in the first to second hour after the spill reached concentrations of approximately 40 micrograms per liter. Not surprisingly, the majority of these compounds were lower molecular weight mono- and dicyclic aromatics. Toluene was present at the highest concentration, approaching 12 micrograms per liter within 2 hours of the spill.

Within 3 to 6 hours after the spill event (Figure 4-31) concentrations of these compounds declined rapidly with the onset of columnar ice formation, under the surface oil slick, which effectively decoupled or removed the source of hydrocarbons from the water column. Thus, by 24 hours after the spill, most of the lower molecular weight compounds had been removed from the water column by subsurface advection. When the break-up event occurred, the concentrations of several lower molecular weight aromatics remaining in the oil (such as the xylenes, C_3-benzenes, and 2-methylnaphthalenes) were still high enough in the oil such that concomitant water column concentrations still exceeded the initial concentrations of these compounds in the water column by a factor of 3 to 5. The concentrations of dissolved toluene at least equalled the initial spike levels measured immediately after the spill. The dicyclic, higher molecular weight aromatics, naphthalene, 1-methylnaphthalene, and 2,6-dimethylnaphthalene, with their higher m-values were not present in the water column immediately following the spill event. It was only after the break-up event and the introduction of wave turbulence that concentrations of these compounds reached substantial levels. Table 4-13 presents time-series concentrations of each of the resolved aromatic hydrocarbons in the water column following the spill and break-up events. The data follow the same general pattern exhibited in Figure 4-31; with the formation of columnar ice

274
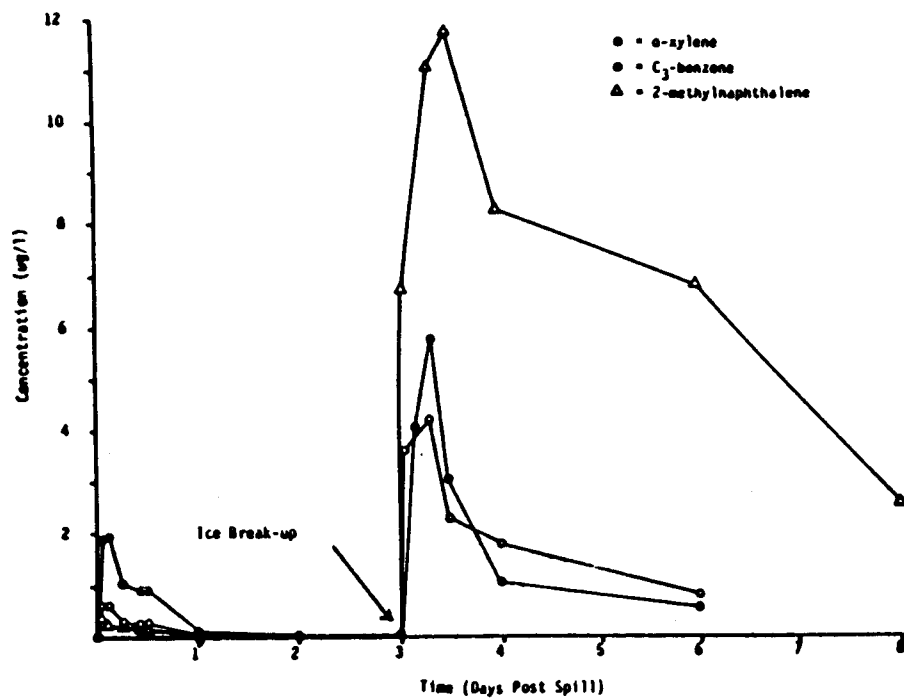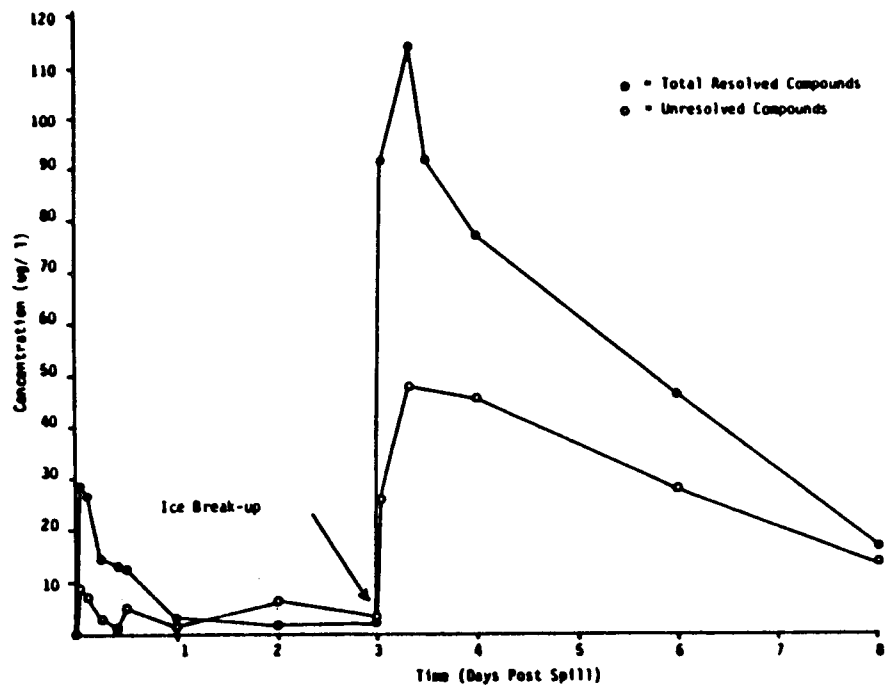
Figure 4-31.--Selected Dissolved Hydrocarbon Concentrations versus Time
from an Oil Spill in Multi-Year Ice.
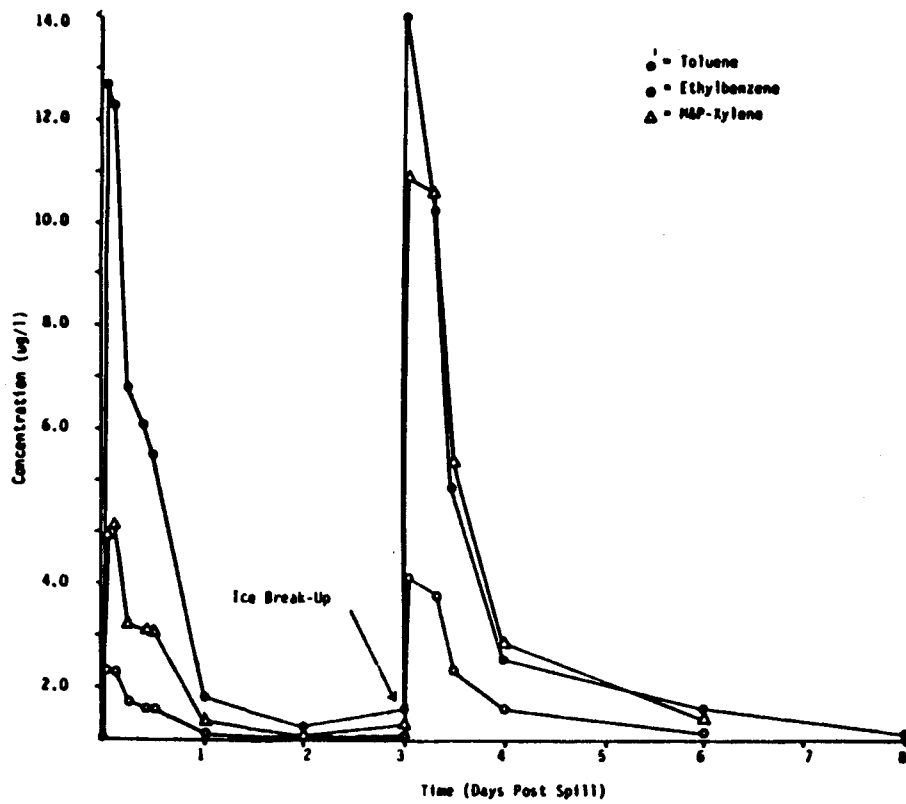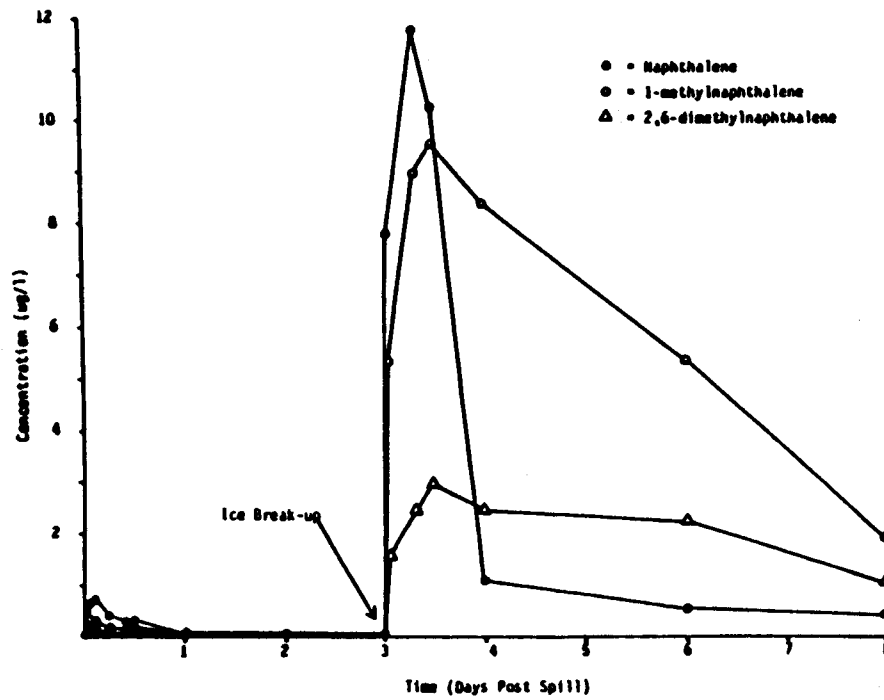
Figure 4-31.--(Continued)

276

Table 4-13.—Dissolved Hydrocarbons from an Oil Spill in Multi-Year Ice.

| | Concentration (ug/l) | | | | | | | | | | | | | | |
| | Time Post Spill | | | | | | | | Time Post Break-up | | | | | | |
Compound	1 hour	3 hours	6 hours	10 hours	12 hours	24 hours	48 hours	3 days	1 hour	4 hours	8 hours	12 hours	24 hours	3 days	5 days
Toluene	12.7	12.3	6.72	6.07	5.50	.839	.228	.654	14.0	9.97	10.3	4.80	1.51	.525	.0577
Ethylbenzene	1.31	1.30	.728	.673	.679	.0974	.0238	.0800	3.13	2.02	2.79	1.35	.651	.232	ND
m&p-Xylene	3.98	4.16	2.26	2.11	2.09	.335	.0687	.278	10.9	7.53	10.6	5.40	1.89	.979	ND
o-xylene	1.90	1.94	1.07	.948	.963	.143	.0250	.102	-	4.08	5.82	3.03	1.09	.529	ND
Isopropylbenzene	.130	.125	.0642	.0656	.0689	ND	ND	ND	.540	.342	.638	.277	.240	.966	ND
n-propylbenzene	.189	.186	.0950	.981	.102	.0223	ND	.0150	1.04	.613	1.10	.557	.505	.221	ND
C_3-benzene	.650	.642	.352	.333	.330	.624	.0145	.0538	3.57	2.35	4.26	2.32	1.83	.842	.0432
C_3-benzene	.209	.205	.103	.106	.113	.0232	ND	.0174	1.46	.905	1.69	.977	.939	.415	ND
1,3,5-trimethylbenzene	.284	.286	.157	.146	.151	.0266	ND	.0212	1.73	1.16	2.11	1.22	1.19	.451	ND
C_3-benzene	.730	.730	.402	.372	.245	.0758	.0259	.0602	5.07	3.43	6.44	3.90	2.96	1.53	.0942
C_4-benzene	.438	.442	.260	.227	.244	.0528	.0309	.0493	3.40	2.31	4.41	2.89	3.35	1.13	.0872
Tetramethylbenzene	.128	.137	.0735	.0376	.0585	.0471	ND	ND	.204	.188	.0824	ND	ND	ND	ND
Naphthalene	.657	.680	.428	.343	.345	.0618	.0191	.0397	7.73	6.00	11.7	10.3	1.09	.520	.472
2-methynaphthalene	.408	.378	.240	.202	.207	.0467	.0177	.0306	6.76	5.49	11.1	11.8	8.33	6.90	2.58
1-methynaphthalene	.322	.302	.197	.168	.175	.0373	ND	.0243	5.44	4.40	9.00	9.57	8.41	5.41	1.97
1,1'-biphenyl	.0430	.0199	ND	ND	ND	ND	ND	ND	.909	.690	1.42	1.83	2.01	1.10	.466
2,6-dimethynaphthalene	.121	.0844	.0467	.0380	.0357	ND	ND	ND	1.61	1.23	2.50	3.00	2.49	2.33	1.07
C_2-naphthalene	.139	.0906	.0414	.0352	.0347	ND	ND	ND	1.94	1.65	3.49	4.20	1.55	3.14	1.48
C_2-naphthalene	.0288	.0181	ND	ND	ND	ND	ND	ND	.436	.334	.685	.871	.718	.650	.311
C_2-naphthalene	.0231	ND[a]	ND	ND	ND	ND	ND	ND	.385	.378	.809	.678	.600	.469	.383
2,3,5-trimethylnaphthalene	.0278	ND	ND	ND	ND	ND	ND	ND	.322	.245	.468	.623	.700	.548	.345
Dibenzothiophene	.0206	ND	ND	ND	ND	ND	ND	ND	.237	.155	.332	.450	.633	.453	.321
Phenanthrene	.0220	ND	ND	ND	ND	ND	ND	ND	.225	.179	.357	.498	.633	.456	.362
Total Resolved Compounds	28.1	26.7	14.9	13.2	13.0	2.70	1.27	2.11	91.3	65.7	114	92.2	77.0	46.5	16.8
Unresolved Compounds	8.79	7.35	3.02	1.34	5.00	1.71	6.49	3.85	25.4	13.8	47.7	22.1	45.5	28.4	14.5

a - "ND" indicates "not detected"

277

beneath the oil, many of the higher molecular weight compounds were rapidly removed from the water column. Also, concentrations of the lower molecular weight compounds (toluene, ethylbenzene, and xylene) decreased by several orders of magnitude within 3 days. Nevertheless, the concentrations after break-up were still sufficient to reach levels at least equal to those observed in the first hours after the spill. Furthermore, the higher molecular weight compounds, which were not removed by evaporation dispersed and dissolved into the water at concentrations approaching 1 ppb (see Table 4-13).

Wave turbulence is critical for dispersion of whole oil droplets into the water column. Data from dispersed whole oil droplet concentrations in the water column are presented in Table 4-14. Dispersed oil concentrations were only moderate during the first 1 to 3 hours following the spill. The dispersed oil concentrations, as represented by n-alkanes, then decreased rapidly in the water column after columnar ice formation. After break-up and resumption of 6-10 cm wave turbulence, however, concentrations increased by over two orders of magnitude; at 8 hours post-break-up the total dispersed hydrocarbons concentrations were in excess of 800 ppb. After 12 hours, with water-in-oil emulsification, higher oil viscosities, and the impingement of most dispersed oil droplets onto the under-ice surface, the spike in the dispersed hydrocarbon concentrations decreased. However, the large number of dispersed oil droplets trapped on the underside of the ice surface still provided a significant surface area for interphase mass transfer and, therefore, dissolution of lower and intermediate molecular weight compounds.

Table 4-15 presents the chemical and physical characteristics of the oil spilled in the pseudo "multi-year" ice. The interfacial surface tension and viscosity were not effected as drastically as during the oil in first-year ice experiments (Section 4.2). This is primarily due to differences in the ice behavior during the breakup event. Specifically, the multi-year ice floe was degraded by melting in the warmer (-1.0 to -1.5°C) water and wave radiation (ablation) interactions, as discussed in Pease (1981) and Martin et al. (1983). The first-year ice, on the other hand, was observed to breakup into slush ice with the onset of 6-10 wave turbulence during the spring thaw. Thus, the high

278

Table 4-14.—Dispersed Oil Concentrations from an Oil Spill
in Multi-Year Ice.

Time	Concentration (ug/l)		
	Resolved Compounds	Unresolved Compounds	Total Hydrocarbons
1 hour Post Spill	19.4	18.7	38.1
3 hours " "	22.4	18.4	40.8
6 hours " "	17.6	7.82	25.4
10 hours " "	3.74	4.32	8.06
12 hours " "	5.88	7.41	13.3
24 hours " "	1.99	5.87	7.86
1 hour Post Break-up	2.73	11.7	14.4
4 hours "	3.60	9.29	12.9
8 hours "	220.	589.	809.
12 hours "	3.89	13.2	17.1
24 hours "	4.47	14.9	19.4

Table 4-15.—Chemical and Physical Characteristics of Oil Spilled in Multi-Year Ice.

Time	Hydrocarbon Concentration (mg/g)		Surface Tension (dynes/cm)		Viscosity @ 38° C (centipoise)	Water Content (% by weight)
	Total Resolved	Unresolved Compounds	Oil/Water	Oil/Air		
Starting Crude	119	229	24.6	31.8	30	.03
1/2 hr Post Spill	98.2	182	-a	-	-	.99
3 hrs Post Spill	67.6	161	-	-	-	-
12 hrs Post Spill	91.8	206	-	-	-	-
24 hrs Post Spill	77.1	238	-	-	-	-
9 hrs Post Break-up	20.8	55.2	-	-	-	13.6
24 hrs Post Break-up	28.8	134	-	-	-	-
3 days Post Break-up	19.3	88.5	-	-	-	-
6 days Post Break-up	14.9	98.4	17.4	35.3	2000	28.1

a - limited sample volumes precluded measurements

concentrations of slush ice observed during first-year ice decay created local-ized microscale turbulence under the influence of the surface waves, and this was important for the generation of stable water-in-oil emulsions. In the multi-year ice case, the ice structure appeared to be ablated and worn down more slowly. Thus, a gradual thaw of the ice, rather than physical break-up into grease ice, occurred. As such, localized turbulence was much lower than in the oil/first-year ice study, which resulted in the delayed viscosity increase to 2,000 centipoise (measured on an aliquot in the lab at 38°C) (6 days post breakup) and the minimal water incorporation. The water content in the emulsified crude was 13.6% 9 hours after the break-up event. During oil/first-year ice studies, the water content was 60% just 4 hours after the initiation of wave turbulence. The grinding of slush ice resulted in the increased microscale turbulence responsible for rapid emulsification. Six days after the final break-up event in the multi-year ice study, water content in the oil was still only 28% by weight while the viscosity was similar to that in the first-year ice experiment (i.e., 2,000 centipoise at 38°C). In contrast, water content for Prudhoe Bay crude oil weathering in the presence of firstyear ice was 64% at the same time. Open-ocean wave tank simulations of waterin-oil emulsification with Prudhoe Bay crude oil are somewhat dependent on the formation of surface active agents to stabilize the emulsion and prevent water/water droplet coalescence. Thus, it was only after a longer period of 6-9 days that similar water content and viscosities were observed in sub-arctic open ocean simulations (Payne et al., 1984a).

4.5 SIMILARITIES AND DIFFERENCES IN WAVE TANK SIMULATIONS OF OIL WEATHERING BEHAVIOR IN FIRST- AND MULTI-YEAR ICE

The similarities and differences between oil weathering behavior in first- and pseudo-multi-year ice are considered in the following discussion. First of all, the importance of molecular weight in compound specific aromatic hydrocarbon dissolution, in oil weathering with both first- and multi- year ice, cannot be overemphasized. There was an initial concentration spike of 40 μg/l of lower molecular weight components (toluene, o-, m-, and p-xylene, ethylbenzene and C_3-benzenes) immediately after the oil release in the multi-year ice experiment; however, after freezeup occurred (columnar ice formed

under the oil), water column concentrations returned to near background levels within a 24 hour period. Following columnar ice formation the surface slick weathered by evaporation only. After break-up, there were still suffient lower molecular weight aromatic hydrocarbon concentrations in the slick to at least equal the earlier concentration spike in the water column. Nevertheless, columnar ice growth under oil in calm conditions is extremely important because it decouples oil from the water column. However, this probably will be a factor only under very calm conditions in the field.

In the oil/first-year ice experiments, the initial concentration spike of dissolved aromatics in the water column (before encapsulation in the ice) was also about 40 $\mu g/l$. These concentrations declined over a 24 hour period, except that the seawater-exchange flow rate was three times slower (1 liter/ minute). This slower water flow rate and the greater volume of oil released (5,000 ml vs 750 ml) suggest that aromatic hydrocarbon dissolution was approximately 18 times slower in the oil under first-year ice release. However, the slick was contained in larger, thicker pools on the under-ice surface before encapsulation. Thus, the surface area for interphase mass transfer was greatly reduced. In both experiments the seawater temperature was measured at -1.7 to 1.8°C.

With ice break-up and wave turbulence in both studies, significantly higher dissolved concentrations were again observed, and much higher concentrations of dissolved components on a per ml of oil spilled basis were measured in the multi-year ice case. Specifically, the maximum total dissolved (resolved plus UCM) components three to four hours after break-up were 0.23 and 0.20 (in units of total dissolved aromatics in $\mu g/liter$ of seawater per ml of oil spilled) for the oil in multi-year and first-year ice cases, respectively. However, the seawater flow rate was three times higher in the multi-year ice case, which suggests that the relative oil droplet surface area to volume ratios were approximately three times higher when turbulence was introduced in the multi-year ice break-up event. That is, to reach and maintain a similar dissolved aromatic hydrocarbon concentration on a per gram of oil-spilled basis, when different volumes were spilled and different seawater flushing

rates were encountered, significantly different surface to volume ratios must have been generated. In the first-year ice study, 6.6 times more oil was released at one-third the flushing (seawater turnover) rate, and yet, the total dissolved concentration was only 5.8 times higher on break-up. Thus, there may have been a three fold higher surface area to volume ratio for interphase mass transfer in the multi-year ice case after break-up. Again, in the multi-year ice study there was little droplet dispersion without wave pumping. Then, with just 30 minutes of 6-10 cm wave turbulence, over 80% of the oil was trapped under the fast ice as <1 μm to 1 cm droplets. Alternatively, the very rapid onset of a stable water-in-oil emulsion and the concomitant increase in oil viscosity in the first-year ice study may have slowed or prevented dispersion of smaller oil droplets into the water column.

The coldroom wave tank experiments also suggested that oil may be forced by waves under fast (or stationary) ice to a greater degree than first-year pancakes. Wave-induced pumping can force oil both directions, on top of and beneath smaller, floating ice pans. In fast ice (and presumably larger multi-year floes with stabilizing ridges, etc.) the waves interacting with the ice will also cause the oil to be distributed on top of and underneath the floe (depending on freeboard). That oil which ends up under the floe tends to stay there (as demonstrated in the wave tank with both first- and multi-year ice). It is trapped in under-ice depressions, ridges, and even in the skeletal layer of columnar ice (if present). Oil will tend to remain in place even in the presence of ice/water differential current velocities of up to 15 to 25 cm/sec (Cox et al., 1980). The oil deposited on the upper surface of larger multi-year floes, on the other hand, is subject to repeated washings. Some of the oil (e.g., approximately 10-20%) was washed further back onto the surface layers of ridges, cracks, and rubble (8-12 cm above the water surface), but the majority of the oil, which was initially deposited on the ice "beach face", did not stay there. Small waves (6-10 cm high), which are equivalent to localized wind chop, quickly rinsed the oil back into the water (i.e., the oil did not stick to the smooth multi-year ice surface). Within hours, approximately 90% of the oil ended up in the open water or was deposited on the under side of the ice. This was particularly true if the ice "beach face" sloped down at the ice

water interface. If there was an abrupt verticle face and a surface depression on the ice behind the edge then some oil was splashed up onto the ice, but only if the freeboard was not greater than 10 to 15 cm. If it was, then the oil went under or around the floe. First year pancakes in the wave tank, on the other hand, tended to be smaller and, as such, had less inertia and more bouyancy. Thus, they tended to float higher in the waves, and small waves did not wash oil off. Instead, the smaller pans tended to get pushed along, with oil contained within their rims, by the wind and waves in a less turbulent manner.

Obviously, the laboratory scale by virtue of the tank size and water depth cannot duplicate field conditions. In actual arctic environments higher freeboards would inhibit ice surface contamination, and the oil would be more likely to be confined to dispersion around and under the floes. Nevertheless, in actual oil spills in the presence of active sea ice (e.g. the Bouchard #65 oil spill in Buzzard's Bay, MA in January 1977) as much as 29% of the oil was estimated to ultimately reside in deep oil pools in rafted ice (Baxter et al., 1978). The ultimate fate of the oil (on or under the ice) will be controlled by the stochastic nature of the spill event and environmental conditions. The experiments discribed herein were not intended to simulate all possible spill scenarios; but rather to examine the chemical and physical changes that occurred to the oil and its distribution (on the ice and in the water as dissolved and dispersed entities) under conditions that could be controlled and carefully monitored.

Once the break-up of multi-year ice in the coldroom wavetank was initiated with full-cycle paddle turbulence, the landfast and multi-year ice tended to break up into larger pieces which were not ground into slush ice. Instead, after breaking off of the "fast ice shelf", the pseudo-multi-year ice floes and ridges were subject to in situ melting similar to the decay described for first-year ice bands in the marginal ice zone (Pease, 1981). Presumably, the multi-year ice floe's resistance to degradation into slush ice in the wave tank reflects the lower salinities resulting from previous brine drainage during earlier freeze/thaw cycles and ridge formation. This behavior (i.e.,

lack of grinding into slush) may have implications for inhibited water-in-oil emulsification during the release of oil trapped in multi-year ice ridges. When oil was finally released from under the multi-year ice ridges in the wave-tank system, it did not form a stable water-in-oil emulsion as quickly as the oil released in first-year ice because of the absence of slush-ice induced micro-scale turbulance. This was demonstrated by slower increases in both oil viscosity and final water content in the water-in-oil emulsion.

Also, during the melting/break-up phase of the multi-year ice wavetank experiments, the oil on upper ice surfaces tended to readily wash off the melting ice. Pooled oil on the ice surface remained remarkably fluid despite the cold ice/room temperature. As described in Payne et al. (1984a), viscosity increases in oil due to evaporation alone are not sufficient to affect oil be-havior when stranded as pools on ice surfaces. Mixing and water-in-oil emulsi-fication with melt water from ice or snow (or seawater from wave swash and overflooding) would be required to permanently increase spilled oil viscosity while still stranded on upper ice surfaces. Some of the oil did become trapped (frozen during the initial spill event) in cracks on the ice-floe surface or in the capillary channels of broken chips of rafted columnar ice on the upper ice surface; this trapped oil resisted washing and remained longer on initial wave washing. Nevertheless, with continued wave turbulence and washing, trapped oil was also released in a matter of hours as the ice gradually melted.

During the execution of the oil-in-ice experiments we also endeavored to examine the effect that spilled oil had on ice behavior itself. It can speed up melting when trapped within the ice, but if the oil remains on the ice surface, it will only initially enhance melting by lowering the albedo of the ice. Then, one of two things can happen. First, if the pan is small and mobile and subject to wave washing and erosion, the oil quickly will be washed off the ice. Or, if the ambient temperature drops after melting in a localized spot, then the oil can float on the melt-water and be partially refrozen in place. However, during a subsequent thaw event, this oil can be washed off the ice and end up under the ice or in the open water.

5.

INVESTIGATIONS OF LEAD REFREEZING, BRINE INJECTION
AND DISSOLUTION OF AROMATICS INTO SINKING BRINE

5.1   INTRODUCTION

An important concern for marine pollution research is the potential transport of spilled oil or dissolved hydrocarbon components to benthic environments and prolonged exposure of benthic organisms to the more toxic fractions of oil. However, experience from laboratory and field studies conducted under temperate (ice-free) open-ocean conditions indicates that soluble aromatic hydrocarbons do not reach deep bottom waters or ocean sediments in concentrations that might produce long-term impacts (McAuliffe et al., 1975; Payne et al., 1980a and b; Boehm and Fiest, 1982, McAuliffe et al., 1980; and Gearing et al., 1979). Although hydrocarbons can spread onto and disperse into near-surface water, oil droplets are usually less dense than sea water and return to the surface. Likewise, dissolved compounds are usually confined to the upper mixed layer (generally above the thermocline or pycnocline, if present). As such, they are subject to gradual evaporative removal from the water column. Field measurements at several major open ocean oil spills (the IXTOC I blowout in the Bay of Campeche, Gulf of Mexico being the most notable) have indicated few significant increases in hydrocarbon levels in sediments or bottom-dwelling organisms, even after many months of continuous oil input to the water column (National Academy Press, 1985). There generally appears to be very limited effect from open water oil spills to the benthos, except in the narrow band of shallow coastal waters and in regions of direct vertical mixing of oil with nearshore sediments (e.g., Amoco Cadiz spill; Gundlach et al., 1983).

Hydrocarbons released in or under ice in arctic waters can be rapidly incorporated into the ice cover, which implies little opportunity for dissolution, advection, or transport of hydrocarbons to the bottom. Weeks and Weller (1984) stated that "ice (would) assist in confining the oil to a relatively small area... under the ice and in the absence of high ice/water relative currents the oil will stay in place."

286

However, the ice formation processes that occur during arctic winter conditions in the nearshore regions of the Beaufort and Chukchi Seas provide a previously undescribed mechanism for the potential transport of oil components to bottom water environments. During periods of ice growth, particularly in nearshore leads and polynyas in the Chukchi Sea, salt is exuded into surface waters during frazil and slush ice formation (Bauer and Martin, 1983; Kozo, 1983). CTD measurements in the Chukchi Sea indicate that the exuded brine sinks (due to its higher density) and flows by gravity to the bottom where it can spread laterally and form a highly stable bottom boundary layer that can be 1-2 m thick (Hachmeister and Vinelli, 1985). A salinity cross section (Figure 5-1) obtained from CTD data collected in February 1984 along transect B-1 to B-7 (shown in Figure 4-23 in Section 4.3.1) illustrates the presence of a higher density bottom layer.

Brine formation and sinking can occur in both multi-year and first-year ice areas when open-water leads form (due to ice movement, wind stress, or subsurface currents) and air and water temperatures are suitable for active ice formation (Bauer and Martin, 1983; Kozo, 1983; Martin and Kauffman, 1981; McPhee, 1980). In many areas in the arctic, frazil and grease ice growth can occur during extended periods of the year. For example, satellite imagery shows frequent polynyas and leads in this area, which implies that sea ice formation (if rapid enough) in these open waters may result in continued production of high-salinity waters beyond the initial fall freezeup period (Bauer and Martin, 1983). If an open lead is in shallow water, the extent of the lead and rate of freezing do not have to be as great to produce bottom water with a comparably elevated salinity because dilution of the water mass will be reduced. Aagaard (as cited by McPhee, 1980) reported high salinity bottom waters off Cape Lisburne in the Chukchi Sea, which could have originated from brine exclusion processes during ice formation. Brine layers also have been observed as pools in depressions in shallow and nearshore lagoons in the Beaufort Sea. These layers at times remain through winter and into summer months when the highest seasonal biological production occurs. For example, in Prudhoe Bay in the summers of 1984, 1985, and 1986 a bottom layer with salinities up to 70
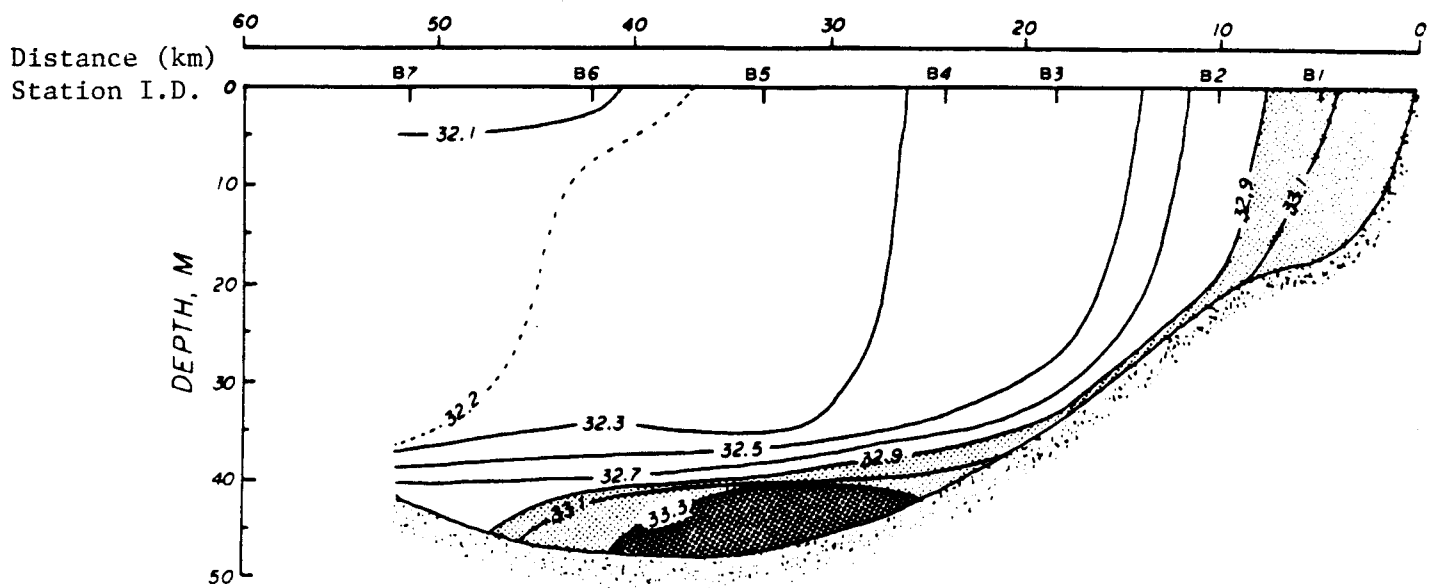
Figure 5-1.--Salinity Profile from Station Transect Line in Northeast Chukchi Sea (see Figure 4-23) During February 1984.

^{o}/oo remained from the winter season into mid-August before being flushed from the area by intense summer storm events (Hachmeister et al., 1986).

If crude oil or refined petroleum (distillate) products were spilled in an open lead during ice growth and brine formation, the more water soluble lower molecular weight aromatic hydrocarbons (McAuliffe, 1966 and 1969; Mackay and Shiu, 1976; Sutton and Calder, 1974, 1975a, 1975b; Clark and MacLeod, 1977; Payne et al., 1984a; and Payne and McNabb, 1984) could be readily incorporated into the sinking brine, where they could then behave as conservative species (similar to salt) and be advected to the bottom with the denser water. Some dilution would be expected due to entrainment of surrounding water during the sinking process; however, this would be minimized in shallower nearshore waters. Once present in the bottom waters, these dissolved aromatics would not be subject to rapid release to the surface and removal by evaporation processes.

Implicit in the hypothesis that soluble aromatics will be transported with sinking brine is that the dissolved components will behave as conservative variables. Conservative behavior is expected based on the fact that virtually all molecular and atomic species (with the exception of helium and hydrogen) have similar diffusion constants (usually around 10^{-5} cm^2/sec) in aqueous environments (Reid et al., 1977; Lymen et al., 1982).

This mechanism for the potential transport of hydrocarbons by a dense (brine excluded) water mass was investigated during three areas of study included in the oil in multi-year ice program. Theoretical calculations of potential aromatic hydrocarbon dissolution and transport were completed based on measured oil/seawater partition coefficients and calculated rates of brine generation during frazil/slush ice formation. This topic is discussed in Section 6.9 of this report. Simulated brine generation and sinking experiments were then completed in a laboratory test-tank (Section 5.2 below). Finally, a chemical and physical oceanographic field program was completed in the Chukchi Sea near Pt. Franklin in which an aromatic hydrocarbon mixture was released into a refreezing near-shore lead. Water samples subsequently were collected

from beneath the ice and analyzed chemically to monitor transport of dissolved hydrocarbons in the bottom waters (Section 5.3).

5.2   LABORATORY STUDIES OF BOTTOM WATER GENERATION PHENOMENA

5.2.1   Background

To demonstrate the phenomenon of surface brine formation, sinking and gravity induced flow along the bottom, a series of laboratory experiments were conducted to model two sets of environmental conditions typically encountered in arctic coastal waters during the winter. The first experiment modeled the fall freeze-up; the initial conditions include a vertically mixed (typical of late Fall conditions in shallow water) water column with no ice present at the start of the freeze-up process. The second experiment modeled the deep winter, with 10/10ths ice coverage and a newly opened lead located approximately 15 km offshore. This lead remains open for several days in the model and then closes, thus terminating the rapid freezing process and the generation of brine. Data collected during the laboratory experiment included photographs of the phenomenon, water samples collected from the experimental tank, and in situ measurements of the water's conductivity and temperature. Photographic data provided information on depth and "offshore" position of the brine layer and upper convective layer. In addition, information on the velocity field was obtained by using vertical dye lines as a tracer element. Analysis of water sample data produced information on vertical density profiles and water movement from the nearshore to offshore regions.

5.2.2   Scaling Parameters

The laboratory experiments were intended simply as a demonstration that the phenomena described in Section 5.1 can occur. A secondary goal was to evaluate the entrainment (dilution) of the brine and estimate water velocities induced by the freeze-up process. In the field, the region to be modeled consists of the coastal boundary from the shoreline to approximately 50 km offshore. In the laboratory experiment, it was desirable to keep tank-end and

290

side-wall boundary effects to a minimum. Therefore a scale model as large as can be accommodated is preferred. For this experiment side-wall effects were limited to within 1-2 cm of the wall; therefore, in our two-dimensional experimental 50-cm-wide tank, only 4-8 percent of the water column was affected by the wall boundary layers. Previous experiments, with a moving salt intrusion forming a slowly advancing front, were used to guide the selection of the proper tank dimensions. Therefore, 5.7 m of an available 15 m test tank were used for the experiment, modeling the 50-km wide slope by 5 m in the tank (Figure 5-2). Turbulence was not modeled in the tank, and initial conditions of vertical stratification were assumed to be typical of late-fall early-winter shallow-water conditions (i.e., non-stratified). These factors were not considered to be critical for the demonstration of the phenomena.

To insure proper scaling of laboratory results to the field case, the Richardson number given by

$$R_i = g \frac{\Delta \rho}{\rho_o} \frac{h \cos\theta}{U^2} \tag{1}$$

must be preserved in the laboratory model. We begin the scaling analysis by first defining nondimensional variables (primed):

$x = \ell_x x'$	horizontal distance	$u = \ell_u u'$	horizontal velocity
$z = \ell_z z'$	vertical distance	$\Delta\rho = \ell_{\Delta\rho} \Delta\rho'$	density differences
$t = \ell_t t'$	time	$\cos\theta = \ell_{\cos\theta} \cos'\theta$	slope

For the purpose of this modeling effort we were partially constrained by the dimensions of the tank (which was designed for horizontal intrusion studies), and our desire to limit the vertical to horizontal exaggeration to no more than 100:1. Therefore we assumed that

$$\frac{\ell_{x\text{ model}}}{\ell_{x\text{ field}}} = \frac{1}{10,000} , \quad \frac{\ell_{z\text{ model}}}{\ell_{z\text{ field}}} = \frac{1}{100} , \quad \frac{\ell_{\cos\theta\text{model}}}{\ell_{\cos\theta\text{field}}} = 1 \tag{2}$$

291
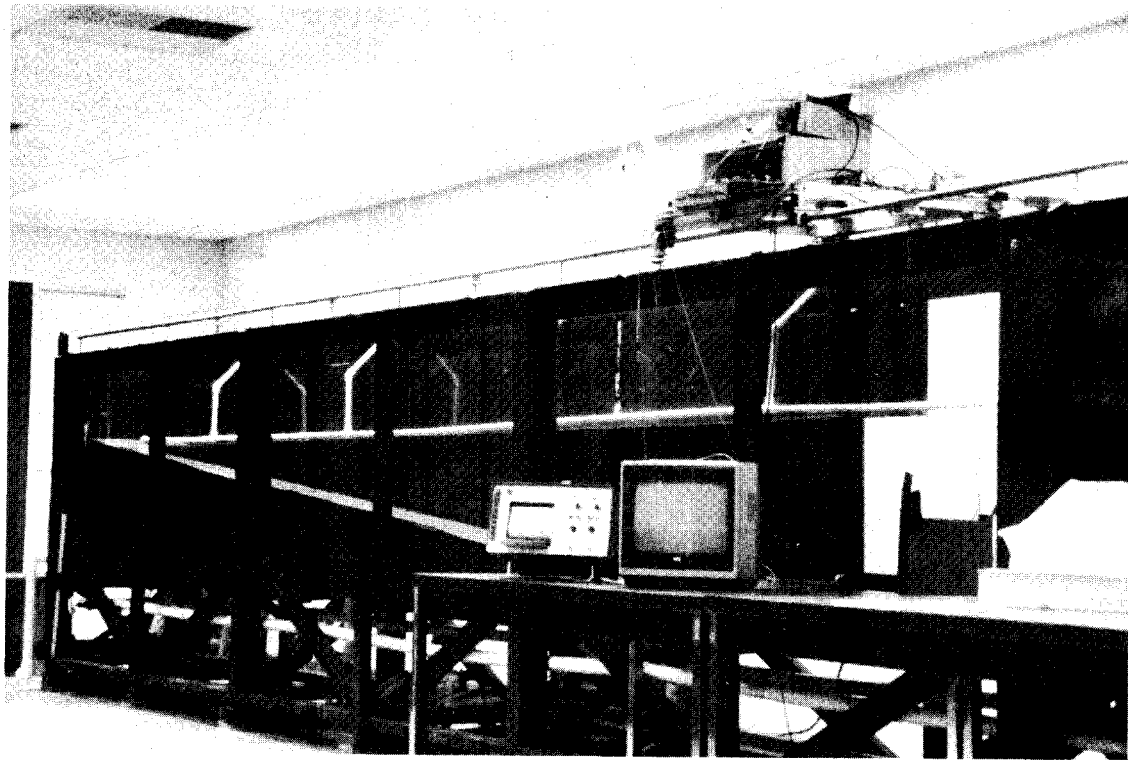
Figure 5-2.--SAIC/Northwest Experimental Tow Tank with Slope and Brine
Delivery Channels Installed.

Richardson number scaling requires that

$$\frac{R_i \text{ model}}{R_i \text{ field}} = \frac{\ell_{\Delta\rho_m}}{\ell_{\Delta\rho_f}} \frac{\ell_{z_m}}{\ell_{z_f}} \frac{\ell_{\cos\theta_m}}{\ell_{\cos\theta_f}} \frac{\ell^2_{u_f}}{\ell^2_{u_m}} = 1 \qquad (3)$$

Substituting,

$$\frac{\ell^2_{u_m}}{\ell^2_{u_f}} = \frac{1}{100} \frac{\ell_{\Delta\rho_m}}{\ell_{\Delta\rho_f}} \qquad (4)$$

If we model the stratification effects as

$$\frac{\ell_{\Delta\rho_m}}{\ell_{\Delta\rho_f}} = 10 \qquad (5)$$

then velocities scale as

$$\frac{\ell^2_{u_m}}{\ell^2_{u_f}} = \frac{1}{10} \quad \text{and} \quad \frac{\ell_{u_m}}{\ell_{u_f}} = \frac{1}{3.16} = 0.316 \qquad (6)$$

From the definition of velocity

$$(\frac{U}{x/t})_{\text{model}} = (\frac{U}{x/t})_{\text{field}}, \qquad (7)$$

which yields a temporal scaling law

$$\frac{\ell_{t_m}}{\ell_{t_f}} = \frac{\ell_{u_f}}{\ell_{u_m}} \frac{\ell_{x_m}}{\ell_{x_f}} = 3.16 \times \frac{1}{10,000} = 3.16 \times 10^{-4} \qquad (8)$$

Scaling laws therefore become

$$\frac{\ell_{x_m}}{\ell_{x_f}} = \frac{5 \text{ m}}{50,000 \text{ m}} = \frac{1}{10,000} \tag{9}$$

$$\frac{\ell_{z_m}}{\ell_{z_f}} = \frac{0.5 \text{ m}}{50 \text{ m}} = \frac{1}{100} \tag{10}$$

$$\frac{\ell_{\Delta\rho_m}}{\ell_{\Delta\rho_f}} = \frac{0.005 \text{ gm/cc}}{0.0005 \text{ gm/cc}} = 10 \tag{11}$$

$$\frac{\ell_{u_m}}{\ell_{u_f}} = \frac{1}{10} \frac{\ell_{\Delta\rho_m}^{\frac{1}{2}}}{\ell_{\Delta\rho_f}^{\frac{1}{2}}} = 0.316 \tag{12}$$

$$\frac{\ell_{t_m}}{\ell_{t_f}} = \frac{\ell_{u_f}}{\ell_{u_m}} \frac{\ell_{x_m}}{\ell_{x_f}} = 3.16 \times 10^{-4} \tag{13}$$

Table 5-1 gives examples of corresponding basic unit scaling parameters for the modeling program.

Table 5-1.--Scaling Parameters for Tow Tank Model Studies.

Parameter	Field Scale	Model Scale
x	1 km	10 cm
z	1 m	1 cm
$\Delta\rho$	0.0005 gm/cc	0.005 gm/cc
u	1 cm/sec	0.32 cm/sec
t	1 day	27.3 sec

To calculate the amount of brine produced during the fall freeze-up process, we started with the assumption that 2.2 gm of salt are released per square cm for each 1 meter of ice formed (assuming 32 ppt seawater and 0 ppt ice; Martin, 1985; personal communication). If we assume -20°C temperature during freeze-up and allow ~0.65 m of ice to form over 20 days we will produce $2 m^3$ of 40 ^{o}/oo brine per square meter of ocean (Martin, 1985; personal communication). In the laboratory this will scale to 2 cc of 40 ^{o}/oo brine introduced into each square centimeter of surface over a period of ~10 minutes.

For the winter lead experiment, model scaling is slightly different. We assumed that a midwinter lead opens to a uniform width of 500 m under conditions of -30°C and 10-knot along-axis winds. To simplify the modeling effort, this lead is assumed to remain open for a total of four days and then close. We also assumed that ice is being formed at a uniform rate such that 24 cm of ice results over the 96 hour period. Also, newly formed ice is assumed to be advected along the axis of the lead out of the study section. This will, in turn, produce a 0.72 m layer of 40 ^{o}/oo brine over each square meter of the lead which will be modeled by 0.72 cm in the laboratory. Approximately 50 cc of 40 ^{o}/oo brine will then be added per model day (27 sec) to the 5 x 50 cm model lead. Again, it is important to recognize that we were only attempting to demonstrate the phenomena of brine cabeling in shallow, near-shore waters.

5.2.3   Experiments

Laboratory experiments were conducted to model brine formation during two conditions: (1) fall freeze-up when considerable open water is present and (2) refreezing of a newly opened lead. These two cases will be called the open-water freeze-up and lead refreezing experiments, respectively.

5.2.3.1 General Description

Initial stratification conditions in the modeled nearshore waters were intended to be both horizontally and vertically homogeneous in temperature, salinity and density, thus simulating the conditions which occur during rapid

surface cooling and vertical convection but prior to the actual formation of ice. Freezing was assumed to occur uniformly throughout the nearshore region as modeled by the uniform input of brine over the entire water surface. In order to achieve a spatially uniform addition of dense brine to the surface while preventing the brine from immediately sinking to the bottom, the brine was initially heated to a temperature where its density is less than the ambient density of the underlying water. The decreased density of the upper brine layer is sustained only by its elevated temperature and as surface cooling occurs, the brine layer gradually achieves a density greater than that of the fluid below it and sinking occurs. Dilution of the brine temperature and salinity begins during its addition to the surface of the tank through mixing salt finger formation, and heat loss to the air. These effects resulted in surface water dilution such that surface waters rapidly achieved an excess density of ~0.004-0.006 gm/cc over ambient water. This range encompasses the 0.005 gm/cc desired for the start of the brine-formation simulations (see Section 5.2.2). PVC tubing suspended near the water surface down the entire length of the tank comprised a brine delivery system that proved to be quite efficient in depositing the brine into a 1.0-1.5 cm thick layer with very little initial mixing. The experiment start time was defined as the time that the first warm water began to spread along the water surface.

5.2.3.2 Open-Water Freeze-up Simulation

Two open-water simulations were conducted during the series of experiments. The first was intended to study the formation of the upper-ocean thermohaline convective layer and the vertical transport of brine into the water column. The second was intended to study the bottom boundary-layer flow and horizontal velocity profile induced by the dense brine flow. Table 5-2 gives the initial conditions present for each of the two open-water freeze-up experiments.

Table 5-2.--Open-Water Freeze-up Initial Conditions (Laboratory Model).

Experiment	Total Depth (cm)	S ocean (ppt)	S brine (ppt)	T ocean (°C)	T brine (°C)	ρ ocean (20°C) (σt)	ρ brine (20°C) (σt)	ρ brine at T_i (σt)
Run I	52.8	34.5	40.9	20.5	57.0	23.5	28.1	15.5
Run II	51.7	31.3	40.0	20.0	62.5	22.0	27.5	14.5

Tests were conducted in a 7.5 m section of a 15 m stratified tow tank. A 10% slope, 5 m long, was constructed at one end of the tank which terminated in a flat plane 2 m long (Figure 5-2). At the start of the experiment, brine at 40.9 °/oo and 54.0°C was added to the entire surface of the experimental section over a 2.5-min period, through fill channels suspended at the water surface as shown in Figure 5-3.

Measurements taken during the experiment included conductivity, temperature and depth (CTD) profiles, water samples, and visual recordings. The visual records consisted of 35 mm slides and VCR videotapes. Both rhodamine and fluorescein dyes were used to aid in the collection of visual records. Verbal observations were recorded on VCR audio tracks and handheld magnetic tape recorders.

A subsequent open water freeze-up simulation was performed under similar conditions (Table 5-2). Pre- and post-experimental measurements were made of the temperature, salinity and density fields as in the previous experiment. Time-lapse photographs of initially vertical dye lines were made to deduce vertical profiles of the horizontal velocity field.
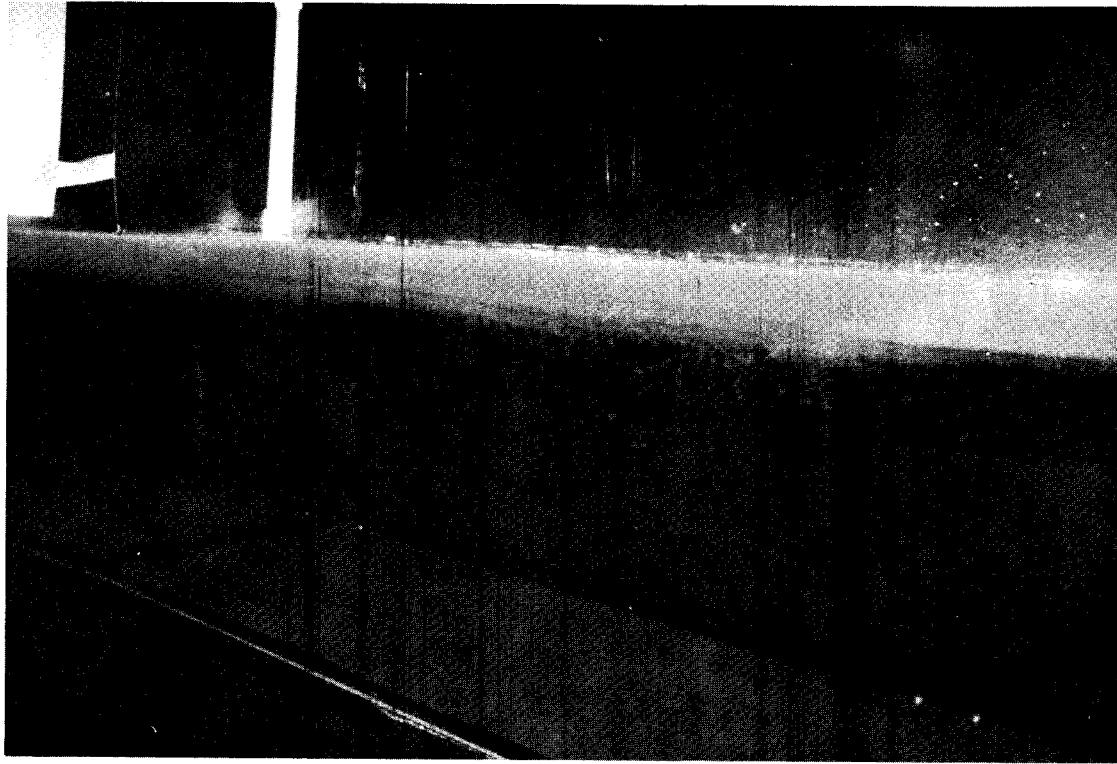
Figure 5-3.--Fill Channels While Dyed Brine is Put into Surface of Water.

5.2.3.3 Lead Freeze-up Simulation

A single lead freeze-up experiment was conducted. For this experiment a 5 x 50 cm "lead" was constructed at the location of the 15 cm depth (1.5 m from the modeled coastline). This lead was intended to be two-dimensional and to simulate a 500 meter wide opening of the ice at the shear zone during off-ice winds. The initial conditions for this experiment are given in Table 5-3.

Table 5-3.--Lead Freeze-up Initial Conditions (Laboratory Model).

Experiment	Total Depth (cm)	S ocean (^{o}/oo)	S brine (^{o}/oo)	T ocean (°C)	T brine (°C)	ρ ocean (20°C) (σt)	ρ brine (20°C) (σt)
Run III	51.5	31.7	38.2	20.3	20.1	21.5	26.5

For this experiment a 5 x 50 cm box was floated at the water surface to contain the added brine (Figure 5-4). At the start of the experiment, brine was added uniformly across the lead at a rate of 100 cc/min. For the first minute, brine marked with fluorescein dye was added to the tank. For the next 30 seconds, brine marked with rhodamine dye was added at the same rate. For the final minute, fluorescein-marked brine was again added. Horizontal velocity profiles were determined from time-lapse photographs of initially vertical dye lines.

5.2.4 Results

Experimental results for the two sets of environmental conditions are discussed below in separate sections. Results for both of the open-water freeze-up experiments are given together because the environmental parameters were very similar.
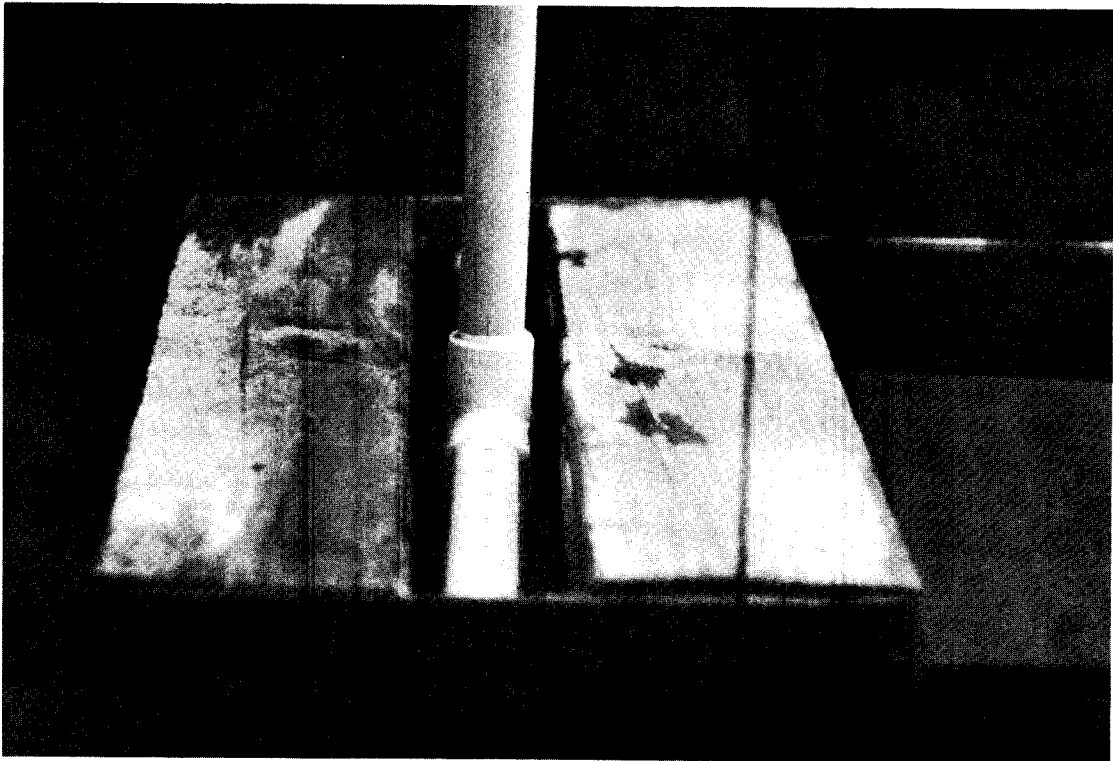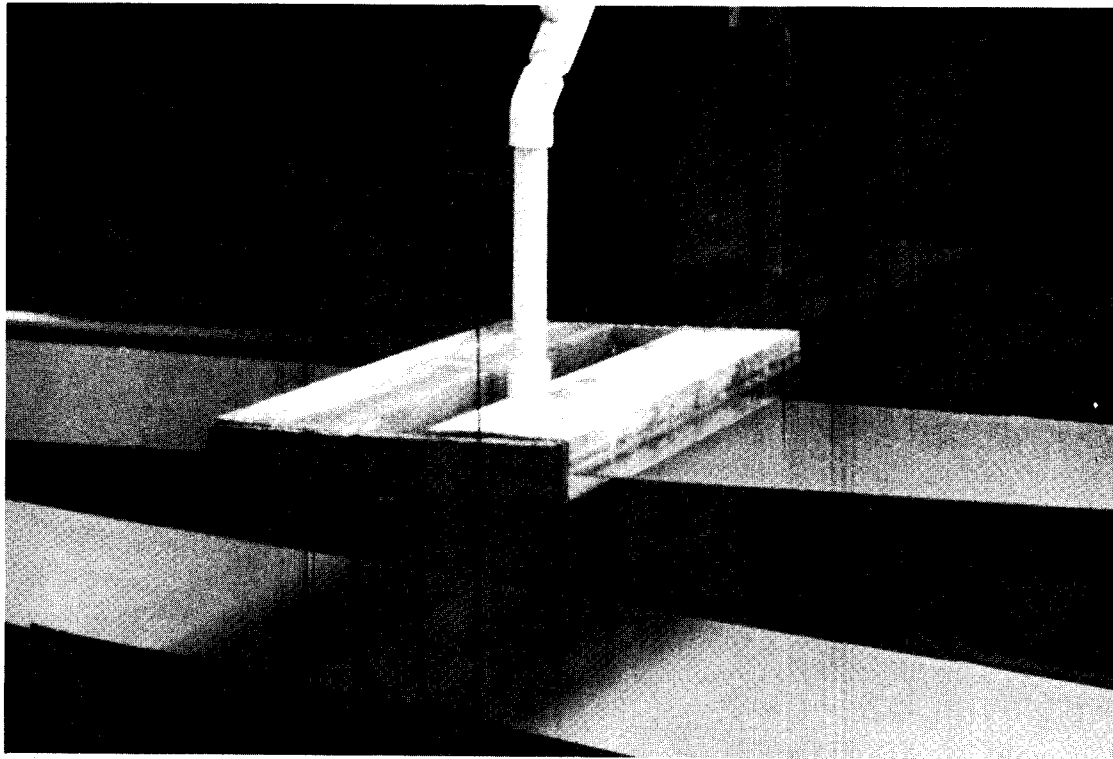
Figure 5-4.--Experimental 5 x 50 cm Lead Model with Brine Fill
Channel in Place.

5.2.4.1 Open-Water Freeze-up Results

Figures 5-5A and 5-5B show the initial temperature, salinity and density profiles in the experimental section of the tank for the two open-water freeze-up experiments. Note that the conductivity cell displays anomalous behavior near the water surface and readings for the first 1-2 cm should be ignored. There is also a slight cooling effect observed near the tank surface which may lower the surface temperature by as much as a degree prior to the beginning of the experiment. This surface cooling is relied upon later during the experiment to rapidly cool the heated surface brine to a temperature where its density is greater than the underlying water density. Figures 5-6A and 5-6B show the temperature, salinity and density profiles in the tank 5.5 min (BW2) and 5.0 min (BW12) after the warm brine has been added to the surface water in each experiment. Both casts were taken at the end of the slope at a distance 5 m from the modeled coastline. Note that, in the cast of BW2, mixing of the heated brine occurred down to a depth of 20 cm, whereas in the case of BW12 mixing has occurred down to a depth of 40 cm and a distinct bottom layer with salinities greater than 35 ^{o}/oo was observed. This layer of brine is confined to the lower 2 cm of the water column (Figure 5-7).

A third cast was taken at 50 min (BW4) and 49 min (BW13) into each experiment. Data from these profiles are shown in Figures 5-8A and 5-8B. Note that considerably more heat and salt are retained in the upper layers of the water column in BW4 than in BW13. However, in both cases, the bottom brine layer developed very similarly with respect to its thickness and the increased salinity and density relative to the ambient water. The minimal temperature deviation between the two experiments indicated similar mixing processes.

A final CTD cast (BW5) was taken 127 minutes into Run I (Figure 5-9). A bottom layer of approximately 10 cm thickness had developed in the tank at this time. This layer was observed as a region of increased dye concentration at the time of the cast.
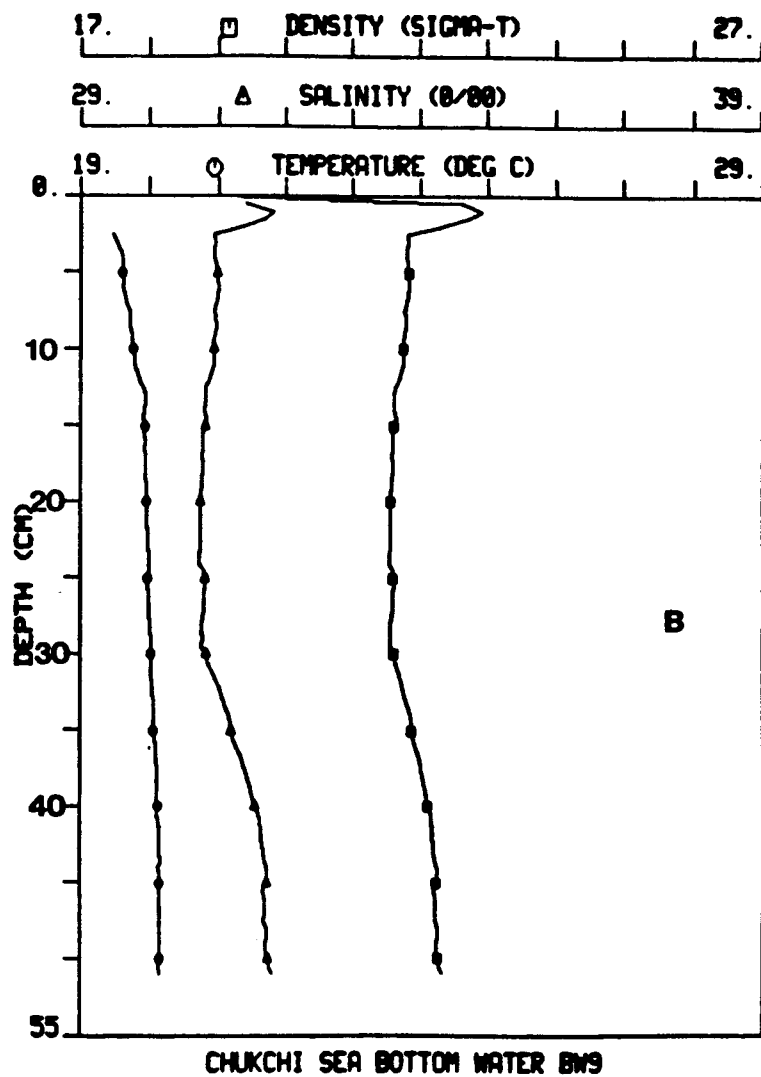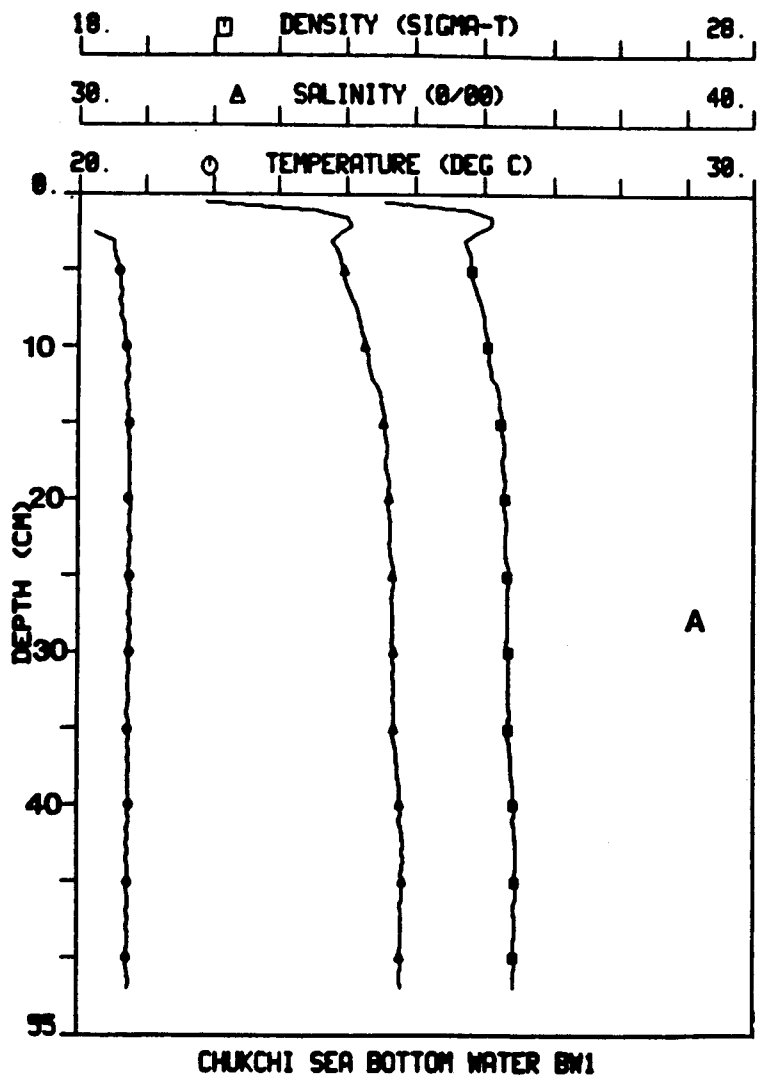
Figure 5-5.--Initial (Time = 0) Temperature, Salinity and Density Profiles for Laboratory-Scale Open-Water Freeze-up Experiments: (A) No. 1, and (B) No. 2. (Casts BW1 and BW9 at base of slope, 5 m from modeled coastline.)
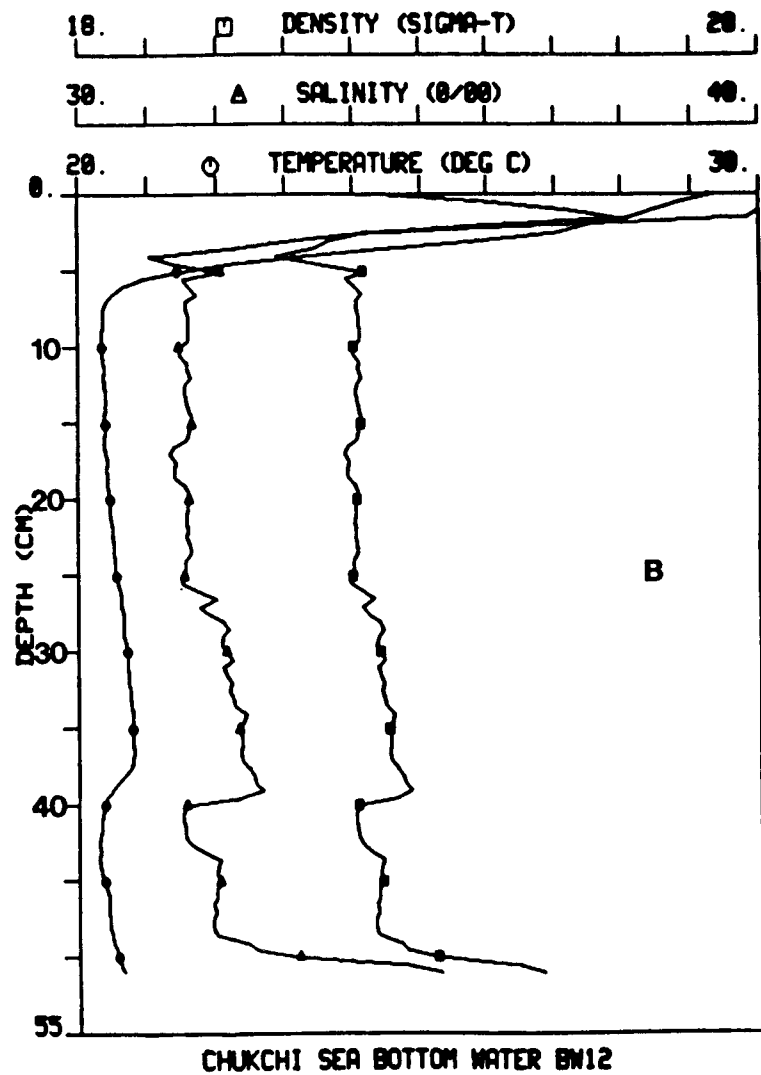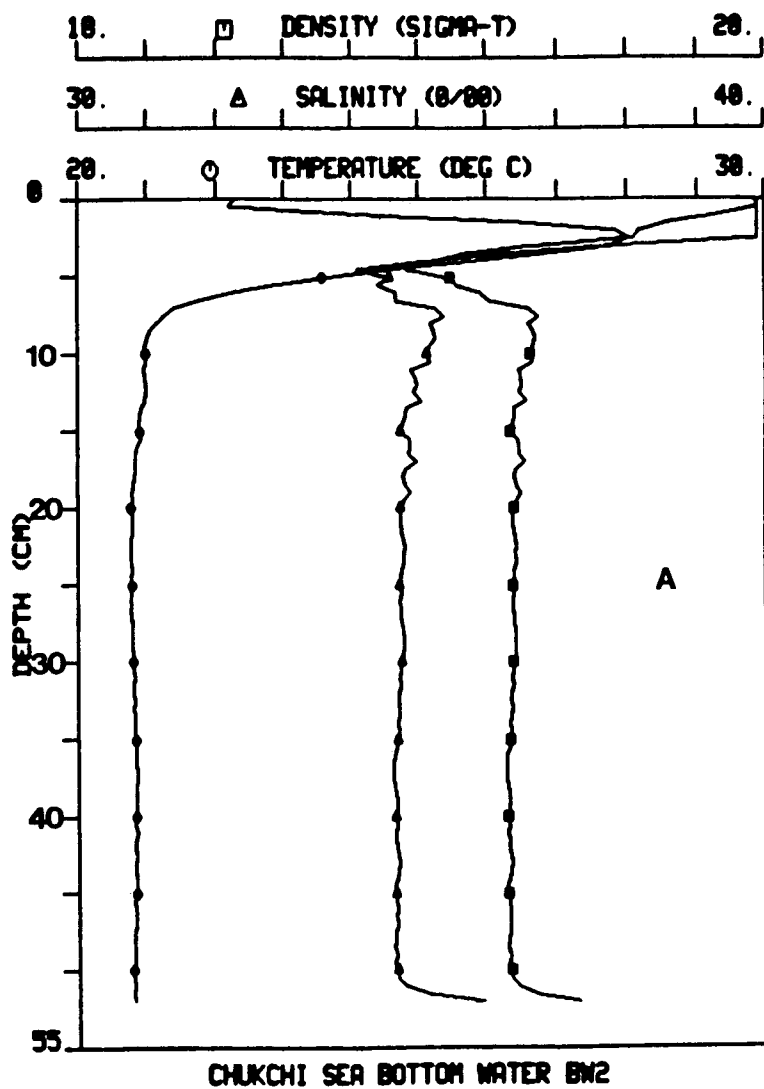
Figure 5-6.--Temperature, Salinity and Density Profiles Taken During Laboratory-Scale Open-Water Freeze-up Experiments: (A) No. 1 at 5.5 minutes, and (B) No. 2 at 5.0 minutes. (Casts BW2 and BW12 at base of slope, 5 m from the modeled coastline.)
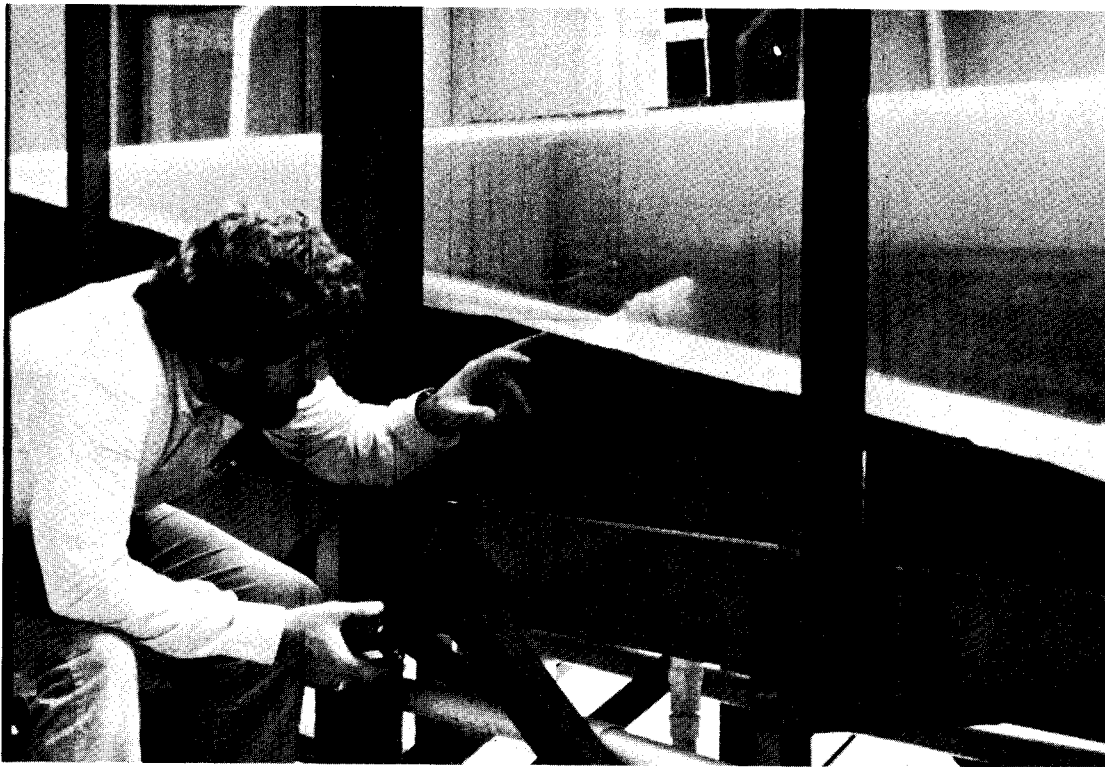
Figure 5-7.--Dyed Brine Mixed to Approximately 20 cm Depth.
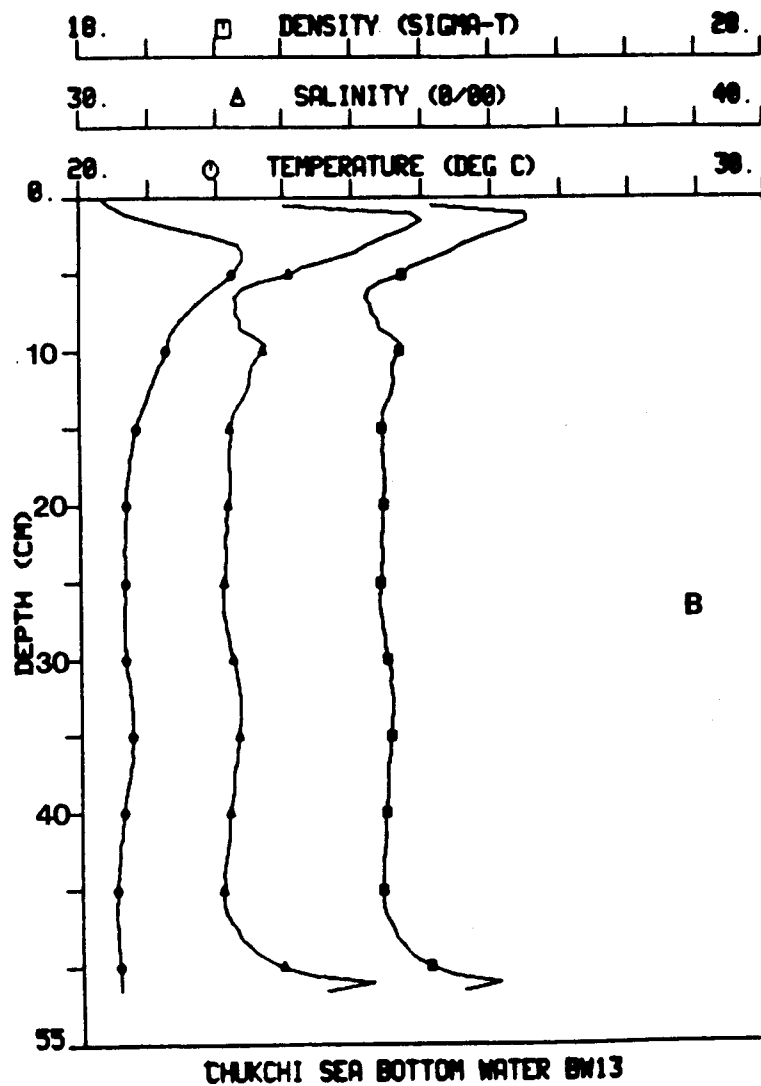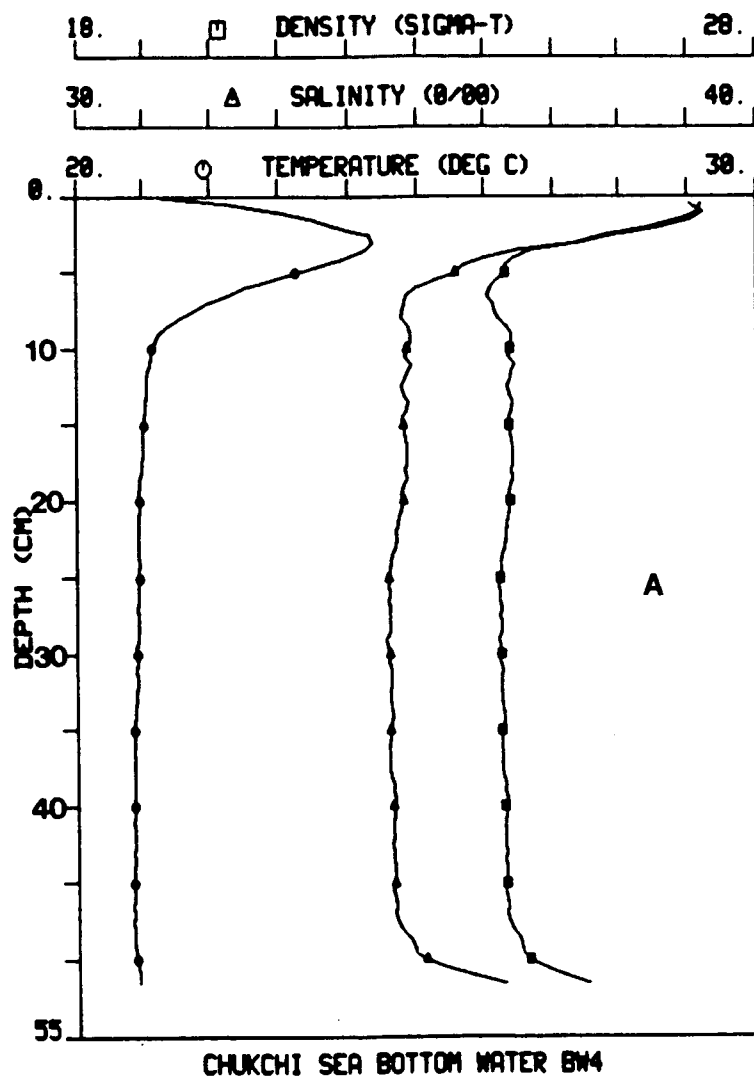
Figure 5-8.--Temperature, Salinity and Density Profiles Taken During the Laboratory-Scale Open-Water Freeze-up Experiments: (A) No. 1 at 50 minutes, and (B) No. 2 at 49 minutes. (Casts BW4 and BW13 at base of slope, 5 m from modeled coastline.)
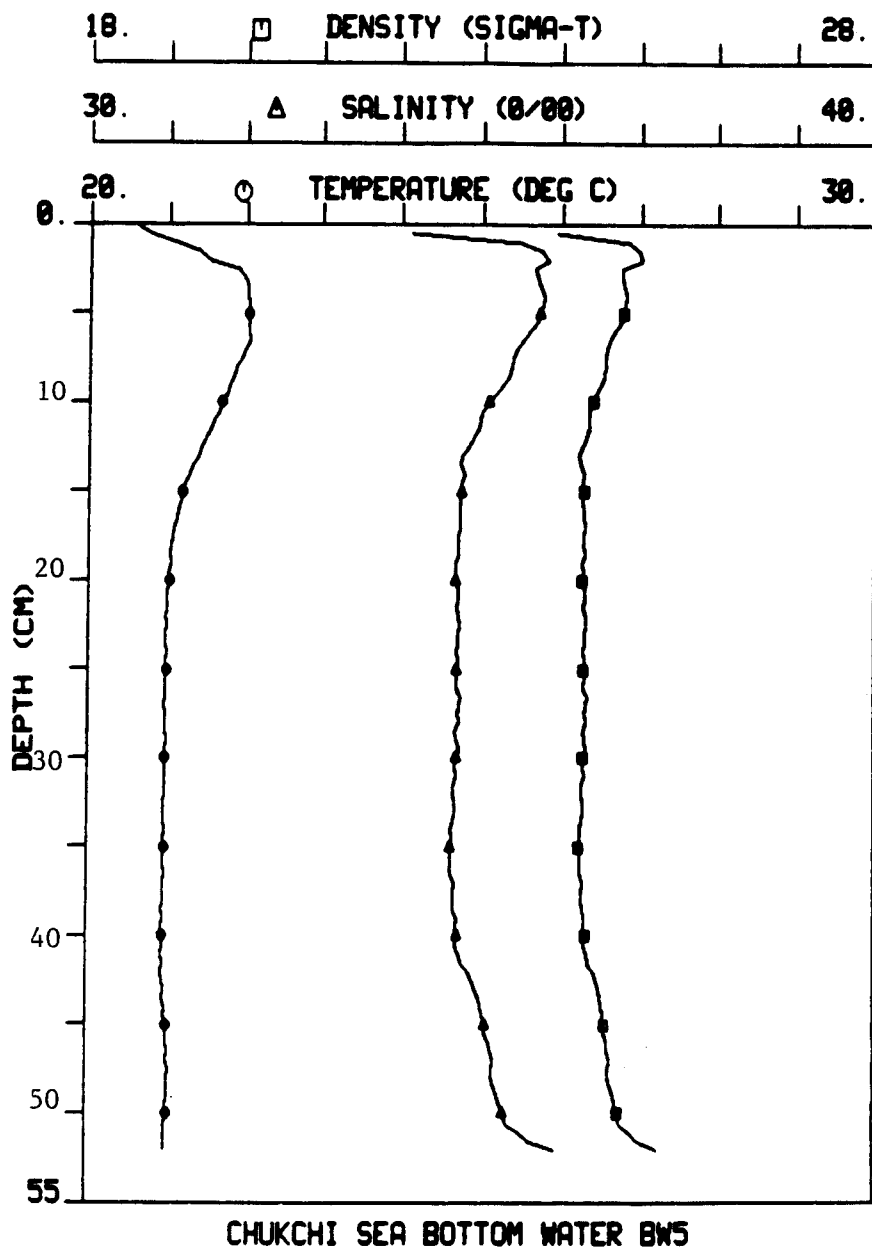
Figure 5-9.--Temperature, Salinity and Density Profiles Taken 127 Minutes into Laboratory-Scale Open-Water Freeze-up Simulation No. 1. (Casts BW5 at base of slope 5 m from the modeled coastline.)

The velocity data show similar down slope speeds for each of the open-water freeze-up experiments. Measurements of the advancing bottom brine layer give the same value (0.53 cm/sec) for fronts near the 5 m mark at 16 minutes and near the 2 m mark at 5 minutes into the experiments. Figures 5-10A and 5-10B show velocity profiles at the 2 m mark for the two experiments at 5 minutes. Although the shape of the profiles varies considerably, the maximum bottom layer speed is approximately 0.53 cm/sec in both profiles. This maximum value is consistent with the observed speed for the advance of the bottom boundary layer front given above. Figure 5-10C shows the velocity profile at the 3 m mark, 19 minutes into Run No 2. By this time an off-slope flow is seen in the upper 6 cm of the water column. Down-slope flow in the bottom boundary layer, however, remains nearly 0.53 cm/sec.

Time series temperature and salinity measurements of the bottom brine layer front at the 5.0 m mark are shown in Figure 5-11. There is a rapid increase in temperature observed as the front passes. Assuming the measured frontal speed of 0.53 cm/sec, water would have traveled from as far as 2.38 m up the slope to the site of the CTD probe during the 7.5 min recording period. Given the average speed of the front, the water forming the leading edge began its descent down the slope about 5 minutes into the experiment. This is consistent with observations which indicated that an upper-layer flow toward the coastline was present at 3.5 minutes into the experiment and the upper convective layer had mixed to 10 cm at the 2.0 m mark and to 15 cm (i.e., to the bottom) at the 1.5 m mark by 4.5 minutes into the experiment. Presumably this denser fluid, now at the bottom in the region between the coastline and 1.5 m offshore, would begin to flow down the slope. A bottom brine layer was clearly visible at 7.8 minutes between the 1.5 and 2.0 m marks, as was an upper-layer-onshore/lower-layer-offshore flow field.

Dilution or entrainment of ambient water into the falling brine can be calculated by knowledge of the initial brine concentration, the ambient salinity of the water, and the final salinity at the bottom brine layer. For a
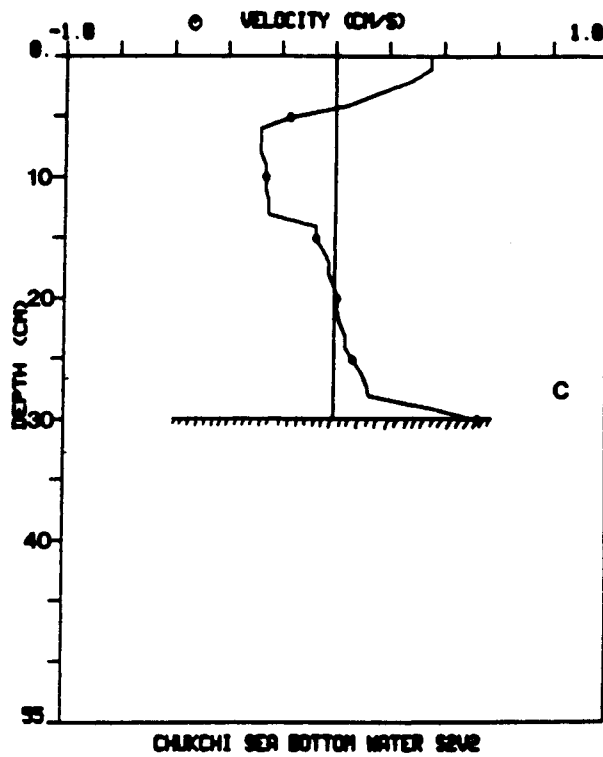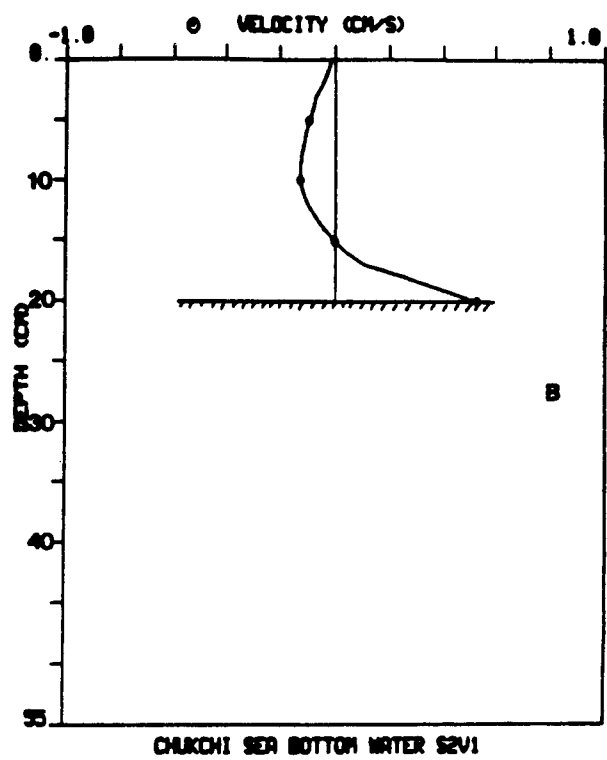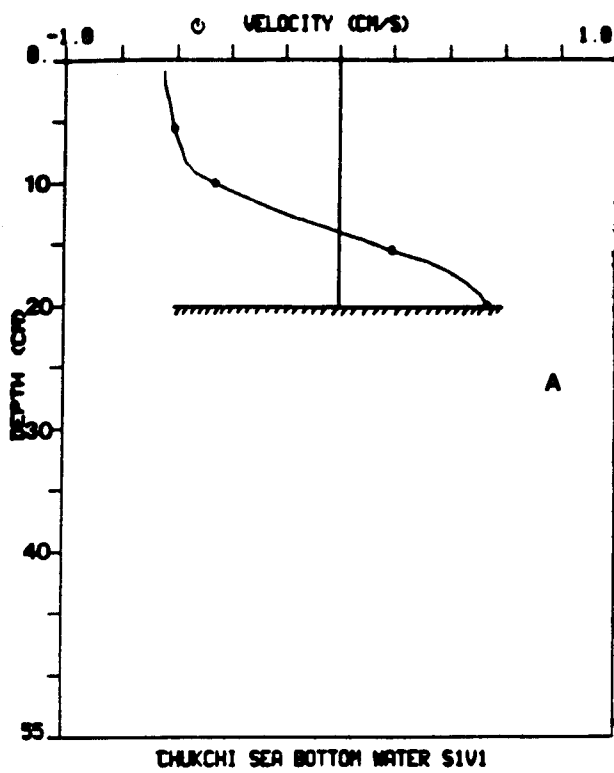
Figure 5-10.--Velocity Profiles from Laboratory-Scale Open-Water Freeze-up
Experiments: (A) No. 1 at 2.0 m from the modeled coastline at 5 minutes;
(B) No. 2 at 2.0 m from the modeled coastline at 5 minutes; and (C) No. 2 at
3.0 m from the modeled coastline at 19 minutes.
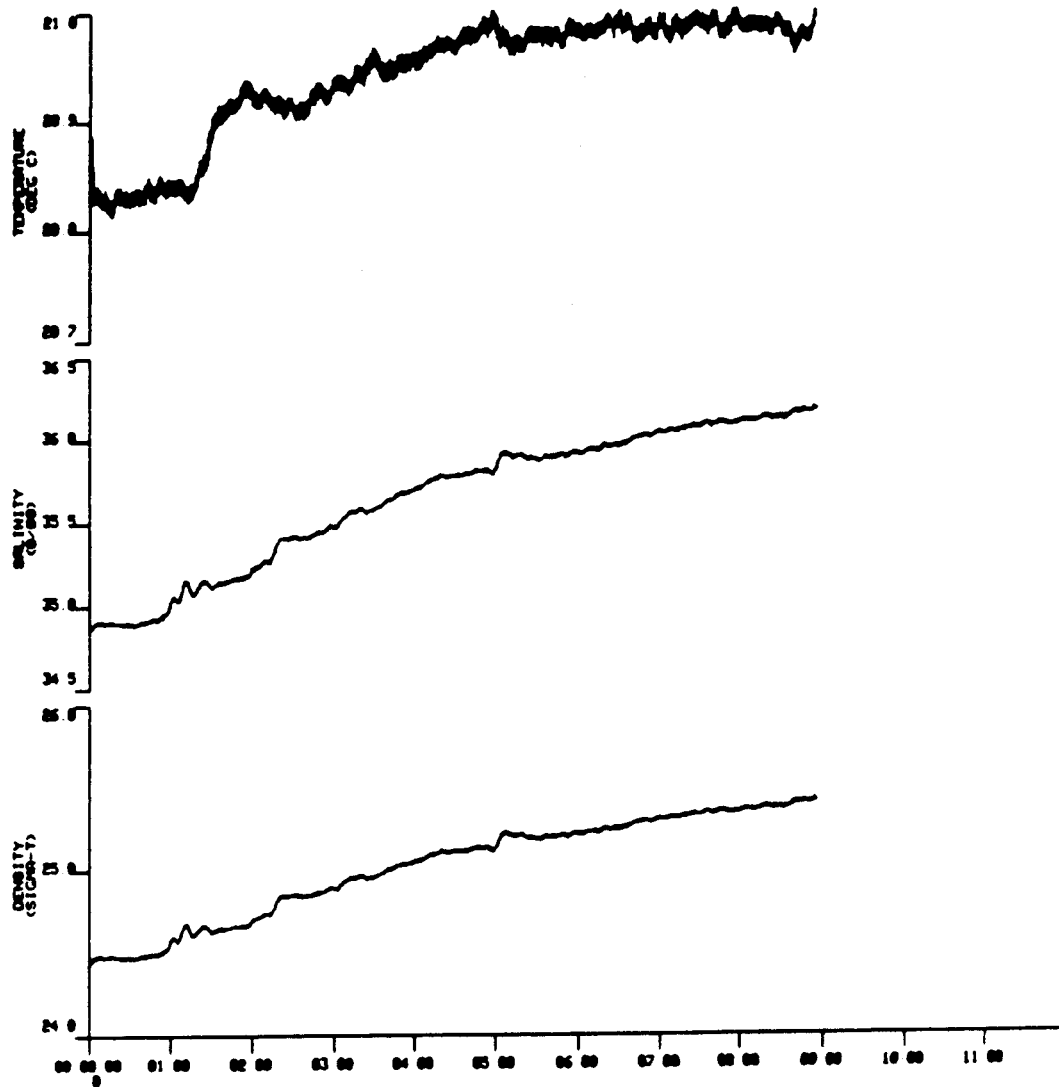
CHUKCHI SEA BOTTOM WATER BW3
DENSITY FLOW OBSERVATION AT 5.0 METERS

Figure 5-11.--Temperature, Salinity and Density Time Series in Advancing Bottom Brine Layer as it Arrived at the 5.0-m Mark in Laboratory-Scale Experiment 1.

particular milliliter volume of brine introduced at the surface, the minimum dilution can be expressed in terms of the maximum observed salinity as

$$(S_{brine}) \cdot (1 \text{ ml}) + (S_{ambient}) \cdot (x \text{ ml}) = (S_{btm \text{ layer max}}) \cdot (x+1 \text{ ml}) \qquad (14)$$

Table 5-4 gives computed values for the minimum dilution for several bottom samples taken during the two open water freeze-up experiments.

Table 5-4.--Calculated Brine-Dilution Ratios for Open-Water Experiments.

Experiment	S_{brine} (^{o}/oo)	$S_{ambient}$ (^{o}/oo)	$S_{btm \text{ max}}$ (^{o}/oo)	Minimum Dilution $(x+1)/x$	Elapsed Time (min)
Run I	40.9	34.5	35.2	9.1	84
Run II	40.0	31.3	33.8	3.5	22
Run II	40.0	31.3	33.3	4.4	57

Although elapsed time is shown in this table, time should not be inferred as the dominant variable in determination of the dilution factor. To put these factors in perspective, if 1.0 cm of 40.9 ^{o}/oo brine were added to the surface of 34.5 ^{o}/oo brine and uniformly mixed to a depth of 7.5 cm, 35.25 ^{o}/oo brine would result (see Run I case in Table 5-4 for comparison). Water samples collected at 2.5 cm (35.5 ^{o}/oo), 5.0 cm (35.3 ^{o}/oo), and 7.5 cm (34.8 ^{o}/oo) depths at 65 minutes after the start of Run I show an average salinity of 35.2 ^{o}/oo for the upper 7.5 cm. Water below that upper 7.5 cm layer remains at the pre-run value of 34.8 ^{o}/oo to a depth of 50 cm, where an increase to 35.2 ^{o}/oo is observed for the bottom 2.5 cm of water (Run I).

5.2.4.2 Lead Freeze-up Results

Figure 5-12A shows the initial temperature, salinity and density pro-
files (BW6) for the lead freeze-up experiment. Some difficulty was encountered
during the tank-filling process for this experiment and a density jump was
created at the 40 cm depth. This accident provided some interesting observa-
tions which will be presented later. As discussed in the previous section, the
conductivity cell displays anomalous behavior near the surface and both salin-
ity and density readings for the upper 1-2 cm should be disregarded. Tempera-
ture measurements in this region also indicate a 3 cm thick cooler surface
layer (~19 C°) due to overnight surface cooling.

Observations of dyed brine discharge from the modeled lead indicated
that sinking occurred rapidly (the brine was at ambient temperature) and in a
relatively uniform manner across the 5 x 50 cm lead. Downslope flow began
almost immediately and, at 8 minutes into the experiment, a 1 cm bottom bound-
ary layer was fully established at the 2.0 m mark. The leading edge of the
front was observed to reach the 3.5 m mark at 12:35 into the experiment, yield-
ing a rate of advance of 0.26 cm/sec. Other observations of the advancing
front at the 1.25 m and 2.5 m marks yielded similar velocities of 0.24 and 0.26
cm/sec, respectively, at elapsed times of 1:50 and 6:35 min. The front contin-
ued to advance downslope toward the 4.0 m mark where the density step at the
~35.0 cm depth was encountered (see Figure 5-12A). The downslope flow slowed
considerably and eventually stopped near 4.0 m where it began to "pool" in
front of the lens of denser water.

Figure 5-12B shows temperature, salinity and density profiles at the
3.0 m mark, 33 minutes into the experiment, well after the bottom boundary
layer front had reached the position of the cast and had begun to "pool".
Visual observations indicated that the downslope flow had accumulated dyed
fluid to a depth of approximately 5 cm at this position. This observation is
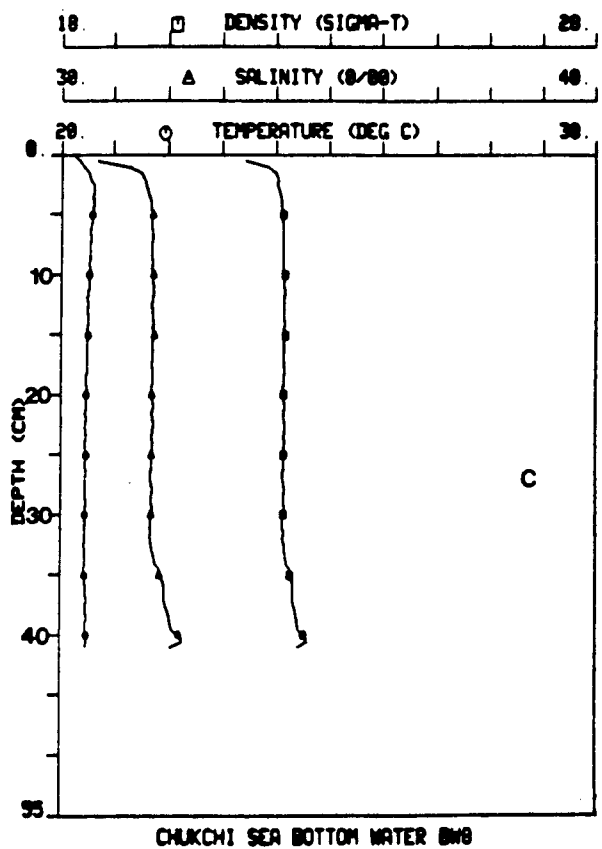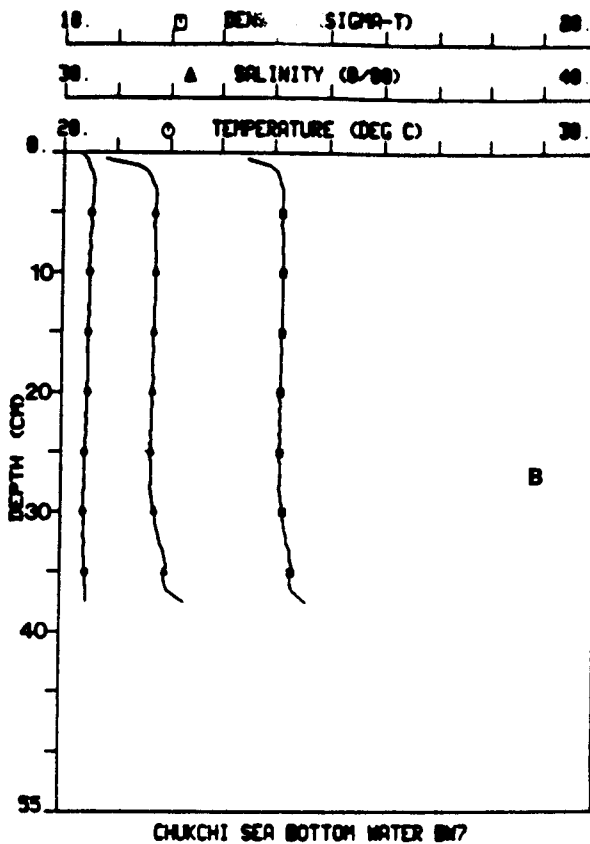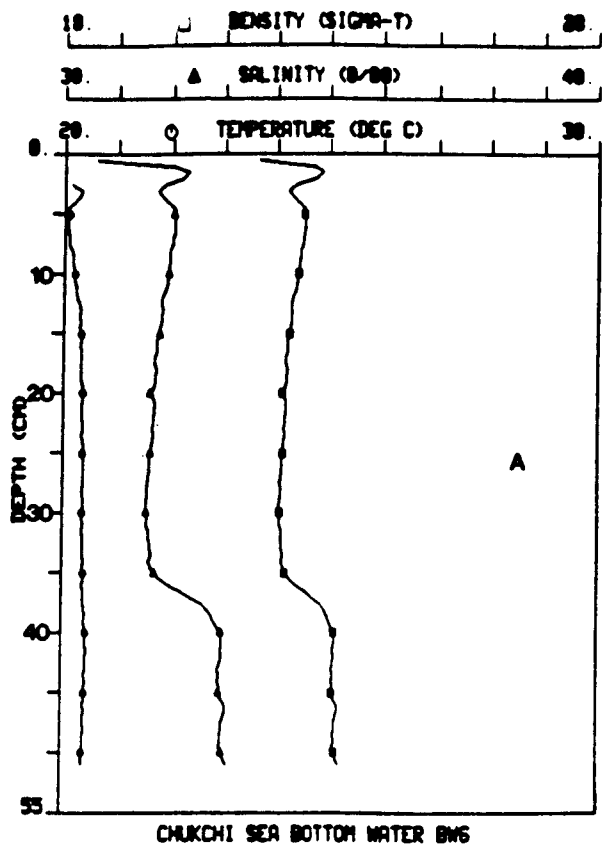
Figure 5-12.--Temperature, Salinity and Density Profile Taken During the Laboratory-Scale Lead Refreezing Experiments: (A) 0 minutes (initial), at the base of slope 5 m from the modeled coastline, (B) 33 minutes, 3.5 m from the modeled coastline, and (C) 79 minutes, 4.0 m from the modeled coastline.

consistent with data collected in the cast (see Figure 5-12B) which shows an increase in the salinity and density data from the pre-experiment values between the depths of 30 and 37 cm. The maximum salinity observed in this layer was 32 ^{o}/oo, which is an increase from the originally measured salinity of 31.6 ^{o}/oo at that depth. At an elapsed time of 79:25 a third profile (Figure 5-12C) was taken at the 4.2 m mark over the layer of pooled brine. The forms of the lower portion of the salinity and density profiles are almost exactly the same as those observed at 3.9 m, displayed lower in the water column when adjusted for the difference in water depth of 3.0 cm. With further elapsed time, the pooled brine at 4.0 m slowly spread horizontally along a depth of equilibrium density (approximately 35 cm) in the original density profile (see Figure 5-12A). The mixed brine did not have sufficient density to continue its advance down the slope along the bottom and was starting to spread laterally along the density interface. This process can be likened to an observed Chukchi Sea situation where dense brine, formed in the nearshore region, flows into Barrow Canyon and then northward along the canyon axis until it reaches the layers of dense Atlantic and intermediate water (Figure 5-13) where it spreads laterally into the Beaufort Sea. Dilution of the original brine (38.2 ^{o}/oo) introduced into the lead was 22:1 (Table 5-5). This is considerably greater than the dilution observed for the open-water cases (Table 5-4) where an average dilution of 6:1 was observed.

Table 5-5.--Calculated Brine-Dilution Ratios for the Lead Experiment (Laboratory Model).

Experiment	S brine (^{o}/oo)	S ambient (^{o}/oo)	S btm max (^{o}/oo)	Minimum Dilution (x+1)/x	Elapsed Time (min)
Run III	38.2	31.7	32.0	21.6	33
Run III	38.2	31.7	32.0	21.6	79
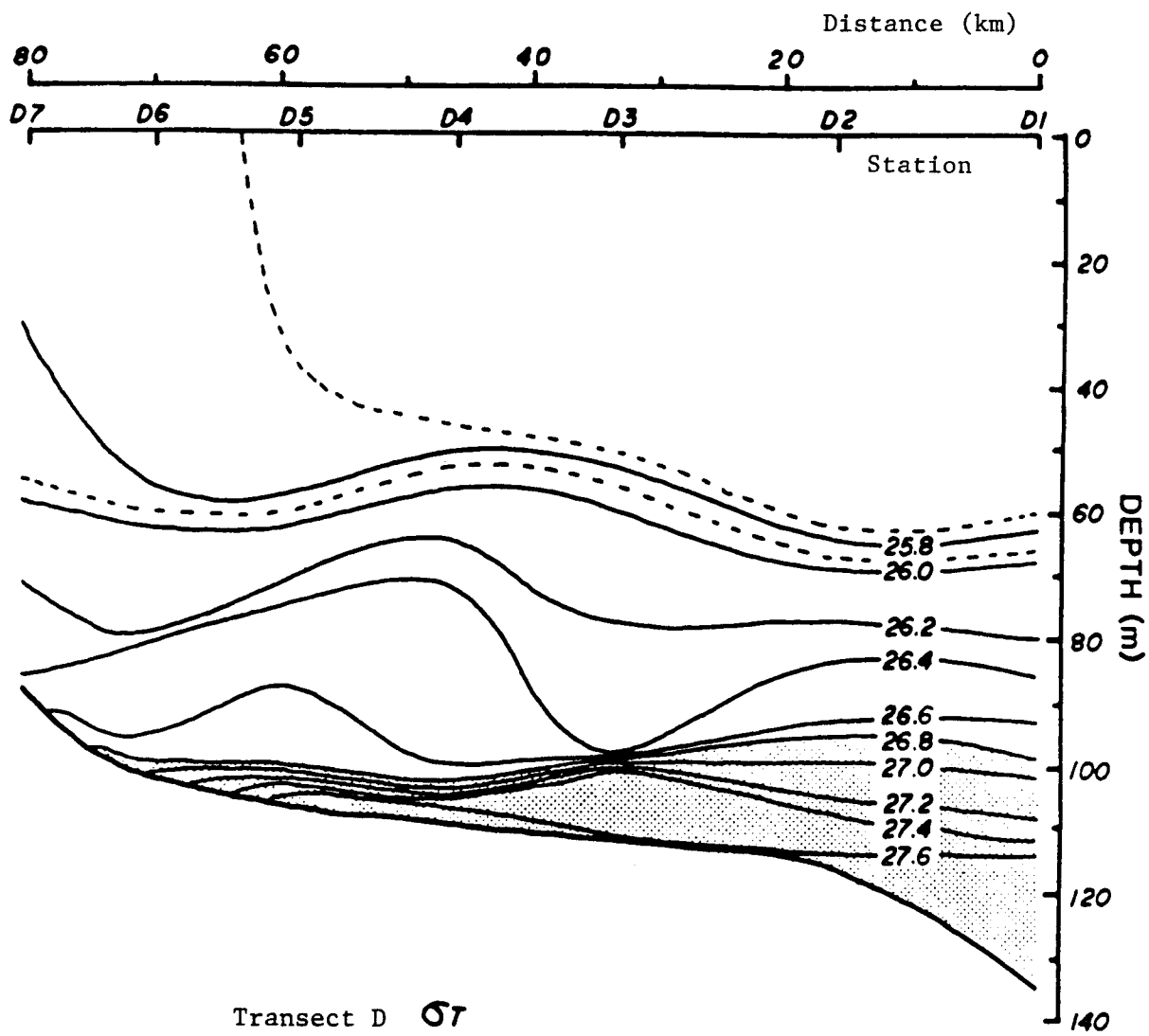
Figure 5-13.--Density Section Along Axis of Barrow Canyon, Showing Depth of Atlantic Water (shaded). (See Figure 4-23 for Transect D station locations.)

This apparent higher dilution rate is a consequence of water depth at the point of brine introduction. In the "refreezing lead" experiment, the brine was introduced and mixed into 15 cm of water. In the "open-water" case, a considerable portion of brine (i.e. that volume introduced inshore of 150 cm) vertically mixed with less than 15 cm of water and produced less dilution and therefore higher salinities. A simple calculation using the 250 ml of brine (equivalent to 1 cm of height in the 5 x 50 cm lead) at 38.2 ^{o}/oo added to the lead and completely mixed with the underlying 15 cm of water at 31.7 ^{o}/oo (15:1 dilution) yields water at 32.1 ^{o}/oo, which is similar to the observed maximum salinity of 32.0 ^{o}/oo pooled at the 4.0 m mark.

Velocity profiles for the lead freeze-up experiment are shown in Figures 5-14A and 5-14B for the 2 m and 3.5 m marks at 7.6 and 12.0 minutes into the experiment. Note that the maximum bottom layer velocity (~0.1 cm/sec) in the fluid behind the front is considerably less than that observed for the advance of the front itself, which was measured at ~0.25 cm/sec. Although temperature and salinity time-series data similar to Figure 5-11 were not taken for this advancing front, it must be assumed that the density of this layer is less than that of the initial front. The majority of the relatively undiluted brine (entering at the lead) proceeded downslope (at 0.25 cm/sec) as a "parcel" of fluid, which was followed by the more dilute and less dense water moving with a slower downslope velocity.

5.2.5 Discussion

The series of experiments conducted to demonstrate the process of dense brine formation in arctic nearshore waters have been extremely informative in illustrating the basic physical phenomena active during fall freeze-up and winter refreezing periods. Important observations relative to the near-shore exchange of water during fall freeze-up can be extrapolated from the laboratory data to field conditions as: (1) the formation of a slow (0.3-0.9 cm/sec) near-surface ($\leq$10 m) onshore flow balancing (2) a more rapid (1.5-1.7 cm/sec) offshore flow in a 2 to 5 m thick bottom layer. (These current esti-mates are consistent with the observed field values described in Section 5.3.3

315
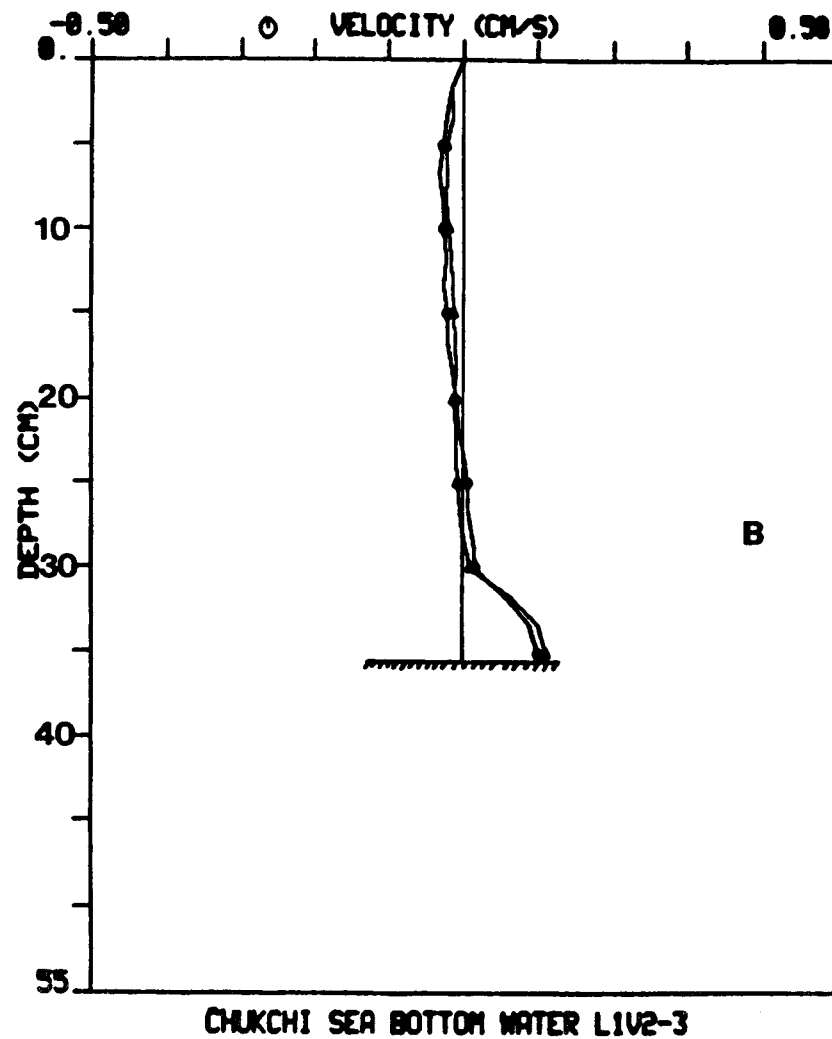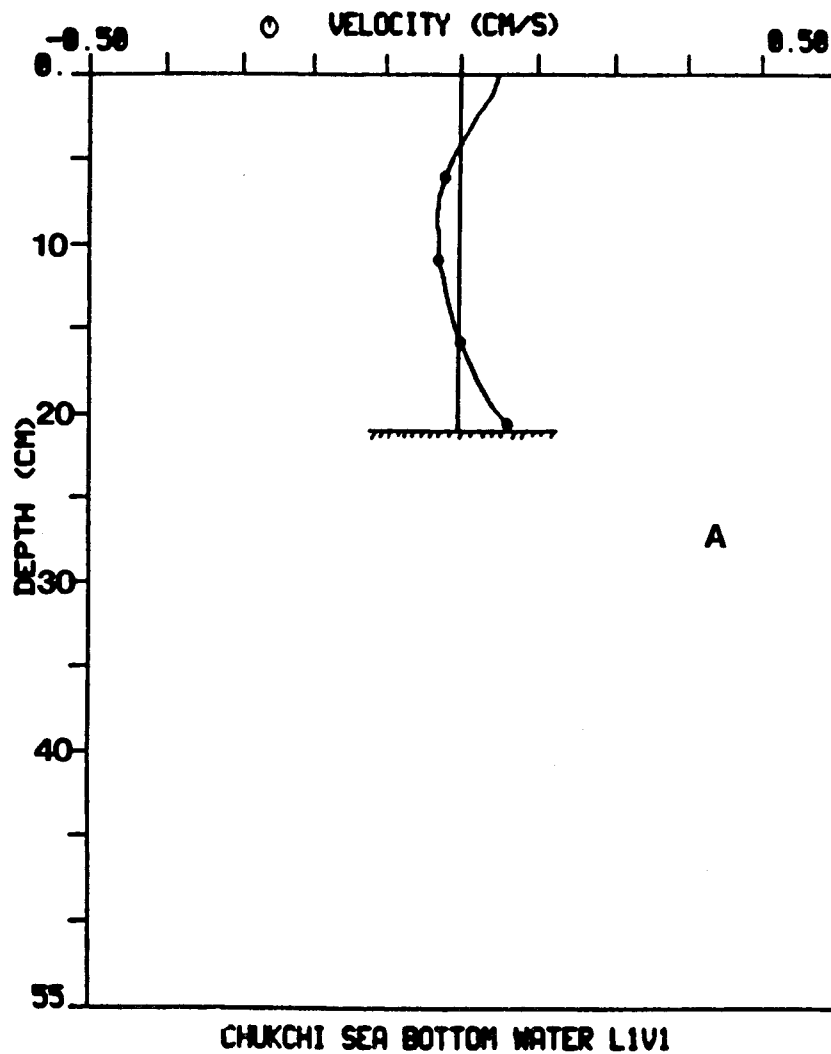
Figure 5-14.--Velocity Profile Taken During the Laboratory-Scale Lead Refreezing Experiments: (A) 7.6 minutes, 2.0 m from the modeled coastline, and (B) 12.0 minutes, 3.5 m from the modeled coastline.

316

on Field Studies.) In the case of a nearshore oil spill this general circulation pattern would tend to concentrate (in the absence of wind effects) surface spilled oil products in the nearshore region. If winds are present they would dominate surface oil movement. Onshore winds would tend to compound such behavior, whereas offshore winds might tend to disrupt the pattern. Winds might also tend to herd surface oil to one end of an open lead system. However, wind effects must be modeled as a stochastic process, so further discussion of perturbations caused by surface winds is unwarranted as the laboratory experiments were not designed to include them.

In nearshore areas, dissolved lighter fractions of the oil would be incorporated into the forming brine and be transported with the brine. In deeper waters the brine (and any associated hydrocarbons) would of course be diluted as the brine is exuded and sinks. These laboratory observations indicate that much of the dense brine formation occurs in water depth less than 20 meters (typically within 15 to 20 km of shore) although scaling-up of the experimental laboratory results relative to vertical entrainment of the surface brine must be done very cautiously. Existing field data do support these laboratory observations that brine formation occurs in this region. Aagaard (1984) observed a thin (<2 m) layer of brine (33-36.5 ^{o}/oo which formed at depths less than 25 m at Pt. Lay. Similar brine layers were observed in his Pt. Franklin and Pt. Barrow salinity sections. Historical data repoted by Garrison (1977) also suggest the near shore formation of dense brine in the Chukchi Sea at depth less than 20 m. The salinity profile shown in Figure 5-1 (from Hachmiester and Vinelli, 1985) also very clearly support the observations from these earlier studies.

A very simplistic model of the freeze-up process for open water is shown in Figure 5-15. Starting with ambient water at 31.6 ^{o}/oo and allowing (per Section 5.2.2) 0.65 m of ice to form over 20 days, 2 m^3 of 40 ^{o}/oo brine will be input uniformly across the nearshore surface waters. The resulting salinity field (Figure 5-15B) is obtained if no horizontal mixing is allowed. As observed in the laboratory experiments, the bottom brine shows maximum off-shore bottom salinity which is characteristic of the water formed at 5-10 km

DISTANCE OFFSHORE (km)

a

DISTANCE OFFSHORE (km)

b
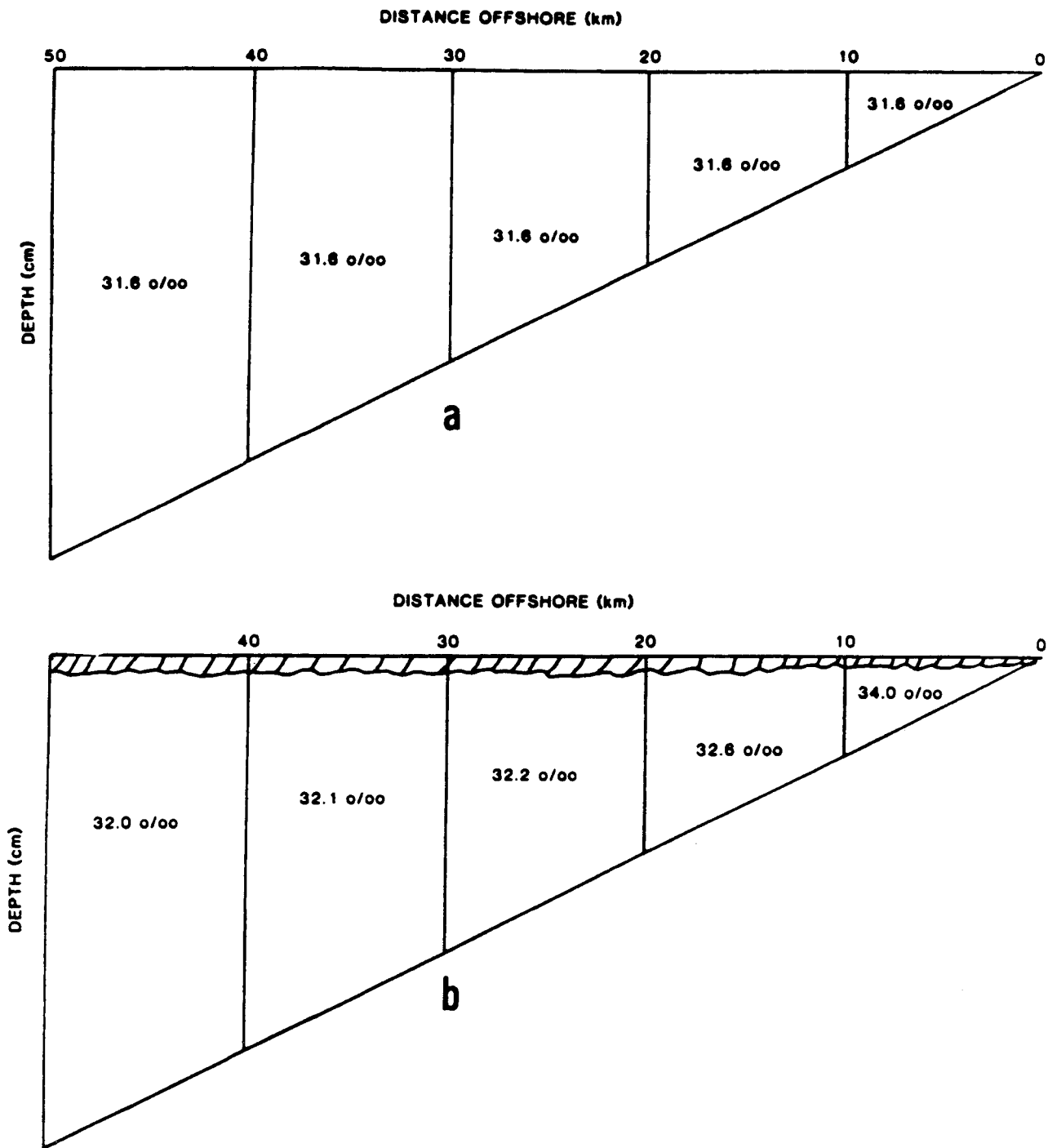
Figure 5-15.--Simplistic Model of the Freeze-Up Processes: (A) Initial
conditions in 10 km-wide cells, and (B) final conditions in 10 km-wide cells
after formation of 65 cm of ice over 20 days assuming no horizontal mixing.
(Results in uniform input of 2-m layer of 40% water across 50-km distance.)

318

offshore (Table 5-4) or 33.3-34.0 $^{o}/oo$. Given the downslope speeds predicted by the open-water freeze-up experiments, in the absence of other external forces, this brine should reach a 20 km offshore position within 20 days of formation. A 1.5 to 2.0 m bottom layer flowing at 1.5-1.7 cm/sec would remove a volume of water equal to that in the 0-10 km region in approximately the same time (17-25 days), thus implying an onshore flow of surface water of equal magnitude and additional dilution to perhaps 33.5 $^{o}/oo$. Measurements made in February 1984, (see Figure 5-1) under ambient salinities of 32.1 $^{o}/oo$ and considerably reduced brine formation rates, showed bottom salinities of 33.1 $^{o}/oo$ in a 2 m thick lower layer. With all other processes remaining the same, this would imply a 70% reduction in the brine-formation rate in the nearshore where the 33.1 $^{o}/oo$ water was formed, or additional dilution of the nearshore water as described above through onshore flow, or both. The important fact remains, however, that dilution in both the fall freeze-up and the lead refreezing cases is sufficiently low in the nearshore region to allow for the possibility that significant concentrations of dissolved hydrocarbons from a hypothetical spill might persist in the sinking brine.

5.3   FIELD PROGRAM TO STUDY DISSOLUTION AND TRANSPORT OF SPILLED AROMATIC HYDROCARBON COMPONENTS DURING OPEN LEAD REFREEZING AND BRINE GENERATION PROCESSES IN THE CHUKCHI SEA

5.3.1   Objectives of the Field Program

The field program tested the hypothesis that the dissolved fraction of an oil spill in the upper water layer of a refreezing lead could be incorporated into a denser brine mass that is transported to the bottom as the brine sinks under the influence of gravity. Specific objectives of the field experiments were the following:

1)   demonstrate brine production and its association with the lead system northeast of Pt. Franklin,

2)   demonstrate incorporation of hydrocarbons (from a 38 liter aromatic "cocktail" spilled into the lead surface waters) by brine produced during the refreezing process, and

319

3) track any such brine (and accompanying dissolved hydrocarbons) over time and distance by using acoustic transmitting bottom drifters to aid in station/site selection and collecting water samples for measurements of aromatic hydrocarbon concentrations.

5.3.2   Field Methods and Materials

The field program was conducted in early March 1985 at a nearshore location northeast of Pt. Franklin, Alaska (Figures 5-16 and 5-17). Selection of this test site was based on 1) its proximity to logistics support at Barrow, 2) year-to-year persistence of an open-water lead system in shallow water in the area, 3) anticipated low water current velocities in the area, and 4) previoulsy observed brine formation events during freezing in the area (i.e., February/March of 1982 and 1984; Hachmeister and Vinelli, 1985).

Cocktail Deployment--10 March 1985

For the field oil-spill experiment, an aromatic hydrocarbon "cocktail" mixture (Table 5-6), not whole crude oil, was used. A total of 38 liters was released on 10 March 1985 in the open water of an extensive lead system north-east of Pt. Franklin, Alaska (see Figures 5-16 and 5-17). The spill occurred at site 10 (71° 1.4'N, 158° 12.1'W, Figure 4-25) in an open refreezing lead that was approximately 30 m wide. Water depth at the spill site was 29 m, which was slightly greater than the desired depth (15-20 m). However, the solid ice on both the north and south sides of the lead provided stable plat-forms from which the spill was initiated and from which subsequent sampling of near-surface and bottom waters could be performed. CTD measurements were obtained at selected sites and times through holes in the ice cover to monitor relevant water mass properties before and after the spill event.

Conditions at the time of the spill were favorable for the occurrence of brine formation: air temperature was -24°C, and frazil and grease ice were being actively formed. CTD and current meter data collected in the region on 9 March (i.e., the day before the spill) indicated that higher salinity water existing under the lead was sinking and moving in an onshore direction.
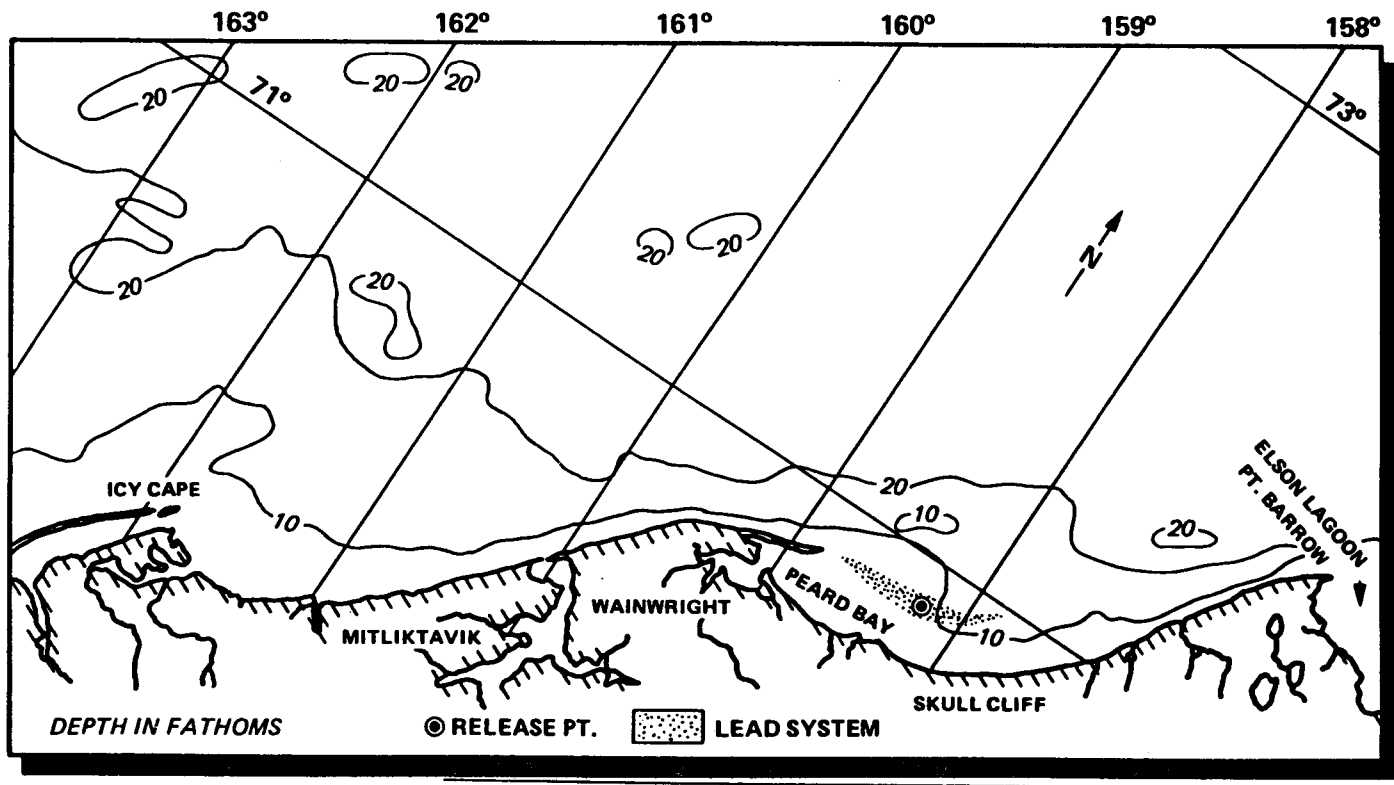
Figure 5-16.--Map of Study Area and Anticipated Lead System
Near Peard Bay.
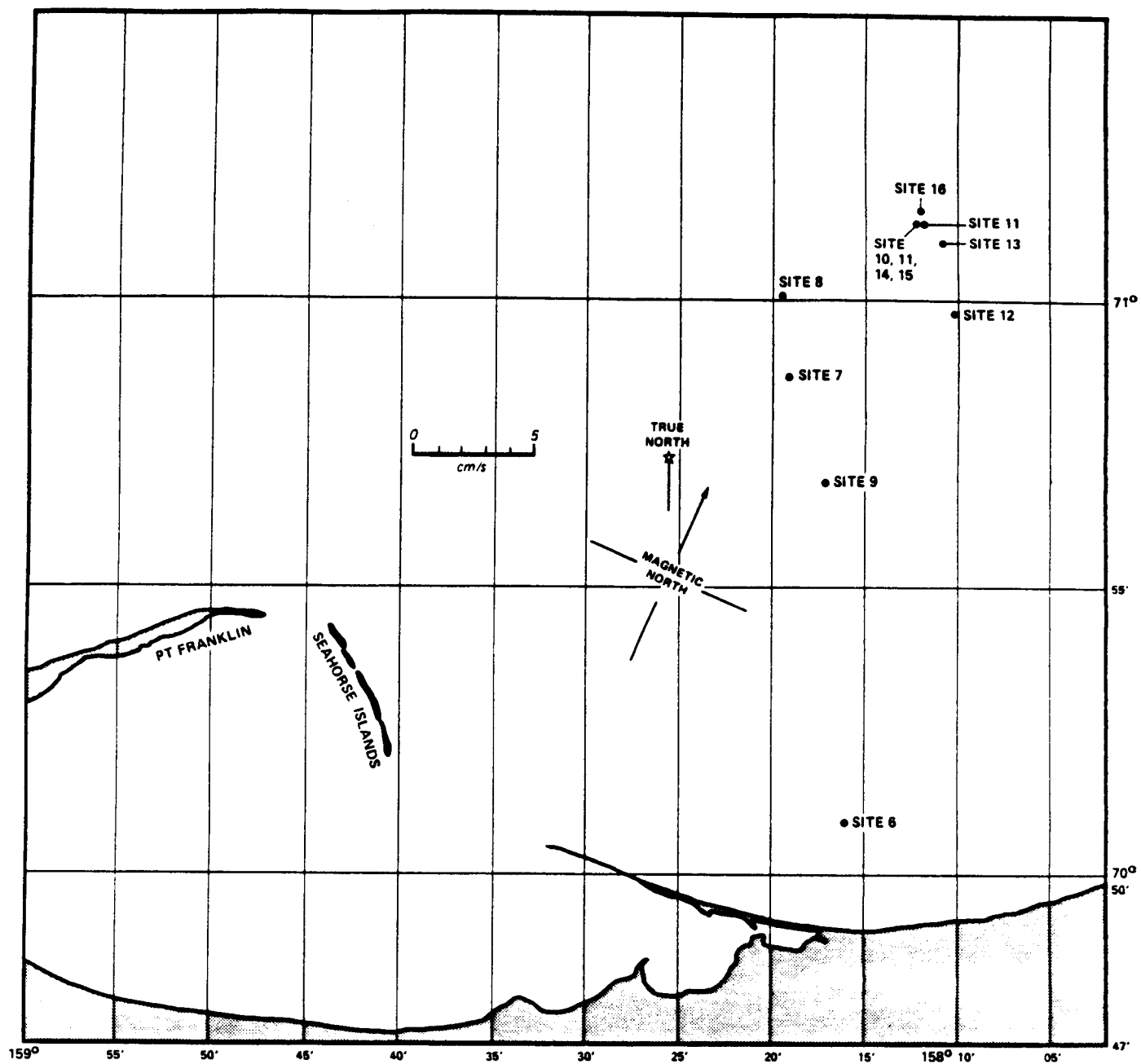
Figure 5-17.--Station Locations in the Chukchi Sea, Pt. Franklin Area.

Table 5.6--Individual Components and Amounts in
the Chukchi Sea Aromatic Cocktail Mixture.

Compound	Amount
Toluene	18.9 liters (5.0 gallons)
Benzene	9.5 liters (2.5 gallons)
p-Xylene	3.8 liters (1.0 gallons)
o-Xylene	3.8 liters (1.0 gallons)
Ethylbenzene	500 grams
Naphthalene	1,000 grams
2-Methylnaphthalene	500 grams
Uranine dye	500 grams

Immediately before the cocktail release, a CTD cast was completed, and prespill surface and bottom water samples were obtained with Nansen bottles deployed through a 25 cm diameter hole augered through the ice. An Inter Ocean S4 current meter was deployed directly into the lead at the site approximately 15 minutes before the spill to measure current speed and direction (5 minute vector averages). This meter indicated a bottom current with a speed of 1.5 cm/sec and a heading of 25°-35° (i.e., NNE) at the time of the spill.

At 1405 hrs, the spill mixture (Table 5-6) was released over a 10 minute period into the middle of the lead at a depth of 2-4 cm below the water surface. After release of the mixture, two transponders were deployed into the lead. A 27.0 kHz acoustic seabed drifter was deployed with a drogue flotation collar (to impart neutral density in 33-38 ^{o}/oo, -1.8°C seawater) to track the bottom water movement, and a 37.0 kHz transponder, with no flotation, was released to mark the deployment site.

The cocktail had approximately 20-25 minutes to mix with the forming slush ice and associated brine. The uranine dye in the mixture very clearly allowed differentiation between the cocktail that was floating on accumulating slush ice and associated pieces of broken ice chunks and that which was actually mixed into the surface waters. Specifically, the cocktail that was spilled or pooled on top of existing or freshly formed ice was still in the oil (toluene) phase, and the uranine dye retained a dark red color. When the cocktail mixed with the water the uranine turned a bright yellow-green.

Five to ten minutes after the release of the cocktail, additional 1-liter near bottom and surface (1 m below the bottom of the ice cover) water samples were obtained with a Niskin bottle through a 25 cm diameter hole augered in a small ice floe approximately 15 m from the release site. (This location (sample) was identified as Station 10.)

Between 20 and 30 minutes after the experimental spill was initiated, it became apparent that the lead was closing. At first, it appeared that the lead was only filling up with excessive slush and grease-ice covered pans, but then observations of the ice in the rubble field on the northern side of the lead clearly indicated that the entire rubble field was moving slowly towards the pan from which the cocktail had been released. Eventually, the rubble field from the other side of the lead pushed grease ice and larger ice chunks in front of it as it approached. Larger chunks (1-2 m) were up-ended and forced against, under and on top of the edge of the southern floe that supported the scientific party and all field equipment. After slightly more than an hour (1512 hrs or 68 min post-spill) the moving rubble field had completely closed the lead, and some of the dye-stained (red, yellow and green) ice had actually been subducted and forced beneath the rubble field and (presumably) under the pan from which the observations were being made. Approximately half of the dye-stained ice ended up ridged against the stationary observation pan, and the rest was ground up or incorporated into or under the rubble field that now occupied the lead where the experimental spill had been initiated an hour earlier. Schematic plan views of the experimental spill site and lead system before and after closing are presented in Figure 5-18.

In designing the experiment, we had hoped to work in a lead system that remained open with active ice formation for 2-3 hours after the spill release. Therefore, as a result of the lead closing, there was some uncertainty as to how much of the hydrocarbon cocktail actually dissolved into the sinking brine at the time. This confounded subsequent attempts to estimate the rate of initial mixing or dilution of the aromatic cocktail.

The S4 current meter was retrieved at 1450 hrs, and the scientific party retreated from the observation pan (Station 10) and occupied an adjacent more stable ice floe (100 m by 200 m) which had been used as a staging area where the helicopter had landed prior to the experiment. This location was approximately 50 meters to the south of the spill site (see Figure 5-18B).

True
North
↑

(a)   1400 hours

Smooth Ice

Site of Cocktail
Deployment

Refreezing Lead/Open Water

Rubble

Current Vector

Site 10

Station 10
Current
Data: 1.5 cm/sec
          25-35 °True
          at 1415 Hrs

0 _____ 100m

(b)   1500 hours

Ice

Open Water

1m Ridge

Closed Lead
Rubble Field

Current
Vector

Site 10

Site of Cocktail
Deployment

Station 11

Smooth Ice

Helicopter landing
site

Station 11
Current Data:
          1.6 cm/sec
          25° True
          1655-1835Hrs

0 _____ 100m

Figure 5-18.--Plan View of the Lead/Ice System on 10 March 1985:
(A) 1400 hours and (B) 1500 hours.

While it could not be observed from the original pan at Station 10 or the adjacent floe by the helicopter, there was a large new lead (100 to 150 m wide) opening up approximately 30 m north of the rubble field that resulted from the closure of the initial experimental lead. This new lead (Figure 5-18B plan view) was discovered during the helicopter flight to Station 11, which was 300 to 400 m to the west of the initial spill release point.

After completing a CTD cast and deploying the current meter at Station 11 at 1655 hrs, a directional EFCOM sonar receiver system was used to obtain direction headings on the two transponders that had been released at site 10. The receiver system was assembled by attaching the sonar head to six 1-meter long, 7.5 cm diameter PVC extensions for under-ice depth and directional control. The electrical leads for the sonar head were contained within the PVC tubing, and these were attached to an EFCOM sonar receiver system that was contained in an Igloo^{TM} cooler. The cooler was equipped with an automobile battery and heater that maintained the unit at a necessary temperature level such that the liquid crystal frequency display could be used to tune to the 27.0 and 37.0 kHz transponders.

At 1720 hrs the ice pan at Station 10 was still intact, so it was reoccupied (identified as Station 10A) and another sampling hole drilled. Two additional 1-liter water samples (at 26 m bottom and 14 m intermediate depths) were collected with a Nansen bottle. The sonar receiver system was then reassembled and an additional fix on the 37.0 and 27.0 kHz pingers obtained. At 1740 hrs the two deployed transponder units were separated by approximately 15 degrees, but an exact distance separation between the two could not be obtained because the sonar receiver system was located almost directly over the

transponders. Open water to the north of the spill site and safety considera-
tions prevented occupation of additional stations on 10 March. Therefore, we
returned to Station 11 to retrieve the S4 current meter at 1835 hrs, and the
scientific party returned to base at UIC/NARL.

Water Column Sampling--11 March 1985

The general area of the spill site was surveyed, and Station 12 (see
Table 5-7 and Figure 5-17) was occupied immediately to the southeast of a 500
meter wide rubble field and ridge system approximately 2 miles south/southeast
of the spill site. CTD and current meter data were collected from 1225-1445
hrs, and a near bottom current was detected with a velocity of 1.1 cm/sec and a
direction of 161 degrees True (toward the south/southeast). Surface (just
below the ice), and near bottom (0.5-1m above the bottom) water samples were
collected for hydrocarbon analyses, and the EFCOM sonar receiver system was
assembled to locate the positions of the fixed 37 kHz and seabed drifting 27
kHz transponder units. No sonar signal could be detected from either trans-
ponder. Presumably, this was because of the vertical dimensions of the rubble
field and ice ridge systems to the northwest of the area (i.e., ridges had
elevations in excess of 3 m and estimated keel depths of 15 to 20 m).

At 1520 hrs Station 13 was occupied 1.9 km to the north/northwest of
Station 12 (see Figure 5-17). Station 13 was characterized by much smoother
ice, and directional readings for the two transponders were successfully
obtained. Water samples were again obtained at the surface and bottom depths.

Station 14 was located on smooth ice approximately 300 m southeast of
the original spill site. Surface (just below the ice) and bottom water samples
were collected, and sonar fixes were obtained for the two transponder units.
From the position-fix obtained for the helicopter and triangulation of the
sonar readings at Stations 13 and 14, it was apparent that the surface ice had
not moved relative to the 37 kHz transponder beneath the spill site. The
seabed drifting transponder (27 kHz) had travelled approximately 500 to 1000 m
in a direction of 25-30° True from the original release site. Because of

Table 5-7.—Station Locations and Bottom Current Meter Readings for 1985 Field Program.

Date	Station number	Latitude (°N)	Longitude (°W)	Bottom depth (m)	CTD	Speed (cm/s)	Near bottom current Direction (° True)	Time	Depth (m)
(North of Pt. Barrow, equipment checks)									
3/8/85	001	71°31.3'	155°22.7'	22	X	3.2	275	1150-1430	21
						3.9	91	1440-1530	21
3/8/85	002	71°28.3'	155°19.5'	20	X				
3/8/85	003	71°24.4'	155°15.1'	18	X				
3/8/85	004	71°19.3'	155°11.1'	--	X				
3/8/85	005	71°33.5'	155°30.3'	120	X				
(Pre-spill)									
3/9/85	006	70°50.9'	158°16.0'	11	X				
3/9/85	007	70°58.7'	158°19.0'	21	X	3.0	154	1335-1545	21
3/9/85	008	71° 0.1'	158°19.3'	26	X				
3/9/85	009	70°56.9'	158°17.1'	20	X				
Spill event: 1405-1415 hours 3/10/85, Station 010									
3/10/85	010	71° 1.4'	158°12.1'	29	X	1.5	35	1455	28
3/10/85	011	71° 1.4'	158°12.4'	28	X	1.6	25	1655-1835	27
3/11/85	012	70°59.8'	158°10.2'	24	X	1.1	161	1225-1445	23
3/11/85	013	71° 1.0'	158°10.7'	27	X				
3/11/85	014	71° 1.4'	158°12.1'	29	X				
3/11/85	015	71° 1.4'	158°12.1'	26					
3/10/85	016a	71° 1.6'	158°12.0'	29	X	3.0	284	1255-1355	27
3/10/85	016b	71° 1.6'	158°12.0'	26		3.1	272	1405-1455	25
3/12/85	016c	71° 1.6'	158°12.0'	26		3.9	265	1505-1545	25
3/12/85	017	71° 1.6'	158°12.0'	26					
3/12/85	018	71° 1.6'	158°12.0'	26					
3/12/85	019	71° 1.6'	158°12.0'	25					
3/12/85	020	71° 1.6'	158°12.0'	25					
3/12/85	021	71° 1.6'	158°12.0'	26					

extremely thin ice to the north of the original spill site, however, no stations could be occupied in this direction (i.e., where the 27 kHz seabed drifting transponder was detected).

The spill site itself was then reoccupied now designated as (Station 15), and the original experimental lead was observed to be completely covered by a partially frozen rubble field. The broad expanse of open water that had opened to the north of Site 10 just after the spill event (see Figure 5-18B) had begun to refreeze, but neither it or the rubble field over the initial spill site were explored further due to uncertainties regarding their stability. At 1730 hrs (26-27 hours post-spill) two additional water samples (subsurface and bottom) were obtained through a freshly drilled auger hole at Station 15, which was located 7 m from the original spill site.

Water Column Sampling--12 March 1985

Observations during the flight from Barrow to Pt. Franklin indicated that considerable refreezing of the offshore lead system had occurred over the previous 48 hours. Therefore, the original spill site location (Station 10/15) was reoccupied. Figure 5-19 presents a schematic plan view of the original spill location as well as Stations 16 through 21 which were occupied on 12 March 1985. All of the latter stations were located on the freshly refrozen lead that had opened to the north of the original spill site (Figure 5-18B) within one to two hours of the start of the experiment 48 hrs earlier. The ice thickness at these stations was now 12 to 18 cm, and open pools of fresh seawater or cracks in the ice were occasionally encountered in the area. Station 16 was occupied, and the seabed drifting transponder (27 kHz) was located by triangulation using the EFCOM sonar receiver system at Site 16C and auger boring Site X further to the west (see Figure 5-19). The transponder was approximately 500 to 750 m from the original spill release point, and appeared to be trapped in the under-ice ridge system between Stations 16 and 17. The location of the seabed drifting transponder at this time was consistant with bottom current directions that had been measured during the first two hours following the spill. However, the estimated distance from the spill site

330

True
North

Open Leads

Auger
Boring ✕
Site

3 cm/sec

1200-1500 hrs
3/12/85

16a 16b 16c

27 kHz
Transponder

17

18

19

20

21

15

Site of
Cocktail Deployment

0   100m
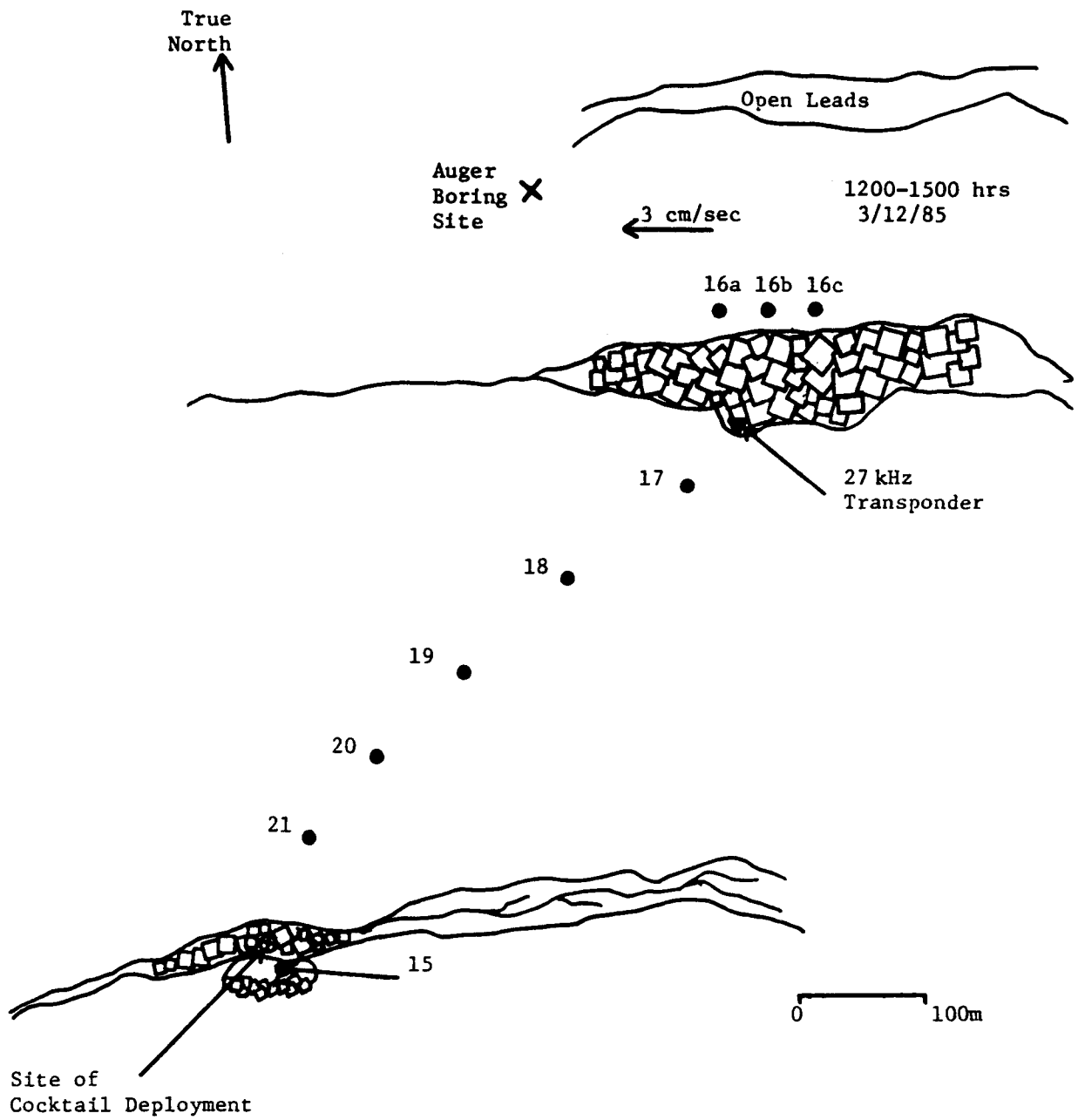
Figure 5-19.--Station Area Overview on 11-12 March 1985.

331

indicated that the transponder may have become trapped in the subsurface ice ridge system in the first 1 to 2 hours after its release. This ridge system was quite extensive, with upper surface relief up to 3-4 m and estimated under-ice relief of 15 to 23 m. It was possible that portions of this under-ice relief extended all the way to the bottom sediment, although this could not be determined from the surface. At certain locations on the northern slope of the ice ridge system (i.e., near Station 16), the ice was sufficiently thick immediately adjacent to the ridge to support the helicopter and thereby expedite sampling operations.

A series of water samples were obtained near the location of the seabed drifting transponder for an east-west transect of auger holes at Stations 16A, B and C and from Station 17. An ice thickness of 5-6 m prevented boring of a sampling hole immediately over the transponder. Four 1.3 meter long auger bits were connected in the attempt to drill in this area, and open water beneath the ice was never reached. Therefore, Station 17 was located as close as possible to the transponder on a direct line between it and the original spill site (Figure 5-19). Surface and near bottom water samples for hydrocarbon analyses were collected at Stations 17 through 21, which were located on a direct line between the seabed drifting transponder and the spill site. A single CTD cast was taken at site 16A.

During the later sampling events on 12 March, the wire angles on the hydrowire for water sampling casts indicated currents with directions of 268° True at Station 20 and 254° at Station 21. All field sampling efforts concluded with Station 21.

5.3.3   Sample Analyses for Aromatic Hydrocarbons

At the time of collection, all water samples were placed in 580 ml plastic-jacketed screw cap containers to prevent freezing. These containers had been pre-cleaned and rinsed prior to use. Each container was filled completely with seawater to minimize headspace, and while in the field, the

filled containers were stored in Igloo coolers as a further precaution against freezing and sample loss due to container breakage.

Subsets of selected water samples were used for calibration of the CTD data. Upon receipt in the laboratory, all remaining samples were stored at 4°C until analysis for hydrocarbons by GC/MS. Hydrocarbon spiked control samples as well as field and method blanks were analyzed to insure against sample degradation (by either volatilization or microbial activity) and/or contamination during handling and analysis. No evidence of either of these analytical problems was encountered.

For analysis, water samples for hydrocarbon measurements were allowed to come to room temperature before the sample container was opened. The entire sample (580 mls) was transferred to a cleaned and kiln-fired, two-neck, 1000 ml roundbottom flask. To recover hydrocarbons of interest, the flask was fitted for gas purging with an attachment for in-series, back to back Tenax[R] traps. Before exposure to a water sample, the Tenax[R] traps were first "blanked" with the sample extraction and analysis procedure (see procedure below for GC/MS with Selected Ion Monitoring mode). For a sample, water in the round bottom flask was purged for two hours with Ultra-pure helium gas at a flow rate of 30 mls/min. After this purge cycle, the front and back Tenax[R] traps were immediately capped with stainless steel Swage-Lok[R] fittings. The entire purging process was conducted in a laminar flow hood to minimize sample contamination from laboratory sources of volatile organic compounds.

The GC/MS analyses of Tenax[R] trap samples were conducted within 30 minutes of their removal from the purging apparatus. Both front and back traps were analyzed separately to determine if any sample analyte breakthrough from the front trap had occurred during the gas purging process. For GC/MS analysis, each trap was attached to a Tekmar LSC-2 Liquid Sample Concentrator[R] and backflushed while being rapidly heated to 180°C to thermally desorb any trapped volatile aromatic compounds. The compounds were then transferred directly into the inlet of a Finnigan 4021 gas chromatograph, where they were subsequently separated on a 2.8 meter x 2 mm I.D. glass column packed with 1% SP-1000 on

Carbopak 3, 60/80 mesh. Compound identification and quantitation was accomplished in the Selected Ion Monitoring Mode in a Finnigan 4021 quadrupole GC/MS. Absolute amounts of benzene and toluene were determined by comparing specific ion area counts for each compound (78 and 91 m/z, respectively) against 500 pg standard of each. Method detection limits for benzene and toluene were 0.01 ng/l.

5.3.4   Results and Discussion

Field locations for the water samples, CTD measurements and current speed/direction estimates are summarized in Table 5-7 and Figure 5-17. Data from the CTD casts (Table 5-8) and current speed/direction measurements are particularly important in explaining the measured levels of benzene and toluene in bottom and near-surface water samples from selected field locations.

5.3.4.1 Analyses of Seawater Samples for Dissolved Aromatic Hydrocarbons

Table 5-9 presents the results of the "purge and trap" GC/MS analyses of the seawater samples. Benzene and toluene were detected at low part per trillion levels in a number of samples, while other samples had undetectable levels (below the part per quadrillion level). Those samples having undetectable levels for benzene and toluene also serve as additional defacto field/method blanks. It should be noted that the other higher molecular weight compounds in the original field spike mixture (i.e., Table 5-6) were not detected in any of the water samples. The latter absence presumably derives from a combination of: 1) lower water solubilities for these compounds (see Sections 6.8 and 6.9 for a complete discussion of partitioning behavior and estimated amounts of water-soluble components contained in crude oil in general, and Prudhoe Bay crude in particular), 2) and the fact that not all of the initial spill "cocktail" was effectively introduced into the refreezing lead as originally planned. It is also significant that of these other components, o- and p-xylene were only introduced in limited (3.8 l) amounts, and only 0.5 to 1.0 kg quantities of the other components were in the original mixture (see Table 5-6). Nevertheless, absence of the higher molecular weight

Table 5-8.--CTD Data from Stations 7 to 16 for 1985 Field Program.

CONS. CAST #: 7   DATE 3/85/ 9   LATITUDE 70-58.7N   BOTTOM DEPTH: 21
CRUISE ID: TIME: 21:20 GMT LONGITUDE 158-19.0W CAST DEPTH: 0.
LOCATION:

PRESS	TEMP	SAL	SIG-T	S-VEL	DYN-DEP	PRESS	TEMP	SAL	SIG-T	S-VEL	DYN-DEP
0.6	-0.676	31.316	25.185	1441.0	0.000	12.2	-1.796	32.933	26.522	1438.2	0.021
2.0	-1.239	32.133	25.861	1439.6	0.003	13.2	-1.801	33.003	26.579	1438.3	0.023
3.2	-1.423	32.426	26.103	1439.1	0.006	14.2	-1.803	33.030	26.601	1438.4	0.024
4.3	-1.768	32.477	26.152	1437.6	0.008	15.3	-1.805	33.067	26.631	1438.4	0.026
5.4	-1.770	32.575	26.231	1437.7	0.010	16.6	-1.807	33.129	26.681	1438.5	0.027
6.5	-1.779	32.700	26.332	1437.9	0.012	17.7	-1.801	33.344	26.855	1438.9	0.029
7.5	-1.786	32.752	26.375	1437.9	0.014	18.8	-1.820	33.670	27.120	1439.3	0.030
8.6	-1.788	32.779	26.397	1438.0	0.015	19.9	-1.822	33.697	27.142	1439.3	0.031
9.7	-1.790	32.806	26.419	1438.0	0.017	20.9	-1.820	33.699	27.143	1439.3	0.032
11.1	-1.792	32.848	26.483	1438.1	0.019						

CONS. CAST #: 8   DATE 3/85/ 9   LATITUDE 71- 0.1N   BOTTOM DEPTH: 26.
CRUISE ID: TIME: 23: 0 GMT LONGITUDE 158-19.3W CAST DEPTH: 0.
LOCATION:

PRESS	TEMP	SAL	SIG-T	S-VEL	DYN-DEP	PRESS	TEMP	SAL	SIG-T	S-VEL	DYN-DEP
3.1	-1.660	32.873	26.470	1438.6	0.005	15.9	-1.836	33.704	27.148	1439.2	0.021
4.4	-1.792	32.948	26.534	1438.1	0.007	17.2	-1.836	33.719	27.160	1439.2	0.022
5.7	-1.794	32.975	26.556	1438.2	0.009	18.2	-1.836	33.728	27.167	1439.3	0.023
7.0	-1.794	32.984	26.563	1438.2	0.011	19.5	-1.836	33.732	27.171	1439.3	0.024
8.1	-1.796	33.021	26.593	1438.3	0.012	21.0	-1.836	33.742	27.179	1439.3	0.025
9.4	-1.805	33.309	26.827	1438.7	0.014	22.3	-1.838	33.748	27.184	1439.3	0.027
10.7	-1.825	33.507	26.988	1438.9	0.016	23.8	-1.836	33.758	27.192	1439.4	0.028
12.1	-1.829	33.583	27.050	1439.0	0.017	24.9	-1.836	33.760	27.193	1439.4	0.029
13.5	-1.831	33.625	27.084	1439.1	0.018	26.1	2.102	33.627	26.887	1457.3	0.030
14.6	-1.833	33.657	27.110	1439.1	0.020						

CONS. CAST #: 9   DATE 3/85/10   LATITUDE 70-56.9N   BOTTOM DEPTH: 20.
CRUISE ID: TIME: 0:10 GMT LONGITUDE 158-17.1W CAST DEPTH: 0.
LOCATION:

PRESS	TEMP	SAL	SIG-T	S-VEL	DYN-DEP	PRESS	TEMP	SAL	SIG-T	S-VEL	DYN-DEP
0.2	-1.442	31.839	25.628	1438.2	0.000	11.9	-1.794	32.951	26.536	1438.2	0.024
1.6	-1.368	31.744	25.549	1438.4	0.003	13.1	-1.803	33.066	26.646	1438.4	0.026
2.9	-1.609	31.887	25.670	1437.9	0.006	14.2	-1.807	33.141	26.691	1438.5	0.028
4.1	-1.732	31.948	25.722	1437.0	0.009	15.3	-1.809	33.204	26.742	1438.6	0.029
5.3	-1.734	31.960	25.732	1437.0	0.012	16.5	-1.807	33.266	26.792	1438.7	0.031
6.3	-1.734	31.974	25.743	1437.1	0.014	17.6	-1.801	33.268	26.793	1438.8	0.032
7.5	-1.736	32.046	25.802	1437.2	0.017	18.7	-1.796	33.283	26.806	1438.8	0.034
8.9	-1.753	32.548	26.209	1437.8	0.020	19.8	-1.790	33.285	26.807	1438.9	0.035
10.4	-1.777	32.836	26.443	1438.1	0.022						

335

Table 5-8.--(Continued)

```
        CONS. CAST #:    10      DATE   3/85/10    LATITUDE   71- 1.4N   BOTTOM DEPTH:    29
        CRUISE ID:               TIME: 23:19 GMT   LONGITUDE 158-12.1W   CAST DEPTH:       0.
        LOCATION:
```

PRESS	TEMP	SAL	SIG-T	S-VEL	DYN-DEP	PRESS	TEMP	SAL	SIG-T	S-VEL	DYN-DEP
1.5	-1.697	33.066	26.627	1438.7	0.002	15.8	-1.838	33.888	27.297	1439.4	0.018
2.5	-1.773	33.023	26.594	1438.3	0.004	17.1	-1.840	33.897	27.305	1439.5	0.019
4.5	-1.790	33.229	26.762	1438.5	0.006	18.7	-1.838	33.893	27.301	1439.5	0.020
6.1	-1.792	33.316	26.832	1438.7	0.008	20.3	-1.840	33.895	27.303	1439.5	0.022
7.2	-1.796	33.326	26.840	1438.7	0.010	21.4	-1.840	33.899	27.306	1439.5	0.022
8.3	-1.803	33.332	26.845	1438.7	0.011	22.8	-1.840	33.903	27.309	1439.6	0.023
9.5	-1.809	33.461	26.950	1438.9	0.012	24.1	-1.838	33.900	27.307	1439.6	0.024
10.7	-1.820	33.594	27.058	1439.0	0.014	25.2	-1.840	33.902	27.309	1439.6	0.025
12.0	-1.827	33.743	27.179	1439.2	0.015	26.3	-1.840	33.901	27.308	1439.6	0.026
13.1	-1.827	33.838	27.256	1439.4	0.016	27.6	-1.838	33.903	27.309	1439.6	0.027
14.2	-1.831	33.873	27.285	1439.4	0.017	28.9	-1.840	33.904	27.310	1439.7	0.028

```
        CONS. CAST #:    11      DATE   3/85/11    LATITUDE   71- 1.4N   BOTTOM DEPTH:    28
        CRUISE ID:               TIME:  2:30 GMT   LONGITUDE 158-11.8W   CAST DEPTH:       0.
        LOCATION:
```

PRESS	TEMP	SAL	SIG-T	S-VEL	DYN-DEP	PRESS	TEMP	SAL	SIG-T	S-VEL	DYN-DEP
2.6	-1.833	33.284	26.807	1438.4	0.003	17.0	-1.836	33.871	27.283	1439.4	0.018
4.1	-1.803	33.183	26.725	1438.4	0.005	18.2	-1.838	33.878	27.289	1439.5	0.019
5.2	-1.803	33.218	26.753	1438.5	0.007	19.2	-1.838	33.877	27.288	1439.5	0.020
6.6	-1.805	33.245	26.775	1438.5	0.008	20.3	-1.838	33.877	27.288	1439.5	0.021
7.9	-1.809	33.299	26.819	1438.6	0.010	21.4	-1.838	33.881	27.291	1439.5	0.022
9.3	-1.812	33.443	26.936	1438.8	0.012	22.5	-1.838	33.880	27.291	1439.5	0.023
10.8	-1.833	33.791	27.186	1439.2	0.013	23.6	-1.838	33.880	27.291	1439.5	0.024
12.2	-1.836	33.773	27.204	1439.2	0.014	24.7	-1.838	33.879	27.290	1439.6	0.024
13.7	-1.831	33.858	27.273	1439.4	0.016	25.7	-1.840	33.881	27.292	1439.6	0.025
14.8	-1.836	33.873	27.285	1439.4	0.017	26.7	-1.840	33.885	27.295	1439.6	0.026
15.9	-1.838	33.875	27.287	1439.4	0.017	27.8	-1.838	33.882	27.292	1439.6	0.027

```
        CONS. CAST #:    12      DATE   3/85/11    LATITUDE   70-59.8N   BOTTOM DEPTH:    24
        CRUISE ID:               TIME: 20: 0 GMT   LONGITUDE 158-10.2W   CAST DEPTH:       0
        LOCATION:
```

PRESS	TEMP	SAL	SIG-T	S-VEL	DYN-DEP	PRESS	TEMP	SAL	SIG-T	S-VEL	DYN-DEP
2.3	-1.703	32.387	26.077	1437.7	0.004	14.0	-1.831	33.736	27.174	1439.2	0.023
3.6	-1.757	32.410	26.097	1437.5	0.007	15.2	-1.831	33.751	27.186	1439.2	0.024
4.8	-1.757	32.460	26.138	1437.6	0.009	16.3	-1.831	33.765	27.197	1439.3	0.025
5.8	-1.762	32.545	26.207	1437.7	0.011	17.5	-1.829	33.767	27.199	1439.3	0.026
6.9	-1.768	32.612	26.261	1437.8	0.013	18.6	-1.827	33.769	27.200	1439.4	0.027
8.3	-1.773	32.686	26.321	1437.9	0.016	19.7	-1.829	33.771	27.202	1439.4	0.028
9.6	-1.786	32.927	26.517	1438.2	0.018	20.8	-1.825	33.770	27.201	1439.4	0.029
10.7	-1.794	33.068	26.631	1438.4	0.019	21.8	-1.822	33.767	27.199	1439.4	0.030
11.7	-1.809	33.439	26.932	1438.9	0.021	22.8	-1.825	33.774	27.204	1439.4	0.031
12.8	-1.822	33.646	27.101	1439.1	0.022	24.0	-1.809	33.766	27.198	1439.5	0.032

336

Table 5-8.--(Continued)

CONS. CAST #:	13	DATE	3/05/12	LATITUDE	71- 1.0N	BOTTOM DEPTH:	27
CRUISE ID:		TIME:	0:20 GMT	LONGITUDE	158-10.7W	CAST DEPTH:	0
LOCATION:							

PRESS	TEMP	SAL	SIG-T	S-VEL	DYN-DEP		PRESS	TEMP	SAL	SIG-T	S-VEL	DYN-DEP
3.6	-1.639	32.748	26.368	1438.6	0.006		15.8	-1.831	33.719	27.157	1439.2	0.021
4.7	-1.777	32.870	26.470	1438.1	0.008		17.1	-1.831	33.724	27.164	1439.3	0.022
6.0	-1.783	32.902	26.496	1438.1	0.010		18.4	-1.829	33.726	27.166	1439.3	0.023
7.1	-1.788	32.962	26.545	1438.2	0.011		19.6	-1.831	33.730	27.179	1439.3	0.025
8.4	-1.788	33.077	26.638	1438.4	0.013		20.8	-1.831	33.742	27.179	1439.3	0.026
9.4	-1.801	33.187	26.728	1438.5	0.015		22.1	-1.829	33.739	27.176	1439.4	0.027
10.9	-1.816	33.624	27.083	1439.1	0.016		23.3	-1.827	33.741	27.178	1439.4	0.028
12.1	-1.827	33.666	27.117	1439.1	0.018		24.4	-1.827	33.740	27.177	1439.4	0.029
13.1	-1.829	33.689	27.136	1439.2	0.019		25.6	-1.827	33.739	27.176	1439.4	0.030
14.4	-1.829	33.703	27.147	1439.2	0.020		26.6	-1.829	33.741	27.178	1439.5	0.031

CONS. CAST #:	14	DATE	3/05/12	LATITUDE	71- 1.4N	BOTTOM DEPTH:	29
CRUISE ID:		TIME:	3: 0 GMT	LONGITUDE	158-12.1W	CAST DEPTH:	0
LOCATION:							

PRESS	TEMP	SAL	SIG-T	S-VEL	DYN-DEP		PRESS	TEMP	SAL	SIG-T	S-VEL	DYN-DEP
2.5	-1.792	33.339	26.851	1438.7	0.003		15.8	-1.831	33.811	27.235	1439.4	0.017
4.0	-1.803	33.264	26.790	1438.9	0.005		17.1	-1.831	33.826	27.247	1439.4	0.018
5.0	-1.801	33.291	26.780	1438.9	0.006		18.5	-1.831	33.830	27.250	1439.4	0.019
6.6	-1.803	33.268	26.794	1438.6	0.008		19.8	-1.836	33.894	27.270	1439.5	0.020
7.6	-1.805	33.309	26.824	1438.6	0.009		21.2	-1.836	33.864	27.278	1439.5	0.022
8.7	-1.809	33.451	26.942	1438.8	0.011		22.5	-1.840	33.873	27.285	1439.5	0.023
9.8	-1.818	33.658	27.110	1439.1	0.012		23.8	-1.840	33.872	27.284	1439.5	0.024
11.0	-1.827	33.769	27.200	1439.2	0.013		25.3	-1.840	33.876	27.287	1439.6	0.025
12.1	-1.829	33.786	27.214	1439.3	0.014		26.7	-1.840	33.885	27.295	1439.6	0.026
13.3	-1.831	33.798	27.224	1439.3	0.015		28.0	-1.842	33.902	27.309	1439.6	0.027
14.6	-1.833	33.799	27.225	1439.3	0.016		29.0	-1.840	33.909	27.314	1439.7	0.028

CONS. CAST #:	16	DATE	3/05/12	LATITUDE	71- 1.6N	BOTTOM DEPTH:	29
CRUISE ID:		TIME:	17: 0 GMT	LONGITUDE	158-12.0W	CAST DEPTH:	0
LOCATION:							

PRESS	TEMP	SAL	SIG-T	S-VEL	DYN-DEP		PRESS	TEMP	SAL	SIG-T	S-VEL	DYN-DEP
3.1	-1.742	32.479	26.153	1437.7	0.006		17.3	-1.829	33.721	27.161	1439.3	0.026
4.2	-1.757	32.475	26.150	1437.6	0.008		18.7	-1.831	33.728	27.167	1439.3	0.027
5.5	-1.757	32.490	26.162	1437.7	0.010		20.0	-1.831	33.732	27.170	1439.3	0.028
7.0	-1.760	32.921	26.187	1437.7	0.013		21.4	-1.829	33.739	27.176	1439.4	0.030
8.7	-1.766	32.714	26.344	1438.0	0.016		22.8	-1.827	33.751	27.186	1439.4	0.031
10.4	-1.796	33.182	26.724	1438.5	0.019		24.0	-1.825	33.753	27.187	1439.4	0.032
11.7	-1.809	33.297	26.817	1438.7	0.020		25.3	-1.825	33.797	27.191	1439.5	0.033
13.0	-1.814	33.509	26.989	1439.0	0.022		26.6	-1.827	33.779	27.208	1439.5	0.034
14.5	-1.822	33.670	27.120	1439.2	0.023		28.1	-1.829	33.781	27.210	1439.5	0.036
16.0	-1.827	33.710	27.153	1439.2	0.025		29.2	-1.827	33.808	27.232	1439.6	0.036

Table 5-9.—Concentration of Aromatic Spike Components in Chukchi Sea
Seawater Samples and CTD Information.

Station No.	Depth(m)	Sampling[a] Depth(m)	Sample Depth	Concentrations[b] (ng/1) Benzene	Toluene	Temp (°C)	CTD Salinity (°/oo)	σ_t
10	29	3	Subsurface	NA	NA	-1.77	33.02	26.63
		28	Bottom	NA	NA	-1.84	33.90	27.31
10A	28	14	Subsurface	.5	ND	-1.83	33.28	26.81
		27	Bottom	.3	ND	-1.84	33.88	27.30
12	24	2	Subsurface	6.9	2.8	-1.70	32.39	26.08
		23	Bottom	76	13	-1.82	33.77	27.20
13	27	4	Subsurface	.6	.04	-1.64	32.75	26.37
		26	Bottom	2.1	.2	-1.82	33.74	27.18
14	29	2	Subsurface	.2	ND	-1.79	33.34	26.85
		28	Bottom	ND	ND	-1.84	33.91	27.31
15	26	2	Subsurface	1.6	.2	NA	NA	NA
		25	Bottom	.9	.02	NA	NA	NA
16A	29	2	Subsurface	16	.5	-1.74	32.48	26.15
		28	Bottom	1.9	.2	-1.83	33.80	27.22
16B	26	2	Subsurface	1.1	ND	NA	NA	NA
		25	Bottom	1.7	.06	NA	NA	NA
16C	26	2	Subsurface	13	ND	NA	NA	NA
		25	Bottom	1.8	ND	NA	NA	NA
17	26	2	Subsurface	2.4	.1	NA	NA	NA
		25	Bottom	.4	.02	NA	NA	NA
18	26	1	Subsurface	.7	ND	NA	NA	NA
		25	Bottom	1.0	.07	NA	NA	NA
19	25	1	Subsurface	.5	.09	NA	NA	NA
		24	Bottom	1.9	.2	NA	NA	NA
20	25	1	Subsurface	.4	.03	NA	NA	NA
		24	Bottom	1.0	.2	NA	NA	NA
21	26	1	Subsurface	.2	ND	NA	NA	NA
		25	Bottom	15	5.5	NA	NA	NA

[a] Bottom sampling depth nominally 0.5-1.0 m above the bottom.

[b] No detectable amounts of ethylbenzene, o ,m-xylenes, naphthalene or
2-methylnaphthalene were found in any samples.

ND Not detected at method detection limit of 0.01 ng/1.

NA Not available.

compounds in the water samples indicates that sample contamination due to handling in the field was not a problem.

Comparison of the measured concentrations for the detectable hydrocarbons (i.e., benzene and toluene) and the salinity data allow for a rational hypothesis to be developed for the hydrocarbon distributions observed in the field (Table 5-9). For example, the highest benzene and toluene concentrations were measured in bottom water samples associated with the largest salinity/density gradients in the water column (e.g., Station 12; Figure 5-20A and Table 5-8). This situation was in contrast to the low or undetectable hydrocarbon levels at stations with little or no density stratification (e.g., Station 14; Figure 5-20B and Table 5-8). Furthermore, benzene and toluene concentrations generally were higher in bottom water compared to surface water (e.g., Stations 12, 13, 16b, 18, 19, 20, and 21). Exceptions to these trends can be explained when ice formation sequences, extensive ridge structures and current measurement data are considered.

Seawater samples collected three hours after the spill at Station 10A contained low (<1 ng/l) but detectable concentrations of benzene and non-detectable (<0.01 ng/l) concentrations of toluene. Based on S4 current meter data collected at the time of the spill, this site was upcurrent from the spill site. Therefore, minimal transport/mixing of water that had been in direct contact with the original surface spill could be expected. The measurable benzene concentrations may simply represent background contamination due to the close (7-10 m) proximity to the spill site.

Bottom water samples collected at Site 12 (23 hours post-spill) contained the highest concentrations of aromatic hydrocarbons of any location examined. These concentrations for benzene and toluene were 76 and 13 ng/l, respectively. The surface water sample (1 m below the ice canopy) at Site 12 contained concentrations of benzene and toluene of 7 and 3 ng/l, respectively. These concentrations likely reflect limited vertical mixing of deeper water toward the surface due to the presence of the extensive ridge/keel system immediately northwest of Station 12. The ice keel associated with this ridge

339
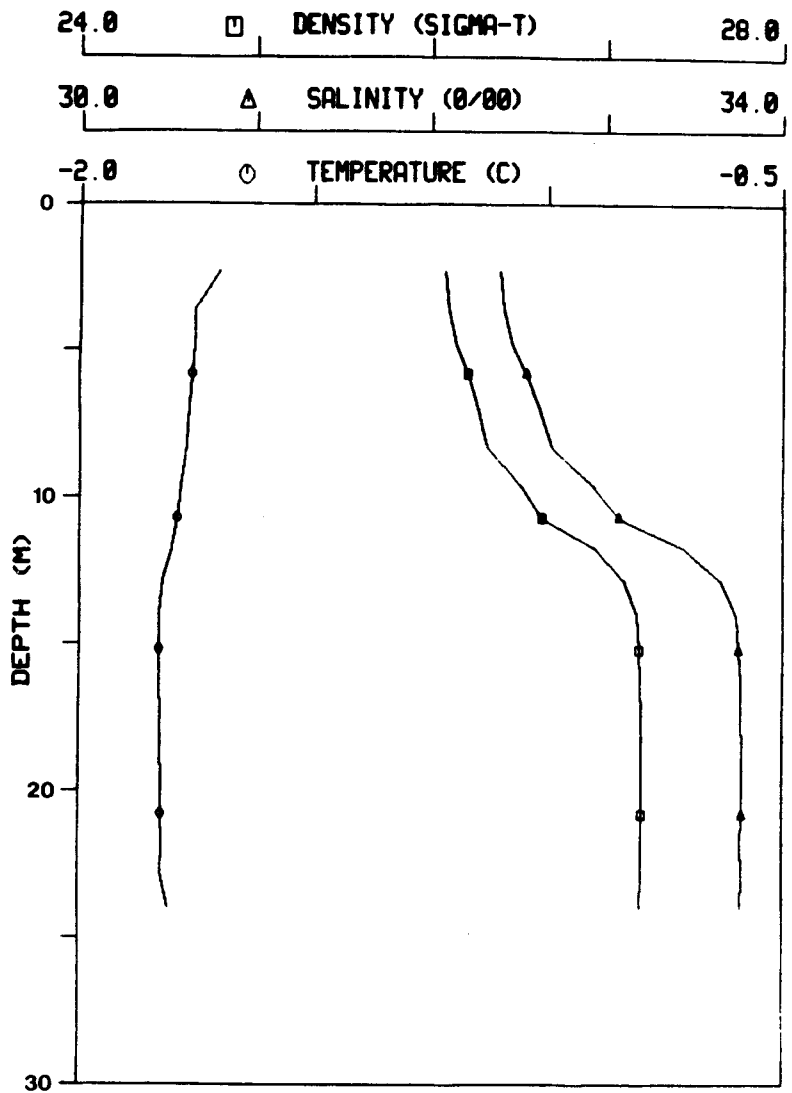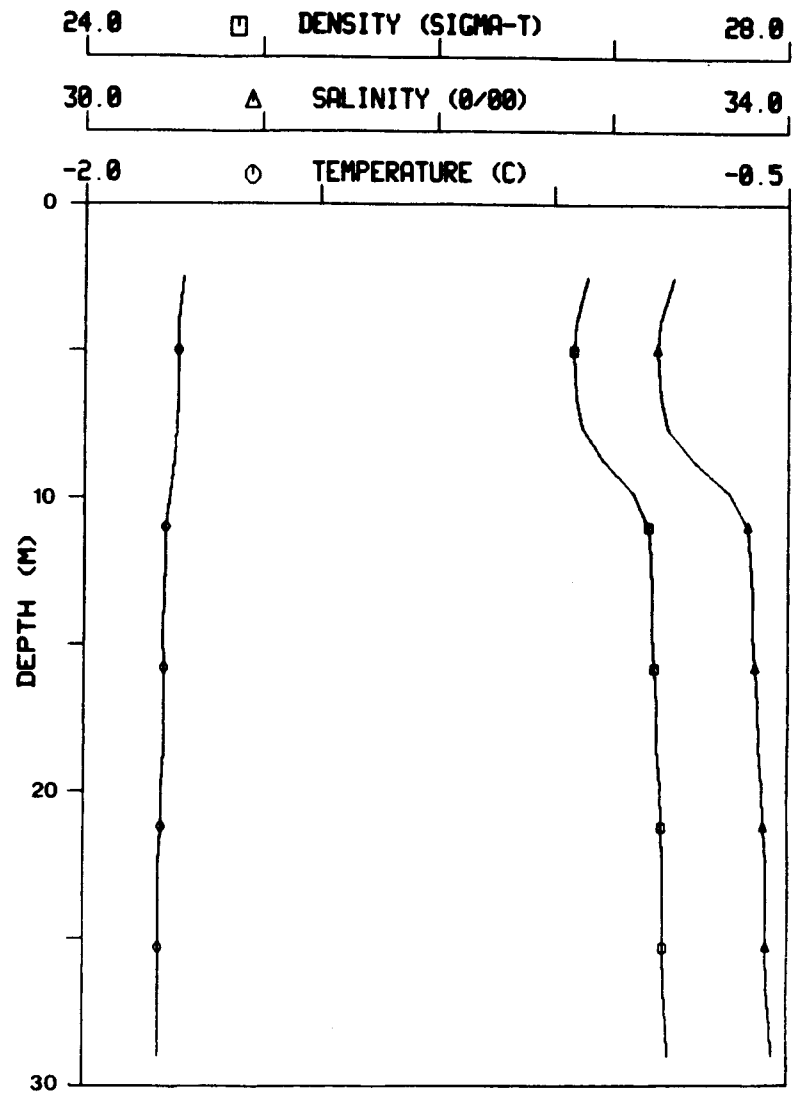
Figure 5-20.—CTD Data from the 1985 Field Program for (A) Station 12 and (B) Station 14.

could promote turbulence around the keel, and thus mix the benzene-enriched bottom water into near surface under-ice waters. Station 12 was 3.2 km southeast of the spill site. Bottom current measurements taken at this site (Table 5-7) indicated a southeasterly flow of bottom water with a velocity of 1.1 cm/sec. Although this current direction could explain the presence of hydrocarbons derived from the initial spill site, the magnitude of the current velocity should have been slightly higher (ca.3.8 cm/sec) to transport the hydrocarbons to Site 12 by the time of sampling. It is possible, however, that higher current speeds with a southeasterly direction could have occurred while the leads north of Station 10 were open during the 24 hour period between the initial spill and the sample collections at Site 12.

Such southeasterly transport of 33.7 ^{o}/oo salinity bottom water at 3.0 cm/sec was in fact, measured the day before the experimental spill at Station 7 on 9 March 1985, when active ice formation was occurring in extensive offshore open-leads in the vicinity of Station 8, which was located on a 50 m diameter stable pan in those leads to the north of Stations 7 and 9 (see Figure 5-17 and Table 5-8). Also, the rather uniform salinity values (up to 32.9 ^{o}/oo at the surface and 33.7 ^{o}/oo at the bottom) at Station 8 suggested the formation and active sinking of brine at that site compared to surface and bottom salinities at Sites 7 and 9 (Table 5-8).

At Station 13, higher concentrations of both benzene and toluene were measured in the bottom water sample (2.1 ng/l and 0.2 ng/l, respectively) as compared to the near-surface sample (0.6 ng/l and 0.04 ng/l, respectively). However, the concentrations of benzene and toluene in the bottom water sample at Station 13 were substantially less than those in the bottom water at Station 12. Because Station 13 was in a region with a relatively smooth surface ice cover about 1.6 km southeast of the initial spill release point, the data suggest that the majority of the dissolved aromatic hydrocarbon plume had been transported past or adjacent to this site by the time the station was occupied (i.e., approximately 26 hours after the spill). That is, the spill released at Site 10 served as a short-term point source (versus a longer term "continuous" source) to the water column due to the initial lead closure shortly after the

spill event. Thus, hydrocarbons reaching the bottom at Station 10 could advect along a line from the release site toward Station 12 and largely miss Station 13.

Benzene and toluene were not detected in the bottom water at Station 14. However, CTD data (Figure 5-20B and Table 5-8) from the area around Stations 14 and 15 suggest that the water column was only weakly stratified (i.e., the surface water salinity of 33.34°/oo was similar to the bottom water salinity of 33.91°/oo). Under weakly stratified conditions, the aromatic hydrocarbons that were dissolved in the water (e.g., benzene) could have been mixed vertically and diluted (below detection limits) more effectively than at stations with more pronounced water column stratification (e.g., Station 12).

Benzene and toluene were both present at concentrations of <2 ng/l in water samples from Station 15 (26-27 hrs post-spill). The concentrations at this site were slightly higher in the surface versus the bottom sample. However, the possibility of accidental sample contamination at this site cannot be discounted completely, even though a new auger hole was drilled in the ice for sampling. Alternatively, cold-room wave-tank studies (Sections 4.4.2 and 4.4.3) have demonstrated that with only minor wave turbulence, dispersed oil droplets can impinge on under-ice surfaces adjacent to leads where the hydrocarbons have been introduced. Entrapment of hydrocarbons on the under-ice surface adjacent to the experimental spill site due to turbulence accompanying the initial lead closure could easily explain the detectable benzene and toluene concentrations in the near surface waters at Site 15.

Stations 16 A, B, and C were on a transect that ran parallel to but 30 m north of a ridge system approximately 500-700 m north-northeast of the spill site (see Figure 5-19). Samples from these three stations contained low concentrations (≤ 0.5 ng/l) of toluene, but variable concentrations (i.e, up to 16 ng/l) of benzene. At Station 16B the benzene and toluene concentrations in the bottom water were 2 ng/l and 0.06 ng/l, respectively, whereas surface water concentrations of benzene were 1 ng/l and toluene concentrations were below detection. However, at Stations 16A and C, the surface water concentrations of

benzene were elevated compared to those in the bottom water. A possible explanation for this variation in concentrations at Station 16 could be the existence of turbulent flow on the downcurrent (northern) side of the ridge system. Such turbulent flow could have mixed benzene-enriched bottom water into the near-surface zone. Alternatively, micro-scale ridge/keel melting could have introduced fresher, lower-density water near the bottom of the water column, and thereby induced an upward mixing of bottom water toward the surface.

Bottom water between Stations 17 and 21 (Figure 5-19) contained relatively uniform concentrations of benzene and toluene. However, the concentrations in the bottom water samples were relatively higher at those stations closest to the original spill site. Surface water concentrations at these stations were uniformly low, except Station 17 immediately adjacent to the northern-most ridge system where the 27 kHz bottom drifting transponder was eventually located. Again, it is conceivable that the nearby 4-6 m ice keel structure produced an irregular flow pattern that resulted in mixing of bottom water toward the surface at Site 17. This could account for the higher aromatic concentrations in the surface water (2 ng/l benzene, 0.1 ng/l toluene) vs the bottom water at that station.

There appeared to be a strong correlation between the relative bottom vs surface water concentrations of dissolved aromatics and the degree of stratification (i.e., vertical density gradient) in the water column. Where the water column was weakly stratified, aromatic hydrocarbon concentrations in both surface and bottom water samples were generally low or undetectable (Tables 5-8 and 5-9 and Figure 5-20). Slightly higher aromatic concentrations were noted in surface waters near ice ridge systems, which could have induced irregular and turbulent flows in the subsurface waters near the ice ridge keels. These results from the field experiment agree with processes observed in smaller scale laboratory studies of brine generation and associated near-bottom flows (Section 5.2) as well as model predictions on the rates and magnitude of aromatic hydrocarbon dissolution into surface brine generated during frazil and grease ice growth (Section 6.9).

5.3.4.2 Transport Scenario for Dissolved Hydrocarbons from the Initial Spill Mixture

Salinity sections (Figures 5-21 and 5-22) derived from CTD and current measurements completed on 9 and 11 March (Tables 5-7 and 5-8) suggest an on-shore (i.e., generally southeasterly) flow of brine along the bottom during the initial 48 hours following the spill event. Between 9 and 11 March, the in-shore salinity increased from 32.8 to 33.3°/oo. A calculation estimating the total volume of water inshore of a location at 15 km (approximately 20 m water depth) indicates that an onshore current velocity of 3 cm/sec in the lower 10 m of the water column and an accompanying offshore current velocity of 3 cm/sec in the upper 10 m of the water column could yield the observed change in salinity.   Onshore (southeasterly) bottom water velocities of 1-3 cm/sec were observed on 9 and 11 March (Table 5-7) and an average current velocity in this range could transport benzene and toluene in a brine generated bottom layer from Station 10 to Station 12 in a period of 24-28 hours as observed. An apparent anomaly, however, is the net under-ice movement of the 27 kHz seabed drifting transponder to the north-northeast and measured benzene and toluene levels at Stations 16 through 21.

These findings can be explained if the rearrangement of the ice canopy and experimental lead system are considered in context with the timing of the cocktail release.   At the time of the spill, a 1.5 cm/sec near-bottom current to the north-northeast was measured immediately beneath the experimental lead (Station 10, Figure 5-18 and Table 5-7).

This current could transport dissolved hydrocarbons in the brine and the 27 kHz bottom drifting transponder toward the north- northeast during the first 1-2 hours after the spill. With the closing of the exprimental lead and the opening of the broad (several 100 meter) expanse of open water to the north of the experimental site, however, a different flow pattern (more closely approximating that observed on 9 and 11 March) might be anticipated. A similar pattern was suggested by the tank experiments in Section 5.2.3.2, Open Water Freeze-up.
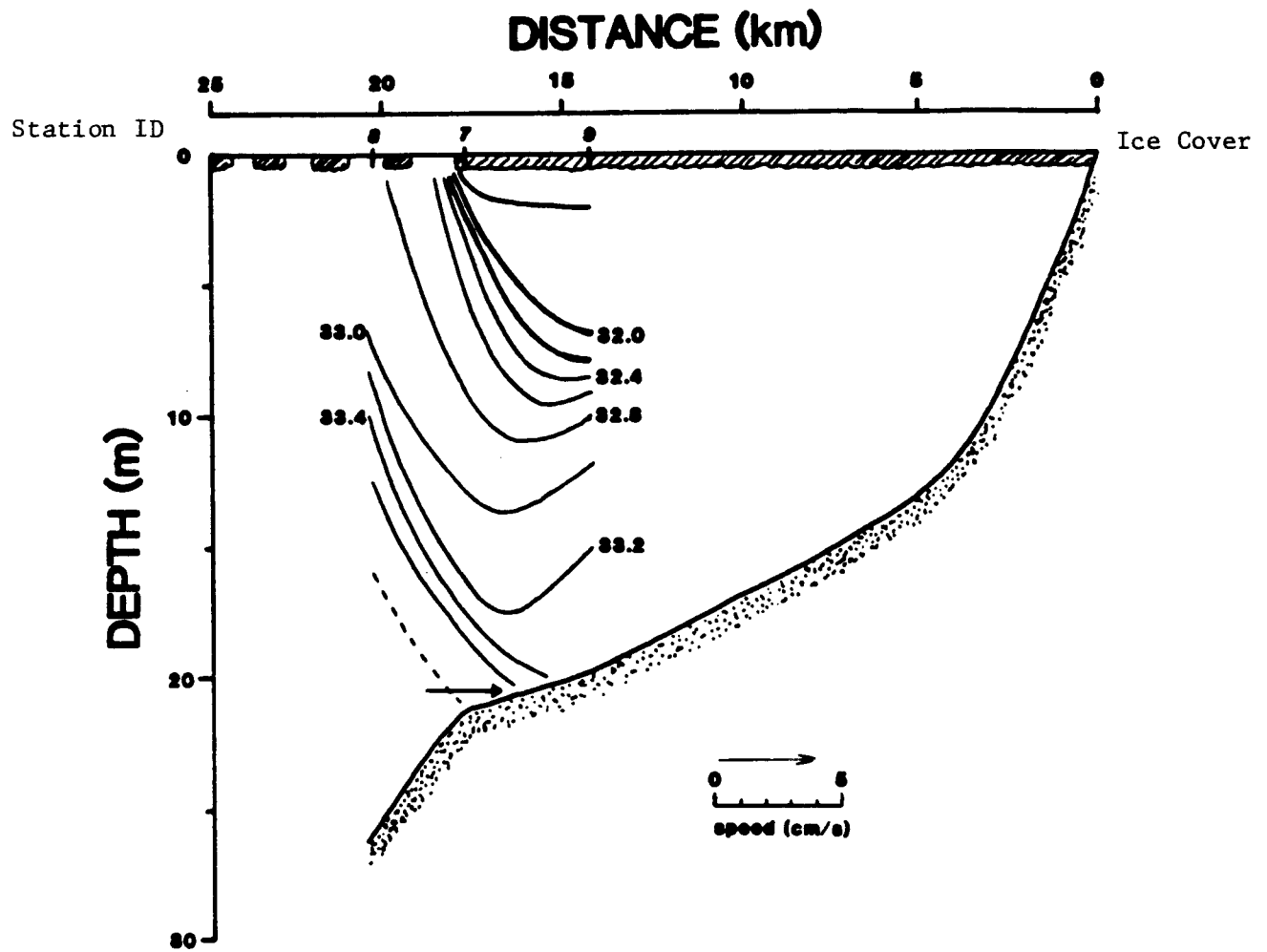
Figure 5-21.—Salinity Section on 9 March 1985 and Average Bottom Velocity Vector Taken at Station 7. (See Figure 5-17 for station locations.)
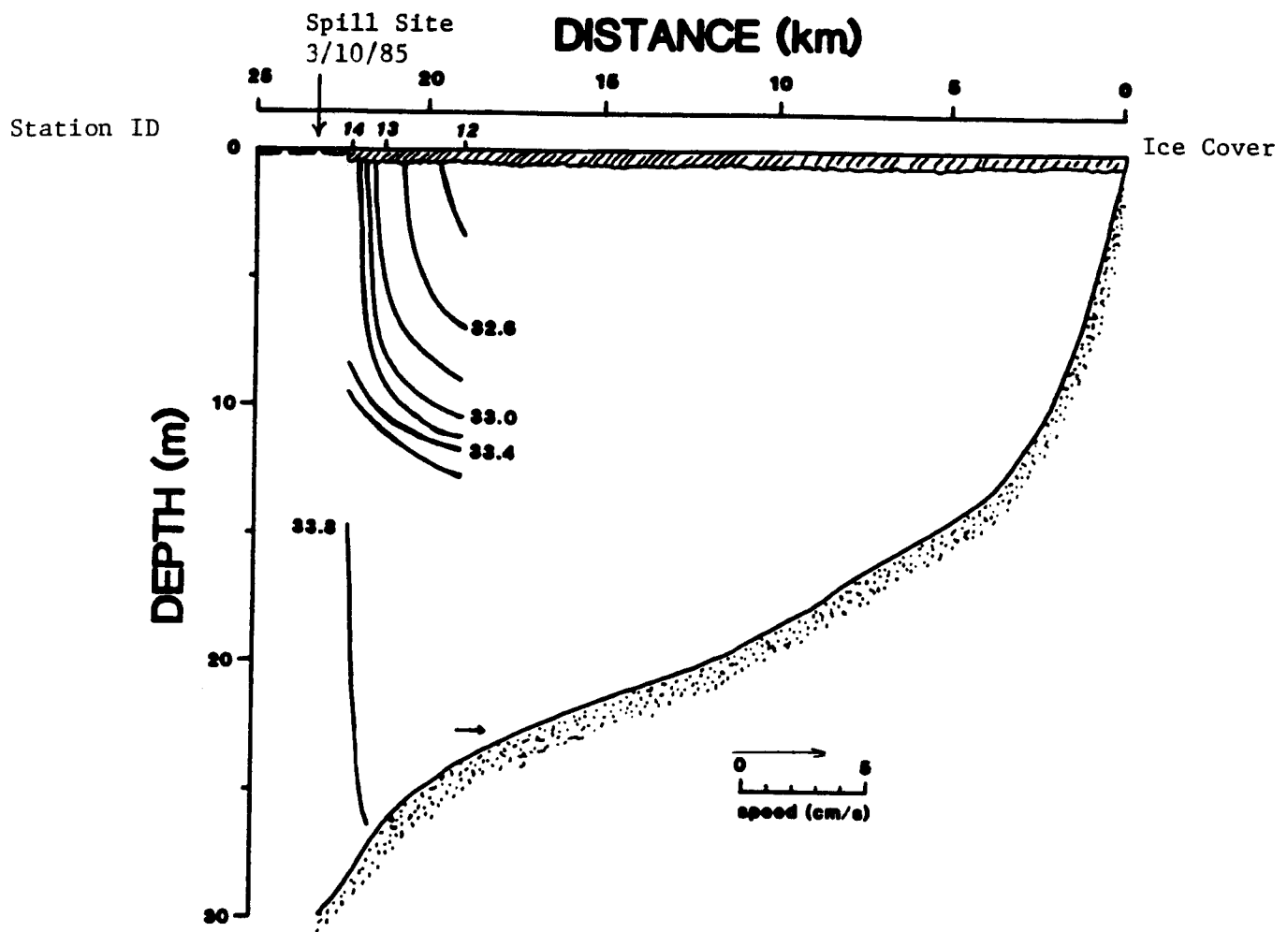
Figure 5-22.—Salinity Section on 11 March 1985 and Average Bottom Velocity
Vector Taken at Station 12. (See Figure 5-17 for station locations.)

346

Figure 5-23 presents idealized vertical cross-sections for flow regimes and ice structures along an approximate northwest-southeast transect line in the study area (also examine Figure 5-17 for station locations). The illustrated current flow patterns are extrapolated from current meter data (Table 5-7), vertical salinity profiles and cross-sections from CTD data for 9-11 March (Table 5-8 and Figures 5-21 and 5-22), and ice movement observations.

As shown in Figure 5-23A, brine appeared to be generated in the experimental lead system at the time of the initial cocktail release (Site 10), while ice fields to the south of this region were continuous. This would tend to generate a weak northerly flow as measured in the field at the initiation of the experiment (shown in Figure 5-23A). After the opening of the larger off-shore lead system to the north of the spill site (Figure 5-23B), water currents under the continuous ice field to the south could have reversed and have a predominantly horizontal component to their flow direction for the next 20-24 hour period following the spill. In contrast, water flow patterns directly under the new offshore lead system to the north would have a greater vertical component during this period due to extensive brine generation and the proximity of a deep ridge keel in this direction (Figure 5-23B). Such currents would serve to further dilute any benzene or toluene introduced into the area initially after the spill, as observed by the low concentrations measured on 12 March 1985 after the freezing in the vicinity of Stations 17 through 21.

Kozo (1983) predicted comparable directional flow regimes using an initial model for arctic mixed layer circulation under a refreezing lead. This model represents idealized circulation under a refreezing lead in the Arctic Ocean and presents mathematical calculations that determine the salt flux to the bottom. The model considers conditions including zero geostrophic current superimposed over the lead circulation system and also geostrophic currents running parallel and perpendicular to the lead system. With a geostrophic current of 2.5 cm/sec perpendicular to the lead axis, a circulation pattern would be established that mimics the distributions of currents and water masses, the temperature and salinity profiles, and the benzene/toluene

347

Northwest

Southeast

16   17   18   19   20   21   lead   15   14   13   12

1.5 cm/sec

Bottom

B

Northwest

Southeast

16   Open Water   15   14   13   12

27 kHz Transponder

1.1 cm/sec

Bottom

37 kHz Transponder

C

Northwest

Southeast

16   17   18   19   20   21   15   14   13   12

27 kHz Transponder

3.0 to 3.9 cm/sec

Bottom

(NOT TO SCALE)

37 kHz Transponder
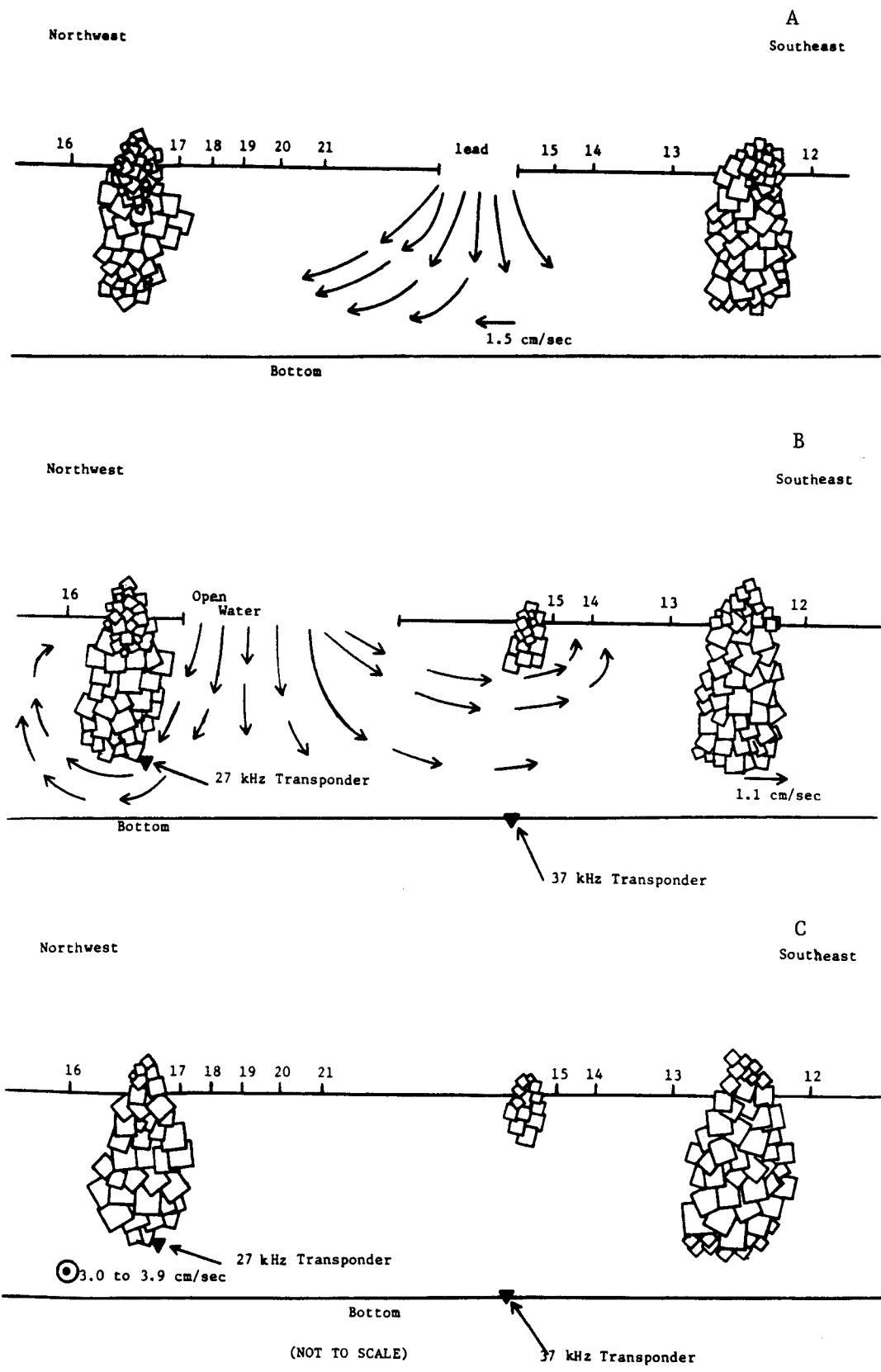
Figure 5-23.--Vertical Ice Conditions for (A) 3/10/85, (B) 3/11/85,
and (C) 3/12/85.

348

concentrations that were measured during this study near the lead at Stations 14 and 15. Kozo's model for mixed layer circulation under a refreezing lead in the absence of geostrophic influence predicts a maximum horizontal flow from brine generation in the range of 2 to 5 cm/sec. These current estimates agree with values measured in this program in March 1985.

In summary, at the time of the hydrocarbon spill for this field study, active freezing occurred in the open lead system with an accompanying production of downward advecting brine. The lead was only open for approximately one hour after the spill. At the beginning of this period the measured bottom current (i.e., 5-minute vector average) was northerly (approximately 25 to 35°T) at a speed of 1.5 cm/sec. The seabed drifter (27 kHz) deployed to track bottom water movement was transported to the north-northeast, until it became trapped in the ridge system 0.5 to 1 km north of Station 10 (see Figure 5-23B).

Bottom topography in the immediate vicinity of the spill site was quite uniform. Therefore, current shifts due to the in situ water column density structures or tidal fluctuations would have been primarily responsible for determining flow directions for the bottom brine layer and any associated dissolved aromatic hydrocarbons. Thus, with the subsequent opening of the larger lead to the north of the spill site, the bottom current would have likely shifted to an approximate southerly direction at the immediate spill site due to brine-mediated flow processes illustrated in Figure 5-23B. The latter flow regime would explain the higher concentrations of aromatics observed in the bottom water samples at Sites 12 and 13 within approximately the first 24-26 hours after the spill event.

Such flow reversals due to brine rejection during refreezing of polynyas have also been reported by Schumacher et al. (1983). These authors suggested that ice formation and accompanying brine rejection affected bottom water flow in the vicinity of the polynya south of St. Lawrence Island. Eleven flow reversals were detected in the regional circulation patterns that could be explained by combinations of brine rejection processes and offshore wind stress. Scaling of a simplified equation of motion yielded results suggesting

density induced quasi-geostrophic flow resulting from brine rejection that was an important element for the circulation patterns. During the study, approximately 5 m of ice formed in the polynya. The estimated increases in water salinities in the northern Bering Sea shelf polynas suggest that this process is comparable in effect, but opposite in phase, to that of runoff. Therefore, brine rejection is an important part of the seasonal salt budget in these waters.

In the case of the present study in the Chukchi Sea, the offshore development of open leads and concomitant brine rejection provide conditions required to generate the observed (1-3 cm/sec) onshore flow patterns of higher salinity bottom water. Under these conditions, the dissolved aromatic hydrocarbons (benzene and toluene) detected in bottom waters are clearly consistent with the source of those water masses from formation of brine in the refreezing lead at the experimental spill site and the measured bottom-water flows. The observation of (only) benzene and toluene transport to the bottom does not exclude the possibility of the transport of other compounds, including other aromatics, and (to a lesser extent) paraffins and naphthas, to the bottom. While benzene and toluene do have water/oil partition coefficients that are larger than other compounds present in crude oil, finite partition coefficients will result in transport of other less soluble components. Only benzene and toluene were detected in the field experiments; however, other parameters that must be specified include the quantity of each compound in the spill itself. In the case of the Chukchi Sea field experiments, these quantities were extremely small compared to the carrier solvent, toluene, and benzene (Table 5-6). From ice chamber wave tank experiments presented in Sections 4.2.3 and 4.4.3, it is clearly evident that there are numerous other water-soluble, lower-molecular weight aromatic hydrocarbons which partition from Prudhoe Bay crude oil into the water colume (see also Sections 6.8 and 6.9). Once present as truly dissolved species in solutions of brine generated during ice growth, these other compounds would be subject to the same transport mechanisms demonstrated in the Chukchi Sea field experiment for benzene and toluene.

The low velocities (1 to 5 cm/sec) associated with both the sinking brine and the horizontal advection of this brine away from the lead system in the lower layers of the water column may result in the motion of the brine being driven by localized currents or tidal movements. Nevertheless, with time, a mean down-slope, offshore movement of brine is expected (especially after closure or complete refreezing of the offshore leads).

The extreme difficulty of field sampling due to weather and the dynamic nature of the ice fields (and experimental lead) in this study limited the synopticity of sampling. Additional water samples and current measurements could have provided further information for tracking the cocktail plume, estimating dilution rates, and evaluating the longer term fate of the soluble hydrocarbons. Nevertheless, dissolution and transport of aromatic hydrocarbons from the surface to the bottom of the water column (and up to 3 km from the spill site) are demonstrated by the results of the field program. The low flow period encountered during this study may not be typical of all conditions in the area. In fact, given the limited size of the spill (38 liters) and location (further offshore and in deeper water than desired), the benzene and toluene components may not have been recoverable under higher flow conditions.

Nevertheless, the observations of aromatic hydrocarbon dissolution suggest a mechanism by which a spill of crude oil or refined products in a refreezing lead system could result in elevated concentrations of aromatics in bottom waters. Once incorporated into a bottom brine layer, these aromatic compounds would persist depending on rates of mixing and dilution. Potential problems with extrapolating results from this experiment to an actual oil spill would involve consideration of the type and volume of oil (or petroleum product) spilled, the degree of weathering of the oil prior to mixing with brine, the duration of the ice (brine) formation process, and the degree of water column density stratification and depth.

6.
OCEAN-ICE OIL-WEATHERING MODEL DEVELOPMENT

6.1   INTRODUCTION

The objectives for a mathematical model of oil weathering in the presence of first and multi-year sea ice are to temporally predict both the mass of oil remaining in the slick and the chemical composition and physical properties of the oil slick. These two objectives require that oil composition be described in terms of both specific components and lumped-component categories, or "pseudocompounds". Pseudocomponent classification has been widely used in the petroleum industry to describe crude oil because of the inherent interest in bulk oil characteristics and accounting for total mass. A specific-component description is of interest in describing spilled oil as a changing source of foreign chemicals to an aquatic ecosystem, but the complexity of oil composition makes it impractical to keep track of bulk oil mass in terms of individual components.

The Ocean-Ice Oil-Weathering Model presented in this report has been developed over the last thirty-six months. The basis for this model is the Open-Ocean Oil-Weathering code that was developed between 1979 and 1984. During this time, additional stand-alone models have been derived and used to guide experimental and development work. Some of these, as well as the open-ocean code itself, are described in detail in Payne et al. (1984a). Others will be presented here.

The most developed models are mass transport models which describe evaporation and dissolution processes. These two processes describe molecular transport, in contrast to the dispersion/oil-weathering process which describes the transport of discrete oil drops into the water column due to wind/wave action and other physical processes.

These models incorporate the concepts of interfacial mass transfer, the considerations of both mechanically well-stirred and stagnant oil phases, the effects of slick spreading, and the boundary conditions imposed on the oil by the environment. In addition, these models include descriptive predictions

of specific compound concentrations in the air and water column in contact with a slick or other spilled oil phase.

Both portions of the model require distinct and independent mathematical formulations. In order to predict the mass of oil remaining in a slick as a function of time, a method of characterizing the bulk oil with respect to the various transport processes that alter and dissipate oil must be utilized. The total oil mass cannot be characterized by its individual components because of both their large number and complexity and the limitations of analysis. To compensate for these limitations, the pseudo-component approach "cuts" oil into a number of fractions, assigning appropriate physical properties to each.

In attempting to predict the mass of oil remaining in a slick, the two most important mass transport processes to consider are evaporation and dispersion. Of these two, evaporation appears to have the greater influence, certainly over short time scales, making vapor pressure an especially important oil characteristic. Adequate description of the dissolution process, on the other hand, requires water solubility information. The pseudo-component approach to describe these processes is to cut the oil into a number of fractions based on properties of distillation fractions (Payne et al., 1984a).

The pseudo-component approach, employed in virtually all previous efforts to model oil weathering, is singularly useful for providing a total material balance versus time for spilled oil (especially for slicks). However, this approach does not predict the time-dependent material balance for specific chemical components. In order to obtain component-specific information, component-specific physical properties (e.g., solubilities, vapor pressures and other phase partitioning parameters) must be used. No other functional component-specific models have been developed to date. Ironically, most of the data generated when an actual oil spill has occurred have been component- specific concentrations across phase boundaries, and virtually no pseudo- component concentration data have been reported.

Although evaporation and dispersion are the oil-weathering processes of greatest importance during the initial stages of a spill, other longer-term

weathering processes also destroy and produce compounds that are important to any component-specific model. In the case of photo- or autoxidation, a compound may chemically react to become an aldehyde, ketone, alcohol or acid, all of which are more soluble in water than the precursor hydrocarbon compounds. Similarly, metabolites of microbial degradation have physical properties markedly different from their corresponding parent compounds. These secondary or long-term processes are typically more complex than the evaporation and dispersion processes, thus increasing the complexity of the mathematical descriptions.

In discussing the segments of the model which follow, three basic aspects have been considered for each oil weathering process:

(1) physical properties (of bulk oil and specific components)

(2) mass balance equations (for specific components and pseudo- components)

(3) environmental parameters (which the oil encounters upon being spilled)

Physical properties include the thermodynamic and transport characteristics required to describe a particular process. In the cases of evaporation and dissolution, thermodynamic properties are the vapor pressures, Henry's Law coefficients, oil/water partition coefficients, and mixing rules, while the transport properties include diffusivities, viscosities and, again, mixing rules.

6.2   MODEL APPROACH

In considering the most useful approach for modeling oil-weathering in the presence of sea ice, a "scenario" approach was selected to provide clarity to the user with maximum flexibility. In this approach, the user is given the freedom to choose a series of environmental conditions and physical locations for the oil to weather. Then, since sea and ice conditions change (for a real or conceptualized situation), they can be changed by the user also. In other words, the user can alter environmental and physical parameters in order to create a "scenario" that best fits the situation for the desired weathering

prediction. Flexibility has been provided in the following manner. Using the open-ocean oil-weathering code as a basis, the model has been compartmentalized into four basic oil-ice configurations: oil in pools on top of ice, oil trapped under (and encapsulated in) a growing ice field, oil on the ocean surface in a broken-ice field, and oil on the open-ocean (no ice). Each of these configurations is offered to the user chronologically but none is required. When a configuration is chosen, the specific environmental parameters required to predict weathering in that configuration are then requested from the user. After this information is supplied the oil is re-characterized so that the user can track the progress of the various pseudo-components and learn about the physical processes that occur during oil weathering. After re- characterization, the user is then offered the next oil-ice configuration. In this way, the user has a large amount of freedom to subject the oil to specific (user-defined) weathering conditions.

In order to introduce users to the operation of the model, a stand-alone users manual has been prepared as a separate volume.

6.3   PHYSICAL PROCESSES CONSIDERED

Predicting the quantity of oil in the slick as a function of time requires that a total mass balance approach be used. It is not possible to write a total material balance for crude oil by using component-specific information. If one tries to use component specific information, it soon becomes apparent that all the components in crude oil will never be identified, thus precluding an accounting of the total mass of the oil. No predictive equations have ever been successfully developed based on specific components for the purpose of predictions a total mass balance for oil.

The question then is raised as to how one uses bulk properties of the oil to make specific predictions? The petroleum industry refers to these bulk properties of oil as "characterization parameters". The characterization of an oil must be done with respect to a specific prediction (process design or mathematical model) as the objective. For example, when the prediction is a process that involves vapor-liquid transport, the characteristic parameters are

355

vapor pressures or partial pressures. When the prediction is the performance of a catalytic reformer where naphthas are converted to aromatics, the characteristics required on the catalytic reformer feedstock are combined contents of paraffins-olefins-naphthas-aromatics, referred to as PONA. Kinetic equations use PONA values as starting concentrations along with kinetic constants to predict the product from the catalytic reforming process. Both of these examples illustrate a pseudo-component model, sometimes referred to as a "lumped" model.

In predicting the mass of oil remaining in an oil slick as a function of time as evaporation proceeds, the oil must be characterized with respect to vapor pressure. An overall mass balance utilizes the vapor pressure and environmental parameters to predict loss of oil and, therefore, mass of oil remaining in the slick. The following discussion considers: 1) the procedure for characterizing crude oils with respect to pseudo-component vapor pressures; and 2) the pertinent equations for describing the overall mass balance as they apply to the oil weathering model.

6.4   PSEUDO-COMPONENT CHARACTERIZATION OF CRUDE OIL

The standard inspections on a crude oil include distillation, density of the distillate cuts, and viscosity of the distillate cuts. Virtually no component-specific data can be obtained which will allow adequate prediction of the bulk properties of the oil. The standard distillation data come from either a true boiling point (TBP) distillation or an ASTM (American Society for Test and Materials) D-86 distillation; both are usually carried out at one atmosphere total pressure. Each of these distillations can also be carried out at 40 mm Hg total pressure to obtain information on the less volatile fractions of the oil.

Either distillation is conducted in a manner such that the distillate fractions are collected separately (i.e., the fraction distilling at 50 to 75°C is physically separated from the fraction distilling at 75 to 100°C). The total number of fractions collected is usually five to seven, but can be as many as 20. Characteristic data for the distillate fractions include the temperatures at the beginning and end of each fraction (or "cut"), sometimes in the

356

form of a continuous curve of temperature vs percent distilled. The API (American Petroleum Institute) gravity and, occasionally, the viscosity of each cut are then measured.

Given the boiling point (1 atm) and API gravity of each cut (or pseudo-component), the vapor pressure of the cut can be calculated as a function of temperature. First, the molecular weight and critical temperature of the cut are calculated according to the following correlation (Fallon and Watson, 1944):

$$Y = C_1 + C_2X_1 + C_3X_2 + C_4X_1X_2 + C_5X_1^2 + C_6X_2^2 \tag{1}$$

where X_1 is the boiling point (°F) at one atmosphere, X_2 is the API gravity, and the constants C_1 to C_6 have the values indicated in Table 6-1. Similarly, the critical temperature can be calculated from the same equation form using the indicated constant values in Table 6-1.

Next the equivalent paraffin carbon number if calculated according to (Gamson and Watson, 1944):

$$N_C = (MW - 2)/14 \tag{2}$$

The critical volume is then calculated according to:

$$V_c = (1.88 + 2.44N_c)/0.044 \tag{3}$$

and the critical pressure is calculated from:

$$P_c = \frac{20.8T}{(V_c - 8)} + P_c' \tag{4}$$

where $P_c' = 10$ to correct the critical pressure correlation from a strictly paraffinic mixture to a naphtha-aromatic-paraffin mixture. Next a parameter (b) is calculated according to

$$b = b' - 0.02 \tag{5}$$

Table 6-1.--Correlation Equation Constants for the Characterization of Narrow Boiling Petroleum Fractions (see text for equation form).

PROPERTY	c_1	c_2	c_3	c_4	c_5	c_6
Molecular weight $t_b \leq 500°F$	6.241E+01	-4.595E-02	-2.836E-01	3.256E-03	4.578E-04	5.279E-04
Molecular weight $t_b > 500$	4.268E+02	-1.007	-7.491	1.380E-02	1.047E-03	2.621E-02
Critical temperature $t_b \leq 500$	4.055E+02	1.337	-2.662	-2.169E-03	-4.943E-04	1.454E-02
Critical temperature $t_b > 500$	4.122E+02	1.276	-2.865	-2.888E-03	-3.707E-04	2.288E-02
b'	1.237E-02	2.516E-01	4.039E-02	-4.024E-02	-----	-----
Kinematic vis, cs @ 122°F API $\leq$ 35	-4.488E-01	-9.344E-04	1.583E-02	-5.219E-05	5.268E-06	1.536E-04
Kinematic vis, cs @ 122°F API > 35	-6.019E-01	1.793E-03	-3.159E-03	-5.1E-06	9.067E-07	3.522E-05

where

$$b' = C_1 + C_2 N_c + C_3 N_c^2 + C_4 N_c^3 \qquad (6)$$

and the values of the constants C_1 to C_4 are indicated in Table 6-1.

A final parameter designated as A is then calculated according to:

$$A = \frac{T_{rb}}{T_{rb}-1} \log_{10}(P_{rb}) + \exp\left[-20(T_{rb}-b)^2\right] \qquad (7)$$

where T_{rb} and P_{rb} are the reduced temperature and reduced pressure at the normal boiling point.

The vapor pressure equation which can be used down to 10 mm Hg is:

$$\log_{10} P_r = \frac{-A(1-T_r)}{T_r} - \exp\left[-20(T_r-b)^2\right] \qquad (8)$$

where A, b, T_c and P_c were determined from the normal boiling point and API gravity of the cut. The temperature at which the vapor pressure is 10 mm Hg can be obtained by the root-finding algorithm of Newton-Raphson.

Below 10 mm Hg, the vapor pressure is calculated according to the Clausius-Clapeyron equation as follows (Gamson and Watson, 1944):

$$\ln \frac{P_2}{P_1} = \frac{\lambda_0}{RT_c} \int_{T_{r_1}}^{T_{r_2}} \frac{(1-T_r)^{0.38}}{T_r^2} dT_r \qquad (9)$$

and is based on the law which states the ratio of the heat of vaporization, λ, to $(1 - T_r)^{0.38}$ is a constant at any temperature. The latent heat of vaporization is calculated from the slope of the natural log of the vapor pressure equation with respect to temperature at the temperature where the vapor pressure is 10 mm Hg. Thus, in the above equation, P_2 is the 10 mm Hg vapor pressure at the temperature, T_r, previously determined.

A sample calculation for the characterization of Prudhoe Bay crude oil is presented in Tables 6-2 and 6-3. Table 6-2 presents the standard inspections (Coleman, 1978; PPC, 1973) for the crude and provides the starting point for the characterization calculations. Note that the distillation in Table 6-2 was conducted at 40 mm Hg for cuts 11 to 15. Thus, these cut temperatures must be corrected to one atmosphere (API, 1976). Table 6-3 presents the computer generated output along with the corrected cut temperatures.

6.5   PSEUDO-COMPONENT EVAPORATION MODEL ON THE OCEAN SURFACE

The evaporation model that predicts the oil remaining in a slick is derived from the physical properties of the oil cuts and a total material balance. From the previous discussion a number of pseudo-components are defined. For each pseudo-component the vapor pressure, molecular weight and initial quantity are known, and a material balance can be written to include each:

$$\frac{dM_i}{dt} = -K_i \ Ax \ P_i^* \ \text{for } i = 1,2,\ldots \ \text{Total number of components} \tag{10}$$

where it is assumed that the oil slick is well stirred and a pseudo-Raoult's law applies as the mixing rule. In this rate equation, M_i is the number of moles of pseudo-component i in the oil slick, P_i^* is the vapor pressure at the prevailing environmental temperature, A is the area of the slick, K_i is an overall mass-transfer coefficient based on partial pressure driving forces, and x_i is the mole fraction of pseudo-component i in the slick. The differential equations are all coupled through the mole fraction term where the total number of moles appears in the denominator.

The over-all mass-transfer coefficient can be calculated using two different methods. One method is the approach of Mackay and Matsugu (1976).

$$K = 0.0292 \ U^{0.78} \ X^{-0.11} \ Sc^{-0.67} \tag{11}$$

where U is the wind velocity in m/hr, X is the slick diameter (assumes circular slick), and Sc is the Schmidt number (2.7). This expression is a correlation

Prudhoe Bay field
Sadlerochit, Triassic
8,890 - 9,008 feet

Alaska
North Slope

GENERAL CHARACTERISTICS

Gravity, specific, 0.893
Sulfur, percent, 0.82
Viscosity, Saybolt Universal at 77° F, 111 sec; 100° F, 84 sec

Gravity, °API, 27.0
Pour point, °F, 15
Color, brownish black
Nitrogen, percent, 0.230

DISTILLATION, BUREAU OF MINES ROUTINE METHOD

Stage 1—Distillation at atmospheric pressure, 741 mm Hg

First drop 81 °F

Fraction No	Cut temp °F	Percent	Sum percent	Sp gr 60/60° F	API 60° F	C I	Refractive index n at 20° C	Specific dispersion	S U visc 100° F	Cloud test °F
1	122									
2	167	2.1	2.1	0.693	72.7	-	1.38591	127.9		
3	212	2.6	4.7	.723	64.2	23	1.40312	139.0		
4	257	3.5	8.2	.752	56.7	27	1.41922	141.9		
5	302	3.6	11.8	.773	51.6	30	1.43082	147.0		
6	347	3.7	15.5	.790	47.6	31	1.43922	149.6		
7	392	3.5	19.0	.801	45.2	30	1.44626	152.1		
8	437	4.3	23.3	.818	41.5	33	1.45528	154.7		
9	482	4.8	28.1	.836	37.8	36	1.46565	157.0		
10	527	5.0	33.1	.851	34.8	38	1.47467	160.5		
Stage 2—Distillation continued at 40 mm Hg										
11	392	2.8	35.9	0.873	30.6	45	1.48218	161.5	40	10
12	437	6.5	42.4	.881	29.1	45	1.48650	168.6	45	30
13	482	6.8	49.2	.897	26.2	49	1.49477	169.4	58	50
14	527	6.0	55.2	.910	24.0	52			93	70
15	572	7.4	62.6	.919	22.5	53			176	90
Residuum		36.3	98.9	.990	11.4					

Carbon residue, Conradson: Residuum 11.6 percent; crude 4.7 percent.

Residuum: Sulfur, percent, - ; Nitrogen, percent, -

APPROXIMATE SUMMARY

	Percent	Sp gr	°API	Viscosity
Light gasoline	4.7	0.710	67.9	
Total gasoline and naphtha	19.0	0.742	54.2	
Kerosene distillate	4.3	.818	41.5	
Gas oil	18.4	.860	33.1	
Nonviscous lubricating distillate	11.0	.887-.911	28.0-23.9	50-100
Medium lubricating distillate	8.1	.911-.922	23.9-22.0	100-200
Viscous lubricating distillate	1.8	.922-.924	22.0-21.6	Above 200
Residuum	36.3	.990	11.4	
Distillation loss	1.1			

Table 6-3.—Illustration of Output from Oil-Weathering Calculations; Fresh Prudhoe Bay Crude Oil Characterization.

SUMMARY OF TBP CUTS CHARACTERIZATION FOR: PRUDHOE BAY, ALASKA

CODE VERSION IS CUTICA OF MAY 84.
ITEM   9, SAMPLE 71011

	TB	API	SPGR	VOL	MW	TC	PC	VC	A	B	T10	VIS	NC	NS
1	1.50E+02	7.27E+01	6.81E-01	2.12E+00	8.35E+01	9.14E+02	3.95E+01	3.66E+02	3.17E+00	1.90E-01	4.47E+02	3.88E-01	3	1
2	1.90E+02	6.42E+01	7.11E-01	2.63E+00	9.39E+01	9.63E+02	3.79E+01	4.07E+02	3.24E+00	2.03E-01	4.78E+02	4.48E-01	3	1
3	2.35E+02	5.67E+01	7.39E-01	3.54E+00	1.06E+02	1.02E+03	3.64E+01	4.54E+02	3.31E+00	2.15E-01	5.13E+02	5.44E-01	3	1
4	2.80E+02	5.16E+01	7.60E-01	3.64E+00	1.19E+02	1.07E+03	3.48E+01	5.07E+02	3.41E+00	2.27E-01	5.49E+02	6.73E-01	3	1
5	3.25E+02	4.76E+01	7.77E-01	3.74E+00	1.34E+02	1.12E+03	3.32E+01	5.65E+02	3.52E+00	2.39E-01	5.86E+02	8.46E-01	3	1
6	3.70E+02	4.52E+01	7.87E-01	3.54E+00	1.51E+02	1.16E+03	3.16E+01	6.32E+02	3.67E+00	2.50E-01	6.23E+02	1.07E+00	3	1
7	4.15E+02	4.15E+01	8.04E-01	4.35E+00	1.67E+02	1.21E+03	3.03E+01	6.98E+02	3.80E+00	2.59E-01	6.60E+02	1.38E+00	3	1
8	4.60E+02	3.78E+01	8.22E-01	4.85E+00	1.85E+02	1.26E+03	2.91E+01	7.67E+02	3.94E+00	2.67E-01	6.98E+02	1.81E+00	3	1
9	5.05E+02	3.48E+01	8.36E-01	5.06E+00	2.00E+02	1.31E+03	2.84E+01	8.28E+02	4.06E+00	2.74E-01	7.36E+02	1.75E+00	3	1
10	5.54E+02	3.06E+01	8.58E-01	2.83E+00	2.21E+02	1.35E+03	2.74E+01	9.09E+02	4.22E+00	2.82E-01	7.77E+02	2.48E+00	3	1
11	6.09E+02	2.91E+01	8.66E-01	6.57E+00	2.52E+02	1.40E+03	2.58E+01	1.03E+03	4.49E+00	2.92E-01	8.26E+02	4.00E+00	3	1
12	6.62E+02	2.62E+01	8.82E-01	6.88E+00	2.81E+02	1.45E+03	2.47E+01	1.15E+03	4.73E+00	2.99E-01	8.73E+02	7.18E+00	3	1
13	7.12E+02	2.40E+01	8.94E-01	6.07E+00	3.13E+02	1.49E+03	2.36E+01	1.27E+03	5.00E+00	3.06E-01	9.19E+02	1.36E+01	3	1
14	7.64E+02	2.25E+01	9.03E-01	7.48E+00	3.51E+02	1.53E+03	2.25E+01	1.43E+03	5.35E+00	3.13E-01	9.68E+02	2.81E+01	3	1
15	8.50E+02	1.14E+01	9.73E-01	3.67E+01	6.00E+02	0.00E+00	0.00E+00	0.00E+00	0.00E+00	0.00E+00	0.00E+00	1.81E+02	0	0

	UOP K	CORRELATION INDEX
1	1.24E+01	1.16E+01
2	1.22E+01	1.66E+01
3	1.20E+01	2.12E+01
4	1.19E+01	2.32E+01
5	1.19E+01	2.43E+01
6	1.19E+01	2.32E+01
7	1.19E+01	2.56E+01
8	1.18E+01	2.90E+01
9	1.18E+01	3.15E+01
10	1.17E+01	3.73E+01
11	1.18E+01	3.66E+01
12	1.18E+01	4.02E+01
13	1.18E+01	4.27E+01
14	1.18E+01	4.36E+01
15	1.12E+01	7.21E+01

BULK API GRAVITY = 28.9

TB = NORMAL BOILING TEMPERATURE, DEG F
API = API GRAVITY
VOL = VOLUME PER CENT OF TOTAL CRUDE
MW = MOLECULAR WEIGHT
TC = CRITICAL TEMPERATURE, DEG RANKINE
PC = CRITICAL PRESSURE, ATMOSPHERES
VC = CRITICAL VOLUME, CC/MOLE
A AND B ARE PARAMETERS IN THE VAPOR PRESSURE EQUATION
T10 IS THE TEMPERATURE IN DEG R WHERE THE VAPOR PRESSURE IS 10 MM HG
VIS IS THE KINEMATIC VISCOSITY IN CENTISTOKES AT 122 DEG F
UOP K IS THE U.O.P. K CHARACTERIZATION FACTOR
CORRELATION INDEX IS DEFINED IN (COLEMAN, 1978)
NC = ERROR CODE, SHOULD BE LESS THAN 20
NS = ERROR CODE, SHOULD BE EQUAL TO 1
IGNORE THE ERROR CODES FOR COMPONENT NUMBER 15 IF IT IS A RESIDUUM

MEAN MOLECULAR WEIGHT OF THE CRUDE = 2.593E+02

and is the proper mass transfer coefficient to multiply by the partial pressure to obtain the rate. Here K is specific to a particular cut i through the Schmidt number.

Implicit in the rate equation for the i-th pseudo-component is the assumption that the partial pressure in the bulk atmosphere is zero. The mass transfer coefficient above takes into account (through the X term) an averaging effect whereby the evaporation rate on the downwind portion of the slick is lower than the upwind portion due to the fact that P_i becomes finite in the air immediately over the oil slick in the down-wind direction.

Another approach to calculating overall mass transfer coefficients is that of Treybal (1955) and Liss (1974):

$$\frac{1}{k} = \frac{1}{k_g} + \frac{H^*}{k_\ell} \tag{12}$$

where k_g is the individual gas-phase mass-transfer coefficient, K is the individual liquid-phase mass-transfer coefficient and H* is the Henry's law coefficient which is defined by:

$$P_i = H^* X_i \tag{13}$$

The units on k_g for a <u>partial pressure</u> driving force are typically moles/(m^2 hr atm), the units on k_g for a <u>mole fraction</u> driving force are moles/(m^2 hr), and the units on H* are atm. The individual mass transfer coefficients, K and k_g, must then be obtained from actual data in a manner similar to that used to deduce K.

The other bulk property of interest for the oil slick is its viscosity. When oil is spilled on the ocean surface, the viscosity is low enough so that mixing into the water column occurs, and the well-mixed oil-phase assumption is valid. However, as evaporation occurs the bulk viscosity increases because the low-viscosity fractions are removed. The viscosity "blending" relationship used to predict the bulk viscosity as a function of composition is:

$$\frac{\mu}{\mu_0} = \exp(K_4 F) \tag{14}$$

where μ_0 is the viscosity of the unweathered oil at 25°C, F is the fraction weathered (i.e., how much has evaporated and dissolved), and K_4 is an oil-dependent constant (Tebeau, et al., 1982).

The bulk viscosity predicted from equation (14) is scaled with respect to temperature according to the Andrade equation (Gold, 1969) which is

$$\ln \frac{\mu_1}{\mu_0} = B \left[\frac{1}{T_1} - 0.00335 \right] \tag{15}$$

where μ_0 is the viscosity of the bulk oil at 25°C, and B is an oil-dependent constant. None of the above viscosity equations take into account water-in-oil emulsion (mousse) formation (Mackay, 1980).

The area for mass transfer in equation (10) is calculated from the rate at which the oil spreads on the water surface. Considerable research has been devoted to the spreading of oil on calm water surfaces; however, many of the resulting models are still relatively elementary. The model of Elliott (1986) was evaluated for these considerations. The major assumption of this spreading model is ...... "oil was modelled as a distribution of droplets whose individual buoyancies depended on droplet size......". The major conceptual problem with this assumption is the connection between the oil slick itself and the oil droplets in the water column. This concept was not discussed. In order to integrate the defining partial differential equation (page 121 of reference) a source of oil droplets must be available. Instead, the model is "carried out" by injecting "mathematically" 1000 droplets and calculating the spatial positions. This model is not plausible because it assumes the oil slick exists as droplets and spreads as droplets. There is no discussion presented on how much of an oil slick exists as droplets and how much exists as oil on the surface.

The type of data needed for a spreading model such as Elliott's to be mechanistically plausible is the rate of production of oil droplets (from the

364

slick), their size distribution, and the rate of return to (or loss from) the slick. The Mackay et al. (1980) spreading model was selected for our purposes because this model is based on observations.

Using arguments based on observations the area of the slick is calculated according to the differential equation

$$\frac{dA}{dt} = K_2 K_3 \ Z^{1.33} A^{0.33} \qquad (16)$$

where A is the slick area, Z is the thickness, K_3 is a constant, and K_2 is the factor by which spreading is inhibited in a broken-ice field. This equation, without K_2, is sometimes referred to as the thick-slick area (Mackay, et al., 1980). Other spreading equations, such as those based on gravity-surface tension theories have been found to be inadequate on the open sea surface and would be of even less use in predicting spreading in the presence of ice. predicting spreading in the presence of ice.

The prediction of water-in-oil emulsification (mousse) is important in oil-weathering material balances because of the viscosity change due to the incorporation of water into oil. Descriptions of water-in-oil emulsification formation are based on three equations from Mackay, et al. (1980) and a fourth which describes the increase in mousse formation rate due to broken-ice (see Section 4.2.2).

$$(1-K_2 W) \ exp \left[\frac{-2.5W}{1-K_1 W} \right] = exp \ (-K_3 K_4 T) \qquad (17a)$$

where W is the weight fraction water in the oil-water mixture, K_1 is a constant in a viscosity equation (Mooney, 1951), K_2 is a coalescing-tendency constant, K_3 is a lumped water-incorporation rate constant and K_4 is the broken-ice field multiplier. The viscosity equation from Mooney (1951) is:

$$\mu = \mu_0 \ exp \left[\frac{-2.5W}{1-K_1 W} \right] \qquad (17b)$$

where μ_0 is the parent oil viscosity and K_1 is usually around 0.62 to 0.65 and apparently does not change much with respect to different types of oils. The

constant K_2 above must satisfy the relation $K_2W < 1$ in order for the water incorporation rate term (right-hand side of equation 17a) to be > 0. Thus, K_2 is the inverse of the maximum weight fraction of water in the mixture. K_3 is the water incorporation rate constant and is a function of the wind speed.

The dispersion (oil into water) weathering process is described by two equations (Mackay et al., 1980). These equation are:

$$F = K_a K_c (V + 1)^2$$

$$F_B = (1 + K_b u^{1/2} \delta X)^{-1}$$

(17c)

(17d)

where F is the fraction of oil on the sea surface subject to dispersions per second, V is the wind speed in m/sec and K_a is a constant. F_B is the fraction of droplets of oil below a critical size which do not return to the slick, K_b is a constant, μ is the oil viscosity in centipoise, X is the slick thickness in meters, δ is the oil/water interfacial surface tension in dynes/cm, and K_c is the factor by which dispersion is increased in a broken-ice field due to enhanced lead matrix pumping. The mass fraction that leaves the slick as dispersed droplets is F_b/F; this fraction applies to <u>each cut of oil</u> simultaneously.

6.6   OIL-ICE CONFIGURATIONS

The interaction of oil with first and multi-year ice in the Arctic environment can be described with varying degrees of complexity. A very detailed description would include discussions of a variety of ice types (grease, frazil, etc.) and formations (brine channels, leads, etc.), the dependence of ice growth (or melt) on environmental conditions, and many other considerations. A more general description of oil-ice interactions, however, would seek to discuss only the most important variables and conditions that affect oil-ice behavior phenomena. In developing a computer model to predict such interactions, a more generalized approach must (at first) be undertaken for many reasons. First, in constructing and testing a model, the processes that will be dominant should be added first. After these processes are adequately described, other more minor effects can be added. Second, many of the more detailed effects (such as brine channel migration, variation of ice type, etc.) are stochastic

in nature and thus difficult to predict. Third, a generalized model can be used more effectively to identify further required experimental efforts and to utilize the results of those efforts.

Because of the above, and in order to make the most use of the existing open-ocean oil-weathering model, the ocean-ice oil-weathering code has been developed so that generalized oil-ice configurations are considered. The configurations chosen are currently considered to be the major logical sets of conditions that determine oil-weathering. With time, and a continued improvement in our understanding of the Arctic, more configurations can be added and existing configurations can be improved. Below is a discussion of the three existing oil-ice configurations, preceded by a discussion of why a fourth one was not included in the computer code except as a separate stand-alone model to predict pseudo-component loss due to dissolution alone. As will be noted, this mechanism effects such a small percentage of the overall oil mass, that it is not factored into mass balance calculations embodied in the main oil weathering code.

6.6.1   Under-Ice Weathering

When oil is spilled <u>under</u> sea ice, most of the weathering processes that occur in the open-ocean are not operative. Evaporation is prevented by the ice cover, dispersion and mousse formation are inhibited by the lack of strong turbulence, and the oil does not spread significantly under ice. While it is known that spreading of oil under ice does occur and is current dependent, the macroscopic configuration of the oil will not have an effect on its weathering. In addition, the dissolution of aromatic hydrocarbons into the water column is slow enough (as evidenced by Sections 4.2.3 of this report), that the oil will be encapsulated before a significant amount of oil can dissolve. Furthermore, even if all of the 1-2% of the oil that is soluble were to dissolve, this would not impact the API gravities and volume percents of the TBP cuts that are utilized as input to each section of the oil-weathering code. Thus, since oil under ice is limited to a very small weathering effect, it has not been included as an oil-ice configuration in the ocean-ice oil-weathering model at this time.

6.6.2   Oil in Pools on Top of Ice

In spring when the temperature rises, the encapsulated oil travels to the ice surface through brine channels or because the ice above melts away. Evaporation begins when the oil is exposed to the atmosphere. For the cases when oil is released over a long period of time, the evaporation must be modeled by considering incremental releases of oil on the ice surface. This technical approach was used to model the continuous release of oil on ocean surface where discrete "patches" of oil are identified (B.E. Kirstein, 1984). Varying amounts of water will be present in the on-ice pools, but spreading, mousse formation, and dispersion will certainly be much less important than in the open-ocean or later as the ice breaks up (see Broken Ice Field). Thus, for this section of the ocean-ice model, evaporation is the only mass-transfer process considered. The user is prompted for the environmental temperature (the ice temperature), the number of hours for weathering to occur, and other parameters relating to evaporation. The model then performs the integration required to "weather" the oil and re-characterizes the oil in the same manner described in Section 6.4. This allows each pseudo-component of the oil to be tracked through the course of the weathering scenario, enables the user to monitor the bulk properties of the oil, and provides intermediate results that can be compared with real data from field experiments (pseudo-components lost as determined by TBP distillation or simulated by FID-GC analyses).

The results of the intermediate characterization of the oil are subsequently used as input for any weathering specified later in the weathering scenario (such as broken ice and ultimately, open ocean conditions).

6.6.3   Broken-Ice Field

After further ice melting takes place, the oil can reach the ocean surface and weather in the broken-ice field. Because the oil is in contact with water it is important to consider the spreading, mousse formation, and dispersion processes. The effect of varying ice cover on the rates of these processes, however, is not well known. For this reason the code has been

368

written such that constants that describe the dependence of these processes on ice cover are required model input.

Data from the wave tank experiments at Kasitsna Bay (See Section 4) indicate that the mousse formation rate (K_3) in broken ice is increased by about an order of magnitude. It must be emphasized that this observation cannot be scaled easily to natural sea-ice conditions because very little is quantitatively known about this process. Dispersion without sea ice is still a research topic. Therefore, field observations with similar situations is highly desirable. A value of 10 is used in the mousse equations to take the previously mentioned increase into account. This value can be changed by the user as more data are collected. For example, in wave tank experiments examining oil weathering behavior in "pseudo multi-year ice" where slush ice and grinding ice flows were not present, mousse formation rates appeared intermediate between open ocean and broken floe/slush ice conditions.

The data for oil droplet dispersion are even less indicative of an ice cover dependence. However, a constant (K_c) of 10 has been chosen to describe the increase of (initial) dispersion in broken ice. As emulsified oil viscosity increases limiting continued dispersion, the constant can once again be changed as the data-base increases.

For the oil spreading rate a linear dependence with ice cover has been assumed; thus a 50% ice cover will decrease the spreading rate (area) 50% and a 75% ice cover will decrease the spreading rate (area) 75%, etc. The assumption of a linear spreading function for ice cover may not be true since theoretical predictions are not possible. As data becomes available, possibly from the State of Alaska Tier II work, a more realistic algorithm or correlation can be used.

6.6.4   Open Ocean

When all of the ice has melted, the oil undergoes open-ocean weathering. Thus all of the weathering processes are in effect as described in the open-ocean oil-weathering users manual (Payne et al., 1984a).

Figure 6-1 presents an abbreviated flow chart of the calculation performed in the Ocean-Ice oil-weathering code. The majority of the coding calculates the required physical properties and kinetic constants. The actual integration routine is relatively small.

Tables 6-4 through 6-6 present examples of abbreviated numerical output (80-column) for the weathering of Prudhoe Bay crude. The cut information which numbers 1-15 presents the physical properties of the cuts: molecular weight, vapor pressures, density and boiling point. The kinetic parameters are contained in the mass-transfer coefficient code (2 in this case), wind speed and temperature. The integrated material balance presents the volume remaining in the slick, the density, area, thickness, weight % water-in-oil, evaporation rate, mass per unit area and compositional information. Note that the user has chosen three different weathering compartments (pools on ice, Table 6-4; then oil in broken ice, Table 6-5; then open ocean conditions, Table 6-6) and output is presented for each compartment with an oil characterization at the beginning of each. A more detailed output was also generated but it is quite lengthy; an example of this output is presented in the User's Manual which is a stand-alone companion document to this report.

In summary the open-ocean oil-weathering code considers the following processes:

- evaporation

- dispersion

- spreading

- physical property changes

- mousse formation

The Ocean-Ice oil-weathering code User's Manual (a separate document) presents detailed input-output information along with a code listing. It is imperative that the user understands the common terms used to describe oil in the environment. Thus, the User's Manual and the code itself were written to aid the user in gaining the necessary knowledge. All that is required to use the code is the User's Manual and an installed copy of the computer code.
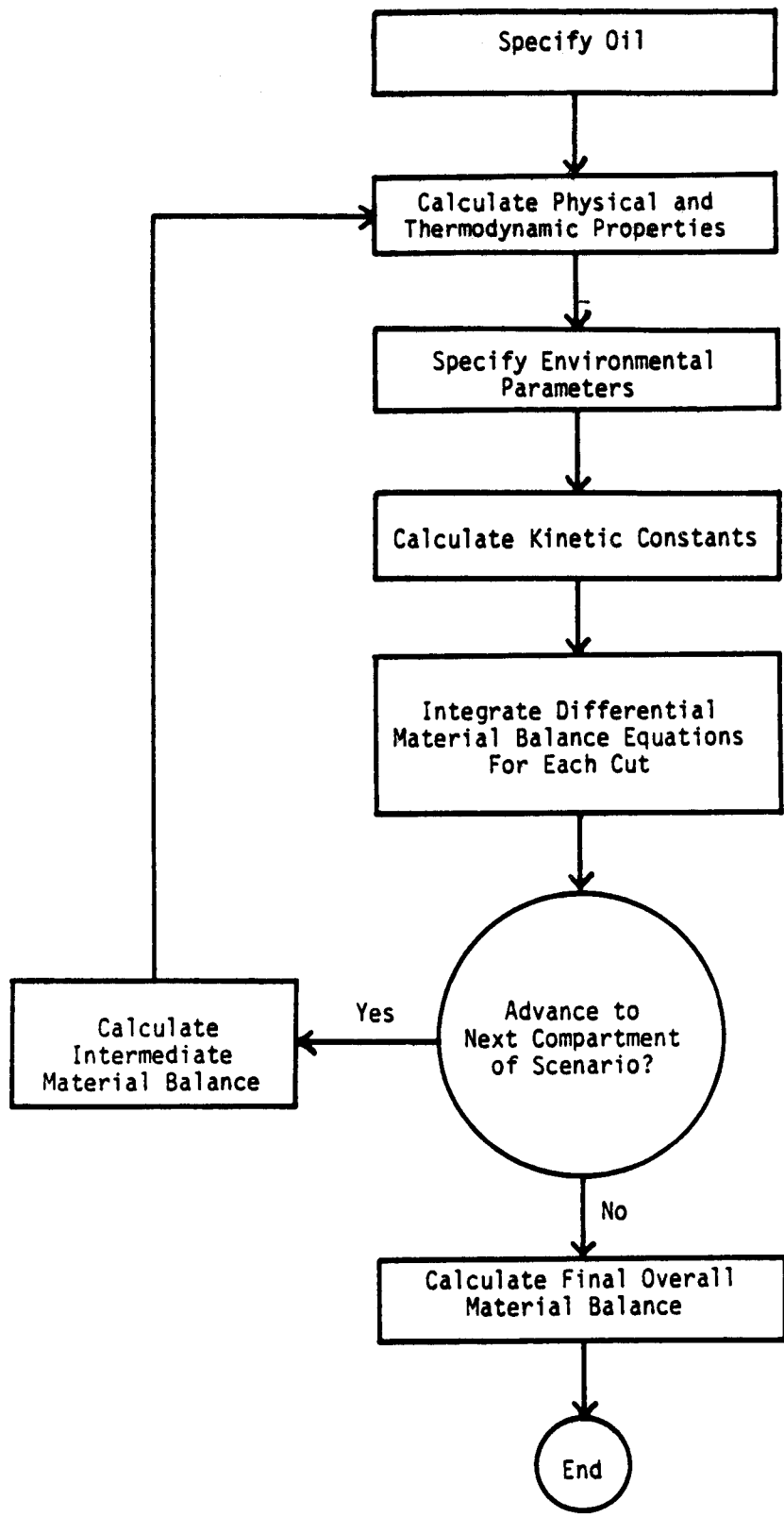
Figure 6-1.--Ocean-Ice Oil Weathering Model Flow Chart.

Table 6-4.--Illustration of 80-Column Output from Ocean-Ice Oil-Weathering Code; Prudhoe Bay Crude Oil; Weathering of Oil in Pools on Top of Ice at 32°F.

WEATHERING OF OIL IN POOLS ON TOP OF ICE

OIL: PRUDHOE BAY, ALASKA
TEMPERATURE= 32.0 DEG F, WIND SPEED= 10.0 KNOTS
SPILL SIZE= 1.000E+04 BARRELS
MASS-TRANSFER COEFFICIENT CODE= 2

FOR THE OUTPUT THAT FOLLOWS, MOLES=GRAM MOLES
GMS=GRAMS, VP=VAPOR PRESSURE IN ATMOSPHERES
BP=BOILING POINT IN DEG F, API=GRAVITY
MW=MOLECULAR WEIGHT

CUT	MOLES	GMS	VP	BP	API	MW
1	2.74E+05	2.29E+07	4.09E-02	1.50E+02	7.27E+01	83
2	3.15E+05	2.96E+07	1.35E-02	1.90E+02	6.42E+01	93
3	3.91E+05	4.14E+07	3.25E-03	2.35E+02	5.67E+01	105
4	3.67E+05	4.37E+07	7.05E-04	2.80E+02	5.16E+01	119
5	3.43E+05	4.60E+07	1.40E-04	3.25E+02	4.76E+01	133
6	2.92E+05	4.41E+07	2.44E-05	3.70E+02	4.52E+01	150
7	3.30E+05	5.53E+07	3.98E-06	4.15E+02	4.15E+01	167
8	3.41E+05	6.31E+07	5.86E-07	4.60E+02	3.78E+01	184
9	3.34E+05	6.69E+07	8.22E-08	5.05E+02	3.48E+01	200
10	1.74E+05	3.84E+07	8.24E-09	5.54E+02	3.06E+01	220
11	3.58E+05	9.01E+07	4.12E-10	6.09E+02	2.91E+01	251
12	3.41E+05	9.59E+07	2.02E-11	6.62E+02	2.62E+01	281
13	2.75E+05	8.59E+07	8.60E-13	7.12E+02	2.40E+01	312
14	3.04E+05	1.07E+08	1.96E-14	7.64E+02	2.25E+01	351
15	9.42E+05	5.65E+08	0.00E+00	8.50E+02	1.14E+01	600

MOUSSE CONSTANTS: MOONEY= 0.00E+00, MAX H20=-1.00, WIND**2= 0.00E+00
DISPERSION CONSTANTS: KA= 1.08E-01, KB= 3.00E+01, S-TENSION= 1.00E+00
VIS CONSTANTS: VIS25C= 3.50E+01, ANDRADE = 9.00E+03, FRACT = 1.05E+01

FOR THE OUTPUT THAT FOLLOWS, TIME=HOURS
BBL=BARRELS, SPGR=SPECIFIC GRAVITY, AREA=M*M
THICKNESS=CM, W=PERCENT WATER IN OIL (MOUSSE)
DISP=DISPERSION RATE IN GMS/M*M/HR
ERATE=EVAPORTION RATE IN GMS/M*M/HR
M/A=MASS PER M*M OF OIL IN THE SLICK
I=FIRST CUT WITH GREATER THAN 1% (MASS) REMAINING
J=FIRST CUT WITH GREATER THAN 50% (MASS) REMAINING
DISPERSION WAS TURNED OFF
SPREADING WAS TURNED OFF

TIME	BBL	SPGR	AREA	THICKNESS	W	DISP	ERATE	M/A	I	J
0	1.0E+04	0.88	7.9E+04	2.0E+00	0	0.0E+00	0.0E+00	1.8E+04	1	1
1	9.8E+03	0.88	7.9E+04	2.0E+00	0	0.0E+00	1.7E+02	1.7E+04	1	1
2	9.7E+03	0.88	7.9E+04	1.9E+00	0	0.0E+00	1.3E+02	1.7E+04	1	2
3	9.7E+03	0.88	7.9E+04	1.9E+00	0	0.0E+00	9.5E+01	1.7E+04	1	2
4	9.6E+03	0.88	7.9E+04	1.9E+00	0	0.0E+00	7.5E+01	1.7E+04	1	3
5	9.6E+03	0.89	7.9E+04	1.9E+00	0	0.0E+00	6.2E+01	1.7E+04	1	3
6	9.5E+03	0.89	7.9E+04	1.9E+00	0	0.0E+00	5.2E+01	1.7E+04	1	3
7	9.5E+03	0.89	7.9E+04	1.9E+00	0	0.0E+00	4.5E+01	1.7E+04	1	3
8	9.4E+03	0.89	7.9E+04	1.9E+00	0	0.0E+00	4.0E+01	1.7E+04	2	3
9	9.4E+03	0.89	7.9E+04	1.9E+00	0	0.0E+00	3.6E+01	1.7E+04	2	3
10	9.4E+03	0.89	7.9E+04	1.9E+00	0	0.0E+00	3.3E+01	1.7E+04	2	3
11	9.4E+03	0.89	7.9E+04	1.9E+00	0	0.0E+00	3.0E+01	1.7E+04	2	3
12	9.4E+03	0.89	7.9E+04	1.9E+00	0	0.0E+00	2.8E+01	1.7E+04	2	3
13	9.3E+03	0.89	7.9E+04	1.9E+00	0	0.0E+00	2.6E+01	1.7E+04	2	3
14	9.3E+03	0.89	7.9E+04	1.9E+00	0	0.0E+00	2.4E+01	1.7E+04	2	3
15	9.3E+03	0.89	7.9E+04	1.9E+00	0	0.0E+00	2.2E+01	1.7E+04	2	3
16	9.3E+03	0.89	7.9E+04	1.9E+00	0	0.0E+00	2.1E+01	1.7E+04	2	4
17	9.3E+03	0.89	7.9E+04	1.9E+00	0	0.0E+00	2.0E+01	1.7E+04	2	4
18	9.3E+03	0.89	7.9E+04	1.9E+00	0	0.0E+00	1.9E+01	1.6E+04	2	4
19	9.2E+03	0.89	7.9E+04	1.8E+00	0	0.0E+00	1.8E+01	1.6E+04	2	4
20	9.2E+03	0.89	7.9E+04	1.8E+00	0	0.0E+00	1.7E+01	1.6E+04	2	4
21	9.2E+03	0.89	7.9E+04	1.8E+00	0	0.0E+00	1.6E+01	1.6E+04	2	4
22	9.2E+03	0.89	7.9E+04	1.8E+00	0	0.0E+00	1.6E+01	1.6E+04	2	4
23	9.2E+03	0.89	7.9E+04	1.8E+00	0	0.0E+00	1.5E+01	1.6E+04	2	4

Table 6-5.--Illustration of 80-Column Output; Prudhoe Bay Crude Oil; Broken Ice Field Weathering at 32°F Following Weathering in Pools on Top of Ice.

```
WEATHERING OF OIL IN A BROKEN ICE FIELD
AFTER ICE POOL WEATHERING FOR 2.400E+01 HOURS

OIL: PRUDHOE BAY, ALASKA
TEMPERATURE=  32.0 DEG F, WIND SPEED=   12.0 KNOTS
SPILL SIZE=  9.195E+03 BARRELS
MASS-TRANSFER COEFFICIENT CODE=   2

FOR THE OUTPUT THAT FOLLOWS, MOLES=GRAM MOLES
GMS=GRAMS, VP=VAPOR PRESSURE IN ATMOSPHERES
BP=BOILING POINT IN DEG F, API=GRAVITY
MW=MOLECULAR WEIGHT
```

CUT	MOLES	GMS	VP	BP	API	MW
1	1.87E-01	1.57E+01	5.99E-02	1.50E+02	7.27E+01	83
2	3.11E+03	2.92E+05	2.06E-02	1.90E+02	6.42E+01	93
3	1.31E+05	1.38E+07	5.42E-03	2.35E+02	5.67E+01	105
4	2.90E+05	3.46E+07	1.24E-03	2.80E+02	5.16E+01	119
5	3.28E+05	4.39E+07	2.59E-04	3.25E+02	4.76E+01	133
6	2.90E+05	4.37E+07	4.81E-05	3.70E+02	4.52E+01	150
7	3.30E+05	5.52E+07	8.33E-06	4.15E+02	4.15E+01	167
8	3.41E+05	6.31E+07	1.31E-06	4.60E+02	3.78E+01	184
9	3.34E+05	6.69E+07	1.95E-07	5.05E+02	3.48E+01	200
10	1.74E+05	3.84E+07	2.12E-08	5.54E+02	3.06E+01	220
11	3.58E+05	9.01E+07	1.17E-09	6.09E+02	2.91E+01	251
12	3.41E+05	9.59E+07	6.39E-11	6.62E+02	2.62E+01	281
13	2.75E+05	8.59E+07	3.03E-12	7.12E+02	2.40E+01	312
14	3.04E+05	1.07E+08	7.87E-14	7.64E+02	2.25E+01	351
15	9.42E+05	5.65E+08	0.00E+00	8.50E+02	1.14E+01	600

```
MOUSSE CONSTANTS: MOONEY= 6.20E-01, MAX H20= 0.70, WIND**2= 1.00E-02
                 K4=1.000E+01
DISPERSION CONSTANTS: KA= 1.08E-01, KB= 5.00E+01, S-TENSION= 3.00E+01
                 KC=1.000E+01
FRACTION OF ICE COVER=6.600E-01
VIS CONSTANTS: VIS25C= 3.50E+01, ANDRADE = 9.00E+03, FRACT = 1.05E+01

FOR THE OUTPUT THAT FOLLOWS, TIME=HOURS
BBL=BARRELS, SPGR=SPECIFIC GRAVITY, AREA=M*M
THICKNESS=CM, W=PERCENT WATER IN OIL (MOUSSE)
DISP=DISPERSION RATE IN GMS/M*M/HR
ERATE=EVAPORTION RATE IN GMS/M*M/HR
M/A=MASS PER M*M OF OIL IN THE SLICK
I=FIRST CUT WITH GREATER THAN  1% (MASS) REMAINING
J=FIRST CUT WITH GREATER THAN 50% (MASS) REMAINING
CUT  1 GOES AWAY IN MINUTES, THEREFORE IT WAS DELETED AND THE CUTS RENUMBERED
```

TIME	BBL	SPGR	AREA	THICKNESS	W	DISP	ERATE	M/A	I	J
0	9.2E+03	0.89	7.9E+04	1.8E+00	0	7.6E+01	0.0E+00	1.6E+04	1	1
1	9.1E+03	0.89	1.1E+05	1.3E+00	29	7.3E+01	2.5E+01	1.2E+04	1	1
2	9.0E+03	0.89	1.4E+05	1.1E+00	48	4.4E+01	2.3E+01	9.5E+03	1	2
3	9.0E+03	0.89	1.6E+05	9.2E-01	60	2.8E+01	2.1E+01	8.2E+03	1	2
4	8.9E+03	0.89	1.7E+05	8.2E-01	66	1.9E+01	1.9E+01	7.3E+03	1	2
5	8.9E+03	0.89	1.9E+05	7.4E-01	69	1.5E+01	1.7E+01	6.7E+03	1	3
6	8.8E+03	0.89	2.0E+05	6.9E-01	70	1.3E+01	1.5E+01	6.1E+03	1	3
7	8.8E+03	0.89	2.2E+05	6.4E-01	70	1.3E+01	1.3E+01	5.7E+03	2	3
8	8.7E+03	0.90	2.3E+05	5.9E-01	70	1.2E+01	1.2E+01	5.3E+03	2	3
9	8.7E+03	0.90	2.5E+05	5.6E-01	70	1.2E+01	1.1E+01	5.0E+03	2	3
10	8.6E+03	0.90	2.6E+05	5.3E-01	70	1.2E+01	9.6E+00	4.8E+03	2	3
11	8.6E+03	0.90	2.7E+05	5.1E-01	70	1.1E+01	8.7E+00	4.5E+03	2	3
12	8.5E+03	0.90	2.8E+05	4.8E-01	70	1.1E+01	7.9E+00	4.3E+03	2	4
13	8.5E+03	0.90	2.9E+05	4.6E-01	70	1.1E+01	7.3E+00	4.2E+03	2	4
14	8.5E+03	0.90	3.0E+05	4.5E-01	70	1.1E+01	6.8E+00	4.0E+03	2	4
16	8.4E+03	0.90	3.1E+05	4.3E-01	70	1.0E+01	6.3E+00	3.9E+03	2	4
17	8.4E+03	0.90	3.2E+05	4.2E-01	70	1.0E+01	5.9E+00	3.8E+03	2	4

Table 6-5.--(Continued)

18	8.3E+03	0.90	3.3E+05	4.1E-01	70	9.8E+00	5.5E+00	3.6E+03	3	4
19	8.3E+03	0.90	3.4E+05	3.9E-01	70	9.6E+00	5.2E+00	3.5E+03	3	4
20	8.3E+03	0.90	3.4E+05	3.8E-01	70	9.4E+00	4.9E+00	3.4E+03	3	4
21	8.2E+03	0.90	3.5E+05	3.7E-01	70	9.2E+00	4.6E+00	3.3E+03	3	4
22	8.2E+03	0.90	3.6E+05	3.6E-01	70	9.0E+00	4.3E+00	3.3E+03	3	4
23	8.1E+03	0.90	3.7E+05	3.5E-01	70	8.8E+00	4.1E+00	3.2E+03	3	4
24	8.1E+03	0.90	3.7E+05	3.5E-01	70	8.6E+00	3.9E+00	3.1E+03	3	4
25	8.1E+03	0.90	3.8E+05	3.4E-01	70	8.4E+00	3.7E+00	3.0E+03	3	4
26	8.0E+03	0.90	3.9E+05	3.3E-01	70	8.2E+00	3.5E+00	3.0E+03	3	4
27	8.0E+03	0.90	3.9E+05	3.2E-01	70	8.0E+00	3.3E+00	2.9E+03	3	4
28	8.0E+03	0.90	4.0E+05	3.2E-01	70	7.8E+00	3.1E+00	2.9E+03	3	4
29	7.9E+03	0.90	4.1E+05	3.1E-01	70	7.6E+00	2.9E+00	2.8E+03	3	4
31	7.9E+03	0.90	4.1E+05	3.0E-01	70	7.4E+00	2.8E+00	2.7E+03	3	4
32	7.9E+03	0.90	4.2E+05	3.0E-01	70	7.3E+00	2.6E+00	2.7E+03	3	4
33	7.8E+03	0.90	4.3E+05	2.9E-01	70	7.1E+00	2.5E+00	2.6E+03	3	4
34	7.8E+03	0.90	4.4E+05	2.8E-01	70	6.9E+00	2.4E+00	2.6E+03	3	5
35	7.7E+03	0.90	4.4E+05	2.8E-01	70	6.8E+00	2.3E+00	2.5E+03	3	5
37	7.7E+03	0.90	4.5E+05	2.7E-01	70	6.6E+00	2.2E+00	2.5E+03	3	5
38	7.7E+03	0.90	4.5E+05	2.7E-01	70	6.5E+00	2.1E+00	2.4E+03	3	5
39	7.7E+03	0.90	4.6E+05	2.7E-01	70	6.3E+00	2.0E+00	2.4E+03	3	5
40	7.6E+03	0.90	4.6E+05	2.6E-01	70	6.2E+00	1.9E+00	2.4E+03	3	5
41	7.6E+03	0.90	4.7E+05	2.6E-01	70	6.1E+00	1.8E+00	2.3E+03	3	5
42	7.6E+03	0.90	4.7E+05	2.5E-01	70	6.0E+00	1.8E+00	2.3E+03	3	5
43	7.5E+03	0.90	4.8E+05	2.5E-01	70	5.8E+00	1.7E+00	2.3E+03	3	5
44	7.5E+03	0.90	4.8E+05	2.5E-01	70	5.7E+00	1.7E+00	2.2E+03	3	5
45	7.5E+03	0.90	4.9E+05	2.4E-01	70	5.6E+00	1.6E+00	2.2E+03	3	5
46	7.5E+03	0.90	4.9E+05	2.4E-01	70	5.5E+00	1.6E+00	2.2E+03	4	5
47	7.4E+03	0.90	5.0E+05	2.4E-01	70	5.4E+00	1.5E+00	2.1E+03	4	5
48	7.4E+03	0.90	5.0E+05	2.3E-01	70	5.3E+00	1.5E+00	2.1E+03	4	5
49	7.4E+03	0.90	5.1E+05	2.3E-01	70	5.2E+00	1.4E+00	2.1E+03	4	5
50	7.4E+03	0.90	5.1E+05	2.3E-01	70	5.1E+00	1.4E+00	2.1E+03	4	5
51	7.3E+03	0.90	5.2E+05	2.3E-01	70	5.0E+00	1.4E+00	2.0E+03	4	5
61	7.1E+03	0.90	5.6E+05	2.0E-01	70	4.2E+00	1.1E+00	1.8E+03	4	5
71	6.9E+03	0.90	5.9E+05	1.8E-01	70	3.5E+00	8.4E-01	1.7E+03	4	5
81	6.7E+03	0.91	6.3E+05	1.7E-01	70	3.0E+00	6.8E-01	1.5E+03	4	5
91	6.6E+03	0.91	6.6E+05	1.6E-01	70	2.6E+00	5.6E-01	1.4E+03	4	6

Table 6-6.--80-Column Output; Prudhoe Bay Crude Oil; Open-Ocean Weathering Following Weathering in Pools on Top of Ice and Broken Ice Field Weathering.

OPEN OCEAN WEATHERING
AFTER:

       ICE POOL WEATHERING FOR 2.400E+01 HOURS
       BROKEN ICE FIELD WEATHERING FOR 1.000E+02 HOURS

OIL: PRUDHOE BAY, ALASKA
TEMPERATURE= 40.0 DEG F, WIND SPEED= 20.0 KNOTS
SPILL SIZE= 6.428E+03 BARRELS
MASS-TRANSFER COEFFICIENT CODE= 2

FOR THE OUTPUT THAT FOLLOWS, MOLES=GRAM MOLES
GMS=GRAMS, VP=VAPOR PRESSURE IN ATMOSPHERES
BP=BOILING POINT IN DEG F, API=GRAVITY
MW=MOLECULAR WEIGHT

CUT	MOLES	GMS	VP	BP	API	MW
1	4.40E-02	5.25E+00	1.77E-03	2.80E+02	5.16E+01	119
2	1.04E+04	1.40E+06	3.84E-04	3.25E+02	4.76E+01	133
3	1.26E+05	1.90E+07	7.40E-05	3.70E+02	4.52E+01	150
4	2.33E+05	3.90E+07	1.33E-05	4.15E+02	4.15E+01	167
5	2.62E+05	4.84E+07	2.18E-06	4.60E+02	3.78E+01	184
6	2.60E+05	5.21E+07	3.40E-07	5.05E+02	3.48E+01	200
7	1.36E+05	3.00E+07	3.86E-08	5.54E+02	3.06E+01	220
8	2.79E+05	7.03E+07	2.29E-09	6.09E+02	2.91E+01	251
9	2.66E+05	7.49E+07	1.33E-10	6.62E+02	2.62E+01	281
10	2.14E+05	6.70E+07	6.76E-12	7.12E+02	2.40E+01	312
11	2.37E+05	8.34E+07	1.91E-13	7.64E+02	2.25E+01	351
12	7.35E+05	4.41E+08	0.00E+00	8.50E+02	1.14E+01	600

MOUSSE CONSTANTS: MOONEY= 6.20E-01, MAX H20= 0.70, WIND**2= 1.00E-03
DISPERSION CONSTANTS: KA= 1.08E-01, KB= 5.00E+01, S-TENSION= 3.00E+01
VIS CONSTANTS: VIS25C= 3.50E+01, ANDRADE = 9.00E+03, FRACT = 1.05E+01

FOR THE OUTPUT THAT FOLLOWS, TIME=HOURS
BBL=BARRELS, SPGR=SPECIFIC GRAVITY, AREA=M*M
THICKNESS=CM, W=PERCENT WATER IN OIL (MOUSSE)
DISP=DISPERSION RATE IN GMS/M*M/HR
ERATE=EVAPORTION RATE IN GMS/M*M/HR
M/A=MASS PER M*M OF OIL IN THE SLICK
I=FIRST CUT WITH GREATER THAN 1% (MASS) REMAINING
J=FIRST CUT WITH GREATER THAN 50% (MASS) REMAINING

TIME	BBL	SPGR	AREA	THICKNESS	W	DISP	ERATE	M/A	I	J
0	6.4E+03	0.91	6.8E+05	1.5E-01	70	3.5E+00	0.0E+00	1.4E+03	1	1
1	6.4E+03	0.91	6.9E+05	1.5E-01	70	3.4E+00	1.0E+00	1.3E+03	1	1
2	6.4E+03	0.91	7.0E+05	1.5E-01	70	3.4E+00	1.0E+00	1.3E+03	1	2
3	6.4E+03	0.91	7.1E+05	1.4E-01	70	3.3E+00	9.8E-01	1.3E+03	1	2
4	6.3E+03	0.91	7.1E+05	1.4E-01	70	3.2E+00	9.5E-01	1.3E+03	1	2
5	6.3E+03	0.91	7.2E+05	1.4E-01	70	3.2E+00	9.2E-01	1.3E+03	1	2
6	6.3E+03	0.91	7.3E+05	1.4E-01	70	3.1E+00	8.9E-01	1.2E+03	1	3
7	6.3E+03	0.91	7.4E+05	1.4E-01	70	3.1E+00	8.6E-01	1.2E+03	1	3
8	6.2E+03	0.91	7.5E+05	1.3E-01	70	3.0E+00	8.4E-01	1.2E+03	2	3
9	6.2E+03	0.91	7.5E+05	1.3E-01	70	2.9E+00	8.1E-01	1.2E+03	2	3
11	6.2E+03	0.91	7.6E+05	1.3E-01	70	2.9E+00	7.9E-01	1.2E+03	2	3
12	6.2E+03	0.91	7.7E+05	1.3E-01	70	2.8E+00	7.6E-01	1.2E+03	2	3
13	6.1E+03	0.91	7.8E+05	1.3E-01	70	2.8E+00	7.4E-01	1.1E+03	2	3
14	6.1E+03	0.91	7.9E+05	1.2E-01	70	2.7E+00	7.3E-01	1.1E+03	2	3
15	6.1E+03	0.91	7.9E+05	1.2E-01	70	2.7E+00	7.1E-01	1.1E+03	2	3
16	6.1E+03	0.91	8.0E+05	1.2E-01	70	2.6E+00	6.9E-01	1.1E+03	2	3
17	6.1E+03	0.91	8.1E+05	1.2E-01	70	2.6E+00	6.8E-01	1.1E+03	2	3
18	6.0E+03	0.91	8.1E+05	1.2E-01	70	2.5E+00	6.6E-01	1.1E+03	2	3
19	6.0E+03	0.91	8.2E+05	1.2E-01	70	2.5E+00	6.5E-01	1.1E+03	2	3
20	6.0E+03	0.91	8.3E+05	1.2E-01	70	2.5E+00	6.3E-01	1.1E+03	2	3
21	6.0E+03	0.91	8.3E+05	1.1E-01	70	2.4E+00	6.2E-01	1.0E+03	2	3
22	6.0E+03	0.91	8.4E+05	1.1E-01	70	2.4E+00	6.1E-01	1.0E+03	2	3
23	6.0E+03	0.91	8.4E+05	1.1E-01	70	2.3E+00	6.0E-01	1.0E+03	2	3

Table 6-6.--(Continued)

25	5.9E+03	0.91	8.5E+05	1.1E-01	70	2.3E+00	5.8E-01	1.0E+03	2	4
26	5.9E+03	0.91	8.6E+05	1.1E-01	70	2.2E+00	5.7E-01	9.9E+02	2	4
27	5.9E+03	0.91	8.7E+05	1.1E-01	70	2.2E+00	5.5E-01	9.8E+02	2	4
29	5.9E+03	0.91	8.7E+05	1.1E-01	70	2.2E+00	5.4E-01	9.7E+02	2	4
30	5.8E+03	0.91	8.8E+05	1.1E-01	70	2.1E+00	5.3E-01	9.6E+02	2	4
31	5.8E+03	0.91	8.9E+05	1.0E-01	70	2.1E+00	5.2E-01	9.5E+02	2	4
32	5.8E+03	0.91	8.9E+05	1.0E-01	70	2.0E+00	5.0E-01	9.4E+02	2	4
34	5.8E+03	0.91	9.0E+05	1.0E-01	70	2.0E+00	4.9E-01	9.3E+02	3	4
35	5.8E+03	0.91	9.1E+05	1.0E-01	70	2.0E+00	4.8E-01	9.2E+02	3	4
36	5.7E+03	0.91	9.1E+05	1.0E-01	70	1.9E+00	4.7E-01	9.1E+02	3	4
37	5.7E+03	0.91	9.2E+05	9.9E-02	70	1.9E+00	4.6E-01	9.0E+02	3	4
39	5.7E+03	0.91	9.3E+05	9.8E-02	70	1.9E+00	4.5E-01	8.9E+02	3	4
40	5.7E+03	0.91	9.3E+05	9.7E-02	70	1.8E+00	4.4E-01	8.8E+02	3	4
41	5.7E+03	0.91	9.4E+05	9.6E-02	70	1.8E+00	4.3E-01	8.7E+02	3	4
42	5.6E+03	0.91	9.4E+05	9.5E-02	70	1.8E+00	4.2E-01	8.7E+02	3	4
44	5.6E+03	0.91	9.5E+05	9.4E-02	70	1.7E+00	4.1E-01	8.6E+02	3	4
45	5.6E+03	0.91	9.6E+05	9.3E-02	70	1.7E+00	4.1E-01	8.5E+02	3	4
46	5.6E+03	0.91	9.6E+05	9.2E-02	70	1.7E+00	4.0E-01	8.4E+02	3	4
47	5.6E+03	0.91	9.7E+05	9.2E-02	70	1.6E+00	3.9E-01	8.3E+02	3	4
49	5.6E+03	0.91	9.7E+05	9.1E-02	70	1.6E+00	3.8E-01	8.3E+02	3	4
50	5.5E+03	0.91	9.8E+05	9.0E-02	70	1.6E+00	3.7E-01	8.2E+02	3	4
51	5.5E+03	0.91	9.8E+05	8.9E-02	70	1.6E+00	3.7E-01	8.1E+02	3	4
62	5.4E+03	0.91	1.0E+06	8.3E-02	70	1.4E+00	3.1E-01	7.6E+02	3	4
72	5.3E+03	0.91	1.1E+06	7.8E-02	70	1.2E+00	2.7E-01	7.1E+02	3	4
82	5.2E+03	0.91	1.1E+06	7.4E-02	70	1.1E+00	2.4E-01	6.8E+02	3	4
92	5.1E+03	0.91	1.1E+06	7.0E-02	70	9.4E-01	2.1E-01	6.4E+02	3	5
102	5.0E+03	0.91	1.2E+06	6.7E-02	70	8.4E-01	1.9E-01	6.1E+02	3	5
112	4.9E+03	0.91	1.2E+06	6.4E-02	70	7.6E-01	1.7E-01	5.9E+02	3	5
122	4.8E+03	0.91	1.2E+06	6.2E-02	70	6.9E-01	1.6E-01	5.6E+02	4	5
132	4.7E+03	0.91	1.3E+06	5.9E-02	70	6.3E-01	1.5E-01	5.4E+02	4	5
142	4.7E+03	0.91	1.3E+06	5.7E-02	70	5.7E-01	1.4E-01	5.2E+02	4	5
152	4.6E+03	0.91	1.3E+06	5.5E-02	70	5.3E-01	1.3E-01	5.1E+02	4	5
162	4.5E+03	0.91	1.3E+06	5.4E-02	70	4.8E-01	1.2E-01	4.9E+02	4	5
172	4.5E+03	0.92	1.4E+06	5.2E-02	70	4.5E-01	1.1E-01	4.7E+02	4	5
182	4.4E+03	0.92	1.4E+06	5.0E-02	70	4.1E-01	1.0E-01	4.6E+02	4	5
192	4.4E+03	0.92	1.4E+06	4.9E-02	70	3.8E-01	9.7E-02	4.5E+02	4	5
202	4.3E+03	0.92	1.4E+06	4.8E-02	70	3.6E-01	9.0E-02	4.4E+02	4	5
212	4.3E+03	0.92	1.5E+06	4.6E-02	70	3.3E-01	8.5E-02	4.3E+02	4	5
222	4.2E+03	0.92	1.5E+06	4.5E-02	70	3.1E-01	7.9E-02	4.2E+02	4	5
232	4.2E+03	0.92	1.5E+06	4.4E-02	70	2.9E-01	7.5E-02	4.1E+02	4	5

6.7   DISCUSSION OF DISTILLATION DATA NEEDED FOR THE MACKAY EVAPORATION
        MODEL

6.7.1   Requirements for Compatibility with the Existing NOAA/SAIC Oil
        Weathering Code

        The evaporation calculation used in the oil-weathering model developed
by Mackay (1982) which is utilized by many of the existing oil-weathering mo-
dels, requires as input the slope and intercept of a distillation curve. For
most petroleum products (including crude oil), distillation curves (liquid
boiling point vs volume fraction distilled) are linear over the range of boil-
ing temperatures of the components that will weather under environmental condi-
tions. Thus, if such data are available, the method of least squares can be
used to find the slope and intercept (initial boiling point) of the distilla-
tion curve over this range.

        There are many different distillation methods and conditions, some
standardized and some not. For instance, one could use an ASTM D-86 distilla-
tion or a true boiling point (TBP) distillation. These are only two of a num-
ber of standardized methods for distilling oil. However, neither of these
methods is appropriate since they do not directly simulate environmental oil-
weathering. In both of these methods the vapor leaving the boiling liquid con-
denses and revaporizes (refluxes) before leaving the apparatus. This counter-
current flow of material produces greater separation of components than in a
simple no-reflux distillation. Since no reflux occurs in the evaporation of
oil in the environment, the required distillation should also involve no re-
flux. Further, the input data for the Mackay model should be from a batch dis-
tillation since an environmental spill will generally involve a finite amount
of material. Thus, a simple, batch, no-reflux distillation is required.

        A simple batch distillation is not routinely performed on petroleum,
however. Thus, in order to use the Mackay model, this distillation must be
performed in the lab or the curve must be calculated from physical data. The
second approach will be developed here.

The mathematical description of a simple, batch distillation is as follows. If v is the vapor removal rate of the distillation in moles per time, then a material balance over L moles of the bulk oil is:

$$dL/dt = -v \qquad (18)$$

Then, if m_i is the number of moles of the i-th component in the oil, and y_i is the mole fraction of the i-th component in the vapor, a material balance over the i-th component is:

$$dm_i/dt = -y_i v \qquad (19)$$

However, $dt = -(1/v)dL$ from above, so substitute for dt in Equation (19) to obtain:

$$-v (dm_i/dL) = -y_i v \qquad (20)$$

or

$$dm_i/dL = y_i \text{ for } i=1,2,3,\ldots,n \qquad (21)$$

where n is the number of components.

Equation (21) must be integrated for each component with the following constraints and initial conditions. Since the material is always at its bubble point, the sum of the vapor pressures (p_i) os the components should be 1.0 atmosphere. If Dalton's Law is assumed, then

$$y_i = P_i/P_T \qquad (22)$$

where P_T = total pressure = 1.0 atm. Thus,

$$\sum_i y_i = 1 \qquad (23)$$

Next, assume Raoult's Law:

$$P_i = x_i P_i \qquad (24)$$

where x_i is the mole fraction of the i-th component in the liquid phase and P_i is the pure component vapor pressure of component i. Combining equations (22), (23), and (24) gives

$$\sum_i \frac{x_i P_i}{P_T} = 1 \tag{25}$$

The final constraint is:

$$\sum_i x_i = L \tag{26}$$

where

$$x_i = \frac{m_i}{\sum_i m_i} \tag{27}$$

A number of different numerical integration methods could be used for this problem. The method chosen here is a simple Runga-Kutta integration (Greenspan, 1971). The integration proceeds as follows:

1. Specify m_1, m_2, ...,m_n at start of integration step.

2. Calculate bubble point temperature using interval-halving trial and error. This also yields y_1, y_2, y_3, ...,y_n.

3. Take an integration step and use y_1, y_2, ...,y_n to calculate new m_1, m_2, ...,m_n.

These three steps are repeated until the desired fraction of the oil has been distilled.

The existing NOAA open-ocean oil-weathering model calculates all of the parameters required to perform the integration (distillation) described above. Instead of using each individual compound of the oil (which is impossible), the oil is broken up into "cuts" according to a TBP distillation so that many compounds of similar volatility are considered together as one "pseudo-component". The TBP data for many different petroleum products are readily available. These data are input to the model, which then calculates the number of moles, the specific gravity, the molecular weight, and the vapor pressure versus temperature for each cut. At the end of each integration step above, the following values are calculated:

1. Boiling point of remaining liquid (°K)

2. Total volume fraction distilled = $\sum_i \dfrac{m_i (MW)_i}{(SPGR)_i}$ + initial volume

   where $(SPGR)_i$ = specific gravity of cut i

   $(MW)_i$ = molecular weight of cut i in grams per mole

These values of volume fraction distilled versus boiling point are then input to a least squares linear curve fitting routine to calculate the "best" initial boiling point (intercept) and boiling curve gradient (slope). These values can then be used as direct input to the Mackay evaporation model.

6.7.2   Calculation of the Input Parameters for the Mackay Evaporation Model

The oil-weathering model developed by Mackay (1982) employs an analytical expression in which the vapor pressure of the oil is expressed as a function of the fraction evaporated. Thus, the oil as a whole is assigned one vapor pressure. Other physical data, such as enthalpy of vaporization, molar volume and boiling point curve are either measured for each oil or measured and "averaged" for many oils to give bulk physical properties.

The NOAA evaporation model, however, uses a pseudo-component approach and focuses much more on the calculation of oil physical properties than the Mackay model. This is important since some physical parameters such as heat of vaporization and molecular weight can vary widely over the range of TBP cuts for any one oil. Furthermore, other parameters such as mean molecular weight vary significantly from oil to oil, and this is particularly important for re-fined petroleum products, such as light diesel or gasoline. For this reason, it is more appropriate and accurate to assign values for these physical proper-ties to a range of cuts rather than to assign a single value to the bulk oil.

The ability of the NOAA model to calculate many physical properties for a range of pseudo-components (distillate cuts) enables it to calculate the bulk oil constants and input parameters that are required by the Mackay evapor-ation model. No further input is required for these calculations and the model itself is not affected in any way. The following is a discussion of the Mackay

380

evaporation model and the procedure for calculating the input constants for Mackay's equation using the NOAA model.

The Mackay evaporation calculation (Mackay, 1983) is:

$$\Delta F = \Delta\theta \cdot H \qquad (28)$$

where

F — Volume fraction evaporated

H — Henry's law constant (dimensionless)

θ — Evaporative exposure, a dimensionless parameter defined by:

$$\theta = K A t/V \qquad (29)$$

where

K — Mass transfer coefficient (m/sec)

A — Area of slick (m^2)

t — Time (seconds)

V — Initial slick volume (m^3)

Thus

$$\Delta\theta = KA\Delta t/V \qquad (30)$$

K, A, V, and t are all "bulk" properties. Therefore, the NOAA model will not improve upon the value of θ.

The Henry's law constant is calculated as follows:

$$H = \frac{\text{Concentration in gas phase}}{\text{Concentration in liquid phase}} = \frac{\dfrac{n_g}{V_g}}{\dfrac{n_\ell}{V_\ell}} = \frac{\dfrac{P_g}{RT}}{\dfrac{1}{V_\ell}} = \frac{P_g V_\ell}{RT} \qquad (31)$$

where

381

P_g is the vapor pressure of the evaporated oil (pascals)

V is the molar volume of the oil (m^3/mole)

R is the gas constant (8.314 $Pa \cdot m^3$/mole$\cdot ^\circ K$)

T is the temperature ($^\circ$Kelvin)

P_g can be calculated further using the Clausius-Clapeyron equation and boiling point data. It should be noted, however, that this equation is not strictly applicable to mixtures (Denbigh, 1971). At atmospheric pressure, though, the error introduced by using this equation is probably small in comparison to the overall errors associated with other necessary assumptions of the model. The Clausius-Clapeyron equation is:

$$\ln(P_1/P_2) = \frac{\Delta H}{R} \left[\frac{1}{T_2} - \frac{1}{T_1} \right] \tag{32}$$

where ΔH is the enthalpy of vaporization of the material.

Let $P_2 = 1$ atm, then $T_2 = T_b$, the boiling point of the liquid. The result is:

$$P_1 = \exp \frac{\Delta H}{R} \left[\frac{1}{T_b} - \frac{1}{T_1} \right] \tag{33}$$

and

$$\Delta F = \Delta \theta \frac{V_\ell}{RT} \exp \frac{\Delta H}{R} \left[\frac{1}{T_b} - \frac{1}{T_1} \right] \tag{34}$$

At this point, use an average value for V_ℓ and Trouton's rule ($\Delta H_v = 88\ T_b$) for an average value of ΔH_v to obtain:

$$P_1 = \exp \frac{88T_b}{R} \left[\frac{1}{T_b} - \frac{1}{T_1} \right] \tag{35}$$

and

$$\Delta F = \Delta \theta \exp \left[6.3 - 10.6 \frac{T_b}{T} \right] \tag{36}$$

Further, the Mackay model uses a "boiling point curve" (B.P. vs fraction evaporated) to determine the prevailing boiling point: T_b = initial BP + (F)·(boiling point curve gradient).

The NOAA model is capable of calculating values of V_ℓ and ΔH_V and of calculating the initial boiling point and boiling point curve gradient. The details of these calculations are below:

V_ℓ: The molar volume of the oil is the mean molecular weight of the oil in grams per mole divided by the density in grams per m^3, both of which are calculated by the NOAA model.

$$V_\ell = \text{mean molecular weight/density}$$

ΔH_V: ΔH_V for petroleum fractions has been correlated with API gravity and boiling point (Fallon and Watson, 1944), both of which are input to the NOAA model. This correlation is:

$$\Delta H_V = 232.2 - .2441(TB) - .6937(API)$$
$$- 3.58 \times 10^{-4}(TB)(API) + 1.024 \times 10^{-4}(TBP)^2$$
$$+ (1.037 \times 10^{-4})(API)(API)$$

where

    ΔH_V is in BTU/lb
    TB is the cut boiling point in °F
    API is the API gravity

TBP (Boiling Point Curve):

    For most petroleum products (including crude oil), the boiling point vs fraction distilled curve is linear over the range of compounds that evaporate under normal environmental conditions. The distillation curve required for input to the Mackay model is a simple, batch distillation, and can be calculated using the physical properties calcu-

lated by the NOAA model. The details of that calculation are presented in the previous section. Once the distillation curve (volume fraction vs boiling point) is calculated, it is fit to a straight line by the method of least squares:

$$T_b = \text{initial boiling point} + (\text{gradient})(\text{fraction evaporated})$$

Following calculations of V_ℓ, ΔH_V, and the linear boiling point curve, the Mackay evaporation equation can be constructed as follows:

ΔH_V for each cut is divided by the molecular weight of the cut (to convert to Joules/mole) and by the boiling point of the cut in order to find a "Trouton's rule" constant. The "Trouton's rule" constants (one per cut) are then averaged. This average constant (TR) is then used in place of the classical value of 88 J/°K mole. The evaporation equation then becomes:

$$\Delta F = \Delta\Theta \ \frac{V_\ell}{RT} \ \exp\left[\frac{TR}{R} \left(1 - \frac{T_b}{T}\right)\right] \tag{37}$$

where

T_b — Initial boiling point + (TBP gradient)(F)   (in °K)

T — Environmental temperature (°K)

R — Gas constant (8.314 Pa·m^{3}mole·°K)

V_ℓ — Molar volume of the oil (m^3/mole)

TR — Average Trouton's rule constant (Joules/°K·mole)

These calculations are performed by the ocean-ice oil-weathering code as an add-on calculation. The output from these calculations are the input parameters for the Mackay Evaporation Model. These values are calculated using existing literature data and do not require experimental work for most oils.

384

6.8   COMPONENT-SPECIFIC DIFFUSION THROUGH AN OIL "SLAB" AND DISSOLUTION IN-
TO THE WATER COLUMN IN THE ABSENCE OF EVAPORATION

When oil is released under sea ice the primary weathering process is thought to be the dissolution of soluable hydrocarbons into the water column. The oil is not exposed to the atmosphere and the water currents are relatively weak (see Section 3.5). Thus evaporation, dispersion, mousse formation, and spreading do not occur to any large extent. It becomes important then to predict the rate at which individual components will transfer from the oil phase to the water phase. The mathematics to describe such mass-transfer will depend heavily on whether the oil phase can be considered "well mixed" or whether it behaves like a "slab". The following presents derivations for both of these situations. The solutions of the equations below, along with the experimental data presented in Sections 4.2 and 4.4, can be used to determine which state the oil is likely to be in in the environment and to determine which resistances to mass-transfer are dominant for dissolution.

The dissolution of specific components from an oil slick into the water column is described mathematically in much the same way as evaporation. The pertinent physical property required to describe dissolution is the liquid-liquid partition coefficient which is the analogy of Henry's Law for e-vaporation.

Unfortunately there is no characterization process for dissolution that can be applied to the bulk oil in the same manner that distillation is used to characterize the oil with respect to evaporation. There have been two attempts to classify the oil into pseudo-components with respect to solubility, one by Yang and Wang (1977) which was not carried through to the quantitative stage, and another by Mackay (1980) where only two major "cuts" were recognized. Since dissolution apparently accounts for a relatively small mass loss from the slick, an independent component-specific approach to dissolution is presented here.

The physical property data required are liquid-liquid partition co-efficients, referred to in the content of this work as M-values. It must be

emphasized that pure component solubility data alone are not useful in obtaining M-values, because these types of data only yield information about the chemical potential of the species in the aqueous phase. What is required along with pure component solubility data is the chemical potential of the species in the oil phase. Henry's Law data coupled with solubility and vapor pressure data will provide M-values through calculation, while liquid-liquid equilibrium experiments measure the M-values directly.

6.8.1 "Slab" Case

For the case of a species dissolving from an oil "slab" into the water column, consider a water column which is well-stirred (i.e., of uniform concentration) and in contact with a stagnant oil slick of thickness ℓ. The diffusion of a compound in the oil is described by:

$$\frac{\partial C_o}{\partial t} = D_o \frac{\partial^2 C_o}{\partial X^2} \qquad 0 < x < \ell, \ t > 0 \qquad (38)$$

where C_o is the oil concentration of the species of interest, t is the time, X is the distance from the oil/water interface, and D_o is the diffusivity of the species in the oil. The water column concentration is zero at t - 0 so that

$$C_w(X) = 0 \qquad at \ t=0 \qquad (39)$$

where C_w is the water column concentration.

For this derivation mass transfer does not occur across the x- ℓ boundary, so

$$\frac{dC_o}{dX} = 0 \qquad at \ x = \ell, \ t > 0 \qquad (40)$$

At the oil-water interface the mass fluxes from the oil and into the water must be equal, which yields

$$A\delta \frac{dC_w}{dt} = AD_o \frac{dC_o}{dX} \qquad at \ x = 0, \ t > 0 \qquad (41)$$

where A is the interfacial area, and δ is the water-phase thickness. Thus $A\delta$ is the volume of water. This equation is rewritten as

$$\frac{dC_w}{dt} = \frac{D_o}{\delta} \frac{dC_o}{dX} \qquad \text{at } x = 0, \, t > 0 \qquad (42)$$

The component flux from the oil is written as

$$AD_o \frac{dC_o}{dx} = AK_o(C_o - C_o^{*}) \qquad \text{at } x = 0, \, t > 0 \qquad (43)$$

where C_o^{*} is a hypothetical oil-phase concentration that is in equilibrium with the water-phase concentration, and K_o is an over-all mass-transfer coefficient based on oil-phase concentrations. The above equation is analogous to a heat transfer equation for the flux of energy across a film resistance. However, mass transfer requires that some form of a potential be used to write the driving force rather than observable concentrations. It is not correct to write the driving force for mass transfer as the concentration difference between the two phases. The reason for this is apparent when a simple system such as pure benzene and water is considered. At equilibrium the concentration of benzene in the water is on the order of 1700 ppm. Thus, the benzene concentration difference between the two phases is not zero, yet mass transfer, does not occur. Therefore, in order to write a driving force for mass transfer the concentration in one of the phases must be related to the other phase on a thermodynamic basis. Once this relationship is defined, the mass transfer problem looks like a heat transfer problem where the temperature is the potential for heat transfer. Thus, in the preceding expression C_o^{*} is an oil-phase concentration (hypothetical) in equilibrium with the bulk water-phase concentration C_w. As a result of this problem definition an oil-water partition coefficient is required. The oil-water partition coefficient is defined as follows:

$$m = \frac{C_o}{C_w} \qquad \text{at equilibrium} \qquad (44)$$

At this point do not relate C_o and C_w above to those same symbols appearing in the previous equations. Because of the way the previous equations

are written, it is convenient to keep C_o in them as it appears now. This means C_w must change. The recipe for doing this is embodied in the mass transfer resistance equation $(C_o - C_o^*)$ term. Here C_o^* is that hypothetical concentration in water in equilibrium with the concentration in the oil. Therefore the oil-phase concentration must change according to

$$C_w = \frac{C_o^*}{m} \tag{45}$$

And C_w must be replaced with $\frac{C_o^*}{m}$ in equation (42) above to yield

$$\frac{dC_o^*}{dt} = \frac{D_o}{m\delta} \frac{dC_o}{dx} \quad \text{at } x = 0, \, t > 0 \tag{46}$$

Concelling the area in the component flux equation yields

$$\frac{dC_o}{dx} + \frac{K_o}{D_o}(C_o - C_o^*) = 0 \tag{47}$$

Finally, the initial concentration in the oil is C_o^o.

The set of differential equations and boundary conditions above can be solved analytically using the technique of Laplace transforms which is described in Carslaw and Jaeger (1967). The analytical solution for the water-phase concentration is

$$\frac{C_w}{C_o^o} = \frac{\ell}{m\ell + \delta} - \frac{2\ell H^2}{\delta} \sum_{j=1}^{\infty} \frac{\exp(-\alpha_j^2 T)}{P_n} \tag{48}$$

and for the oil-phase concentration

$$\frac{C_o}{C_o^o} = \frac{m\ell}{m\ell + \delta} + 2H^2 \sum_{j=1}^{\infty} \frac{\alpha_j \cos\left[\alpha_j(1 - \frac{x}{\ell})\right]\exp(-\alpha_j^2 \tau)}{\sin \alpha_j \, P_{\alpha_j}} \tag{49}$$

where α_j is the j-th positive root of

$$\text{Tan } \alpha_j = \frac{H\alpha_j}{\alpha_j^2 - K' H} \tag{50}$$

$$H = \ell h$$

$$h = \frac{K_0}{D_0}$$

$$K' = \frac{m\ell}{\delta}$$

$$T = \frac{D_0 t}{\ell^2}$$

$$\tau \equiv time$$

and

$$P(\alpha_j) = \alpha_j^4 + \alpha_j^2 (H^2 + H - 2K' H) + K' H^2 (1 + k') \tag{51}$$

These equations provide useful information in that the effect of the parameters of the problem can readily be determined. For example, note that the parameter K' is a ratio of the capacitance of each phase for the component of interest, and that the partition coefficient M multiplies the water phase thickness δ to yield an equivalent water-phase thickness.

6.8.2   Well-Mixed Oil Phase Case

For the case of a "well-stirred" oil-phase in contact with a "well-stirred" water-phase, the concentration of the compound of interest is not a function of distance in either phase (i.e., both phases are uniform).

The flux equation for this case is

$$A\ell \frac{dC_0}{dt} = -AK_0 (C_0 - C_0^*) \tag{52}$$

From the "slab" case

$$C_0^* = mC_w \tag{53}$$

Thus, cancelling the area from both sides, substituting for C_0^*, and rearranging gives

$$\frac{dC_0}{dt} = -\frac{K_0}{\ell}(C_0 - mC_w) \tag{54}$$

However, a mass balance for the system gives

$$C_w A\delta + C_0 A\ell = C_0^0 A\ell \tag{55}$$

so

$$C_w = \frac{\ell}{\delta}(C_0^0 - C_0) \tag{56}$$

substituting into the flux equation gives

$$\frac{dC_0}{dt} = -\frac{K_0}{\ell} \quad C_0 - \frac{m\ell}{\delta}(C_0^0 - C_0) \tag{57}$$

or

$$\frac{dC_0}{dt} = -\frac{K_0 C_0}{\ell} + \frac{K_0 m}{\delta}C_0^0 - \frac{K_0 m}{\delta}C_0 \tag{58}$$

$$\frac{dC_0}{dt} = -K_0 \quad C_0 \frac{m\ell + \delta}{\ell\delta} - C_0^0 \frac{m}{\delta} \tag{59}$$

This differential equation, along with boundary conditions specified in the previous section are solved to give

$$\frac{C_0}{C_0^0} = C_2 + (1 - C_2)\exp(-C_1 K_0 t) \tag{60}$$

and

$$\frac{C_w}{C_0^0} = C_3 \quad 1 - \exp(-C_1 K_0 t) \tag{61}$$

where

$$C_1 = \frac{m\ell + \delta}{\ell\delta}$$

$$C_2 = \frac{m\ell}{m\ell + \delta}$$

$$C_3 = \frac{\ell}{m\ell + \delta}$$

In order to make the analytical solutions for component-specific dissolution usable they have been programmed in FORTRAN to allow easy investigations of the results. The details of this particular code, input-output information, and a code listing are presented in Appendix A of this report: Code Description for Component-Specific Dissolution from slicks.

6.8.3   Stirred Chamber Experiments Conducted to Measure Component-Specific Dissolution - La Jolla, California

Mass transfer and diffusivity coefficients were determined for seven aromatic compounds with regard solely to their dissolution from Prudhoe Bay crude oil into seawater. Using a specially constructed chamber, designed to eliminate whole oil droplet dispersion and compound evaporation, the rates and amounts of compound dissolution were determined experimentally. To obtain mass transfer and diffusivity coefficients, theoretically predicted values were adjusted until they matched the experimental values. These data will ultimately be required for predicting the component specific dissolution of aromatics into seawater as a result of a below-ice oil-release incident. While such information may not be required for mass balance considerations, it is important for assessing potential biological impacts.

An air tight, cylindrical chamber was constructed, primarily of glass, with the dimensions shown in Figure 6-2. The chamber was equipped with a water sampling port 5.1 cm from the bottom, a water replacement port 15 cm from the top, an oil sampling port located on the glass cover plate, and an oil addition port with a glass tube positioned to deliver the oil within a few millimeters of the cover plate. The glass cover plate was seated on a viton lip and clamped in place to form an airtight seal. The entire chamber was housed on a steel

CONSTANT HEAD REPLACEMENT WATER

OIL ADDITION SETUP

OIL SAMPLING PORT

AIR TIGHT GLASS COVER PLATE

29.4 cm

15 cm

42 cm

WATER SAMPLING PORT

5.1 cm
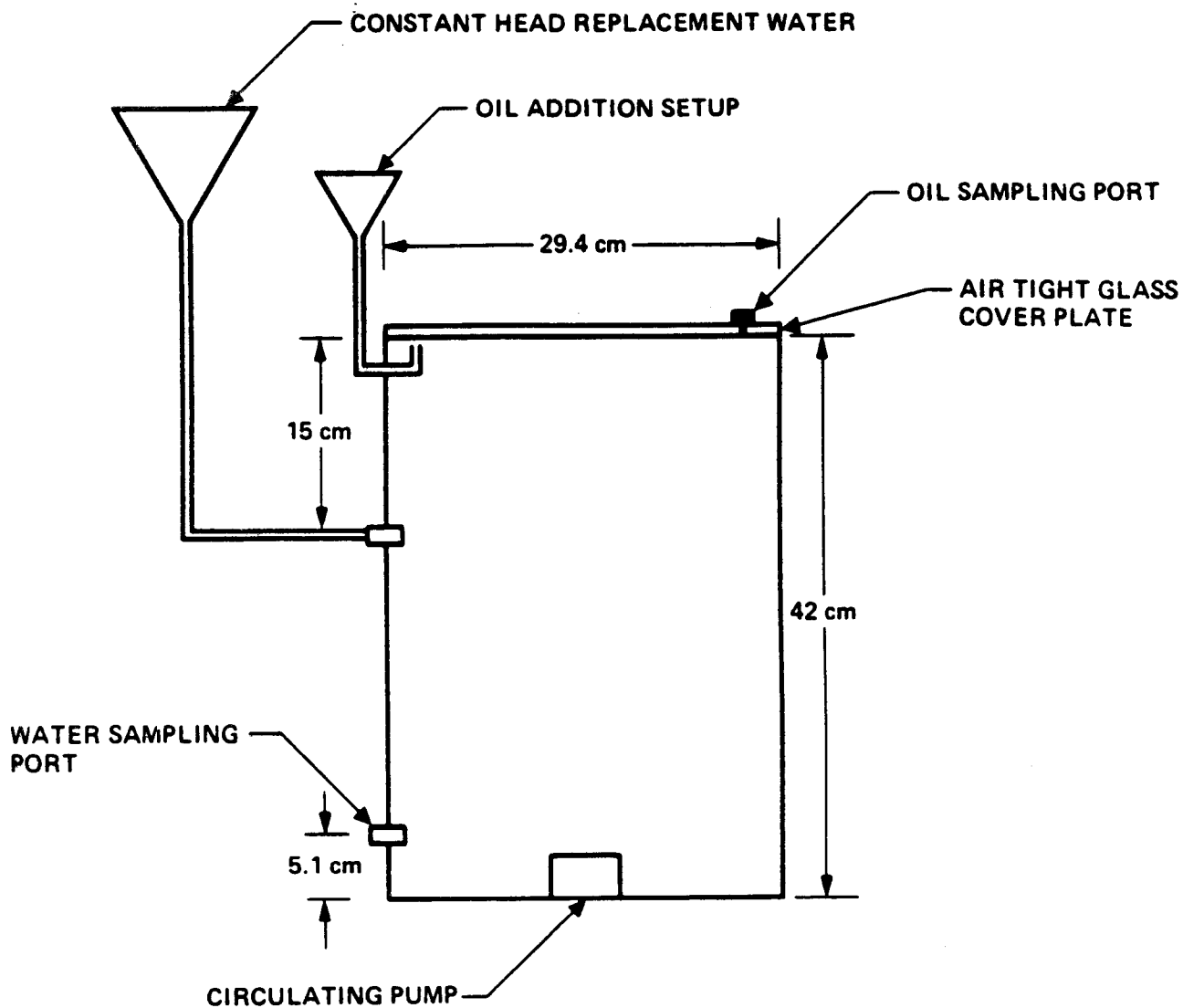
CIRCULATING PUMP

Figure 6-2.--Stirred Chamber for Mass Transfer and Diffusivity Determinations.

plate containing four leveling screws. Water column mixing was accomplished by placing a submergible circulating pump (Little Giant Model 1) in the chamber; water column mixing was further enhanced by a series of one inch stainless steel baffles, which were positioned vertically around the circumference inside the chamber, but not into the oil.

The experiment was initiated by the addition of 1000 ml (a 1.47 cm thick slab) of Prudhoe Bay crude oil over a period of ten minutes. This was

accomplished by gravity feeding the oil into a funnel - attached to a glass entry tube, which extended upwards to within a few millimeters of the glass cover plate. A tube extending from the water sampling port was positioned such that concurrent with the addition of the oil, a similar volume of water was forced out of the tank. In this manner, the oil was layered uniformly and smoothly on top of the seawater, with minimal oil dispersion and no air introduced into the chamber. As soon as the entire 1000 ml of oil had been added, the funnel and tube were disconnected and the port was stoppered.

Water samples (200 ml) were obtained according to the following schedule: prespill, 10 minutes, four hours, eight hours, 12 hours, 24 hours, two days, three days, four days, five days, seven days, nine days, 11 days, 13 days, 15 days, and 17 days after the spill. As the 200 ml sample was drawn off, fresh replacement seawater was simultaneously added via the constant head arrangement. A stopcock, positioned between the funnel and then entry tube, was closed (except during sampling) to prevent any backflushing. In order to minimize evaporation of the more volatile dissolved compounds, all water samples were extracted and analyzed immediately after collection.

Triplicate oil samples were collected, though a Teflon sampling port located on the cover plate, at the initiation and termination of the experiment.

All water samples were filtered (to remove any discreet oil droplets) then extracted three times with 50 mls of CH_2Cl_2. The effect of the filtration step on the concentration of dissolved compounds in the water was investigated by splitting one sample into two equal portions - one aliquot was filtered while the other remained unfiltered - and no differences were noted in final concentrations. Solvent reduction was accomplished by using standard Kaderna-Danish evaporation techniques as described elsewhere (Payne et al., 1984a). Before instrumental analysis (capillary column FID-GC) all samples were spiked with d_{10}-phenanthrene as an internal standard.

Triplicate oil samples were first weighed (~ 50 mg) and then taken up in approximately one ml of hexane. The oil was fractionated into its aliphatic and aromatic constituents by SiO_2 liquid chromatography and analyzed by capillary FID gas chromatography.

Compound identification was accomplished by analyzing one representative water sample extract with a Finnegan 4000 quadrupole GC/MS. Quantification of the selected compounds was achieved by generating a response factor on the FID-GC for each of the seven compounds, from an aromatic standard containing those compounds.

M-values were calculated by dividing each compounds oil phase concentration by its water phase concentration at equilibrium. M-values of the components of interest are presented in Table 6-7. Using curve-fitting techniques, values for mass transfer coefficients were found to range from 2.5×10^{-4} cm/sec to 4.0×10^{-4} cm/sec and diffusivities were found to be no less than 1.0×10^{-6} cm/sec. Ultimately these values will be used for estimating dissolved phase aromatic concentrations in oil weathering simulations as described in Section 6.9.2.4.

Table 6-7.--M-Values Determined from the Stirred Chamber Experiment.

Compound Name	M-Value[a]
ethylbenzene	3300
m & p-xylene	3600
o-xylene	5900
1,3,5-trimethylbenzene	19000
naphthalene	7800
2-methylnaphthalene	46400
1-methylnaphthalene	35800

a - the M-value is defined as the compound concentration in oil divided by the compound concentration in water at equilibrium.

6.9   DISSOLUTION OF HYDROCARBONS AND TRANSPORT TO BOTTOM WATERS

This section investigates the effect of freezing ocean conditions on the potential transport of dissolved oil to sensitive areas of the marine environment (see also Section 5).   As a very simplistic summary, when the surface water freezes, ice is formed that is lower in salinity than the water from which it is formed. The "excess" salt water is denser than the surrounding water and will sink creating a downward vertical current. This has been considered a potential mechanism for the transport of pollutants to bottom waters in the Arctic environment.

With regard to an oil spill in freezing Arctic conditions, it is believed that the spill of oil into an open lead would present the "worst case scenario" for haline transport of dissolved oil since the freezing (ice formation) rates for an open lead have been shown by numerous investigators to be considerably higher than freezing rates in open water (Foster 1972, Schaus and Galt 1973).   A high freezing rate would induce rapid transport of surface material to bottom waters. An analysis of potential pollutant transportation rates based on measurements taken in Arctic leads in included in Section 6.9.3.

To assess an "upper bound" effect of an oil slick on dissolved species transport, calculations have been made to estimate the amount of material that will dissolve out of the slick into the surrounding water. The material that does dissolve is generally considered as having an oil/water partition coefficient that is less than about 150,000. This implies that when an equal amount of water and oil is contacted, the water phase concentration of the compound of interest will be $^1/150,000$ of that in the oil. When dilution is further taken into account as specified in an environment situation, the water-phase concentration is always considerably less. Calculations in Section 6.9.2 indicate that very little oil is dissolved directly from the slick as it effects the slick mass balance; however, using the flow estimates in Section 6.9.3, the amount of dissolved material reaching the bottom waters could be in the range of 0.2 to 3 ppm. These numbers are strictly upper bound estimates and were calculated by specifying environmental parameters from a list of

observed parameters in such a manner that the calculated concentration would be a maximum. No effort was made to also determine an average because of the paucity of published data. This also implies that the maximum values reported here could be higher due to the fact that the extremes in nature have not necessarily been observed.

The primary source of transport of oil species to the bottom waters would be through the dispersion of fine drops into the water column. The transport of small dispersed oil droplets would occur due to the downward current exceeding the droplet's Stokes rising velocity. A five micron diameter oil droplet will rise at 1.5 cm/hour (0.0004 cm/sec) while a salt-rejection plume velocity can be much greater than this. However, it must be noted that dispersed oil has always been studied with the objective of a material balance of the oil slick, not with the objective of the droplet size leaving the slick. Nevertheless, at the present, dissolution from either the slick or oil droplets is all that can be postulated to provide an estimate of "oil" transported to the bottom. As discussed in Section 6.9.2, the small droplet size (1-50 μm) allows for greater dissolution of oil species than that obtained from the slick directly.

6.9.1   A Discussion of the "Solubility" of Petroleum

One of the fundamental mass transfer processes that occurs when crude or refined petroleum is spilled on water is dissolution. This process, which results in oil components being dissolved (on a molecular scale) into the water phase, has also been called solubilization, incorporation, and accommodation.

When an overall mass balance is derived for oil spilled on water, the total mass dissolved (resulting from the dissolution of many different components) into the water is small compared to the original oil mass. It is important to be able to quantify this mass balance, however, since biological impact will, in part, be determined by this result. There is some confusion and misunderstanding in the literature about what is important and/or required to quantify dissolution and some misuse of terminology.

The following discussion is designed to point out the important aspects of the mass transfer of petroleum components into water, particularly the resulting concentration (at equilibrium) of those components in the two phases (water and oil). The main point to be made is that crude oil (or refined petroleum) is a very complex, continuum of components that behaves differently than single components alone.

In order to illustrate the proper use of the term "solubility" and then illustrate how it does not apply to oil, consider the definition. The solubility of a compound in water is the concentration obtained at equilibrium when a finite amount of the pure compound is (still) present. In applying this definition to benzene or sugar, the compound is added to (and dissolved in) water until no more will go into solution. When no more goes into solution, the pure compound phase is visible. The reason this definition of solubility does not apply to oil is that oil is not a pure compound. Some of the compounds in oil are soluble and at the other extreme some are essentially (for practical purposes) insoluble. Thus, for compounds present in oil that are soluble, a liquid-liquid equilibrium exists for the component because it distributes between both phases and a ratio of the concentrations in each phase <u>at</u> <u>equilibrium</u> is the important parameter to measure. It is this ratio that is <u>usually</u> constant over concentration ranges near zero, and it is this ratio that is required to determine how much "oil" will distribute (not dissolve) into water. This distribution concept is illustrated below.

First consider the following system: 1 ml of benzene is layered on top of 10 ml of water in a closed system so that evaporation is prevented. The system is allowed to come to equilibrium. At equilibrium, the concentration of benzene in the water phase is found to be 1700 parts per million (ppm). This concentration is what is normally called the <u>solubility</u> of benzene in water. The important concept is that the relative volumes of the two phases (benzene and water) do not affect the concentration of benzene in the water. In other words, if 1 ml of benzene was equilibrated with 1000 ml of water, the resulting concentration of benzene in the water would again be 1700 ppm. However, the above cannot be said of petroleum, or for any other mixture of compounds. To illustrate this, consider a second system: 1 ml of crude oil (which contains

benzene) is equilibrated with 10 ml of water in a closed system. The numbers will vary from oil to oil, but for a typical set of conditions, the concentration of benzene in the oil and water phases at equilibrium will be 1000 mg/l and 1 mg/l, respectively. Next, consider another system in which 1 ml of crude oil is equilibrated (closed system) with 1000 ml of water. In this case, the oil and water phase concentrations of benzene are 505 mg/l and 0.505 mg/l, respectively. The crucial point is that, unlike with pure benzene, the concentration of benzene in the water phase is not independent of the relative volumes of the two phases. The quantity that is independent of these volumes is the ratio of the concentrations of benzene in the two phases. This ratio is called the partition coefficient and is defined for each component of the system as:

$$\text{partition coefficient} = \frac{\text{concentration in oil}}{\text{concentration in water}} = \frac{1000}{1} = \frac{505}{.505} = 1000$$

Each component in each oil will have a different partition coefficient. For this reason, it is difficult to define the "solubility" of a mixture (such as crude oil) since the concentration of the components of the mixture in the water will depend on the volumes of the two phases and their initial concentration in the mixture.

Most authors have ignored this fact and have measured what they call solubility with a particular volume ratio of water and oil and in some cases the solubility varies three or four orders of magnitude. For example, Boehm and Quinn, 1974, measured "oil solubility" by equilibrating 4 mg of oil with 1.0 liter of water (volume ratio = 200,000) while Mackay and Shiu, 1976, used 10 ml of oil and 100 ml of water (volume ratio = 10). These authors tested different oils so their results cannot be compared. However, the point is that both authors report their results as the "solubility of crude oils" without any indication of the experimental conditions (i.e., volume ratios). Using the results of a derivation presented later in this report, it can be shown that a four order of magnitude difference in volume ratio can produce a one-to-two order of magnitude difference in measured concentration for the more soluble petroleum compounds.

In addition to the difficulty in defining a solubility for mixtures, it must be realized that an equilibrium experiment does not reproduce the dynamics of dissolution in the environment. Since the ocean is turbulent, "clean" water is usually (except possibly in a bay or lagoon) flowing past the oil. Thus, the partitioning behavior described above can deplete the oil of the components that have small partition coefficients and thus distribute these components to the water phase in appreciable quantities (see definition of partition coefficient above). To illustrate this, consider the system described above in which 1 ml of oil is equilibrated with 1000 ml of water. The resulting benzene concentrations are 505 mg/l in the oil and 0.505 mg/l in the water. Now imagine removing the water phase and bringing 1000 ml of fresh water into contact with the remaining oil. After equilibration, the oil and water phase concentrations of benzene are 253 mg/l and 0.253 mg/l, respectively. Thus, the benzene concentration in the oil has been reduced from 1000 mg/l (originally) to 253 mg/l. With further equilibrations, the benzene would eventually be removed completely from the oil phase.

It becomes apparent, then, that the desired data, at least from a biological impact point of view, are the total mass fraction of components that will dissolve in a chosen period of time under the dynamic conditions described above in which "clean" water is flowing past the oil. A published value for this is about three percent (Murray, et al., 1984). However, this number is expected to vary from oil to oil and especially for refined products such as gasoline, which is known to contain large amounts of individually-soluble aromatic components. The following sections discuss a number of mathematical models and experimental methods that have been used to obtain or predict the necessary data to quantify dissolution.

6.9.2   Experimental Method for Measurement of Total Soluble Fraction of Petroleum

When water is brought into contact with petroleum in a closed system and allowed to equilibrate, mass transfer from the oil phase to the aqueous phase takes place. A chemical analysis of the resulting aqueous phase reveals that many compounds are present. Repeated equilibrations of the oil phase with clean water will eventually remove all of these individual components from the

oil.   The   following discussion presents the theory and experimental protocol for   measuring   the   "total   soluble fraction" of a crude or refined petroleum. Results from such experiments follow these discussions.

6.9.2.1   Theory

Consider the Equilibration of a Volume of Oil with a Volume of Water

V_w—volume of water

V_o—volume of oil

X—original mass of the component of interest

M_o—mass of component of interest in oil after equilibration

M_w—mass of component of interest in water after equilibration

Now define the volume ratio and partition coefficient:

$$r = \text{volume ratio} = V_w/V_o$$

$$m = \left[\frac{\text{concentration of component in oil}}{\text{concentration of component in water}} \right]_{\text{at equilibrium}} = \frac{M_o}{V_o} \frac{V_w}{M_w}$$

As mass is conserved, write:

$$X = M_o + M_w \tag{62}$$

Now   substitute in the above definitions and solve for the concentration of the component in the water (M_w/V_w), which is directly observable.

$$M_w = -X - M_o \tag{63}$$

$$= X - \frac{mV_o\, M_w}{V_w} \tag{64}$$

$$= X - \frac{mM_w}{r} \tag{65}$$

$$rM_w = rX - mM_w \tag{66}$$

$$M_w = \frac{rX}{(r+m)} \tag{67}$$

$$\frac{M_w}{V_w} = \frac{rX}{V_w(r+m)} = \frac{X}{V_o(r+m)} \tag{68}$$

or inverting, write

$$\frac{V_w}{M_w} = \frac{V_o(r+m)}{X} \tag{69}$$

Thus, since r and V_o are known and (V_w/M_w) is the reciprocal of the concentration of the component of interest in the water phase (which can be measured), a series of equilibrations of fresh oil with water at varying volume ratios (r) will yield a plot $(V_w/M_w$ vs r) with slope V_o/X and intercept $(V_o m)/X$. An examination of the equation above indicates that a significant difference in the measured concentration (M_w/V_w) will only be "seen" when r is on the order of m or bigger. Since typical oil-water partition coefficients for aromatic hydrocarbons are in the range of 10^3-10^5, the series of equilibrations must include volume ratios in this range and larger if possible.

6.9.2.2 Experimental

In order to verify the above theory and measure the "total soluble fraction" of fresh Prudhoe Bay crude oil, the following experimental protocol was followed. A Hamilton S-1500 1.5 liter super-syringe, fitted with a luer-lock adaptor, was filled with approximately 1300 ml of seawater. All air bubbles were expelled from the syringe and then a known volume of fresh Prudhoe Bay crude oil was introduced to the syringe chamber through the luer-lock fitting using a smaller syringe of appropriate volume. The large syringe was tipped such that the displaced seawater could flow out of the luer-lock fitting as the oil was added. A luer-lock valve was then attached to the large syringe

to close the system from the room air. The syringe was then agitated (by hand) continuously for 20 minutes and then allowed to sit for an additional 40 minutes with occasional agitation.

Next, the luer-lock valve was replaced by a 0.45 micron filter and luer-lock needle. The syringe was then inverted and configured as in Figure 6-3. A 1.0 liter round bottom flask containing 100 ml of fresh hexane was placed under the syringe so that the syringe needle was immersed in the hexane. This was done so that the seawater, after filtration, would not be exposed to the room air, thus preventing evaporation of volatile compounds.

The back-pressure created by the 0.45 micron filter was too large for one person to filter the sea water so the platform arrangement in Figure 6-3 was constructed. Extra supporting rods (plungers) were added to the syringe and attached to a wooden platform. Lead bricks (~60 lbs) were then placed on the platform to supply the necessary force to filter the aqueous phase. Approximately 1.0 liter of seawater was filtered; the remaining water and oil discarded. The seawater/hexane mixture was then put into a separatory funnel and shaken. After settling, the hexane phase was removed, and the aqueous phase was extracted twice with 100 ml of methylene chloride. The hexane and methylene chloride fractions were then combined and concentrated to approximately 1 ml and analyzed by GC-FID. An analytical standard mixture of typical aromatic hydrocarbons was utilized to calibrate the chromatograph.

The above procedure was repeated for varying volume ratios, e.g., $r = 10, 10^2, 10^3, 10^4, 10^5$. Concentration versus r data were then prepared for each peak in the resulting chromatograms and m (partition coefficient) and X (original mass) were calculated. The following section presents these results.

6.9.2.3 Results

Fresh Prudhoe Bay crude oil was utilized to perform the experiment described above. Table 6-8 is a summary of the oil and seawater volumes utilized
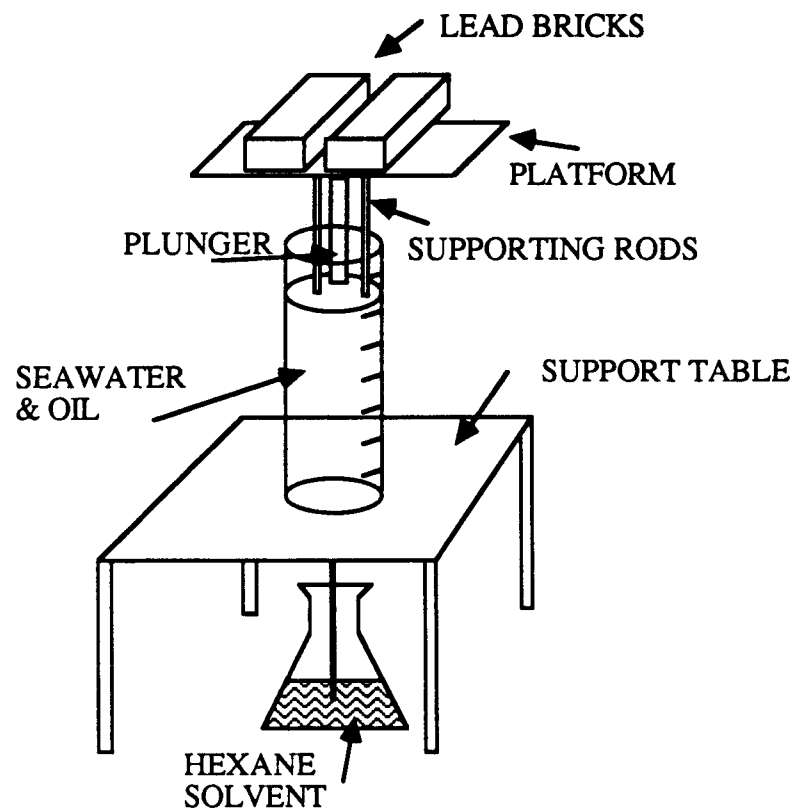
Figure 6-3.--Experimental System Used to Measure Total Soluble Fraction
of Prudhoe Bay Crude Oil.

Table 6-8.--Volumes and Volume Ratios for Experiment to Measure Total Soluble Fraction of Prudhoe Bay Crude Oil.

Equilibration Sample No.	Oil Volume (V_O)	Sea Water Volume (V_W)	Volume Ratio $(r = V_W / V_O)$
1	$1 \mu l$	$1.28 l$	1.28×10^6
2	$10 \mu l$	$1.32 l$	1.32×10^5
3	$100 \mu l$	$1.29 l$	1.29×10^4
4	$1 m l$	$1.30 l$	1.30×10^3
5	$10 m l$	$1.31 l$	1.31×10^2

Table 6-9.--Results of Partitioning Experiments, Compound of Interest: 2-Methyl Naphthalene.

Equilibrium Sample No.	Concentration of 2-Methyl-Naphthalene	Volume Ratio (r)
1	$0.39 \mu g/l$	1.28×10^6
2	$3.53 \mu g/l$	1.32×10^5
3	$7.6 \mu g/l$	1.29×10^4
4	$10.9 \mu g/l$	1.30×10^3
5	$25.4 \mu g/l$	1.31×10^2

in five separate equilibrations. As shown, the volume ratio for these samples varied from 1.31×10^{2} to 1.28×10^{6}.

Table 6-9 presents the results of the experiment for one compound, 2-methyl naphthalene. When the data in Table 6-9 (1/concentration vs r) are linearized, the following are the results:

$$1/C_w = (1.95 \times 10^{-6})r + 6.61 \times 10^{-2}$$

correlation coefficient = 0.9995

Thus, from the theory presented above,

$$\text{slope} = V_o/X = 1.95 \times 10^{-6}$$

$$\text{intercept} = (mV_o)/X = 6.61 \times 10^{-2}$$

When these equations are solved for the X/V_o (original oil concentration) and m (partition coefficient), we find:

$$X/V_o = 0.51 \text{ g/l}$$

$$m = 33,900$$

These values of X/V_o and m are in the range of literature values. This analysis can be performed on the other peaks in the GC trace with similar results.

In order to apply the above theory to determine the total soluble fraction in (Prudhoe Bay) crude oil the chromatographic data from each component (that distributes appreciably) is linearized so that values for X/V_o and m are found. Table 6-10 presents these data for all the observed components. As shown in the table, the total concentration of distributing components is

Table 6-10.—Partition Coefficients and Total Oil-Phase Concentrations for Observed Oil Components.

Retention Time	Partition Coefficient (m)	Oil-Phase Concentration (x/V_o) (g/l)
3.14	3700	1.36
5.11	3700	0.31
5.37	4000	0.84
6.11	6400	0.57
7.24	5900	0.037
8.37	8800	0.064
8.69	10000	0.23
9.38	17000	0.15
9.93	41000	0.69
11.10	31000	0.33
13.75	59000	0.15
17.97	21000	0.38
22.58	34000	0.51
23.25	52000	0.37
27.51	148000	0.22

Total = 6.21 g/l

Table 6-11.—Groupings of Individual Oil Components into "Pseudocomponents."

Retention Time	m	Oil-Phase Concentration		
3.14	3700	1.36	"Cut" 1	m = 3800
5.11	3700	0.31		C = 2.51g/l
5.37	4000	0.84		
6.11	6400	0.57		
7.24	5900	0.037		
8.37	8800	0.064	"Cut" 2	m = 12000
8.69	10000	0.23		C = 1.43 g/l
9.38	17000	0.15		
17.97	21000	0.38		
9.93	41000	0.69		
11.10	31000	0.33		
13.75	59000	0.15	"Cut" 3	m = 51000
22.58	34000	0.51		C = 2.31 g/l
23.25	52000	0.37		
27.51	148000	0.22	"Cut" 4 (remaining oil)	m = ∞ C = 873.8 g/l

6.21 g/l. This value does not, however, include benzene, which is the only low molecular weight aromatic that cannot be measured with the capillary column used for the analysis. Quantitation of benzene could be achieved with another column. Since the purpose of the experiment was to develop a technique for measuring total soluble fraction (and not exact quantitative results), this second column analysis was not performed. Using the density of Prudhoe bay crude oil (880 g/l) the total weight fraction of these soluble components is (6.21/880)(100) = 0.71% (excluding benzene) which is in line with estimates from the literature.

6.9.2.4 Use of Experimental Data for Predictions of Water Column Concentrations

The experimental data presented above (concentration and partition co-efficient) are important because they indicate how much of the distributing components are present in the oil and how large the driving force for dissolution is. They do not, however, represent the complete set of data required to assess water column concentrations in dynamic systems, such as in the open ocean or under ice. The remaining data needed are mass transfer coefficients (K_i), which indicate, in a loose sense, how fast components can travel across the oil/water boundary, and diffusivities (D_i), which indicate the speed at which components diffuse through the oil phase.

Once these data are known, mathematical models can be written to pre-dict the flux of distributing components into the water column as a function of time. Then, if the flowrate of water past the slick is known, the final water column concentration can be calculated. For example, in the case of oil in an open ice lead, this flowrate can be approximated as discussed in the following sections by the rate at which brine is formed and flows down into the water column.

SAIC and others have measured mass transfer coefficients and dif-fusivities of oil components. One such experiment is described in Section

407

6.8.3 of this report. In this experiment, oil was spilled on a tank of seawater and covered so that evaporation was prevented. Time series water column concentrations were then measured and the data fit to a model to "back out" mass transfer coefficients and diffusivities. Mass transfer coefficients ranged from 0.9 to 2.25 cm/hr, and diffusivities were found to be no less than 1.0×10^{-6} cm^2/sec. Cohen (Cohen, et al., 1980) reports mass transfer coefficients of about 1.0 cm/hr. Liquid phase diffusivities are typically in the range of 10^{-5} to 10^{-6} cm^2/sec. Thus the experimental data agree well with the literature.

The set of required kinetic and thermodynamic data is thus complete. The discussions that follow present the simple models that predict the flux of components from oil as a function of time, and then actual predictions utilizing the experimental data for Prudhoe Bay crude oil.

6.9.2.5 Dissolution from a Well-Stirred Oil Slick into a "Clean" Water Column

Consider a slick of oil with volume V and area A in contact with a "clean" (semi-infinite) water column. A differential mass balance on a distributing component of the oil is:

$$V \frac{dC_o}{dt} = A K_w (C_w^* - C_w) \tag{70}$$

where

C_o = oil-phase concentration

K_w = wate r-phase mass transfer coefficient

C_w = water-phase concentration

and C_w* is the hypothetical water-phase concentration that would be in equilibrium with the oil-phase concentration. Or,

$$m = C_o/C*_w \tag{71}$$

where m is the partition coefficient. We now assume that the water phase concentration is zero ($C_w=0$) since in general "clean" water will be flowing past the slick. Substitution of (71) into (70) gives

$$\frac{dC_o}{dt} = \frac{A}{V} \frac{K_w}{m} C_o \tag{72}$$

The appropriate boundary condition is:

$$C_o = C_o o \qquad at \qquad t = 0 \tag{73}$$

The solution to (72) and (73) is:

$$\frac{C_o}{C_o^o} = \exp\left[-\frac{A}{V} \frac{K_w}{m} t \right] \tag{74}$$

An implicit assumption for this model is that the oil-phase is well-stirred. This assumption eliminates the need for consideration of the diffusion of oil components through the oil. This assumption will be evaluated later when the experimental data are used as input to this model. Equation (74) does show, however, that the required data (as discussed above) are the mass transfer coefficients (K_w), partition coefficients (m), and initial oil-phase concentrations ($C_o o$), as well as geometrical factors (A,V).

6.9.2.6 Dissolution of Prudhoe Bay Crude Oil Components from a Slick

The model developed above enables us to predict the dissolution of Prudhoe Bay crude oil from a slick using the experimental data above. One approach would be to apply Equation (74) to every distributing component using the data from Table 6-10. This would be tedious, though, and would obscure the point that will be made. The approach taken here will be to "cut" the oil up into four parts which we will call pseudocomponents. The pseudocomponents will be comprised of individual components that have similar partition coefficients and thus similar driving forces for mass transfer (into the water column). Table 6-11 shows how these pseudocomponents have been chosen. Each pseudocomponent is assigned a partition coefficient which is the weighted average (by concentration) of the partition coefficients of the individual components.

A typical value for mass transfer coefficient, 1.0 cm/hr, will be used. A/V is just the inverse of the slick thickness. A typical slick thickness of 1 cm will be used, i.e. $A/V = 1\ cm^{-1}$. With these data and those from Table 6-11, Equation (74) predicts the following half-lifes for the pseudocomponents in the oil:

Pseudocomponent	Half-life (1 cm slick)	Half-life (1 mm slick)
1	110 days	11.0 days
2	0.95 yrs	34.5 days
3	4.0 yrs	146 days
4	~∞	~∞

These results indicate that dissolution from a well-stirred oil slick will not result in significant water-phase concentrations of distributing components.

Now return to the discussion above about the mechanical state of the oil. If the oil-phase was modeled as a stagnant slick rather than wellstirred, the diffusivity of the pseudocomponent would have to have been considered. However, if this were done, the half-lives calculated above would be even longer because of the __added__ resistance to mass transfer within the oil- phase. Thus, the simple "well-stirred" model is sufficient for the purpose here, that being to illustrate the __very slow__ rate of dissolution from slicks.

Another possible mechanism for transport of oil components to the water phase is dissolution from small oil droplets that have been dispersed (mechanically or chemically) into the water column. The following sections explore this mechanism.

6.9.2.7 Dissolution from Oil Droplets into an Infinite Water Column

Consider a spherical oil droplet of radius a in an infinite well-stirred water column (r>a). Let the diffusivity of an oil component be D. The concentration of the component in the droplet is C_o, initially C^o_o. The water column concentration is C_w. The diffusion equation for the component in the oil is

$$ \frac{dC_o}{dt} = D \left[\frac{\partial^2 C_o}{\partial r^2} + \frac{2}{r} \frac{\partial C_o}{\partial r} \right] \tag{75} $$

At the oil/water interface, the diffusive flux must equal the flux of component across the interface:

$$ - A D \frac{\partial C_o}{\partial r} = A K_w (C^*_w - C_w) \quad \text{(at } r = a) \tag{76} $$

411

where

    K_w — water-phase mass mass transfer coefficient

    A — droplet surface area

    C^*_w — hypothetical water-phase concentration in equilibrium with oil-phase concentration

such that

$$m = C_o/C^*_w \tag{77}$$

The appropriate initial condition is:

$$C_o = C^o_o \qquad (t = 0) \tag{78}$$

The system of Equations (75), (76), and (78) can be solved by the method of Laplace Transforms. Carslaw and Jaeger (1959) present the solution:

$$\frac{C_o}{C^o_o} = \frac{2h}{r} \sum_{n=1}^{\infty} \frac{(a\alpha_n)^2 + (1-ah)^2}{\alpha_n^2 \left[\alpha_n^2 a^2 + ah(ah-1) \right]} \sin(\alpha_n r) \sin(\alpha_n a) \, e^{-D \alpha_n^2/t} \tag{79}$$

where

$$h = k_w/Dm \tag{80}$$

and αn are roots of:

$$(a\alpha_n) \cos(a\alpha_n) = (1-ah)\sin(a\alpha_n) \qquad \text{for} \quad n = 1,2,3,\ldots. \tag{81}$$

Thus, Equations (79-81) comprise a model for the prediction of dissolution from oil droplets.

6.9.2.8 Dissolution of Prudhoe Bay Crude Oil Components from Droplets

The model above (Eqs. 79-81) has been programmed on the SAIC computer so that predictions can be plotted. A code listing of this model is presented in Appendix B of this report: Code Description for Component-Specific Dissolution from Droplets. The data presented below utilize the same experimental data as before with the addition of a value for the oil phase diffusivity, D, of 1×10^{-5} cm^2/sec (a typical value found in the literature). Once again, the pseudocomponent approach will be taken.

Figures 6-4A through 6-4C present plots of the average dimensionless concentration of the pseudocomponents in the oil phase as a function of time for three different droplet radii. These average concentrations are obtained by integrating Equation (79) over the range 0<r<a and dividing by the volume of the drop (4/3 πa^3).

As shown in the plots, the half-lives for the three pseudocomponents are very sensitive to drop radius. For drops of radius 10^{-1} cm, the half-life of Cut 1 is about 3-4 days. This value drops to a few hours for drops of radius 10^{-3} cm. The reason for this decrease in half-life is the increased amount of surface area of the drops in proportion to their volume. It becomes very important then to predict the drop size or size distribution in order to make accurate estimates of the flux of soluable oil components into water.

The results presented in Figures 6-4A, B and C agree well with an approximate equation for dissolution half-lives given by Mackay, 1983.

6.9.2.9 Summary and Implications for Oil/Ice Systems

The preceding sections have illustrated two important facts concerning oil dissolution:

1) Petroleum is a complex mixture of components whose dissolution behavior cannot be described simply by a single measurement of

413
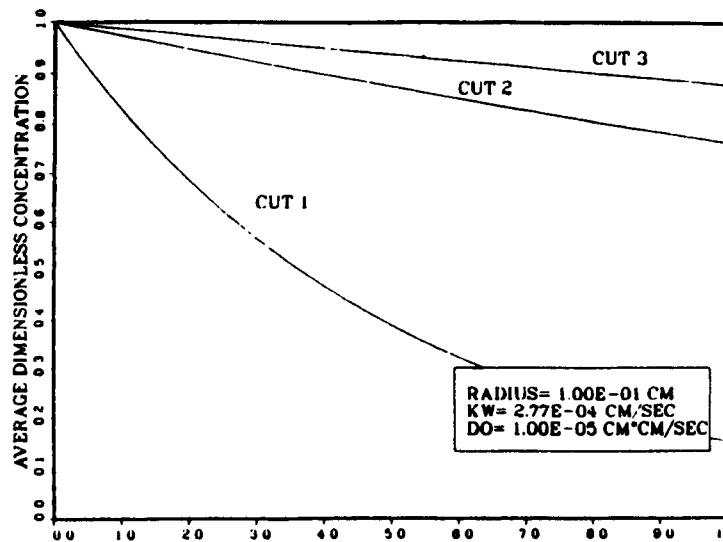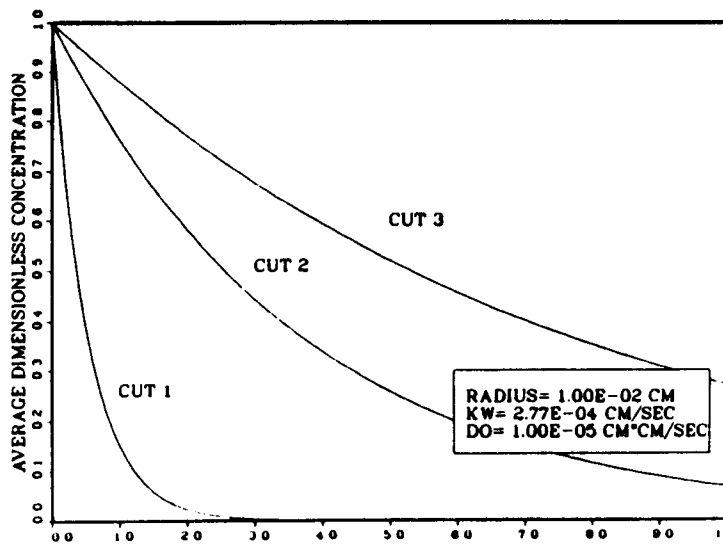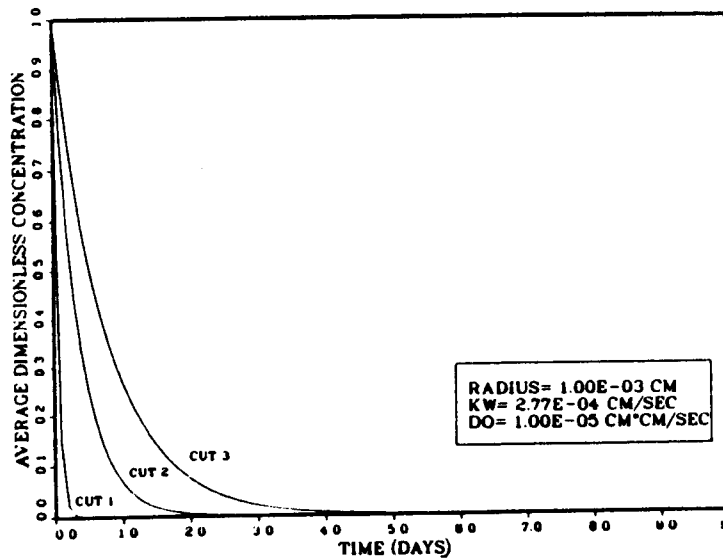
Figure 6-4.--Predicted Diffusion and Dissolution from a Droplet into an Infinite Medium for Droplet Radii of (A) 0.1 cm, (B) 0.01 cm, and (C) 0.001 cm.

414

"solubility." Such a description requires both kinetic and thermodyanmic data. Methods of measuring these data and mathematical models to predict dissolution using them are given.

2) Oil dissolution from an oil slick is a very slow process. Dissolution from very small oil droplets is much faster, chiefly because of the increased surface area per volume in small droplets.

The first implication of these facts is the need for research into the mechanism(s) that produce very small oil drops (5-50 microns). This droplet size has a been observed frequently by many investigators but the details of the process that creates them is not known (Shaw 1973; Gordon , et al. 1973). In some oil-water-electrolyte systems, spontaneous oil-in-water emulsions form in the absence of turbulence. Presumably, this "natural" process would be accelerated by ocean turbulence. Whatever the mechanism is, however, more information is needed before accurate prediction of droplet-size distribution can be made.

Secondly, the results above indicate that unless oil droplets are broken up or formed from sub-surface turbulance for under ice release (pipeline rupture or blow out) very little dissolution will occur from oil spilled under ice. Typically, slicks under ice are on the order of centimeters thick (very small surface area per volume) and are subject to small levels of turbulence. Thus, the time scale for dissolution from these large pools will be very large in comparison to the time scale for encapsulation of the oil into the ice. If smaller oil droplets are distributed, as observed in wave tank simulations (Sections 4.2 and 4.4) or in simulated blowouts under first year ice in the field (DOME, 1981) then dissolution would be significantly enhanced. In the following section, model-predicted water column concentrations of total dissolved species as observed measurements are presented for a subsurface oil spill under growing first year ice.

It is more difficult to make such statements about the later stages of oil/ice weathering, i.e., in the spring when the ice thaws. During this period

415

(after release), the oil begins to spread (increase surface area) and the hydrodynamic conditions are more turbulent. In addition, the oil comes into contact with the atmosphere so evaporation competes with dissolution. In general, the components that dissolve are also very volatile in an evaporation sense. For these reasons, the prediction of the oil droplet size distribution as a function of hydrodynamic conditions and percent ice cover becomes important. As noted in Section 4.2, grinding slush ice can enhance smaller oil droplet dispersion.

The dissolution of oil in open leads during freezeup is similar to that during thaw. The mass transfer from the parent slick will be slow, but if small droplets are being produced that transfer would be increased.

6.9.3   Determination of Ice Production and Salt Rejection Rates in Open Leads

The following model for ice production and salt rejection rates is primarily based on the model of Bauer and Martin (1983). Other similar models are also available (Schaus and Galt, 1973; Foster, 1972). The model used here has been simplified and modified to obtain order-of-magnitude estimates of brine flow rates.

The ice production rate is a function of the heat fluxed through the open lead. The model presented is only applicable for open water. Salinity plumes occur under all freezing ice but at much lower rates of ice production and salinity rejection. Bauer and Martin (1983) estimated coverage times for leads of various size, wind speeds and air temperatures ranging from three hours for a 50 m fetch at -40°C with wind speeds of 10 m/s to 200 hours for a 500m fetch at -10°C and 90 m/s winds. Twenty-four hours for coverage seems to be a reasonable average time for a small fetch (250 m) with mild winds (20 m/s) and temperatures -20°C. The calculated heat flux values are therefore reasonable for times of hours to a few days.

416

The total heat fluxed is Q* where

$$Q* = Q_H + Q_E \quad (W/m_2)$$

and $\quad Q_H$ = sensible heat flux

$= (0.485 \, k_n + 1.9 \, W_2)(T_W - T_A)$

$k_n = 8.0 + 0.35 \, (T_W - T_A)$

W_2 = wind speed at 2 m (m/s)

T_A = air temperature (°C)

T_W = water temperature (°C)

Q_E = latent heat flux

$= (0.76 k_n + 2.95 \, W_2)(e_{SW} - e_a)$

e_a = atmospheric va por pressure (mbars)

e_{SW} = saturated water vapor pressure (mbars)

Q* often includes values for radiant heat flux which is gene rally small compared to Q_H and Q_E and close to zero in cloudy weather or with very thin ice cover (10^{-6} cm). For this model, radiant heat flux is assumed to be zero.

The <u>ice production rate</u> is then (from Bauer and Martin, 1983)

$$I \ (kg/m^2 \ hr) = \frac{3.6 \, Q^{\bullet}}{(L - C_P \, T_W)} \quad (82)$$

L = freshwater latent heat of fusion

= 335 kJ/kg

C_P = specific heat of ice

= 2.12 kJ/kg°C

T_W = water temperature (°C)

The temperature of the sea water at freezing can be obtained from tables of freezing temperature versus salinity (the freezing temperature of 31 °/oo water is -1.73°C). A formula for this relationship is given by (Zubov, 1943)

$$T_F(°C) = -0.054 \ S(°/oo) \tag{83}$$

Salinity rejection rates are based on ice production, where the amount of ice formed gives a direct indication of the salt rejection. There is considerable disagreement in the literature as to the amount of salt retained in newly-formed ice. Bauer and Martin (1983) assume that no salt is retained; Foster (1972) assumes the ice has a salinity 30 $°/oo$ less than sea water (4 $°/oo$ in ice for 34 $°/oo$ water); and Schaus and Galt (1973) assume 8 $°/oo$. Zubov (1943) relates observed values of 5-10 $°/oo$ for an air temperature of -16°C to -40°C with the maximum observed salinities at 25 $°/oo$ (also at --40°C). Ice salinity is a function of air temperature, age and speed of formation with salinity decreasing with age of the ice (see for example, Tables 4-2, 4-10 and 4-12 for sea ice salinities measured in this program). Foster (1969) also observed experimental ice salinities of 25 $°/oo$ to 30 $°/oo$.

For this model, it is conservatively assumed that newly-formed ice contains 10 $°/oo$ so that the <u>salt rejection rate</u> becomes

$$\overline{S} \ (kg/m^2 \ hr) = \frac{3.6 \ Q^*}{(L - C_p \ T_W)} \ \frac{S}{(1000 - S)} \ \frac{(S - 10)}{S} \tag{84}$$

Using Equations (82) and (83) and values for L and C_p, Equation (84) becomes

$$\overline{S} \ (kg/m^2 \ hr) = \frac{3.6 \ Q^*(S - 10)}{(335 + 0.114S)(1000 - S)}$$

or

$$\overline{S} \ (kg/m^2 \ s) = \frac{0.001 \ Q^*(S - 10)}{(335 + 0.114S)(1000 - S)} \tag{85}$$

6.9.3.1 Salinity Plumes and Salt Flux

Table 6-12 gives a summary of salinity values for the top and bottom of plumes associated with open leads (Payne 1985). The average value observed at the surface is 32.9 ^{o}/oo and at the bottom is 33.8 ^{o}/oo giving a difference of 0.9 ^{o}/oo. Salinity profiles observed by various authors show a wide variation in surface values and bottom values; the numbers considered here are used to obtain rough estimates only. A difference of 0.9 ^{o}/oo may, in fact, be higher than other observed values (Foster, 1972) for open leads, but this would yield conservative results for estimating flow rates.

The salt fluxed from the surface may be determined using the equation

$$\text{Salt Fluxed (kg/m}^3) = \Delta S \; \rho_{SW}$$

where ρ_{SW} = density of sea water

$$\simeq 1.023 \text{ gm/cm}^3 \text{ at } 0°C$$

For the data from Table 6-12, this value is approximately

$$\text{Salt Fluxed (kg/m}^3) = [0.9 \text{gm}/1000 \text{gmSW}][1.023 \text{gmSW/cm}^3][\text{kg}/1000 \text{gm}][100 \text{cm/m}]^3$$
$$= 0.92 \text{ kg/m}^3$$

6.9.3.2 Volumetric Flow Rates

A volumetric flow rate may now be determined from the previous calculations and assumed values.

$$\text{Vol Flow (m}^3\text{/s) per unit surface area} = \frac{\text{Salt Rejection Rate (kg/m}^2 \text{ s})}{\text{Salt Fluxed (kg/m}^3)}$$

419

Table 6-12.—Summary of Salinity Plume Measurements
(see also Table 5-8).

Site	Depth	S_O	S_B	DS
10	30m	33.1 ppt	33.9 ppt	0.8 ppt
11	28m	33.2 ppt	33.9 ppt	0.7 ppt
12	24m	32.4 ppt	33.8 ppt	1.4 ppt
13	27m	32.8 ppt	33.7 ppt	0.9 ppt
14	29m	33.3 ppt	33.9 ppt	0.6 ppt
16	29m	32.5 ppt	33.8 ppt	1.3 ppt

S_O = at surface measurement

S_B = at bottom measurement

Table 6-13.—Heat Flux Values from Bauer and Martin (1983) with Corresponding Rejection Rates Based on a Salinity of 32.9 $°/_{oo}$ and Volumetric Flow Rates.

Air Temp (°C)	Water Temp (°C)	Wind Speed (m/s)	Heat Flux (W/m^2)	Salt Reject Rate (kg/m^{2}s)	Vol. Flow Rate* (m^3/s)
-10°	-2°	10	290	2.0 E-5	2.2 E-5
		30	700	4.9 E-5	5.3 E-5
		90	1850	1.3 E-4	1.4 E-4
-20°	-2°	10	600	4.2 E-5	4.6 E-4
		30	1350	9.4 E-5	1.0 E-4
		90	8500	2.4 E-4	2.7 E-4
-30°	-2°	10	940	6.6 E-5	7.1 E-5
		30	2000	1.4 E-4	1.5 E-4
		90	5200	3.6 E-4	3.9 E-4
-40°	-2°	10	1330	9.3 E-5	1.0 E-4
		30	2700	1.9 E-4	2.1 E-4
		90	6900	4.8 E-4	5.2 E-4

* per unit surface area

A summary of heat flux values from Bauer and Martin and salt rejection rates calculated from the assumed initial salinity of 32.9 $^\circ$/oo is given in Table 6-13. Volumetric flow rates were also calculated using the salt fluxed value of 0.92 kg/m^3. This gives a range of flow rates that might be used to transport dissolved species to the bottom water layers. A change in initial salinity to 35 $^\circ$/oo with no change in Δs will lower the volumetric flow rates by one order of magnitude while using the increased salinity and decreasing Δs by one half will halve the flow rates so that within reasonable estimation ranges, changes in salinity values have only small affects on the results.

6.9.4   Dissolved Oil Concentration Transported to Bottom Waters

The results of the last two sections can now be used to estimate the maximum dissolved oil concentration in water under forming ice. The dissolution rate of oil from a slick is considered to be the sum of the dissolution rates of pseudocomponents (these dissolution or solubility pseudocomponents are not strickly the same as those used when considering volatility). From Section 6.9.2 the concentration of individual pseudocomponents in the oil phase is:

$$ C_o = C_o^o \ \exp\left[-\frac{A}{V} \ \frac{Kw}{m} \ T\right] \tag{86} $$

The environmental temperature is used implicitly in the dissolution calculations through the temperature dependence of the partition coefficient, m. This temperature dependence is "weak", and as a result, the water temperature due to thermal coupling, is always used to specify the environmental oil temperature, even though the air temperature may be different.

The mass y of each pseudocomponent is (assuming the volume is roughly constant)

$$ y = C_o^o \ V \ \exp\left[-\frac{A}{V} \ \frac{Kw}{m} \ T\right] \tag{87} $$

421

Differentiating Equation (87) yields an equation for the rate of loss of mass $(-dy/dt)$

$$\left(-\frac{dy}{dt}\right) = -c_o^o \, v \, \frac{A}{V} \, \frac{Kw}{m} \cdot \exp\left[-\frac{A}{V} \, \frac{Kw}{m} \, T\right] \qquad (88)$$

Simplifying and dividing by A gives the rate of loss of mass per unit area.

$$\frac{dy}{dt} = c_o^o \, \frac{Kw}{m} \cdot \exp\left[-\frac{A}{V} \, \frac{Kw}{m} \, T\right] \qquad (89)$$

At $T = 0$, when the dissolution rate is at its maximum

$$\frac{dy}{dt} = \frac{c_o^o \, Kw}{m} \qquad (90)$$

This result indicates that the <u>initial</u> rate of loss of mass is independent of the thickness of the slick. This appears to be a contradictory to the results of Section 6.9.2 in which it was found that increased surface area per volume increases mass transfer rates from slicks. It is only for the special case of $\tau = 0$ that the rates are identical. At later times, mass transfer is enhanced for thinner slicks (larger A/V).

For the first dissolution-pseudocomponent, the mass concentration is about 0.3 percent, the "m-value" (partition coefficient) is 3800, and the bulk oil density is approximately .88 gm/cc. Thus, the rate of loss of mass of pseudocomponent 1 (per meter squared area) is:

$$\frac{dy}{dt} = \frac{(0.003)(.88 \text{ gm/cc})(1 \text{ cm/hr}) \, 10^4 \text{ cm/m}^2}{3800} = 0.007 \text{ g/hr/m}^2$$
$$= 0.17 \text{ g/day/m}^2$$

The (water) flow rate per square meter due to a salinity plume is approximately 1×10^{-4} m³/sec or 8.64 m³/day or approximately 8.64×10^6 g/day.

Therefore an upper bound estimate of the dissolved oil concentration of pseudo-component one in the water due to dissolution from a slick is approximately:

$$\frac{0.17 \text{ g/day/m}^2}{8.6 \times 10^6 \text{ g/day/m}^2} = 0.02 \text{ ppm}$$

For pseudocomponents two and three the dissolved concentrations are 0.003 and 0.0015 ppm, respectively, giving a total dissolved concentration of 0.025 ppm. It must be emphasized that these calculations are based on the pseudocomponents as defined in Table 6-10. These are not the same pseudocomponents that are used in evaporation calculations. Thus, these dissolution pseudocomponents are to be used only in the scenario described. Further, these calculations illustrate how the dissolution (or partition coefficient) is used in the prediction. Because all compounds have a finite partition coefficient, they can be transported, albeit the transport could be quite small.

As mentioned in Section 6.9.2, however, dispersion of small oil droplets can significantly increase the dissolution rates of the pseudocomponents. A 600-fold increase in droplet dispersion rate and concomitant increase in dissolved components was measured in the cold-room test tank immediately after the introduction of 4-6 cm wave turbulence (Section 4.2.2). This was primarily due to small-scale turbulence in the undulating ice field. Thus, in order to calculate an estimated rate of mass loss from a slick that has undergone dispersion, the following particle size distribution will be used.

droplet diameter	% of total mass of dispersed oil
10 μm	30%
100 μm	50%
1 mm	20%

The above droplets sizes were chosen so that the results of Section 6.9.2 (Figures 6-4A, B and C) can be utilized to calculate initial mass loss rates from droplets, and thus water phase concentrations. For these calculations, the initial slope of the plots is used to calculate the initial rate of loss of mass from the oil droplets.

423

Two hypothetical situations will be considered: a 2 cm thick slick with 10% dispersion and a 1 mm thick slick with 10% dispersion. Tables 6-14 and 6-15 present the results. The total mass loss rates in Tables 6-14 and 6-15, when divided by the calculated volumetric flow rates (Section 6.9.3), give total estimated water column dissolved concentrations of 3.1 and 0.18 ppm, respectively.

It should be noted that the above calculations do not consider evaporation and they represent an upper bound calculation. The water that flows past the oil at the initial moment of the spill will eventually mix with less concentrated water and thus be diluted.

The calculations above do not consider, however, the dissolution of benzene. Thus, the results presented here could possibly be low by a factor proportional to the the concentration of benzene in crude oils (or refined products) relative to the other water soluble compounds which were measured.

The results presented in this section illustrate and reinforce those of Section 6.9.2. The rates of dissolution of oil components into the water column are strongly dependent on the surface area to volume ratio. When small droplet dispersion occurs before significant evaporation takes place, dissolution of hydrocarbons becomes an important process. This importance is not due to a large impact on the mass balance of the slick itself, but rather because of the possible transfer of oil components to localized water bodies or flows, such as brine drainage from a lead.

6.10   THE M/V CEPHEUS SPILL - SAIC MODELLING AND ANALYTICAL SUPPORT TO NOAA RESPONSE

6.10.1   Background of the Spill Event

The M/V Cepheus grounded at approximately 0640 hours (1-21-84) on the shallow point on the western side of Knik Arm almost due west of Carin Pt. An estimated 200,000 gal (~4800 bbls) of JP-5 (Jet A) aircraft fuel had been lost during both the grounding incident and movement of the ship to the dock. NOAA

424

Table 6-14.--Initial Mass Loss Rates (g/day/m^2) for 2-cm Slick and 10% Dispersion.

Source	pseudocomponent			
	1	2	3	Total
Parent slick	.17	.028	0.012	0.21
10mm	15.8	2.1	1.9	19.8
100mm	5.3	0.40	0.33	6.0
1mm	0.2	0.014	0.01	0.22
			Total	26.21

Table 6-15.--Initial Mass Loss Rates (g/day/m^2) for 1-mm Slick and 10% Dispersion.

Source	pseudocomponent			
	1	2	3	Total
Parent slick	.17	0.028	0.012	0.21
10mm	0.79	0.11	0.10	1.0
100mm	0.27	0.020	0.017	0.31
1mm	0.01	0.0007	0.0005	0.011
			Total	1.51

trajectory estimates suggested that JP-5 may have been deposited in the mud flats to the north of the grounding site as far as Sixmile Creek (about half way between Carin Pt. and Eagle River). With subsequent tides, the spilled product may have moved to the southwest at least as far as Fire Island. At the time of the grounding, ice coverage was estimated to be ~60-80% and the air temperature was in the -23 to -32°C range.

6.10.2 <u>Observations and Activities Completed During the Site Investigation</u>

SAIC (J. Payne and D. McNabb) visited the spill site, collected samples of both JP-5 and seawater containing the spilled product, and made visual observations of the spill behavior. Visual examination of "Chain of Custody" JP-5 samples collected by the Coast Guard showed the material to be a clear, low-viscosity and low density (0.7 - 0.8 g/ml) fluid, which was quite similar in appearance to intermediate distillate cuts of Prudhoe Bay Crude, distilled into fractions for GC characterization (see, for example, pp 3-28 to 3-40 of Payne et al., 1984a).

At approximately 1600 hours on 1/28/84, pancake ice ranging in size from 1-3 meters (diameter) and ice rafts approaching 10-20 meters (across) were fast against the ship. With the ice cover pressing against the ship, no evidence of any spilled product (JP-5) could be observed from a distance of 5 to 10 meters above the surface. With the outflow of the ebb tide current around 1615 hours, several 10-20 meter wide leads opened adjacent to the hull and JP-5 could be observed bubbling to the surface (Figure 6-5). The fuel appeared as a dull grey film against the opaque olive-green color of the sediment-laden water. No color sheen was observed. With the outgoing tide the oil and broken ice moved parallel to and away from the vessel at an estimated speed of 1-2 knots. The oil was not visible after a distance of 10-20 meters. Very little could be done to contain the spill in the presence of the moving ice. Also, contamination of intertidal mud flats in the Knik Arm and south of Anchorage was of concern, and during the 1-28-84 overflight there was one location south and west of Fire Island where the presence of surface product was suspected. It was extremely difficult, however, to document the extent of this spill from

Figure 6-5.--Sampling JP-5 from the MV Cepheus. With incoming tides the ice
was pressed fast to the hull. As the tide ebbed, an open lead approximately
4 m wide was generated and the oil could be observed surfacing as a dull sheen
after its release from a below-waterline rupture in the number 2 hold.

helicopter or fixed wing aircraft overflights due, in part, to the fact that Cook Inlet in the Anchorage area was covered at the time by 50-80% ice.

Approximately 3 liters of the JP-5 cargo were obtained from the punctured hold of the Cepheus. The JP-5 cargo analyzed by FID-GC at the Kasitsna Bay Laboratory was characterized by n-alkanes ranging from nC6 through nC16, with the maximum n-alkane concentrations between nC10 and nC11. The chromatographic profile also showed evidence of numerous branched and cyclic aliphatic and alkyl-substituted aromatic components. Table 6-16 illustrates the types of components which could be present in each of the distillate cuts (data from Prudhoe Bay Crude Oil) as re-defined to produce the synthetic JP-5.

A True Boiling Point (TBP) distillation on the bulk samples was performed to allow additional JP-5 characterization. Physical properties data for five distillate cuts of the JP-5 are presented in Table 6-17; FID-GC chromatograms of whole fuel and of the corresponding distillate cuts are shown in Figures 6-6 and 6-7. From comparisons with FID-GC chromatograms of Prudhoe Bay Crude distillate cuts (see Payne et al., 1984a), it is apparent that the JP-5 is generally devoid of many of the higher boiling compounds that comprise the heavier distillate cuts and pot residue of the crude oil.

Partition coefficients or M-values were determined for specific components of the JP-5 by layering 3 ml of the jet fuel on top of 37 ml of seawater, allowing the oil and water phases to equilibrate, and then analyzing the relative concentrations of individual compounds in each phase. The measured M-values for several aromatic compounds present in the JP-5 are shown in Table 6-18. Compounds with lower M-values are more soluble in seawater, and thus have a greater tendency to partition from the oil to the water phase. Chromatograms of extracts of the oil and water phase are shown in Figure 6-8. These chromatograms indicate that a relatively greater proportion of the lower molecular weight compounds partition from the oil into the water phase.

Table 6-16.—Distillate Cut Boiling Point Ranges and the Associated Aliphatic
and Aromatic Components of JP-5 from the MV Cepheus Spill.

P.B. Crude Cut No.	JP-5 Cut no.	Boiling Point (°F)	n-alkanes in CEPHEUS JP-5 Cargo *,***	Aromatics that may occur within boiling point range**
2	1	186 - 212	$C_6 - C_7$	benzene, toluene
3	2	213 - 257	$C_8 - C_9$	ethyl benzene; o,m,p xylenes cumene, n-propylbenzene
4	3	258 - 302	KOVAT 950 - 1030	p-cumene, mesitylene
5	4	303 - 347	KOVAT 1040 - 1150	butylbenzene, C_4 benzene
6	5	348 - 392	KOVAT 1150 - 1230	naphthalene, benzothiophene n-hexylbenzene
7	6	393 - 437	KOVAT 1230 - 1380	1-methylnaphthalene, biphenyl,2,6 dimethyl-naphthalene
8	7	438 - 482	KOVAT 1380 - 1490 (?)	naphthalene
9	8	483 - 527	$nC_{15} - nC_{16}$	trimethylnaphthalene and fluorene

* boiling point range estimated from data in Payne et al. (1984)

** aromatics chromatograph within the respective n-alkane Kovat index range

*** Kovat Retenetion Index (Kovats, 1958)

Table 6-17.--Physical Properties of JP-5 and Prudhoe Bay Crude Distillate Cuts.

Sample Cut		Density (g/ml)	Viscosity (centistokes)	Oil/Air Interfacial Tension(dynes/cm)	Oil/Water Interfacial Tension (dynes/cm)
JP-5	Cut 3	.746	.842	43.8	27.3
"	Cut 6	.762	.941	37.6	27.7
"	Cut 9	.770	1.18	36.7	28.0
"	Cut 12	.790	1.65	36.7	30.4
"	Cut 15	.826	2.66	3.90	29.1
Prudhoe Bay	Cut 2	.734	.632	41.9	25.7
" "	Cut 4	.770	.822	35.0	26.6
" "	Cut 7	.822	1.79	34.0	29.8
" "	Cut 9	.848	3.21	29.0	31.9
" "	Bottom	.937	407.	30.3	35.5
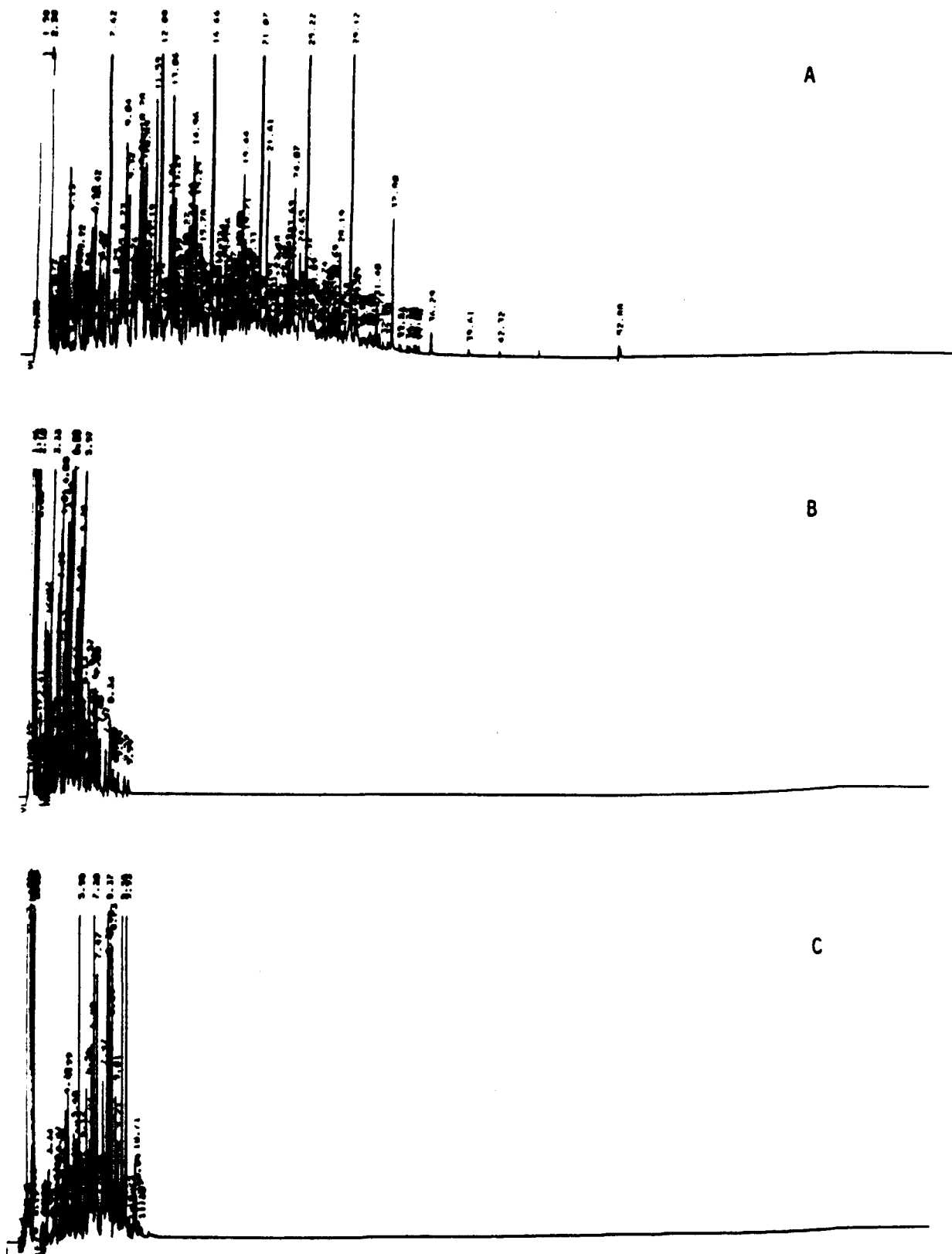
Figure 6-6.--FID-GC Chromatograms of Distillate Cuts of JP-5 Jet Fuel:
(A) whole fuel before distillation, (B) cut 3 (280-293°F), and (C) cut 6
(313-324°F).

431
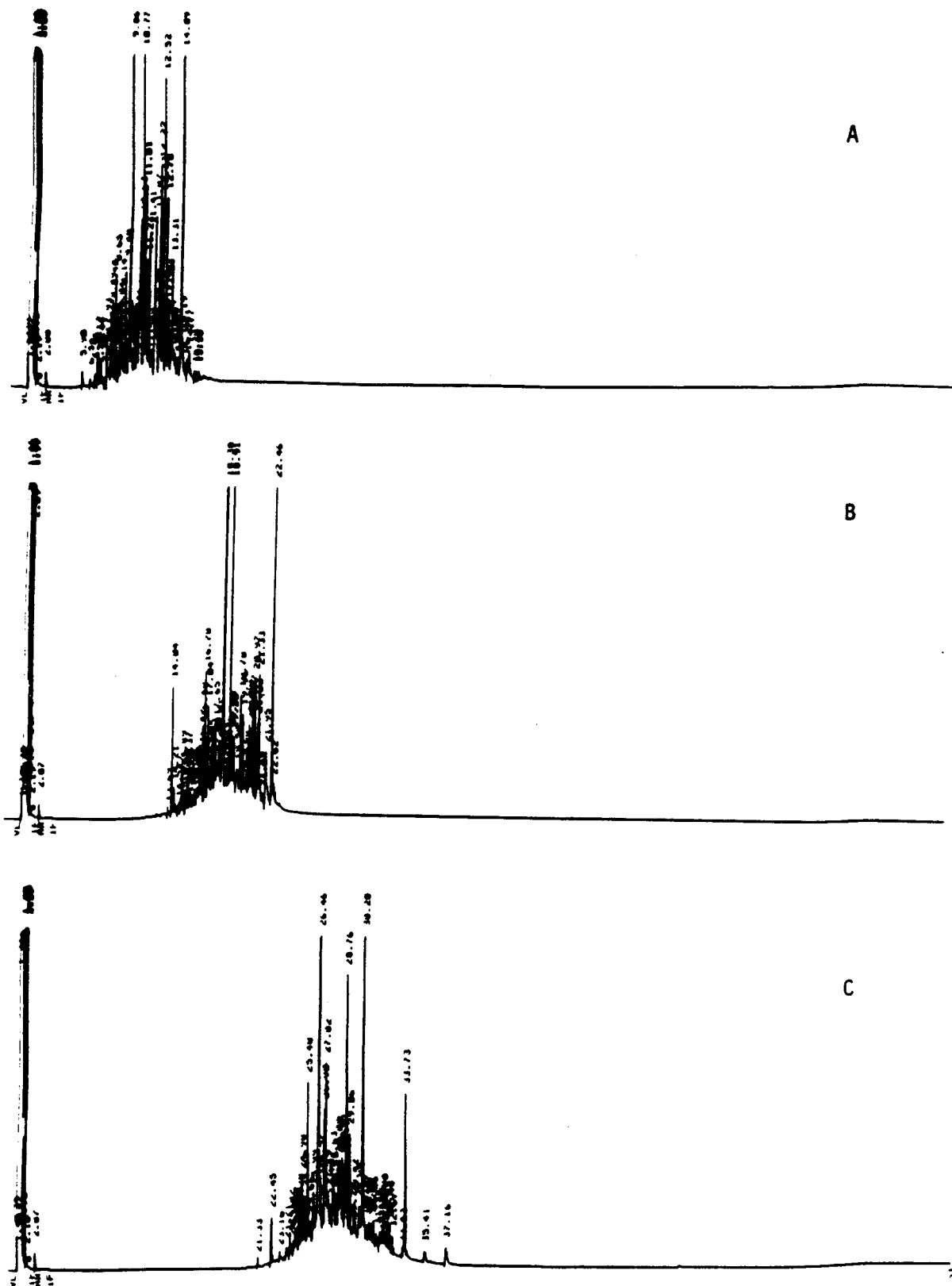
Figure 6-7.--FID-GC Chromatograms of Distillate Cuts of JP-5 Jet Fuel:
(A) cut 9 (347-370°F), (B) cut 12 (415-437°F), and (C) cut 15 (482+ °F).

432

Table 6-18.--M-Values and Concentrations Determined by Partitioning
JP-5 Jet Fuel Against Seawater.

| Compound | Concentration (ug/g) | | M-Value[a] |
	Oil Phase	Water Phase	
Ethylbenzene	378	.113	3350
m & p-xylene	2660	.549	4850
o-xylene	4670	.401	11600
1,3,5-trimethylbenzene	4430	.0701	63200
C_3-benzene	2840	.113	25100
C_3-benzene	17300	.322	53800
C_4-benzene	4060	.194	20900
Tetramethylbenzene	1690	.198	8540
Naphthalene	3160	.187	16900
2-methylnaphthalene	6830	.0933	73200

a - the M-value is defined as the oil phase concentration divided by the water phase concentration at equilibrium.
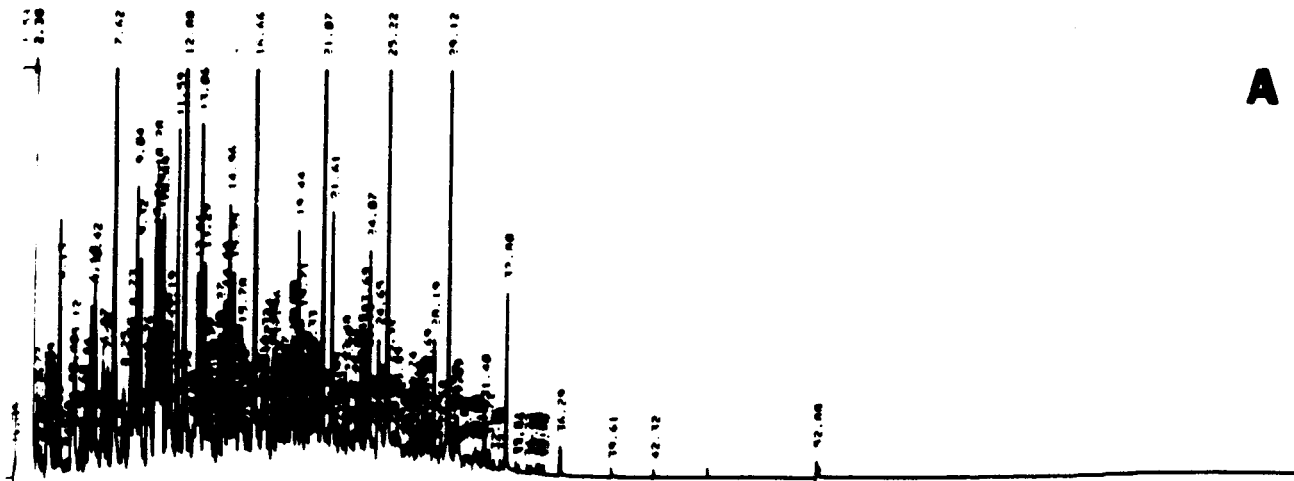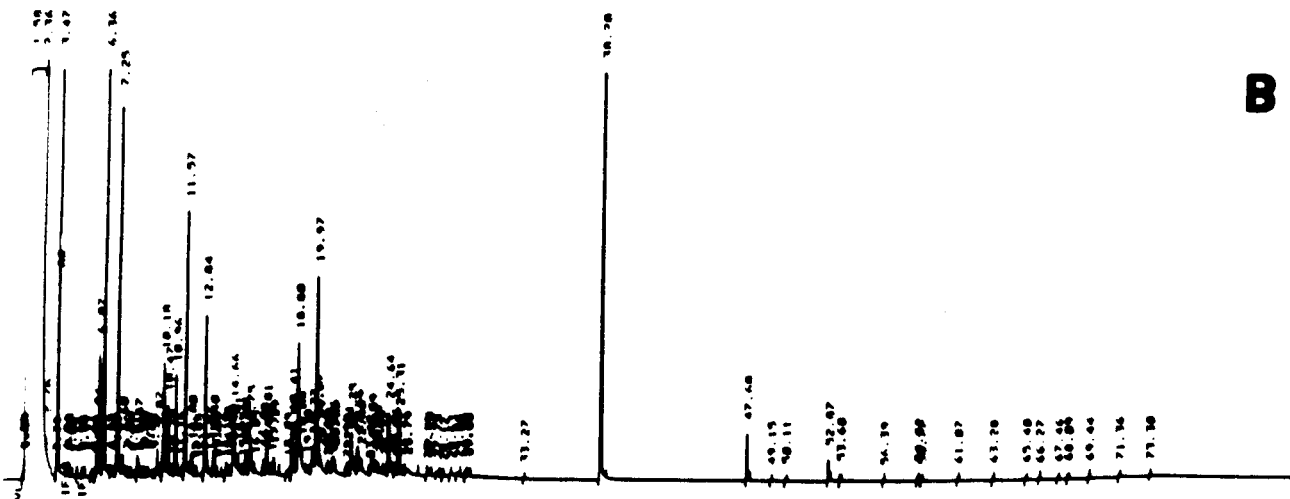
Figure 6-8.--JP-5 Cargo Obtained from MV Cepheus Grounding. FID-GC profiles
of m-value determinations: (A) oil phase, and (B) water phase.

434

Several weathering simulations were run on JP-4 (already in the Model code) and on a "synthesized" JP-5 fuel (made by combining distillate cuts of fractionated Prudhoe Bay crude oil, as described below, to obtain a real-time estimate of JP-5 weathering behavior). Examination of estimated boiling point ranges for Jet Fuel, as provided in Curl and O'Donnell (1977), suggested that JP-4 may be too volatile for adequate simulation of the behavior of the cargo lost from the M/V Cepheus. Therefore, a "synthetic" jet fuel was generated for model simulation by combining PB crude oil distillation cuts 3 through 9 (boiling point 257° to 527°F) and cuts 2 through 9 (boiling points 212° to 527°F) (data for Prudhoe Bay crude oil are given on page B-43 of Appendix B in Payne et al., 1984a). Gas chromatographic and physical properties analyses demonstrated that the choice of cuts 2 through 9 provided the best match with the cargo lost from the vessel (see Table 6-17).

Oil weathering simulations were run on the SAIC computer system for the simulated JP-5 mixture at temperatures of -20 and 0°F with a 10 knot wind. Data were obtained out to 200 hours and subsequently provided to USCG and NOAA personnel. Model simulations indicated that 60% of the cargo would still present after 10 days at -20°F with a 10 knot wind. This estimate agreed with values predicted by the HAZMAT group for jet fuel evaporation at various temperatures:

HAZMAT DATA

Temperature	Percent Remaining				
	Day 1	Day 2	Day 3	Day 4	Day 5
10°C (+32°Z)	67	48	36	29	23
-10°C (+14°F)	81	67	56	48	42
-20°C (-4°F)	90	81	74	67	61
-30°C (-22°F)	94	90	85	81	77

The Oil Weathering Model output at -20°F showed almost no additional mass lost in the 5 to 10 day interval; thus, the overall mass balance of the slick predicted by the two models was similar.

QUALITY ASSURANCE/QUALITY CONTROL PROCEDURES IMPLEMENTED
AS A COMPONENT OF THE ANALYTICAL PROGRAM

The results of environmental measurements are only valuable insofar as they are accurate and precise. This is particularly true if results of the measurements of chemical levels or properties from this program are to be used for predictive assessments in decision-making processes. Therefore, particular attention toward generating reliable data has been an important consideration during the experimental stages of this program.

The specific QA/QC measures taken during various experiments included the routine analysis of system and method blanks, replicate sampling and analyses, spike and recovery tests for matrices of interest, and instrumental recalibration at prescribed intervals. This section presents the results of the experimental QA/QC data generated during the program as well as pertinent results from our participation in the NOAA Status and Trends interlaboratory intercalibration program in force during the completion of this project.

7.1   WAVE TANK STUDIES

Prior to all of the oil/ice interaction experiments conducted in the cold room at Kasitsna Bay, a number of QA/QC measures were undertaken that primarily addressed seawater extraction efficiency and potential contamination sources. The experimental wave tank used for studies was scrupulously cleaned by 1) physical removal of residual oil remaining from any previous spill experiments, 2) thorough solvent washing, 3) soap and water washing and 4) allowing the system to flush with seawater. A seawater/method blank was analyzed before experimental spill initiation to ensure that all residual sources of contamination had been removed. An example of an FID-GC chromatogram depicting such a wave tank blank is presented in Figure 4-14A. Furthermore, the sample preparation method was investigated for extraction efficiency by conducting two spike and recovery experiments. In the first of these tests, known quantities of aliphatic and aromatic hydrocarbons were spiked directly into clean seawater before sample extraction. Compound recoveries are presented in Table 7-1. Approximately 81% of the aliphatic and aromatic hydrocarbons were recovered in

Table 7-1.--Kasitsna Bay Spike and Recovery Experiment Results.

| | Recovery (%) | |
S&R Test	Aliphatic	Aromatic
Seawater Extraction	81.0	80.6
Filtration System[a] (Dissolved)	40.7	77.6
Filtration System[a] (Dispersed)	63.4	18.7

[a] "Dissolved indicates the seawater filtrate, while "dispersed" refers to the extracted filter pad.

this seawater extraction. In the second test, known amounts of aliphatic and aromatic hydrocarbons were introduced to a seawater sample. The sample was then filtered by the method described in Payne et al. (1984a). The seawater filtrate ("dissolved" oil) as well as the filter pad ("dispersed" oil) were then extracted and analyzed separately. For the sum of the "dissolved" and "dispersed" fractions (Table 7-1), 104% of the aliphatics and 96% of the aromatic hydrocarbons were recovered.

During various wave tank experiments, routine analyses of replicates were conducted for seawater hydrocarbon chemistry, surface oil, dispersed oil, seawater and ice salinities, and surface tension measurements. The results of (primarily) duplicate sample analyses are presented in Tables 7-2 through 7-6. These results give indications of experimental and instrumental precision.

Table 7-2 shows results for individual compound concentrations for duplicate seawater samples from one hour, six hour and 12 hour post-spill samples from a wave tank experiment. Good agreement was observed for each set of duplicates.

Table 7-2.--Results of Duplicate Water Sample Analyses.

Compound	Concentration(ug/l)					
	1 hour		6 hours		12 hours	
	Rep 1	Rep 2	Rep 1	Rep 2	Rep 1	Rep 2
Toluene	9.46	15.9	7.87	5.57	5.30	5.70
Ethylbenzene	.961	1.66	.829	.626	.648	.708
m&p-xylene	2.97	4.99	2.58	1.93	2.00	2.17
o-xylene	1.41	2.38	1.21	.927	.930	.995
Isopropylbenzene	.101	.159	.0702	.0582	.0665	.0712
n-propylbenzene	.138	.240	.104	.0860	.0985	.105
C_3-benzene	.478	.822	.402	.302	.307	.353
C_3-benzene	.148	.269	.114	.0923	.104	.122
Trimethylbenzene	.209	.358	.177	.137	.145	.157
C_3-benzene	.536	.924	.449	.356	.381	.406
C_4-benzene	.322	.553	.293	.227	.232	.257
Tetramethylbenzene	.104	.152	.0673	.0796	.0511	.0659
Naphthalene	.468	.847	.485	.371	.327	.363
2-methylnaphthalene	.302	.514	.275	.205	.196	.218
1,1'-biphenyl	.0511	.0348	ND	ND	ND	ND
2,6-dimethylnaphthalene	.0903	.152	.0531	.0403	.0387	.0431
C_2-naphthanlene	.0959	.183	.0478	.0350	.0319	.0374
C_2-naphthalene	.0216	.0360	ND	ND	ND	ND
C_2-napphthalene	.0170	.0292	ND	ND	ND	ND
2,3,5-trimethylnaphthalene	.0214	.0341	ND	ND	ND	ND
Dibenzothiophene	____	.0206	ND	ND	ND	ND
Phenanthrene	____	.0220	ND	ND	ND	ND
Unresolved Compounds	8.93	8.65	3.19	2.84	4.57	5.43
Total Resolved Compounds	21.3	34.9	16.8	12.9	12.3	13.6

Table 7-3.--Results of Replicate Oil Sample Analyses.

| Sample | Hydrocarbon Concentrations (ug/l) | | | |
| | Total Resolved | | Unresolved Compounds | |
	Rep 1	Rep 2	Rep 1	Rep 2
36 hour	80.7	91.7	191	155
1 year residual	6.89	7.90	78.3	74.4
Stranded 1 year	3.07	4.89	38.6	59.2
3 hour	41.3	31.3	96.6	83.2
3 day	33.6	27.4	113	123
Starting Crude	107	68.0	229	236

Duplicate oil sample analyses were conducted on starting Prudhoe Bay crude, 3 hour, 36 hour, 3 day post-spill and one year residual oil sample from wave tank experiments. These results for total resolved and unresolved compounds are presented in Table 7-3. As seen, duplicate analyes were in close agreement.

Replicate filter pad (dispersed oil) samples were extracted and analyzed at the six hour and 12 hour sampling points from a wave tank experiment. These results are shown in Table 7-4. For these types of samples precision is relatively poor (as expected) due to the somewhat random nature of the analyte.

Precision estimates for replicate salinity samples are shown in Table 6-6. The values presented are very close and indicate that he measurments are very reproducable.

Table 7-4.—Results of Replicate Dispersed Oil (Filter Pad) Sample Analyses.

| Sample | Hydrocarbon Concentrations (ug/l) | | | |
| | Total Resolved | | Unresolved Compounds | |
	Rep 1	Rep 2	Rep 1	Rep 2
6 hours	20.8	14.4	7.29	8.35
12 hours	17.1	5.88	23.1	7.41

Table 7-5.—Results of Replicate Salinity Measurements.

| Sample | Salinity (0/00) | | |
	Rep 1	Rep 2	Rep 3
D-2 (field sample)	18.0	17.5	-
Incoming Seawater	30.9	30.1	30.3
Tank Seawater	30.4	31.0	30.5
Ice Surface (1cm)	56.0	59.3	-
6 hr Water	31.6	31.0	-
12 hr Water	31.1	31.2	-
24 hr Water	31.0	31.0	-

Table 7-6.—Results of Replicate Surface Tension Measurements.

| Sample | Surface Tension (dynes/cm) | |
	Rep 1	Rep 2
Starting Crude	32.0	31.5
4-days	32.6	33.8

Replicate sample measurements for bulk physical properties or oil were not attemped for the most part because of 1) the large volumes of oil required for each parameter and 2) the inaccessability of oil in the seawater-ice system. However, duplicate samples were obtained for surface tension measurements at the 4 day sampling point in one experiment along with the starting crude. Table 7-6 shows that precision was excellent.

Because sample collection, work-up and analyses were conducted consecutively (generally on the same day), QA/QC measures related to sample preservation, transportation and storage were circumvented. However, consistent instrument response and reproducibilities were monitored throughout experiments by (at least) daily recalibration of the FID-GC and salinity meter. FID-GC analyses of routine methylene chloride solvent blanks also served as instrument blanks to ensure that system contamination from previous chromatogram carryover was prevented.

The surface tension meter was initially calibrated according to instructions from the manufacturer. The instrument was then tested for accuracy by comparing measured surface tension values against those reported for two solvents. The following lists these measured values and the corresponding literature values.

	Surface Tension(dynes/cm)	
	Measured	Reported
50/50 Methanol/Water	33.3	34.5
Water	75.3	73.1

Good agreement between measured and reported values indicates that surface tension determinations were accurate.

Hydrocarbon concentrations for individual resolved peaks in each gas chromatogram were calculated on a DEC-10 System Computer using the formula given in equation 1. This particular example of the program is for analysis of a seawater sample. Operator-controlled modification of the DEC-10 program allows similar data reduction for sediment, tissue, or individual oil (mousse) samples.

$$\text{ug compound X/L seawater} = (A_x) \times (R.F.) \times$$

$$\frac{P.I.V. + 1.}{Inj.S.Vol.} \times \frac{Pre\text{-}C.S. \; Vol.}{Post\text{-}C.S.Vol.} \times \frac{100}{\%NSL \; on \; LC} \times \frac{100}{\%DW/FW} \times \frac{1}{liters} \quad (1)$$

where:

A_x	=	the area of peak X as integrated by the gas chromatograph (in arbitrary GC area units)
R.F.	=	the response factor (in units of ug/GC area unit)
P.I.V. + 1	=	the post-injection volume (in ul) from which a 1-ul aliquot had been removed for analysis by GC (measured by syringe immediately following sample injection)
Inj.S.Vol.	=	the volume of sample injected into the GC (always 1.0 ul as measured by an HP Automatic Liquid Sampler)
Pre-C.S. Vol. & Post-C.S. Vol.	=	the total solvent volumes before and after an aliquot is removed for gravimetric analysis on a Cahn electrobalance
%NSL on LC	=	the precent of sample non-saponifiable lipid used for SiO_2 column chromatography
%DW/FW	=	the percent dry weight of wet weight in the sediment tissue, or oil sample being analyzed
liters	=	liters of seawater initially extracted (or grams wet weight of oil or sediment).

During analyses of extracts, the Hewlett Packard 5840A gas chromatograph was recalibrated after every 8 to 10 injections, and individual response

factors were calculated for all detected even and odd n-alkanes between nC_8 and nC_{32}. Concentrations of other components (e.g., branched and cyclic aliphatics) that eluted between the major n-alkanes were calculated by linear interpolation of the adjacent n-alkane response factors and the unknown compound peak's KOVAT index. In addition, an aromatic standard was run daily for retention time determinations. By incorporating the post-injection volume (PIV) into the calculation, the amount of hydrocarbons measured in the injected sample was converted to the total hydrocarbon concentration in the sample.

Unresolved complex mixtures (UCM's) were measured in triplicate by planimetry. The planimeter area was converted to the gas chromatograph's standard area units at a given attenuation and then quantified using the average response factors for all n-alkanes occurring within the GC elution range of the UCM (see equation 2).

$$\frac{ug\ UCM}{liter} = Area_p \ x\ (Conv.\ F)\ x\ \frac{S.\ Att.}{Ref.\ Att.}\ x\ (R.F._{a-b})\ x\ [\ldots] \qquad (2)$$

where:

Area = UCM area in arbitrary planimeter units,

Conv. F. = a factor for converting arbitrary planimeter units to GC area units at a specific GC attentuation,

S. Att. and Ref. Att. = the GC attenuation at which the sample chromatogram was run and the reference attenuation to determine the conversion factor (Conv. F.), respectively,

$R.F._{a-b}$ = the mean response factor for all sequential n-alkanes (with carbon numbers a to b) whose retention times fall within the retention time window of the UCM, and

[...] = the same parameters enclosed in brackets in equation 1.

Confirmation of KOVAT index assignment to n-alkanes was done by computer correlation with n-alkane standard retention times and direct data-reduction-operator input.

443

Assignment of a KOVAT index to each branched or cyclic compound eluting between the n-alkanes was done by interpolation using the unknown compound and adjacent n-alkane retention times. Assignment of KOVAT indices to peaks in the aromatic fraction was made by direct correlation of unknown peaks with retention times from the n-alkane and aromatic standard runs completed prior to sample injection.

7.3   FIELD STUDIES

During the field study conducted in the Chukchi Sea, water column samples were collected with Nansen or Niskin sample bottles for analysis of hydrocarbon cocktail components. All sample containers (Thermos bottles) were scrupulously cleaned with soap and water and then rinsed with copious amounts of distilled water prior to use. Collected water samples were placed in the cleaned bottles and capped with no head space (to prevent compound volatilization). Logistical constraints precluded the collection of field replicate samples. All samples were maintained at $4^{\circ}C$ during storage. Sample analyses were conducted according to the methods described in Section 5.3.3. All Tenax[R] traps were baked out and analyzed by Specific Ion Monitoring (SIM) GC/MS prior to sample purging. Therefore, each sample was accompanied by a corresponding GC/MS system blank that ensured no contamination for instrumental analysis. The sample preparation (i.e., purging step) was evaluated as a potential source of contamination by purging one liter of clean seawater prior to an actual sample purging. This sample blank was clean with respect to benzene and toluene. A detection limit of 0.01 ng/liter was established based on the sample volume, response from a 500 pg standard, and a 5 to 1 signal to noise ratio. Compound quantitation was accomplished according to equation 3.

$$\text{Concentration (ng/l)} = (AC \times RF)/V_s \qquad (3)$$

where:

AC   =   the SIM area count in the sample

RF — the response factor for benzene and toluene standards in ng (of standard)/specific ion area counts, and

V_s — sample volume in liters

The specific ions monitored were 78 amu for benzene and 91 amu for toluene.

In addition, a spiked seawater blank was analyzed in order to determine the recovery efficiency of the purging method. One liter of clean seawater was spiked with 100 ng of the actual cocktail, purged, and analyzed by SIM GC/MS according to methods described in Section 5.3.3. Of the 100 ng of cocktail spiked into the blank, 40 ng were recovered (40% method efficiency). This recovery reflects the effects of each compound's solubility properties and Henry's Law coefficients in a seawater matrix.

7.4   INTERLABORATORY INTERCALIBRATION PROGRAMS

While precision is a relatively easy parameter to measure by replicate determinations, accuracy is somewhat more intractable. Spiked sample recovery is valuable as far as determining the efficiency of an extraction procedure for compounds added by the investigator. It does little, however, to determine extraction efficiency of the subject compounds as they are present in an original sample matrix. At this time, there are no Standard Reference Materials (SRM's) to assist in such determinations. Therefore, NOAA has initiated a number of interlaboratory/intercalibration programs wherein the results obtained on real environmental samples (designated as Interim Reference Materials) by a variety of participating laboratories can be compared. Tables 7-7 and 7-8 contain the results from a recent participation effort by SAIC in the NOAA-sponsored Status and Trends Intercalibration Program and compares our data to those of other participating laboratories.

Data in Tables 7-7 and 7-8 reflect variability due to the extraction and analysis of mussel tissue and sediment samples, which are not matrices encountered during oil/multi-year ice experiments. However, they do indicate SAIC's ability to generate reliable aromatic hydrocarbon data and confirm our

sample preparation and instrumental analysis dependability. As indicated in Tables 7-7 and 7-8, SAIC's aromatic hydrocarbon data are seen to fall within reasonable agreement of values reported by the other six participating laboratories.

Table 7-7.--Mean Concentrations (n = 3) in ng/g Dry Weight of Aromatic Hydrocarbons Found in Reference Tissue: Mussel II.

Compound	NAF Set A	NEC Set B	SEC Set C	BOS Set D	SAI Set E	TAM Set F (MS)	TAM Set G (FID)
napthalene	2000	1900	2000	1800	1500	2000	1600
2-methylnaphthalene	7200	7700	8300	6300	6200	7200	12000
1-methylnaphthalene	6200	5800	7100	5300	5200	7000	9000
biphenyl	1300	1500	1600	1300	1400	1500	1500
2,6-dimethylnaphthalene	2500	2700	3200	2700	3200	3300	2800
acenaphthene	**130	1300	790	230	340	330	97
fluorene	900	940	1200	1200	1300	1000	1300
phenanthrene	1200	1200	1500	1300	1500	1300	1200
anthracene	160	150	200	270	170	180	53
1-methylphenanthrene	170	350	1000	460	330	290	230
fluoranthene	860	820	860	930	980	820	560
pyrene	430	430	**560	870	530	490	650
benz(a)anthracene	190	1100	250	210	140	260	180
chrysene	420	340	400	*620	280	350	700
benzo(e)pyrene	180	180	**160	190	*90	170	910
benzo(a)pyrene	74	110	280	<25	120	100	82
perylene	130	56	**200	<30	-	100	100
dibena[a,h]anthracene	31	25	90	<42	-	84	39

* n=1
**n=2

NAF = National Analytical Facility
NEC = Northeast Fisheries Center
SEC = Southeast Fisheries Center
BOS - Battelle Ocean Sciences
SAI = Science Applications International
TAM = Texas A&M University

Table 7-8.—Mean Concentrations (n = 3) in ng/g Dry Weight of Aromatic Hydrocarbons Found in Reference Tissue: Duwamish III.

Compound	NAF Set A	NEC Set B	SEC Set C	BOS Set D	SAI Set E	TAM Set F (MS)	TAM Set G (FID)
napthalene	320	250	330	400	310	370	330
2-methylnaphthalene	160	110	180	210	140	170	150
1-methylnaphthalene	120	80	150	130	88	120	110
biphenyl	39	31	57	48	33	42	48
2,6-dimethylnaphthalene	70	58	76	96	63	72	64
acenaphthene	300	290	420	290	330	320	350
fluorene	310	280	430	460	340	320	360
phenanthrene	2300	2200	3200	3200	2500	2400	2700
anthracene	510	650	730	850	600	590	650
1-methylphenanthrene	220	410	320	330	300	300	310
fluoranthene	3900	3700	5600	5200	4200	4600	4900
pyrene	4100	3900	5800	6600	4800	5500	6000
benz(a)anthracene	1500	1400	2100	2000	1500	2100	2200
chrysene	2600	2100	3600	3500	2500	3000	3000
benzo(e)pyrene	1600	1400	2000	2300	1900	1400	1700
benzo(a)pyrene	1800	1700	2700	2400	1800	1900	2200
perylene	510	460	710	850	580	490	680
dibena(a,h)anthracene	310	310	430	460	430	220	240

* Extraction by NS&T protocol (MacLeod et al., 1985): quantitation by GC/MS
** Extraction based on previous NAF procedure (Brown et al., 1980): quantitation by GC/MS

NAF = National Analytical Facility
NEC = Northeast Fisheries Center
SEC = Southeast Fisheries Center
BOS - Battelle Ocean Sciences
SAI = Science Applications International
TAM - Texas A&M University

447

8.
BIBLIOGRAPHY

Aagaard, K. 1981 Current measurements in possible dispersal regions of the Beaufort Sea. In: Environ Assess of the Alaskan of Marine Pollution and Assessment Wash D.C. p 74.

Aagarrd, K. 1984. Currents, CTD and pressure measurements in possible dispersal regions of the Chukchi Sea. NOAA/OCSEP Final Report, RU 91. p. 77.

Ackley, S. F., W. D. Hibler III, F. K. Kugzruk, A. Kovacs and W. F. Weeks. 1974. Thickness and roughness variations of Arctic multi-year sea ice. AIDJEX Bulletin No. 25. pp. 75-96. University of Washington, Seattle, WA.

Anderson, D. L. 1961. Growth rate of sea ice. Journal of Glaciology, 3: 1170-1172.

API. 1965. 108 Technical Data Book - Petroleum Refining, American Petroleum Institute, Washington, D.C.

Arctec Inc. 1987. Bouchard #650 Oil Spill in Ice Covered Waters of Buzzards Bay, December 1977. Environmental Assessment of the Alaskan Continental Shelf.

Armstrong, T. E., B. B. Roberts and C. W. M . Swithinbank. 1966. Illustrated Glossary of Snow and Ice, Spec. Publ. 4, p. 18, Scott Polar Research Institute, Cambridge, England.

ASTM. 1977. Method D2892-73: Standard Test Method for Distillation of Crude Petroleum (150 Theoretical Plate Column, American Society for Testing and Materials, Philadelphia, PA.)

Barnes, P., E. Reimnitz, L. Toimil and H. Hill. 1979. Open-File Report 79-539. U.S. Geological Survey.

Bauer, J. and S. Martin. 1982. Petroleum (Composition). In: Kirk-Othmer Encyclopedia of Chemical Technology, John Wiley and Sons, Inc.

Bauer, J. and S. Martin. 1983. A model of grease ice growth in small leads. Journal of Geophysical Research, 88: 2917-2925.

Baxter, B., P. C. Deslauriers and B. J. Morgan. 1978. The Bouchard #65 Oil Spill, January 1977. MESA Special Report, NOAA-03-7-022-35105.

Boehm, P. D. and D. L. Fiest. 1982. Subsurface distributions of petroleum from an offshore well blowout. The IXTOC I blowout, Bay of Campeche. Environmental Science and Technology, 16: 67-74.

Boehm, P. D. and J. G. Quinn. 1974. Marine Pollution Bulletin, 5(7): 101.

Bridie, A. L., T. H. Wanders, W. Zegveld and H. G. Van der Heijde. 1980. Formation, prevention, and breaking of sea water in crude oil emulsions "Chocolate Mousses". Marine Pollution Bulletin, 2: 343-348.

Carslaw, H. S. and J. C. Jaeger. 1959. Conduction of Heat in Solids. Oxford University Press.

C-Core, 1975. An Oil Spill in Pack Ice. Memorial University of Newfoundland, St. JHohns, Newfoundland.

Clark, R. C. and W. D. MacLeod. 1977. Inputs, transport mechanisms and observed concentrations of petroleum in the marine environment. In: Effects of Petroleum on Arctic and Subarctic Marine Environments and Organisms. (Malins, D. C., ed.) Academic Press, New York. pp. 91-223.

Cohen, Y., D. MacKay and W. Y. Shiv. 1980. Canadian Journal of Chemical Engineering, 58: 569.

Coleman, H. J., E. M. Shelton, D. T. Nichols and C. J. Thompson. 1978. Analyses of 800 Crude Oils from United States Oil Fields, BETC/RI-78/14, Bartlesville Energy Technology Center, Department of Energy, Bartlesville, Oklahoma.

Cox, J. C., L. A. Schultz, R. P. Johnson and R. A. Shelsby. 1980. The transport and behavior of oil spilled in and under sea ice. ARCTEC, Inc. Final Report to OCSEAP Arctic Project Office. September, 1980.

Curl, H., Jr. and K. O'Donnell. 1977. Chemical and Physical Properties of Refined Petroleum Products. NOAA Technical Memorandum ERL MESA-17. pp. 31.

Denbigh, K. 1971. The Principles of Chemical Equilibrium. Cambridge Univ. Press. Cambridge, MA. pp. 494.

Deslauriers, P.C., B.J. Morson And E.J.C. Sobey. 1979. Field Manual for Cold Climate Oil Spills, Prepared for EPA Report EPA-3-05-009-8, Chapter 8, p. 1-40.

DOME. 1981. Oil and Gas Under Sea Ice. Canadian Offshore Oil Spill Research Association, Project Report, Volume 1. Oil Spill Research Section, Beaufort Sea Production Development Department, Beaufort Sea Division, DOME Petroleum LTD.

Edmister, W. C. and K. K. Okamoto. 1959. Applied Hydrocarbon Thermodynamics Part 13: Equilibrium Flash Vaporizations Correlations for Petroleum Fractions. Petroleum Refiner, 38:117-129.

Elliot, A. J. 1986. Shear Diffusion and the Spread of Oil in the Surface Layers of the North Sea. Dt.hydrogr.Z.39,H.3.

Fallon, J. F. and K. M. Watson. 1944. Thermal Properties of Hydrocarbons. National Petroleum News, June 7, pp. 372.

Foster, T. D. 1969. Experiments in haline convection induced by the freezing of sea water. J. of Geophysical Research, 74(28): 6967.

Foster, T. D. 1972. Haline convection in polynyas and leads. Journal of Physical Oceanography, 2: 462.

Garratt, J. R. 1977. Review of drag coefficients over oceans and continents. Monthly Weather Review, 105: 915-929.

Garrison, G.R. 1977. Oceanographic Measurements in the Chukchi Sea and Baffin Bay - 1976. APL-UW Technical Report 7710. p. 44 plus Apendices.

Gearing, J. N., P. J. Gearing, T. Wade, J. G. Quinn, H. B. McCarthy, J. Farrington and R. F. Lee. 1979. The rates of transport and fates of petroleum hydrocarbons in a controlled marine ecosystem and a note on analytical variability. Proceedings of the 1979 Oil Spills Conference. pp. 555-565.

Gill, A. 1973. Circulation and bottom water production in the Weddell Sea. Deep Sea Research, 20:111-140.

Gold, P. I. and G. Olge. 1969. Estimating Thermophysical Properties of Liquids, Park 10 - Viscosity, Chemical Engineering, July 14.

Gordon, D. C., P. D. Keizer and N. J. Prouse. 1973. Laboratory studies of the accommodation of some crude and residual fuel oils in sea water. Journal of the Fisheries Research Board of Canada, 30(11): 1611.

Greenspan, D. 1971. Introduction to Numerical Analysis and Applications. Markham Pub. Co. Chicago, IL. pp. 182.

Hachmeister, L. E. and J. B. Vinelli. 1985. Nearshore and Coastal Circulation in the Northeastern Chukchi Sea. Science Applications, Inc. Technical Report No. SAI/NW-84-254-26. 93p.

Hachmeister, L. E., K. S. Short, G. C. Schrader, K. B. Winnick and J. W. Johannessen. 1986. Oceanographic monitoring, Part II, Chapter 3. In: Endicott environmental monitoring program, annual report-1985. Prepared by Envirosphere Company, Bellevue, Washington for the U.S. Army Corps of Engineers, Alaska District, Anchorage, Alaska. 160 pages.

Hanley, T. O'D. and G. Tsang. 1984. Formation and properties of frazil in saline water. Cold Regions Science and Technology, 8:209-221.

Horne, E. P. W. 1985. Ice-induced vertical circulation in an Arctic fiord. Journal of Geophysical Research, 90:1078-1086.

Hougen, O. A., K. M. Watson and R. A. Ragatz. 1965. Chemical Process Principles, Part 1 - Material and Energy Balances, 2nd Edition, John Wiley & Sons, Inc.

Kirstein, B. E., 1984. Letter to Lyman Thorsteinson, February 13, 1984, Oil Spill Source Term, Hypothetical Oil spill, RV 3010

Kovacs, A. 1977. Sea ice thickness profiling and under-ice oil entrapment. In "Proceedings 1977 Offshore Technology Conference." Vol. 3. pp. 547-554. Houston, TX.

Kovacs, A. 1979. In:"Environmental Assessment of the Alaskan Continental Shelf." Annual Report Vol. 8. p. 310. NOAA, Boulder, CO.

Kovacs, A., R. Morey, D. Cundy and G. Dicoff. 1981. In: "Proceedings POAC81." Vol. 3. University of Laval, Quebec, Canada. p. 912.

Kowalik, Z. and N. Untersteiner. 1978. A Study of the M_2 Tide in the Arctic Ocean. Dt. Hydrogr. Z., 31, 216-229.

Kozo, T. L. 1983. Initial model results for Arctic mixed layer circulation under a refreezing lead. Journal of Geophysical Research, 88: 2926-2934.

Lewbel, G. S. 1984. Environmental hazards to petroleum industry development. In:Proceedings of a Synthesis Meeting: The Barrow Arch Environment and Possible Consequences of Planned Offshore Oil and Gas Development. (Truett, J.C., ed.) NOAA/OAD. Anchorage, AK. pp. 31-46.

Lewbel, G. S. and B. J. Gallaway. 1984. Transport and fate of spilled oil. In: Proceedings of a Synthesis Meeting: The Barrow Arch Environment and Possible Consequences of Planned Offshore Oil and Gas Development. (Truett, J.C., ed.) NOAA/OAD. Anchorage, AK. pp. 7-29.

Lewis, E. L. 1976. In:"Pacific Marine Science Report 76-12." Institute of Ocean Science, Victoria, B.C., Canada.

Liss, P. S. and P. G. Slater. 1974. Flux of gases across the air-sea interface. Nature, 247: 181-184.

Lyman, W. J., W. F. Reehl and D. H. Rosenblatt. 1982. Handbook of Chemical Property Estimation Methods. McGraw-Hill Book Company. pp. 17-20 to 17-22.

Mackay, D., I. Buist, R. Mascarenhas and S. Paterson. 1980. Oil Spill Processes and Models, Research and Development Division, Environmental Emergency Branch, Environmental Impact Control Directorate, Environmental Protective Service, Environment Canada, Ottawa, Ontario, K1A 1C8.

Mackay, D. and R. S. Matsugu. 1973. Evaporation rates of liquid hydrocarbon spills on land and water. The Canadian Journal of Chemical Engineering, 51: 434-439.

Mackay, D. and W. Y. Shiv. 1976. Aqueous solubilities of weathered northern crude oils. Bulletin of Enviromental Contamination and Toxicology, 15(1): 101-109.

Mackay, D., W. Y. Shiv, K. Hossain, W. Stiver, D. McCurdy, S. Patterson and P. Tebeau. 1982. Development and Calibration of an Oil Spill Behavior Model. Unpublished Report, Department of Chemical Engineering and Applied Science, University of Toronto.

Mackay, D., W. Stiver and P. Tebeau. 1983. Testing of crude oils and petro-leum productions for environmental purposes. In: Proceedings of the 1983 Oil Spills Conference. American Petroleum Institute, Washington D.C.

Mackay, D. and A. T. K. Yeun. 1983. Environmental Science and Technology, 17: 211.

Martin, S. 1979. A field study of brine drainage and oil entrainment in first-year sea ice. Journal Glaciology, 22: 473-502.

Martin, S. 1981a. Frazil ice in rivers and oceans. Annual Review of Fluid Mechanics, 13: 379-397.

Martin, S. 1981b. Anticipated oil-ice interactions in the Bering Sea. In: The Eastern Bering Sea Shelf: Oceanography and Resources. Volume One. (Hood, D.W. and J.A. Calder, eds.) Office of Marine Pollution Assessment, U.S. National Oceanic and Atmospheric Administration. pp. 223-243.

Martin, S. and J. Bauer. 1981. Bering Sea ice-edge phenomena. In: The Eastern Bering Sea Shelf: Oceanography and Resources. Volume One. (Hood, D.W. and J.A. Calder, eds.) Office of Marine Pollution Assessment, U.S. National Oceanic and Atmospheric Administration. pp. 189-211.

Martin, S. and P. Kauffman. 1981. A field and laboratory study of wave damp-ing by grease ice. Journal of Glaciology, 27: 283-314.

Martin, S., P. Kauffman and C. Parkinson. 1983. The movement and decay of ice edge bands in the winter Bering Sea. Journal of Geophysical Research, 88: 2803-2812.

Matthews, J. B. 1981. Observations of surface and bottom currents in the Beaufort Sea new Prudhoe Bay, Alaska., J. Geophys. Res. 86, 6653-6660.

McAuliffe, C. D. 1966. Solubility in water of paraffin, cycloparaffin, olefin, acetylene, cycloolefin, and aromatic hydrocarbons. Journal of Physical Chemistry, 70: 1267-1275.

McAuliffe, C. D. 1969. Determination of dissolved hydrocarbons in subsurface brines. Chemical Geology, 4: 225-233.

McAuliffe, C. D., J. C. Johnson, S. H. Green, C. P. Canevari and J. D. Searl. 1980. Dispersion and weathering of chemically treated crude oils on the ocean. Environmental Science and Technology, 14: 1509-1518.

McAuliffe, C. D., A. E. Smalley, R. D. Groover, W. M. Welsh, W. S. Pickle and G. E. Jones. 1975. Chevron Main Pass Block 41 Oil Spill: Chemical and Biological Investigations. Proceedings of the 1975 Oil Spill Conference. pp. 555-556.

McPhee, M. G. 1980. Physical oceanography of the seasonal sea ice zone. Cold Regions Science and Technology, 2: 93-118.

Mooney, M. 1951. The viscosity of a concentrated suspension of spherical particles. Journal of Colloid Science, 10: 162-170.

Murray, D. A. J., W. L. Lockhart and G. R. B. Webster. 1984. Oil and Petrochemical Pollution, 2(1): 39.

National Academy Press. 1985. Oil in the Sea. Inputs, Fates and Effects. Appendix A (Spill Case Histories).

Nelson, W. G. and A. A. Allen. 1981. Oil migration and modification processes in solid sea ice. In: Proceedings of the 1981 Oil Spill Conference. American Petroleum Institue, Washington, D.C. pp. 191-198.

NORCOR. 1975. The Interaction of Crude Oil with Arctic Sea Ice. Beaufort Sea Technical Report #27, NORCOR Engineering and Research Ltd, Yellowknife, N.W.T.

O&GJ. 1973. Evaluations of World's Important Crudes. The Oil and Gas Journal, Petroleum Publishing Co., Tulsa, Oklahoma.

Payne, J. R., N. W. Flynn, P. J. Mankiewicz and G. S. Smith. 1980b. Surface Evaporation/Dissolution Partitioning of Lower-Molecular-Weight Aromatic Hydrocarbons in a Down-Plume Transect from the IXTOC-I Wellhead. In: Proceedings of a Symposium, Preliminary Results from the September 1979 Researcher/Pierce IXTOC-I Cruise. pp. 239-265. (June 9-10, Key Biscayne, FL) NOAA, Office of Marine Pollution Assessment. Washington, D.C.

Payne, J. R., M. Frydrych, R. E. Jordan, B. Kirsten, J. L. Lambach, G. D. McNabb Jr., W. Paplawsky and R. F. Shokes. 1981. Multivariate Analysis of Petroleum Weathering Under Marine Conditions. Final Report to NOAA/ Outer Continental Shelf Environmental Assessment Program. Juneau, Alaska, pp. 176.

Payne, J. R. and L. E. Hachmeister, 1985. Field Report: Bottom Water Generation in the Chukchi Sea, SAIC, Contract #84-ABC-00121.

Payne, J. R., B. E. Kirstein, G. D. McNabb Jr., J. L. Lambach, C. de Oliveira, R. E. Jordon and W. Hom. 1983. Multivariate analysis of petroleum hydrocarbon weathering in the subarctic marine environment. In: Proceedings of the 1983 Oil Spill Conference American Petroleum Institute, Washington, D.C. pp. 423-434.

Payne, J. R., B. E. Kirstein, G. D. McNabb, Jr., J. L. Lambach, R. Redding, R. E. Jordan, W. Hom, C. De Oliveira, G. S. Smith, D. M. Baxter and R. Eagel. 1984a. Multivariate Analysis of Petroleum in the Marine Environment-Subarctic. In: Environmental Assessment of the Alaskan Continental Shelf; Final Reports of Principal Investigators, Volumes 21 and 22, National Oceanic Atmospheric Administration, Outer Continental Shelf Enironmental Assessment program, Juneau, Alaska.

Payne, J. R., G. D. McNabb, Jr., B. E. Kirstein, R. Redding, J. L. Lambach, C. R. Phillips, L. E. Hachmeister and S. Martin. 1984b. Development of a Predictive Model for the Weathering of Oil in the Presence of Sea Ice. Final Report Submitted to the National Oceanic and Atmospheric Administration, Outer Continental Shelf Environmental Assessment Program, Anchorage, Alaska.

Payne, J. R. and G. D. McNabb, Jr. 1984. Weathering of petroleum in the marine environment. Marine Technology Society Journal, 18(3): 24-42.

Payne, J. R. and C. R. Phillips. 1985. Petroleum Spills in the Marine Environment: The Chemistry and Formation of Water-in-Oil Emulsions and Tar Balls. Lewis Publishers, Inc., Chelsea, MI. 148p.

Payne, J. R., G. S. Smith, P. J. Mankiewicz, R. F. Shokes, N. W. Flynn, V. Moreno and J. Altamirano. 1980a. Horizontal and Vertical Transport of Dissolved and Particulate-Bound Higher-Molecular-Weight Hydrocarbons from the IXTOC-I Blowout. In: Proceedings of a Symposium, Preliminary Results from the September 1979 Researcher/Pierce IXTOC-I Cruise. pp. 119-167. (June 9-10, Key Biscayne, FL) NOAA, Office of Marine Pollution Assessment. Washington, D.C.

Pease, C. H. 1981. Eastern Bering Sea ice dynamics. In: The Eastern Bering Sea Shelf: Oceanography and Resources. Volume One. (Hood, D.W. and J.A. Calder, eds.) Office of Marine Pollution Assessment, U.S. National Oceanic and Atmospheric Administration. pp. 213-222.

Perry, R. H. and C. H. Chilton. 1973. Chemical Engineer's Handbook, 5th Edition, McGraw-Hill.

Petroleum Publishing Co. 1973. Evaluations of World's Import Crude. The Oil and Gas Journal. Tulsa, Oklahoma.

Pollard, R. T. 1977. Observations and models of the structure of the upper ocean. In: Modeling and Prediction of the Upper Layer of the Ocean. (Krause, E.B., ed.) Pergamon Press, New York. pp. 102-117.

Reid, R. C., J. M. Pransintz and T. K. Sherwood. 1977. The Properties of Gases and Liquids, 3rd Edition, McGraw-Hill.

Reimnitz, E., P. W. Barnes, L. Toimil and D. Mauer. 1977. A Word of Caution on the Age of Deep Water Ice Gouges in the Beaufort Sea. In: Environmental Assessment of the Alaskan Continental Shelf, Quarterly Reports, April - June, 2:452-455.

Reimnitz, E. and D. K. Maurer. 1978. Storm surges in the Alaskan Beaufort Sea. USGS open File Report 78-593.

Reimnitz, E., L. Toimil and P. Barnes. 1978. Arctic continental shelf morphology related to sea-ice zonation, Beaufort Sea, Alaska. Marine Geology, 28: 179-210.

Ross, S.L., W. J. Logan and R. Rowland. 1977. "Oil Spill Countermeasures; The Beaufort Sea and the Search for Oil", Dept. of Fisheries and Environment, Otawa, 1977.

Schaus, R. H. and J. A. Galt 1973. A thermodynamic model of an Arctic lead. Arctic, 26(2): 208.

Schumacher, J. D., K. Aagaard, C. H. Pease and R. B. Tripp. 1983. Effects of a shelf polynya on flow and water properties in the northern Bering Sea. Journal of Geophysical Research, 88: 2723-2732.

Shaw, D. G. 1977. Hydrocarbons in the water column. In:Fates and Effects of Petroleum Hydrocarbons in Marine Ecosystems and Organisms (D. A. Wolfe, ed.).

Stringer, W. J. 1981. Nearshore ice characteristics in the Eastern Bering Sea. In: The Eastern Bering Sea Shelf: Oceanography and Resources, Volume 1. (Hood, D. W. and J. A. Calder, eds.) U.S. Department of Commerce, Office of Marine Pollution Assessment. Washington D.C. pp. 167-188.

Sutton, C. and J. A. Calder. 1974. Solubility of higher-molecular-weight n-parafins in distilled water and seawater. Environmental Science and Technology, 8: 654-657.

Sutton, C. and J. A. Calder. 1975a. Reply to correspondence to the editor. Environmental Science and Technology, 9: 365-366.

Sutton, C. and J. A. Calder. 1975b. Solubility of alkylbenzenes in distilled water and seawater at 25.0°C. Journal of Chemical and Engineering Data, 20(3): 320-322.

Tebeau, P. A., D. Mackay, W. R. Shin, W. Stiver, K. Hossain, D. McCurdy and S. Paterson. 1982. Oil Weathering Under Arctic Conditions. Department of Chemical Engineering and Applied Sciences, University of Toronto, Toronto, Canada M55 1A4.

Treybal, R. E. 1955. Mass Transfer. McGraw-Hill.

Van Winkle, M. 1967. Distillation. McGraw-Hill.

Walker, E. R. 1975. "Oil, Ice and Climate in the Beaufort Sea", Beaufort Sea Project #35, December 1975.

Weeks, W. F. 1978. Sea ice conditions in the Arctic. In: Glaciological Data Report GD-2: Arctic Sea Ice Part 1. World Data Center A for Glaciology, Boulder, CO. Reprinted from AIDJEX Bull., 34:173-205.

Weeks, W. F. and G. Weller. 1984. Offshore oil in the Alaskan Arctic. Science, 225: 371-378.

Wilson, D. G. and D. Mackay. 1986. The Behaviour of Oil in Freezing Situations. Final Report for DDS Contract No. KE 145-4-0121. Department of Chemical Engineering and Applied Chemistry, University of Toronto, Toronto, Ontario, M5S/A4. 65p.

Yang, W. C. and H. Yang. 1977. Modeling of oil evaporation in aqueous environment. Water Research, 11: 879.

Zubov, N. N. 1943. Arctic Ice. Naval Ocean. Office and American Meter. Society, N.E.L. San Diego. 491p.

APPENDIX A: CODE DESCRIPTION FOR COMPONENT-SPECIFIC DISSOLUTION FROM SLICKS

The following are code listings and sample output from the FORTRAN code DIFFU.FOR. This code was developed in order to both describe and predict component-specific dissolution of oil from slicks in the absence of evaporation and to aid in the experimental measurement of diffusivities of individual compounds in crude oil. Briefly, the user is prompted for appropriate data, such as oil- water mass-transfer coefficients, oil-water partition coefficients, initial concentration of oil components, and slick thickness and area. The output from the program is time series concentrations of the compound and interest in the water column for both well-mixed and "slab" type slicks.

Details of the derivation of compound-specific dissolution are presented in Section 6.8.1 of this report.

```
C         ********** DIFFU.FOR ***********
C
C         THIS CODE CALCULATES THE WATER COLUMN CONCENTRATION
C         AND TOTAL MATERIAL BALANCES FOR
C         COMPONENT SPECIFIC DISSOLUTION FROM AN OIL SLICK IN
C         A WELL STIRRED TANK.   EVAPORATION IS NOT ALLOWED.
C
C         FOR DETAILS. SEE DERIVATION BY R. REDDING. DEC 1983
C
C
          IMPLICIT REAL*8  (A-H,O-Z)
          REAL*8 L,KW,M,KO,KPRIME,LOTERM,LWTERM,INTE,LH
          DIMENSION ALPHA(300),PAJ(300),CWO(50),COO(50),SUM(300),CMPD(5)
         1,HOURS(50),CW(50),COA(50),TMW(50),TMO(50),TM(50),COOA(50)
         2,CEEW(50)
          OPEN(UNIT=32,DIALOG='DSKD:DIFFU.OUT')
          OPEN(UNIT=34,DIALOG='DSKD:DIFFU.PLT')
          TYPE 10
10        FORMAT(2X,'ENTER A COMPOUND ID')
          ACCEPT 20,(CMPD(I),I=1,4)
20        FORMAT(4A5)
          TYPE 30
30        FORMAT(2X,'ENTER THE NUMBER OF INTERVAL HALVES')
          ACCEPT 40,NHALF
40        FORMAT(I3)
          TYPE 50
50        FORMAT(2X,'ENTER TOTAL NUMBER OF HOURS FOR EXPERIMENT')
          ACCEPT 70,THOURS
          TYPE 60
60        FORMAT(2X,'ENTER THE SLICK THICKNESS IN CM')
          ACCEPT 70,L
70        FORMAT(F10.0)
          TYPE 80
80        FORMAT(2X,'ENTER THE WATER DEPTH IN CM')
          ACCEPT 70,DELTA
          TYPE 90
90        FORMAT(2X,'ENTER THE OVERALL WATER-PHASE MASS TRANSFER
         1 COEFFICIENT IN CM/SEC')
          ACCEPT 70,KW
          TYPE 100
100       FORMAT(2X,'ENTER THE M VALUE (OIL/WATER)-DIMENSIONLESS')
          ACCEPT 70,M
          TYPE 110
110       FORMAT(2X,'ENTER THE DIFFUSIVITY IN CM*CM/SEC')
          ACCEPT 70,DZ
          TYPE 120
120       FORMAT(2X,'ENTER THE NUMBER OF TERMS IN THE SERIES')
          ACCEPT 130,NUM
130       FORMAT(I4)
          TYPE 140
140       FORMAT(2X,'ENTER THE INITIAL OIL CONCENTRATION IN MG/L')
          ACCEPT 70,OILCO
          TYPE 150
150       FORMAT(2X,'ENTER THE SLICK AREA IN CM*CM')
          ACCEPT 70,A
          KO=KW/M
          SMALLH=KO/DZ
          BIGH=L*SMALLH
          KPRIME=M*L/DELTA
          LOTERM=M*L/((M*L)+DELTA)
          LWTERM=L/((M*L)+DELTA)
          C1=((L*M)+DELTA)/(L*DELTA)
C
C         DO INTERVAL HALVING TO FIND THE ROOTS OF THE FUNCTION:
C
C         COT(X)=(X*X-KPRIME*BIGH)/(X*BIGH)
```

458

```
C
C          THEN FIND THE POLYNOMIAL (PAJ)
C
          PI=3.14159265358979323
          DO 180 I=1,NUM
          RH=I*PI
          LH=(I-1)*PI
          DO 170 K=1,NHALF
          XM=(LH+RH)/2.D0
          COT=DCOS(XM)/DSIN(XM)
          FX=XM*COT-((XM*XM-KPRIME*BIGH)/BIGH)
          IF(FX .LT. 0.D0) GO TO 160
          LH=XM
          GO TO 170
160       RH=XM
170       CONTINUE
          ALPHA(I)=XM
          PAJ(I)=ALPHA(I)**4.
          PAJ(I)=PAJ(I)+(ALPHA(I)*ALPHA(I)*(BIGH+(BIGH*BIGH)-(2.*KPRIME
         1*BIGH)))
          PAJ(I)=PAJ(I)+(KPRIME*BIGH*BIGH*(KPRIME+1.))
C
C          NOW FIND THE SUM OF NUM TERMS
C
180       CONTINUE
          SEC=3600.*THOURS
          INTE=SEC/40.
          DO 190 J=1,40
          SUM(J)=0
190       CONTINUE
          HOURS(1)=0.
          CW(1)=0.
          DO 220 J=2,40
          B=J
          TIME=B*INTE
          HOURS(J)=TIME/3600.
          DO 210 I=1,NUM
          ARG=ALPHA(I)*ALPHA(I)*DZ*TIME/(L*L)
          IF(ARG.LT.50.) GO TO 200
          EXPON=0.
          GO TO 210
200       EXPON=DEXP(-(ARG))
          SUM(J)=SUM(J)+EXPON/PAJ(I)
210       CONTINUE
          CWO(J)=LWTERM-(2.*L*BIGH*BIGH/DELTA)*SUM(J)
C
C          NOW CALCULATE THE WATER COLUMN CONCENTRATION, INTEGRATED
C          TOTAL MASS OF COMPONENT IN THE OIL AND MATERIAL
C          BALANCE FOR THE SYSTEM
C
          COOA(J)=LOTERM*L+(2.*BIGH*BIGH*L*SUM(J))
          CW(J)=CWO(J)*OILCO
          COA(J)=COOA(J)*OILCO
          TMW(J)=CW(J)*DELTA*A/1000.
          TMO(J)=COA(J)*A/1000.
          TM(J)=TMW(J)+TMO(J)
220       CONTINUE
C
C          WRITE OUTPUT TO FILE: DIFFU.OUT
C
          IOU=32
          IPU=34
          WRITE(IOU,230)
230       FORMAT(2X,'************* STIRRED TANK RESULTS *************')
          WRITE (IOU,240)THOURS
240       FORMAT(//,2X,'TOTAL HOURS: ',1PE10.3)
```

```fortran
      WRITE (IOU,250)L
  250 FORMAT(2X,'SLICK THICKNESS: ',1PE10.3,' CM')
      WRITE (IOU,260)DELTA
  260 FORMAT(2X,'WATER DEPTH: ',1PE10.3,' CM')
      WRITE (IOU,270)A
  270 FORMAT(2X,'SLICK AREA: ',1PE10.3,' CM*CM')
      WRITE (IOU,280)M
  280 FORMAT(2X,'M-VALUE: ',1PE10.3)
      WRITE (IOU,290)KW
  290 FORMAT(2X,'KW: ',1PE10.3,' CM/SEC')
      WRITE (IOU,300)KO
  300 FORMAT(2X,'KO: ',1PE10.3,' CM/SEC')
      WRITE (IOU,310)DZ
  310 FORMAT(2X,'DO: ',1PE10.3,' CM*CM/SEC')
      WRITE (IOU,320)NHALF
  320 FORMAT(2X,'NUMBER OF INTERVAL HALVES: ',I3)
      WRITE (IOU,330)OILCO
  330 FORMAT(2X,'INITIAL OIL CONCENTRATION: ',1PE10.3,' MG/L')
      WRITE(IOU,340)
  340 FORMAT(///,20X,'**********')
      WRITE(IOU,350)
  350 FORMAT(20X,'*OIL SLAB*')
      WRITE(IOU,360)
  360 FORMAT(20X,'**********')
      WRITE (IOU,370)NUM
  370 FORMAT(/,2X,'RESULTS WITH ',I4,' TERMS IN THE
     1 SERIES')
      WRITE (IOU,380)
  380 FORMAT(//,12X,'ALPHA',8X,'POLYNOMIAL')
      DO 400 I=1,NUM
      WRITE (IOU,390)I,ALPHA(I),PAJ(I)
  390 FORMAT(2X,I4,2(1X,1PE14.7))
  400 CONTINUE
      TMASS=OILCO*A*L/1000.
      WRITE (IOU,410)TMASS
  410 FORMAT(/,2X,'TOTAL INITIAL MASS: ',1PE10.3,' MG')
      WRITE (IOU,420)
  420 FORMAT(//,7X,'TIME',9X,'CW',7X,'MASS/WATER',
     15X,'MASS/OIL',3X,'TOTAL MASS')
      WRITE(IOU,430)
  430 FORMAT(6X,'HOURS',8X,'MG/L',9X,'MG',10X,'MG',10X,'MG')
      DO 450 I=1,40
      WRITE (IOU,440) HOURS(I),CW(I),TMW(I),TMO(I),TM(I)
  440 FORMAT(2X,5(2X,1PE10.3))
  450 CONTINUE
      FINCW=OILCO*LWTERM
      FINMW=FINCW*DELTA*A/1000.
      FINMO=OILCO*A*L*LOTERM/1000.
      WRITE (IOU,460) FINCW,FINMW,FINMO,TMASS
  460 FORMAT(4X,'EQUILIBRIUM',1X,1PE10.3,3(2X,1PE10.3))
C
C     NOW DO WELL MIXED CASE
C
      WRITE(IOU,470)
  470 FORMAT(///,7X,'****************')
      WRITE(IOU,480)
  480 FORMAT(7X,'*OIL WELL-MIXED*')
      WRITE(IOU,490)
  490 FORMAT(7X,'****************')
      DO 500 I=1,40
      CEEW(I)=OILCO*LWTERM*(1.-DEXP(-C1*KO*HOURS(I)*3600.))
  500 CONTINUE
      WRITE(IOU,510)
  510 FORMAT(/,10X,'TIME (HOURS)',8X,'CW (MG/L)')
      DO 516 I=1,40
      WRITE(IOU,514) HOURS(I),CEEW(I)
```

```
514      FORMAT(2X,2(2X,1PE10.3))
516      CONTINUE
C
C         WRITE TO PLOT FILE: DIFFU.PLT
C
         WRITE(IPU,520)(CMPD(I),I=1,4)
520      FORMAT(1X,4A5)
         WRITE(IPU,530)THOURS,M,KW,DZ,OILCO,FINCW,L
530      FORMAT(7(1X,1PE10.3))
         DO 550 I=1,40
         WRITE(IPU,540) HOURS(I)
540      FORMAT(1PE10.3)
550      CONTINUE
         DO 570 I=1,40
         WRITE(IPU,560) CW(I)
560      FORMAT(1PE10.3)
570      CONTINUE
         DO 576 I=1,40
         WRITE(IPU,574) CEEW(I)
574      FORMAT(1PE10.3)
576      CONTINUE
         END
```

************** STIRRED TANK RESULTS **************

```
TOTAL HOURS:  2.500E+02
SLICE THICKNESS:  1.000E+00 CM
WATER DEPTH:  3.900E+01 CM
SLICE AREA:  5.000E+02 CM*CM
M-VALUE:  4.000E+03
KW:  1.000E-04 CM/SEC
KO:  2.500E-08 CM/SEC
DO:  1.000E-05 CM*CM/SEC
NUMBER OF INTERVAL HALVES:  25
INITIAL OIL CONCENTRATION:  3.000E+02 MG/L
```

****
OIL SLAB
****

RESULTS WITH 25 TERMS IN THE SERIES

	ALPHA	POLYNOMIAL
1	5.0861659E-01	1.2945706E-03
2	3.1424094E+00	9.2537591E+01
3	6.2835857E+00	1.5388602E+03
4	9.4250440E+00	7.8457616E+03
5	1.2566570E+01	2.4857788E+04
6	1.5708123E+01	6.0757300E+04
7	1.8849689E+01	1.2606448E+05
8	2.1991262E+01	2.3363734E+05
9	2.5132841E+01	3.9867168E+05
10	2.8274422E+01	6.3870115E+05
11	3.1416006E+01	9.7359720E+05
12	3.4557592E+01	1.4255691E+06
13	3.7699178E+01	2.0191639E+06
14	4.0840766E+01	2.7812666E+06
15	4.3982354E+01	3.7410999E+06
16	4.7123943E+01	4.9302243E+06
17	5.0265532E+01	6.3825381E+06
18	5.3407122E+01	8.1342778E+06
19	5.6548712E+01	1.0224017E+07
20	5.9690302E+01	1.2692668E+07
21	6.2831893E+01	1.5583479E+07
22	6.5973484E+01	1.8942040E+07
23	6.9115075E+01	2.2816274E+07
24	7.2256666E+01	2.7256445E+07
25	7.5398257E+01	3.2315155E+07

TOTAL INITIAL MASS: 1.500E+02 MG

TIME HOURS	CW MG/L	MASS/WATER MG	MASS/OIL MG	TOTAL MASS MG
0.000E+00	0.000E+00	0.000E+00	0.000E+00	0.000E+00
1.250E+01	8.163E-03	1.592E-01	1.498E+02	1.500E+02
1.875E+01	1.190E-02	2.321E-01	1.498E+02	1.500E+02
2.500E+01	1.543E-02	3.009E-01	1.497E+02	1.500E+02
3.125E+01	1.876E-02	3.657E-01	1.496E+02	1.500E+02
3.750E+01	2.190E-02	4.270E-01	1.496E+02	1.500E+02
4.375E+01	2.486E-02	4.847E-01	1.495E+02	1.500E+02
5.000E+01	2.765E-02	5.392E-01	1.495E+02	1.500E+02
5.625E+01	3.029E-02	5.906E-01	1.494E+02	1.500E+02
6.250E+01	3.277E-02	6.391E-01	1.494E+02	1.500E+02
6.875E+01	3.512E-02	6.849E-01	1.493E+02	1.500E+02

7.500E+01	3.734E-02	7.280E-01	1.493E+02	1.500E+02
8.125E+01	3.942E-02	7.688E-01	1.492E+02	1.500E+02
8.750E+01	4.139E-02	8.072E-01	1.492E+02	1.500E+02
9.375E+01	4.325E-02	8.435E-01	1.492E+02	1.500E+02
1.000E+02	4.501E-02	8.777E-01	1.491E+02	1.500E+02
1.063E+02	4.666E-02	9.099E-01	1.491E+02	1.500E+02
1.125E+02	4.822E-02	9.404E-01	1.491E+02	1.500E+02
1.188E+02	4.970E-02	9.691E-01	1.490E+02	1.500E+02
1.250E+02	5.109E-02	9.962E-01	1.490E+02	1.500E+02
1.313E+02	5.240E-02	1.022E+00	1.490E+02	1.500E+02
1.375E+02	5.364E-02	1.046E+00	1.490E+02	1.500E+02
1.438E+02	5.480E-02	1.069E+00	1.489E+02	1.500E+02
1.500E+02	5.590E-02	1.090E+00	1.489E+02	1.500E+02
1.563E+02	5.694E-02	1.110E+00	1.489E+02	1.500E+02
1.625E+02	5.792E-02	1.129E+00	1.489E+02	1.500E+02
1.688E+02	5.885E-02	1.148E+00	1.489E+02	1.500E+02
1.750E+02	5.972E-02	1.165E+00	1.488E+02	1.500E+02
1.813E+02	6.054E-02	1.181E+00	1.488E+02	1.500E+02
1.875E+02	6.132E-02	1.196E+00	1.488E+02	1.500E+02
1.938E+02	6.205E-02	1.210E+00	1.488E+02	1.500E+02
2.000E+02	6.274E-02	1.223E+00	1.488E+02	1.500E+02
2.063E+02	6.340E-02	1.236E+00	1.488E+02	1.500E+02
2.125E+02	6.401E-02	1.248E+00	1.488E+02	1.500E+02
2.188E+02	6.459E-02	1.260E+00	1.487E+02	1.500E+02
2.250E+02	6.514E-02	1.270E+00	1.487E+02	1.500E+02
2.313E+02	6.566E-02	1.280E+00	1.487E+02	1.500E+02
2.375E+02	6.614E-02	1.290E+00	1.487E+02	1.500E+02
2.438E+02	6.660E-02	1.299E+00	1.487E+02	1.500E+02
2.500E+02	6.704E-02	1.307E+00	1.487E+02	1.500E+02
EQUILIBRIUM	7.428E-02	1.448E+00	1.486E+02	1.500E+02

```
*****************
*OIL WELL-MIXED*
*****************
```

TIME (HOURS)	CW (MG/L)		
0.000E+00	0.000E+00		
1.250E+01	8.169E-03		
1.875E+01	1.191E-02		
2.500E+01	1.544E-02		
3.125E+01	1.877E-02		
3.750E+01	2.191E-02		
4.375E+01	2.487E-02		
5.000E+01	2.767E-02		
5.625E+01	3.031E-02		
6.250E+01	3.279E-02		
6.875E+01	3.514E-02		
7.500E+01	3.736E-02		
8.125E+01	3.945E-02		
8.750E+01	4.142E-02		
9.375E+01	4.328E-02		
1.000E+02	4.503E-02		
1.063E+02	4.669E-02		
1.125E+02	4.825E-02		
1.188E+02	4.972E-02		
1.250E+02	5.111E-02	1.813E+02	6.056E-02
1.313E+02	5.242E-02	1.875E+02	6.134E-02
1.375E+02	5.366E-02	1.938E+02	6.207E-02
1.438E+02	5.482E-02	2.000E+02	6.276E-02
1.500E+02	5.593E-02	2.063E+02	6.341E-02
1.563E+02	5.696E-02	2.125E+02	6.403E-02
1.625E+02	5.794E-02	2.188E+02	6.461E-02
1.688E+02	5.887E-02	2.250E+02	6.515E-02
1.750E+02	5.974E-02	2.313E+02	6.567E-02
		2.375E+02	6.616E-02
		2.438E+02	6.662E-02
		2.500E+02	6.705E-02

APPENDIX B: CODE DESCRIPTION FOR COMPONENT-SPECIFIC DISSOLUTION FROM DROPLETS

The following is a code listing from the FORTRAN code DRPLET.FOR. This code predicts component-specific dissolution of oil in the absence of evaporation from oil droplets.

Details of the derivation of component-specific dissolution are presented in Section 6.9.2.7 of this report.

```
           IMPLICIT REAL*8 (A-H,O-Y)
           REAL*8 KW,M,LH
           DIMENSION ALPHA(100),POLY(100),ZTIME(101),CURVES(4,101)
          1,CUR(101),ZCURVS(4,101),ZCUR(101),ZWORDS(20)
          2,ZX(4),ZY(4),ZLINE1(30),ZLINE2(30),ZLINE3(30),ZRAY(30)
           OPEN(UNIT=32,DIALOG='CHECK.OUT')
           TYPE 5
5          FORMAT(1X,'ENTER A IN CM')
           ACCEPT 20,A
           TYPE 10
10         FORMAT(1X,'ENTER DIFFUSIVITY, CM**2/SEC')
           ACCEPT 20,DO
20         FORMAT(F10.0)
           TYPE 21
21         FORMAT(1X,'ENTER KW, CM/SEC')
           ACCEPT 20,KW
           M=1000.D0
           DO 1000 L=1,4
           M=M*10.D0
           H=KW/(DO*M)
           PI=3.141592653589793230
           DO 50 I=1,100
           RH=I*PI
           LH=(I-1)*PI
           DO 40 K=1,50
           XM=(LH+RH)/2.D0
           COT=DCOS(XM)/DSIN(XM)
           FX=XM*COT+(A*H)-1.D0
           IF(FX.LT.0.D0) GO TO 30
           LH=XM
           GO TO 40
30         RH=XM
40         CONTINUE
           ALPHA(I)=XM/A
           POLY(I)=A*A*(ALPHA(I)**2.D0)+((A*H-1.D0)**2.D0)
           POLY(I)=POLY(I)/(ALPHA(I)**4.D0)
           POLY(I)=POLY(I)/(A*A*(ALPHA(I)**2.D0)+A*H*(A*H-1.D0))
50         CONTINUE
           DO 200 J=1,101
           T=(J-1)*86400.D0
           SUM1=0.D0
           DO 100 I=1,100
           SUM1=SUM1+DSIN(A*ALPHA(I))*DSIN(A*ALPHA(I))*POLY(I)*
          1DEXP(-T*DO*(ALPHA(I)**2.D0))
100        CONTINUE
           CURVES(L,J)=SUM1*6.D0*H*H/(A*A)
200        CONTINUE
```

464

```
1000      CONTINUE
          DO 2000 I=1,101
          ZTIME(I)=(I-1)*10./100.
2000      CONTINUE
          DO 3000 I=1,4
          DO 2500 J=1,101
          ZCURVS(I,J)=CURVES(I,J)
2500      CONTINUE
3000      CONTINUE
          ZA=A
          ZKW=KW
          ZDO=DO
          ZM=M
          CALL COMPRS
          CALL NOBRDR
          CALL SCMPLX
          CALL AREA2D(8.,6.)
          CALL YNAME('AVERAGE DIMENSIONLESS CONCENTRATION',35)
          CALL XNAME('TIME (DAYS)',11)
          CALL GRACE(0.0)
          CALL FRAME
          CALL GRAF(0.,1.,10.,0.,0.1,1.)
          CALL BLREC(4.75,.8,3.05,1.0,0.01)
          CALL HEADIN('PREDICTED DIFFUSION AND DISSOLUTION',35,1.8,3)
          CALL HEADIN('FROM A DROPLET INTO AN',22,1.8,3)
          CALL HEADIN('INFINITE MEDIUM',15,1.8,3)
          DO 5000 I=1,4
          DO 4000 J=1,101
          ZCUR(J)=ZCURVS(I,J)
4000      CONTINUE
          CALL CURVE(ZTIME,ZCUR,101,0)
5000      CONTINUE
          ZX(1)=ZTIME(5)
          ZX(2)=ZTIME(20)
          ZX(3)=ZTIME(35)
          ZX(4)=ZTIME(75)
          ZY(1)=ZCURVS(1,4)
          ZY(2)=ZCURVS(2,17)
          ZY(3)=ZCURVS(3,30)
          ZY(4)=ZCURVS(4,55)
          ZMM=1000.
          DO 6000 I=1,4
          ZMM=ZMM*10.
          ENCODE(11,4500,ZWORDS)ZMM
4500      FORMAT('M= ',1PE8.1)
          ZXVAL=ZX(I)
          ZYVAL=ZY(I)
          CALL RLMESS(ZWORDS,11,ZXVAL,ZYVAL)
6000      CONTINUE
          MAXLIN=LINEST(ZRAY,100,23)
          ENCODE(20,7000,ZLINE1)ZA
7000      FORMAT('RADIUS=',1PE9.2,' CM$')
          ENCODE(20,8000,ZLINE2)ZKW
8000      FORMAT('KW=',1PE9.2,' CM/SEC$')
          ENCODE(23,9000,ZLINE3)ZDO
9000      FORMAT('DO=',1PE9.2,' CM*CM/SEC$')
          CALL LINES(ZLINE1,ZRAY,1)
          CALL LINES(ZLINE2,ZRAY,2)
          CALL LINES(ZLINE3,ZRAY,3)
          CALL BLKEY(ID)
          CALL BLOFF(ID)
          CALL LSTORY(ZRAY,3,4.9,1.)
          CALL ENDPL(0)
          CALL DONEPL
          END
```